POLYMER ELECTROLYTES FOR SAFER LITHIUM-BASED BATTERIES: SYNTHESIS, CHARACTERIZATION, AND STRUCTURE-FUNCTION CORRELATION

A Dissertation

Presented to the Faculty of the Graduate School

of Cornell University

In Partial Fulfillment of the Requirements for the Degree of

Doctor of Philosophy

by

Rachna Khurana

August 2014

POLYMER ELECTROLYTES FOR SAFER LITHIUM-BASED BATTERIES: SYNTHESIS, CHARACTERIZATION, AND STRUCTURE-FUNCTION CORRELATION

Rachna Khurana, Ph. D.

Cornell University 2014

Rechargeable Li-metal batteries (LMBs) are conceivably one of the most promising battery technologies to achieve high energy densities for sustainable transport applications and grid-storage components. Electrolytes are a critical component of a battery that allows the ion-transport for the efficient charge-discharge of the battery. Conventional liquid electrolytes (e.g. a mixture of lithium salt and alkyl carbonates) that are employed in a typical Li-ion battery are flammable. Moreover, they can also react with the Li-metal, leading to irreversible reactions and dendrite formation on the lithium metal surface. Solid polymer electrolytes (SPEs) have been reported to limit this reactivity, however their low ionic conductivities at room temperature ($<10^{-4}$ S/cm) have impeded their use in a rechargeable LMB device for ambient temperature operation. This dissertation describes the synthesis, characterization, and applications of new solid polymer electrolytes for lithium battery applications with main emphasis on using poly(ethylene oxide) (PEO) as the ionically conducting segment and semi-crystalline polymers, namely polyethylene (PE) and syndiotactic polypropylene (sPP) as the mechanically rigid segments.

We developed a new class of PE/PEO cross-linked polymer electrolytes using ring opening metathesis polymerization route. These SPEs demonstrated both high

ionic conductivity (>10^{-4} S/cm at 25 °C) and unprecedented levels of dendrite growth resistance. We also formulated new SPE compositions by varying the lithium salts and the plasticizers in these PE/PEO cross-linked systems. To achieve better transport properties, we synthesized Li-ion conducting network polyelectrolytes that contained non-coordinating tetraphenylborate anions tethered to the polyethylene backbone. We also developed syndiotactic polypropylene-*b*-poly(ethylene oxide)-*b*-syndiotactic polypropylene (PEOP) triblock copolymers using azide-alkyne "click" chemistry route. PEOP triblock copolymers containing different block sizes were synthesized and doped with a lithium salt for use as an electrolyte in a lithium battery.

Finally, we established structure-property relationships for several SPEs reported in this dissertation. We anticipate that some of the polymer electrolytes described in this work will provide useful insights for the design of SPEs with superior electrolyte properties, including higher ionic conductivity, better electrochemical stability, and excellent dendrite growth resistance.

BIOGRAPHICAL SKETCH

Rachna Khurana was born in New Delhi, India on August 19, 1985. During her high school education, she enjoyed doing math puzzles and working in chemistry laboratory classes. After graduating from high school in 2003, she decided to major in chemistry and attended St. Stephen's College for undergraduate studies. Her interactions with the chemistry faculty at her undergraduate institution further motivated her to pursue research in chemistry.

For the masters degree program, she got offers from two of the premier research institutions in India – Indian Institute of Technology (Delhi) and Indian Institute of Sciences (Bangalore). She chose to stay closer to her family and attended IIT Delhi for the M.Sc. program in 2006. She decided to pursue research in a biochemistry lab under the supervision of Prof. S. K. Khare. Besides taking chemistry courses, she also took some interdisciplinary courses like biomaterials and enzymology, which inspired her to pursue a Ph.D. degree at the interface of polymer chemistry and biology.

After finishing her postgraduate studies at IIT Delhi, she decided to gain some research experience in the field of materials chemistry before applying for Ph.D. programs. Prof. A. K. Ganguli was kind enough to offer her a position as project assistant in his laboratory in the summer of 2008. During her one year stay there, she made amazing friends, and worked on an independent project which involved the synthesis of nanoparticles using a reverse micellar route.

In the summer of 2009, she moved to the beautiful city of Ithaca for her graduate studies at Cornell University. At Cornell, she joined the laboratory of Prof. Geoffrey Coates, where she worked on the development of new polymer electrolytes for Li-battery applications. During her stay in Coates lab, she made wonderful friends, enjoyed working with her labmates, and learned a lot about US culture. During her graduate studies, she had the opportunity to collaborate with and learn from outstanding scientists both within and outside of Cornell. Upon completion of her Ph.D., she will move to Minnesota, where she will begin her career as a research scientist at 3M.

To my parents.

ACKNOWLEDGMENTS

First and foremost, I would like to thank my advisor Prof. Geoff Coates. His constant guidance and constructive criticism throughout my graduate school have helped me improve as a scientist. His unconventional ideas always motivated me to try exciting things in lab and further inspired me to read scientific articles outside my comfort zone. It is because of him that I know many great things about catalysis and polymers (especially all the analogies!). He gave me the freedom to address the problems that I felt most strongly about while providing his input when I needed it. I also learned a great deal from him about articulating results and scientific writing, which will help me in my future career as a scientist. Geoff is an incredible manager too and I learned a lot about management skills from him as well. It was a pleasure working with him for the past five years.

I also want to thank Prof. Héctor D. Abruña and Prof. William R. Dichtel for serving on my committee. Although I did not get a chance to collaborate with Prof. Abruña or Prof. Dichtel, I have always been an admirer of their research work. Prof. Abruña was always willing to talk to me about my research and teach me about cyclic voltammetry. I am grateful to him for allowing me to attend his battery sub-group meetings. Prof. Dichtel has been a great source of inspiration to me during my time at Cornell. I will never forget the day when Prof. Dichtel gave his tenure talk – it was truly inspirational and one of the best scientific talks I have ever attended.

Next must come my appreciation for Dr. Anne LaPointe, who has been a role model to me. She is a wonderful human being, an excellent scientist, and an amazing

source of technical knowledge. I greatly appreciate all her help for editing my papers and thesis chapters, and teaching me about glove box maintenance.

I have been fortunate to collaborate with some outstanding professors and talented graduate students both in and outside Cornell University. These people include: Prof. Lynden A. Archer, Prof. Nitash P. Balsara, Dr. Jennifer L. Schaefer, Dr. Nicholas Young, and Dr. Didier Devaux. I must thank Jen for educating me about coin cells, dielectric spectroscopy, and rheology.

Besides academic research groups, I have also had the pleasure of collaborating with ExxonMobil Company and QuantumScape. I enjoyed working with Dr. Kate L. Peretti, an alumna from Coates group and currently an employee at ExxonMobil. She provided many insightful suggestions during our phone conversations, and her enthusiasm motivated me to work in industrial research and development division. Working with a start-up company like QuantumScape was an exciting experience. The highly motivated electrolyte team at QuantumScape introduced me to the technical challenges regarding scaling up of a technology, which further inspired me to address some key technical issues in my project.

It was a joy to come to work everyday because of Coates group members (present and past). My stay in the Coates lab will always be memorable because of some awesome friends I made in this lab who are pivotal to my learning experience (not just chemistry!) in life. Angie is the nicest person on the planet and she is one of my best friends. I must thank her for bringing joy to my life and listening to me complaining about random things countless number of times. Thanks to Kristina for teaching me about polymer membranes and film casting tricks. She is an amazing

woman and I am grateful for our friendship. I will cherish my friendship with Yuki forever. She is smart, sweet, funny, and a wonderful human being. Ian is undoubtedly the smartest person I know (although extremely sarcastic at times!), and I am thankful to him for teaching me about US culture and politics. I share a special bond with Tulaza, who taught me a lot about paper formatting and editing. Although technically she is from Nepal, she is more Indian than I am (I hate to admit this though!). I enjoyed doing Bible study with Brandon, and I am thankful to him for bringing me a little closer to God.

The post-doctoral associates and graduate students with whom I have shared lab space and time while my stay at Cornell have contributed a lot to my flourishing as a researcher. I want to acknowledge the help of several people: Dr. Giang Vo, Dr. Chad Ellis, Prof. Brian Long, Prof. Kevin Noonan, Dr. Soumya Sarkar, Dr. Masato Mizutani, Dr. Jeung Kim, Dr. Hisashi Ohtaki, Prof. Chris Goh, 'C', Tam, Nate, Dr. Pasquale Iacano, Dr. Michael Mulzer, Dr. Bryan Whiting, Dr. Rocco Di Girolamo, Dr. Amelia Anderson, Kyle, and Jessica. I would specially like to thank Henry and Erin for supporting me during my visit to 3M, and I look forward to working with them in the future.

In 565 I have had the opportunity to work with amazing colleagues over the past five years. Pete Widger taught me epoxide polymerization and it was fun to make isotactic polyethers in the beginning. Thanks to Jeung for teaching me lab procedures and Schlenk technique. Taz created a fun atmosphere in the lab and I look forward to working with him at 3M. It was a pleasure to teach Will and Qi who are doing exceedingly well in graduate school and I look forward to reading about their

awesome research in future. Julie and Jeff are doing impressive work and I wish them all the best for their bright future.

Financial support from Energy Materials Center at Cornell (EMC^2), an Energy Frontier Research Center funded by the U.S. Department of Energy, is greatly acknowledged. I would also like to thank Dr. Paul F. Mutolo and Bill Dailey for insightful discussions regarding patent application. Special thanks to Suzanne for helping me with the chemical orders and organizing SAB meetings.

I am thankful to the great staff members of the Cornell Chemistry Department. I would specially like to thank Dr. Ivan Keresztes for teaching me about 2D-NMR, ^{11}B NMR, and ^{19}F NMR analysis. I also greatly appreciate Tony Condo's help with TGA, MALDI, and DSC measurements. A big thank you to Kelly for helping me with countless things – ordering chemicals for me, mailing my samples, stocking up the cabinets with supplies, and getting us left-over food from seminars.

Thanks to all my friends – Aditi, Rejy, Susy, Chin, Arthur, Michael Lowe, Jen, David, Aritro da, Siddarth, Deepti, Anand, Amit, Shruti, Pooja, Poornima, Pallavi, Ranga, Aparna, JP, Jahangeer, Menaka, Saroj, Saba, Parag, Debashree, Ritu di, and Kaori for their help, support, encouragement, and good wishes over the years.

Last but not the least, I want to thank my parents for their unconditional love and support over the years. I would also like to thank my sister and brother for their encouragement, love, and prayers without which I wouldn't have been able to conduct my research at Cornell.

TABLE OF CONTENTS

APPENDIX B – Synthesis and Characterization of Perfluorophenylborate Monomers For Ring Opening Metathesis Polymerization

LIST OF FIGURES

LIST OF TABLES

LIST OF SCHEMES

LIST OF ABBREVIATIONS

Block copolymer	BCP
1-butyl-3-methylimidazolium bis(trifluoromethylsulfonyl)imide	BMI-TFSI
N-butyl-N-methylpyrrolidinium bis(trifluoromethylsulfonyl)imide	BMP-TFSI
Cyclooctene	COE
Diethyl carbonate	DEC
Differential scanning calorimetry	DSC
Dimethyl carbonate	DMC
Ethylene carbonate	EC
Ethylene oxide	EO
Ethyl methyl carbonate	EMC
1-Ethyl-3-methylimidazolium bis(trifluoromethylsulfonyl)imide	EMI-TFSI
Gel permeation chromatography	GPC
Gel polymer electrolyte	GPE
Ionic Liquid	IL
Li-ion battery	LIB
Li-metal battery	LMB
Li-metal polymer	LMP
Lithium bis(oxalato)borate	LiBOB
Lithium bis(trifluoromethanesulfonyl)imide	LiTFSI
Polyacrylonitrile	PAN
Polyethylene	PE
Poly(ethylene glycol)	PEG
Poly(ethylene glycol)-grafted-cyclooctene	PEG-*g*-COE
Poly(ethylene oxide)	PEO
Poly(ethylene oxide) cross-linker	PEOX
Poly(propylene oxide)	PPO
Polystyrene	PS
Polystyrene-*b*-poly(ethylene oxide)	PS-*b*-PEO

Polymer Li-ion	PLion
Propylene carbonate	PC
Resonant soft X-ray scattering	RSoXS
Ring opening metathesis polymerization	ROMP
Single-ion conductor	SIC
Small Angle X-ray Scattering	SAXS
Solid electrolyte interface	SEI
Solid polymer electrolyte	SPE
Syndiotactic polypropylene	sPP
Syndiotactic polypropylene-*block*-poly(ethylene oxide)-*block*-syndiotactic polypropylene	PEOP
Thermogravimetric analysis	TGA
Tris-(benzyltriazolylmethyl)amine	TBTA
Vogel-Tammen-Fulcher	VTF
Wide-angle X-ray Scattering	WAXS

LIST OF SYMBOLS

E_a	Activation energy
μ_a	Anion mobility
t_a	Anion transference number
δ	Chemical shift
χ	Crystallinity
J	Current density
t_g	Dendrite growth time
D	Diffusion constant
d	Domain spacing
E	Electric field
e	Elementary charge
ΔH_{fus}	Enthalpy of fusion
T_g	Glass transition temperature
L	Interelectrode distance
C_o	Ion concentration
σ	Ionic conductivity
t_{Li+}	Li ion transference number
T_m	Melting temperature
μ	Mobility
λ	Molar DC ionic conductivity
M_n	Number average molecular weight
M_w/M_n	Polydispersity index
τ_s	Sand's time
θ	Scattering angle
G'	Shear storage modulus
G''	Shear loss modulus
t_{sc}	Short circuit time
rrrr	Syndiotacticity

M_w	Weight average molecular weight
w	Weight fraction

CHAPTER 1

Brief Overview of Polymer Electrolytes for Li-Battery Applications

CHAPTER 1

Brief Overview of Polymer Electrolytes for Li-Battery Applications

1.1 Introduction

Current rechargeable Li-ion batteries (LIBs) have prompted the growth of the market of popular devices such as laptop computers, mobile phones, tablets, and others. These batteries have gained lot of attention due to their many attractive features, such as high energy density, open circuit voltage, and high efficiency. While promising for several applications, these LIBs suffer from many disadvantages, such as a) safety issues due to the use of flammable organic liquids as Li-ion conducting electrolytes, and b) relatively low-energy density because of lithiated graphite as an anode component. Clearly, there is a need to develop safer and higher energy density Li-based battery technology, which can be used for sustainable transport applications (like electric and hybrid electric vehicles) to meet the ever-growing energy demands. One approach for achieving high energy density is by replacing the graphite anode with a Li-metal anode, which has an order of magnitude higher anode capacity compared to the lithiated graphite electrode. Additionally, substituting the flammable liquid electrolytes with less/non-flammable polymer electrolytes could minimize the safety hazards. Although Li-metal polymer (LMP) battery technology offers noteworthy benefits, it has not penetrated the rechargeable battery market due to several practical limitations. Lithium dendrite formation on the anode is one of the primary failure mechanisms in these batteries. Moreover, low ionic conductivities of the solid polymer electrolytes have limited their use in an LMP battery. Extensive research efforts are focused on developing solid polymer electrolytes for LMP batteries that not only exhibit high Li-ion conductivity, but also prevent dendrite nucleation and growth on the Li-metal anode.

1.2 Li-Based Batteries

A battery is an energy storage device that converts chemical energy into electrical energy. It is comprised of two electrodes separated by an ion-conducting medium known as electrolyte. In a rechargeable (or secondary) battery, upon discharge, electrons spontaneously flow from the more negative to the more positive electrode in the external circuit and the ions are transported through the electrolyte maintaining the charge balance. Higher voltage applied in the opposite direction can recharge the battery. A number of rechargeable batteries have been proposed in the last century, such as lead-acid, Ni-Cd, Ni-metal hydride, Li-based batteries, etc. Among these batteries, Li-based battery technologies have received great attention because lithium is the most electropositive (−3.0 V vs. SHE) and the lightest element, thus enabling the fabrication of high energy density batteries.[1,2]

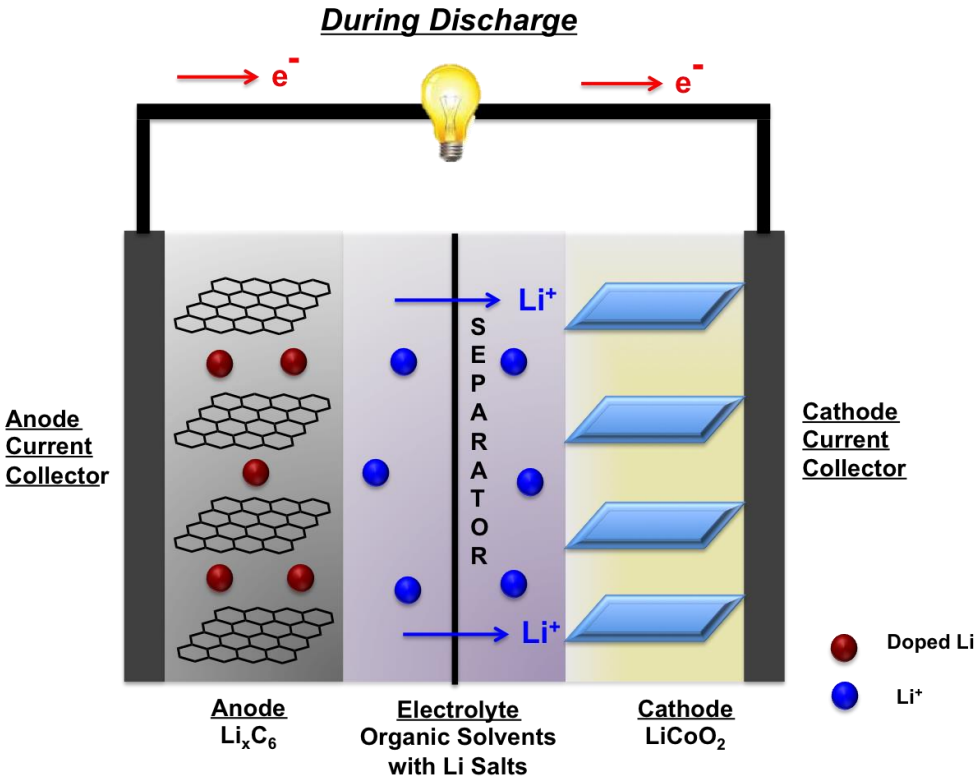

Figure 1.1 Schematic diagram of a Li-ion battery.

The first Li-based rechargeable battery was commercialized by Sony in 1991 and it is known as "Li-ion" or "rocking-chair" secondary battery. A basic schematic diagram of a rechargeable Li-ion battery is shown in Figure 1.1. In a conventional Li-ion battery (LIB), the anode is lithiated graphite (Li_xC_6), the cathode is a transition metal oxide ($Li_{1-x}T^MO_2$, where T^M is a transition metal), the separator is a microporous polyolefin membrane, and the electrolyte is generally comprised of a highly polar organic liquid doped with a lithium salt (for example, 1.0 M solution of $LiPF_6$ in 1:1 (v/v) mixture of ethylene carbonate and dimethyl carbonate). The reversible extraction and insertion of Li-ion (the so-called "rocking-chair" mechanism) in this battery is based on the following reversible redox process:

$$yC + LiT^MO_2 \rightleftarrows Li_xC_y + Li_{1-x}T^MO_2;\ x \sim 0.5,\ y = 6 \qquad (1)$$

The open circuit voltage of a standard LIB is 3.7 V and its energy density is ~180 $Whkg^{-1}$, which is approximately 5 times higher than that of the lead-acid battery.[1] Due to the high open circuit voltage and high energy content, these batteries have revolutionized the consumer electronics market as demonstrated by the production of billions of Li-ion cells each year. Although these batteries are promising for electronic devices, their low energy density cannot meet the high energy demands as well as other standards (safety, power, cost, reliability, and lifetime) required for their application in transportation.[3] Moreover, these batteries have safety hazards associated with them, as both the flammable organic liquids and the reactive cathode materials can cause thermal run-away leading to fires under abusive conditions.

It has been recognized that batteries with high energy density will be needed for their large-scale application in the electric vehicles. One approach of increasing the energy density is to replace the graphitic anode with a higher capacity and lower cost anode material such as lithium metal. Conventional liquid electrolytes cannot be used in Li-metal batteries due to the reaction of these reactive electrolytes with lithium.

Furthermore, lithium has been shown to deposit in a non-uniform way on the anode in aprotic solvents, resulting in short-circuit and thermal run-away.[4] Solid polymer electrolytes (SPEs) have been found to reduce the chemical reactivity of an electrolyte with lithium metal.[5,6] The battery configurations for conventional LIB and Li-metal polymer (LMP) battery are shown in Figure 1.2. Unlike LIBs, LMP batteries are much thinner and hence provide higher energy density. Also, LMP batteries offer significant safety advantages because they contain no flammable solvents. Despite the tremendous potential, two major issues have impeded their practical applications: a) dendrite growth in conjunction with Li-metal that causes battery failure and b) low ionic conductivity of SPEs at room temperature that limits the battery efficiency.

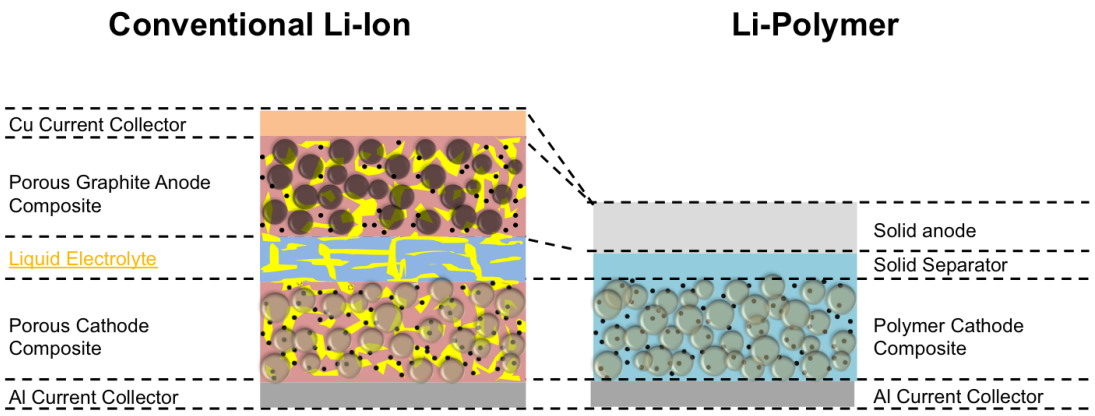

Figure 1.2 Conventional Li-ion vs. Li-metal polymer battery (reference 7).

1.3 Polymer Electrolytes

In contrast to the liquid electrolytes, polymers have the advantage of being flexible and lightweight, and thus allow battery fabrication in different shapes and sizes. Moreover, high molecular weight polymers are essentially non-flammable and therefore much safer than the conventional liquid electrolytes such as $LiPF_6$/ethylene

carbonate. For successful operation of a battery, a polymer electrolyte should possess some desired properties, such as a) *high ionic conductivity* (typically $\sigma > 10^{-4}$ S/cm at 25 °C for an SPE), b) *good mechanical properties*, c) *large electrochemical window*, d) *high cation mobility* (high Li^+ ion transference number), e) *ease of processability*, f) *good interfacial contact with the electrodes*, and g) *excellent chemical and thermal stability*.[6,8]

In 1973, Wright and co-workers discovered the ionic conductivity in the alkali metal salt complexes of poly(ethylene oxide) (PEO).[9] Later, Armand and co-workers proposed the use of alkali metal-doped PEO polymers as a solid polymer electrolyte (SPE) for battery applications for the first time.[10] Theoretical calculations suggest that approximately five oxygens of the PEO chain complex to Li^+ ions and Li^+ ion transport occurs *via* the segmental motion of the PEO matrix, as shown in Figure 1.3.[11] Surprisingly, the majority of the research work in the polymer electrolyte field is still focused on PEO due to its relatively high conductivity when compared with other polymers. However, the room temperature conductivity of PEO-based polymer electrolytes is still very low (Figure 1.4; $\sigma \sim 5 \times 10^{-6}$ S/cm at 25 °C for PEO-LiTFSI

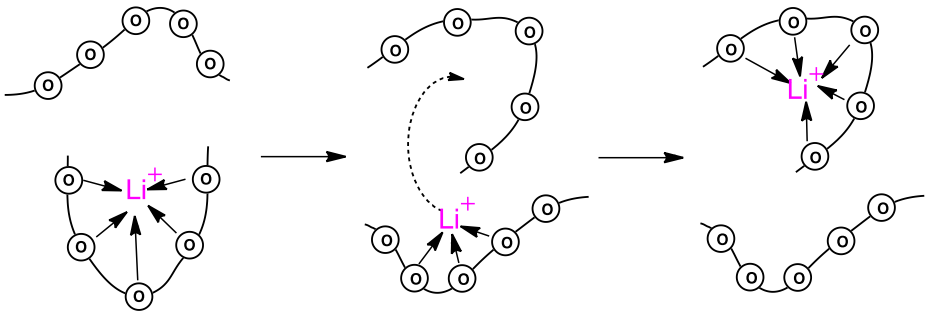

Figure 1.3 Segmental motion in PEO facilitating Li-ion conduction (Adapted from reference 12).

electrolyte) due to the crystalline domains in high molecular weight PEO (M_n ~ 900 kDa). As shown in Figure 1.4, low molecular weight poly(ethylene glycol) (PEG; M_n ~ 250 Da) exhibits higher ionic conductivity at 25 °C ($\sigma \sim 10^{-3}$ S/cm) due to better segmental motion, but the mechanical properties of these oligomers are poor, preventing their use in a solid state battery.

To increase the ionic conductivity of the PEO-based electrolytes, researchers have used different strategies to decrease the crystallinity of PEO: a) block copolymers, b) cross-linked copolymers, c) polyether copolymers, and d) graft copolymers. Although PEO-based polymers have dominated the polymer electrolyte literature, other homopolymers have also been investigated as electrolyte components for Li-based batteries. These homopolymers will be briefly discussed in Section 1.5.1.1, but mainly we will focus on PEO-based polymer electrolytes.

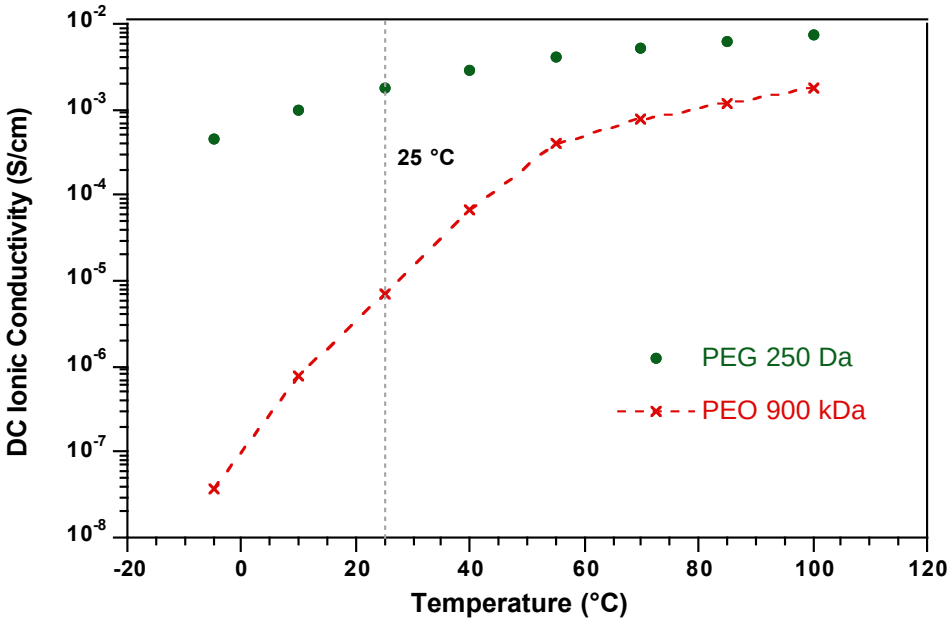

Figure 1.4 Conductivity plot of lithium bis(trifluoromethanesulfonyl)imide salt-doped PEO (M_n ~ 900 kDa) and PEG (M_n ~ 250 Da); [EO]:[Li] = 18.

1.4 General Considerations

1.4.1 Ionic Conductivity

The generally accepted model for the Li^+ ion transport in amorphous domains of PEO is shown in Figure 1.3. Lithium cations coordinate to the lone pairs of oxygen forming a chelate and upon application of external voltage, Li-ions migrate to a neighboring chelation site. The movement of ions is directly coupled to polymer chain mobility; this behavior is thermally activated and is often described by Vogel-Tammann-Fulcher (VTF) (equation 2):[13-15]

$$\sigma = AT^{-1/2} \exp[-B/R(T - T_o)] \quad (2)$$

where A is a pre-exponential factor which may be related to ion mobility and ion association, B is apparent activation energy, which is different from the activation energy (E_a), T_o is the thermodynamic glass transition temperature of the electrolyte, and T is the operating temperature. This model can explain the ion transport of either amorphous polymers or amorphous domains in semi-crystalline polymers. Faster relaxation occurs in low T_g polymers and hence higher conductivity is observed for them.

1.4.2 Electrochemical Stability

A polymer electrolyte is required to have electrochemical stability within the voltage window of the Li-based battery. The electrochemical stability of the electrolyte dictates the type of cathode material suitable for a battery. The voltage of cathode materials, such as $LiCoO_2$, can be as high as 4.5 V and thus requires the polymer electrolyte to be stable in the potential range of 0 to 4.5 V vs. Li^+/Li. PEO-LiTFSI SPEs have shown to be stable up to 4.5 V versus Li^+/Li at ambient

temperature on a smooth blocking electrode.[16,17] Greenbaum and co-workers reported PEO-LiTFSI electrolytes that showed significantly less electrochemical stability when compared to PEO-$LiCF_3SO_3$ SPE at 40 °C.[18] Furthermore, they studied the effect of [EO]:[Li] ratio and ceramic additives on the electrochemical stability of the SPEs. They found that while Al_2O_3 additives did not affect the voltage stability of the PEO-$LiCF_3SO_3$ electrolyte, salt concentration (i.e. [EO]:[Li] ratio) had a dramatic effect on the electrochemical stability at 60 °C. The results of this study indicated that electrolyte salt is one of the main contributors to the electrochemical instability of PEO-based SPEs at high temperatures.

In the pursuit of finding a high energy density battery, researchers have developed new cathode materials that can operate at high potential (ca. 5 V), such as $LiCu_xMn_{2-x}O_4$,[19] $LiNi_xCo_{1-x}PO_4$,[20] etc. However, the practical utility of such high voltage cathode materials is limited by the electrochemical instability of current state-of-the-art electrolytes. Numerous ways have been proposed to increase the electrochemical stability of electrolytes, including development of new electrolyte chemistries, and utilization of various organic and inorganic additives in the electrolyte formulation.[21-28] Some of the additives that have demonstrated to increase the electrochemical stability in a conventional Li-ion battery are shown in Table 1.1.

Among the possible strategies, using fluorinated compounds such as fluorinated lithium salts and fluorinated organic compounds as additives is one of the most extensively used methods for increasing the electrochemical stability window of the electrolytes. Kita and co-workers did an elegant study to determine the structural effects of fluoroorganic lithium salts on the conductivity, electrochemical stability,

Table 1.1 Additives for increasing the electrochemical stability of Li-ion conducting electrolytes

Additive	Chemical Structure	Reference
Lithium Salts		
a) Fluorinated Salts Lithium nonafluorobutanesulfonate $LiC_4F_9SO_3$	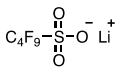	21
Lithium heptadecafluorooctanesulfonate $LiC_8F_{17}SO_3$	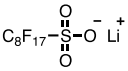	21
b) Borate Salts Lithium bis(oxalato)borate (LiBOB)	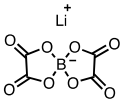	29
Lithium 3,3,9,9-tetrafluoro-2,4,8,10-tetraoxo-1,5,7,11-tetraoxa-6-boraspiro[5.5]undecan-6-uide	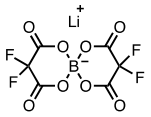	29
Lithium 3,3,4,4,10,10,11,11-octafluoro-2,5,9,12-tetraoxo-1,6,8,13-tetraoxa-7-boraspiro[6.6]tridecan-7-uide	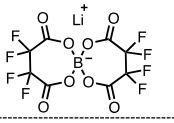	29
Fluorinated Organic Compounds		
Tris(1,1,1,3,3,3-hexafluoro-2-isopropyl)phosphate (HFiP)	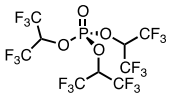	24
4-(trifluoromethyl)-1,3-dioxolan-2-one (TFM-EC)	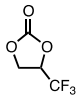	28
4-(perfluorobutyl)-1,3-dioxolan-2-one (PFB-EC)	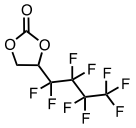	28
4-(perfluorohexyl)-1,3-dioxolan-2-one (PFH-EC)	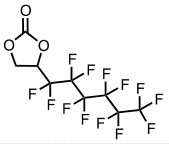	28
Other		
Ethyl methyl sulfone (EMS)		26
Adiponitrile (ADN)	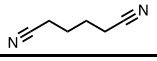	30

aluminum corrosion at high voltage, and cell performance of a Li-ion battery.[21] They found that among a lithium salt series, the anions with longer fluoroalkyl chains showed higher oxidation potential. For instance, the oxidation potentials for $LiCF_3SO_3$, $LiC_4F_9SO_3$, and $LiC_8F_{17}SO_3$ were determined to be 4.8, 6.0, and 6.5 V respectively in propylene carbonate electrolyte. Researchers at Argonne National Laboratory studied the effect of perfluoroalkyl substituted ethylene carbonate additives on the electrochemical performance of the electrolytes in a Li-ion battery.[28]

Sulfones and nitriles have also been explored as the solvents or cosolvents with organic carbonates to increase the oxidative stability of the electrolytes in a Li-ion battery. Xu and Angell studied the properties of ethylmethyl sulfone (EMS) in the presence of high-voltage cathode materials, and found that EMS solutions of high-stability salts such as $LiClO_4$ and LiTFSI were stable up to 5.8 V vs. Li^+/Li.[26] Abu-Lebdeh and Davidson investigated the electrochemical performance of adiponitrile (ADN) as a solvent and cosolvent with ethylene carbonate in a Li-ion battery. An electrolyte solution with the LiTFSI salt showed a wide electrochemical window of 6 V vs. Li^+/Li.[30]

To enhance the electrochemical stability, research efforts are mainly focused on studying the effects of different lithium salts in liquid electrolytes, mainly alkyl carbonates. In contrast to the liquid electrolytes, very little work has been done in the field of polymer electrolytes (for both unplasticized and plasticized) to increase the oxidation potential of these polymer electrolytes. The cyclic voltammetry experiments on the lithium salt-doped electrolytes (small molecules) have shown that the voltage stability window of these electrolytes follow the order: nitriles > carbonates > esters >

ethers.[31] Most likely, the oxidative stability of the polymer electrolytes containing these functional groups will follow a similar trend, i.e. polyacrylonitrile based polymer electrolytes might show highest electrochemical stability when compared to polycarbonates, polyesters, and polyethers (widely studied polymer electrolytes). However, it should be noted that several other electrochemical parameters, such as ionic conductivity, interfacial stability, cyclability (capacity retention), thermal decomposition, etc., would also be different for these polymers.

1.4.3 Lithium Dendrite Growth in Li-Metal Batteries

Lithium dendrite formation is one of the primary modes of failure in a typical rechargeable Li-metal battery. Lithium has been known to deposit in a non-uniform way upon charging on the Li-metal anode.[4] As shown in Figure 1.5, after many charge-discharge cycles, the mossy-like structures of lithium reach over to the cathode and short-circuit the battery, causing thermal run-away and fire. Numerous ways have been reported in the literature to delay the lithium dendrite nucleation and growth, such as alloying of the lithium metal anode,[32] and using additives to improve the uniformity at the solid electrolyte interface (SEI).[33-36] Although these strategies are promising, the performance suffers due to a reduced anode capacity and durability is reduced by consumption of additives to form the SEI films during successive charge-discharge cycles, respectively.

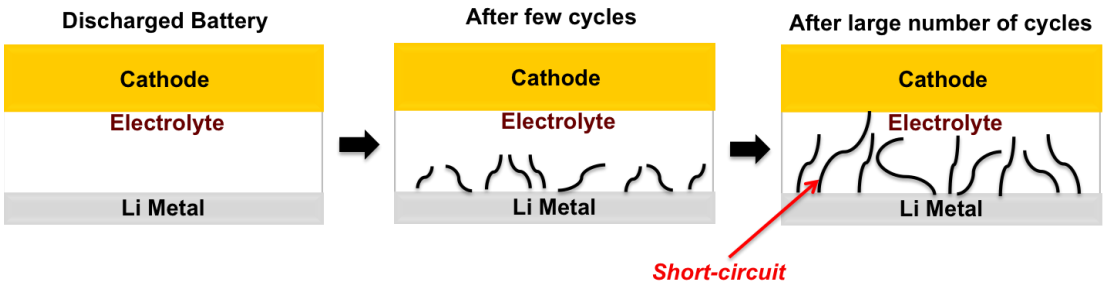

Figure 1.5 Dendrite growth on the lithium metal anode.

Current research efforts are also focused on changing the electrolyte chemistry to delay the dendrite growth.[37-41] Two main theories have been proposed in the literature to understand the dendrite nucleation and growth mechanism in an electrolyte. The Chazalviel model proposes that dendrites arise from anion depletion at the electrode, which leads to large electric field gradients near the lithium electrode causing enhanced electrodeposition and thus leading to dendrite growth. Electrolytes with higher ionic conductivity and reduced anion mobility will delay dendrite nucleation by mitigating anion depletion near the electrode-electrolyte interface.[42] In addition, a second model from Newman and Monroe considers the effect of physical forces such as electrolyte/separator modulus and surface tension on the kinetics of lithium electrodeposition. A prediction from this model is that SPEs with high shear modulus ($G' > 7$ GPa) could be used to suppress the dendrite growth.[43] As a test for this hypothesis, Balsara and co-workers designed mechanically rigid ($G' \sim 0.1$ GPa) microphase separated polystyrene-*b*-poly(ethylene oxide) (PS-*b*-PEO) block copolymers that showed high resistance to Li dendrite growth, supporting the high modulus theory.

1.4.4 Lithium-Ion Transference Number

In an electrolyte containing a binary salt, the measured ionic conductivity has the overall contribution from migration of both the Li^+ cation and the anion. However, for the Li-based battery operation, the rate at which the battery operates is only dependent on the contribution from the fraction of current carried by Li^+ cation. The portion of total current carried by lithium ions is usually referred to as Li^+ ion transference number (t_{Li+}) and is given by:

$$t_{Li+} = \frac{\mu_{Li+}}{\sum_i \mu_i} \quad (3)$$

where μ_i is the mobility of an ion, i in the electrolyte and μ_{Li+} is the mobility of lithium cation.

The majority of the LiX-doped polymer electrolytes reported to date, exhibit low Li^+ ion transference numbers. In particular, PEO-based polymer electrolytes exhibit very low t_{Li+} values of 0.2–0.3.[44] A lithium ion transference number significantly less than 1 is not desirable, because the resultant anion movement and accumulation near electrode surfaces causes concentration polarization during charge–discharge steps in a battery, and leads to significant decrease in the overall power density achievable in the battery. To overcome these limitations and decrease the anion migration, researchers are developing single-ion conductors that have immobilized anions covalently bound to the polymer backbone. These single-ion conductors will be briefly discussed in Section 1.5.1.3.

1.5 Types of Polymer Electrolytes

Polymer electrolytes can be categorized into three different classes based on their chemical composition: 1) *dry (or unplasticized) solid polymer electrolytes*, 2) *plasticized polymer electrolytes*, which typically contain small amounts of plasticizer to increase the free volume and decrease the glass transition temperature, and 3) *polymer composites* that are formed by addition of nanoparticulate ceramics in the polymer host.

1.5.1 Dry (or Unplasticized) Solid Polymer Electrolytes

PEO-based electrolytes are the most extensively studied dry solid polymer electrolytes since their proposed use in a Li-based battery by Armand in 1979.[10] Bathium Canada makes lithium-metal polymer (LMP) batteries, which contains a solid PEO-LiTFSI as the electrolyte component.[45] These LMP batteries power the Bluecar, a small electric vehicle that is available through an electric car-share service launched by Bolloré group in Paris. Despite these attractive applications, these PEO-based LMP batteries suffer from several disadvantages – high operational temperature (>70 °C) are required for better device performance and there is a potential risk of the batteries catching on fire due to dendrite growth at the Li-metal anode.

In a quest to find a better and highly conducting electrolyte for room temperature applications, researchers have also studied non-PEO based polymer electrolytes, such as polypropylene oxide (PPO),[46,47] polysiloxanes,[48-54] polyphosphazenes,[55-58] polyethylene imine,[59] etc. Several representative examples are shown in Table 1.2. Unlike PEO, atactic PPO is completely amorphous, but the Li-ion conductivity values above 60 °C are much lower than those of PEO and the solubility of lithium salts in the polymer is lower as well. This is due to both the lower dielectric constant of PPO, and the methyl group in the side-chain of the polymer backbone that

hinders the complexation of Li^+ cation.[46,47] Poly(ethylene imine) (PEI) is another polymer that has been studied due to strong electron donor properties of nitrogen in the polymer backbone, analogous to the oxygen in PEO polymer chain. Ratner and co-workers studied the conductivity behavior of PEI-$NaCF_3SO_3$ complexes at various salt ratios; the maximum ionic conductivity value observed for amorphous complex was very low (3.1×10^{-7} S/cm at 40 °C).[59]

Other flexible homopolymers with low glass transition temperatures, such as polysiloxanes and polyphosphazenes, have also gained lot of attention; low molecular weight PEG units have been grafted on these low T_g polymers and tested as electrolytes for Li battery applications. Polyphosphazenes have a number of advantages, such as low glass transition temperature, excellent flame retardant properties, and superior electrochemical stability. Seminal work from Allcock and co-workers on highly conducting oligoether-*g*-polyphosphazenes (poly(bis-2-(2-methoxyethoxy)ethoxyphosphazene) (MEEP: Table 1.2, entry 6) SPEs demonstrated the application of these polyphosphazenes as an electrolytes for battery applications.[57] While extremely promising due to good conducting properties, the lithium salt complexes of these polymers were soft solids and hence had poor mechanical properties. Several oligoether-substituted polysiloxanes have been extensively studied as SPEs by research teams of Smid[49,53,54] and Shriver[50-52]. Smid and co-workers reported SPE complexes of $LiClO_4$ with poly((o-methoxy-heptakis(oxyethylene)ethoxy)methylsiloxane) (Table 1.2, entry 5) polymers, which displayed an ionic conductivity of 7.0×10^{-5} S/cm at ambient temperature.[54] These SPEs are viscous liquids and have poor dimensional stability; several methods including cross-linking and blending with high molecular weight PEO have been used as strategies to improve the mechanical properties.

Table 1.2 Homopolymers for Li battery applications

Entry	Polymer	Alkali Metal Salt	Chemical Structure	Ionic Conductivity (S/cm) @ Temperature	Reference
1	Poly(ethylene oxide) (PEO)	LiTFSI		2.0×10^{-6} @30 °C	16
2	Poly(propylene oxide), (PPO)	$LiClO_4$		10^{-8} @20 °C	8
3	Poly(oxymethylene), (POM)	$LiClO_4$		10^{-8} @20 °C	8
4	Poly(ethylene imine), PEI	$NaCF_3SO_3$	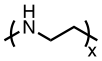	3.1×10^{-7} @40 °C	59
5	Oligoether-*g*-poly(dimethyl siloxane)	$LiClO_4$	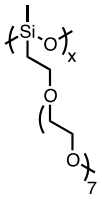	7.0×10^{-5} @25 °C	54
6	Poly(bis-2-(2-methoxyethoxy) ethoxyphosphazene), (MEEP)	LiTFSI	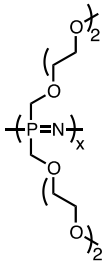	5.0×10^{-5} @25 °C	57

Limitations of all the homopolymer electrolytes, including poor mechanical properties, low ambient ionic conductivities, incompatibility with the electrode materials, etc., have prompted the search for alternative SPE materials. There have been a large number of studies in this field concerning both PEO- and non-PEO based polymer matrices; the PEO-based polymer electrolytes will be the focus of this review. For the PEO-based SPEs, decreasing the crystallinity of PEO domains and increasing the segmental motion of the PEO chains to enhance the ionic conductivity of the SPE has long been recognized as an important goal in the electrolyte field. Numerous strategies have been proposed in the literature to lower the crystallinity of PEO at room temperature, such as PEO-based *block copolymers*,[60-70] and *cross-linked polymers*.[71-78]

1.5.1.1 Block Copolymer Electrolytes

An ideal SPE would have have both high ionic conductivity and good mechanical properties. However, it is challenging to obtain high ionic conductivity values without compromising the mechanical integrity of the electrolyte. Block copolymers (BCPs) are considered to be an excellent way of decoupling the ionic conducting properties of ion-conducting domains from the mechanical properties of the non-conducting block in the block copolymer.[70,79] This is due to the self-assembly of BCPs, which leads to ordered structures with nanoscale domains that may impart desirable mechanical, chemical, and electrical properties for ion-conducting membrane applications. Several PEO-based block copolymers have been studied as a potential electrolyte component for Li-battery applications. [60-69,80]

Table 1.3 Block copolymers as solid polymer electrolytes

Entry	Polymer	Lithium Salt	Chemical Structure	Conductivity (S/cm) @Temperature	Reference
1	Poly(styrene-*b*-ethylene oxide)	LiTFSI	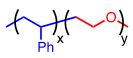	2.5×10^{-4} 90 °C	67
2	Poly(styrene-*b*-oligooxyethylene methacrylate-*b*-styrene)	$LiClO_4$	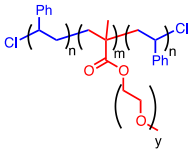	8.0×10^{-5} 30 °C	65
3	Poly(styrene-*b*-(styrene-*g*-ethyleneoxide)-*b*-styrene)	LiTFSI	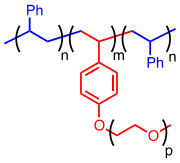	2.0×10^{-5} 25 °C	69
4	Poly(methylmethacrylate)-*b*-poly(oligo oxyethylene methacrylate)	$LiCF_3SO_3$	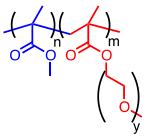	2.0×10^{-6} 22 °C	66

Selected examples of Li-ion conducting PEO-based BCP electrolytes are shown in Table 1.3. Initial studies on the BCP electrolytes were reported by Vincent and co-workers,[61] wherein the BCP was synthesized by grafting PEG units on the polybutadiene block of poly(styrene-*b*-butadiene-*b*-styrene) polymer and doped with $LiCF_3SO_3$. Ionic conductivity values up to 10^{-5} S/cm were observed for these $LiCF_3SO_3$-doped SPEs at 20 °C. Since then, several studies in BCP literature are focused on developing a better understanding of the effects of nanophase separation in the lithium salt-doped BCPs on the ionic conductivity, morphology, and mechanical properties.[60,65,67,81,82] Balsara and co-workers reported nanostructured lamellar LiTFSI-doped polystyrene-*b*-polyethylene oxide (PS-*b*-PEO) SPEs that exhibited an ionic conductivity value of 2.5×10^{-4} S/cm at 90 °C, and had a shear modulus of 0.1 GPa at

90 °C.[67] Epps and co-workers studied $LiClO_4$-doped PS-*b*-PEO SPEs to establish the relationship between ionic conductivity and morphology.[82] Their study indicated that samples with 3D conducting pathways (hexagonally perforated lamellar and hexagonal) exhibited much higher normalized conductivities than the corresponding 2-D conducting pathway (lamellar) morphologies.

Some high modulus BCP electrolytes have also demonstrated enhanced dendrite growth suppression at the lithium metal anode[40,41,83], further demonstrating their potential for a safer Li-metal battery operation. Balsara and co-workers reported high modulus LiTFSI-doped PS-*b*-PEO BCP electrolytes, which showed an order of magnitude higher C_d value (a measure of dendrite growth resistance) than a LiTFSI-doped PEO polymer electrolyte.[40] The increase in dendrite growth resistance was attributed to the microphase separated structure and high modulus ($G' \sim 10^8$ Pa for PS-*b*-PEO compared to $G' \sim 10^4$ Pa for PEO at 90 °C) of these BCPs. These results were found to be in agreement with the theoretical model proposed by Newman, which predicts that high modulus polymers are required to inhibit the dendrite growth at the lithium metal anode.[43] Although, the dendrite inhibition studies on high modulus PS-*b*-PEO polymers by Balsara and co-workers have demonstrated a significant advancement in this area, the low ionic conductivities of these BCP electrolytes have limited their application for medium or room temperature Li-metal battery applications.

Clearly, BCP electrolytes are promising candidates for rechargeable Li-metal batteries, as demonstrated by their excellent mechanical properties and ability to inhibit the dendrite growth at the Li-metal anode. However, due to their low room

temperature ionic conductivities, they cannot be used for ambient temperature batteries. So far, AB diblock and ABA triblock copolymer systems have been investigated for BCP electrolyte applications; ABC triblock systems might be an interesting avenue for the active researchers in this area as well. However, extensive research will be required in this area for the rational design of new BCP electrolytes having both high ionic conductivity at ambient temperature and good dendrite growth resistance.

1.5.1.2 Cross-Linked Polymer Electrolytes

One of the most effective methods to modify both the crystallinity and mechanical properties of the polymer electrolyte is to form a cross-linked structure. Cross-linking increases the amount of amorphous phase in the polymer and gives the polymer rubber-like characteristics.[84,85] To date, numerous PEO based cross-linked polymers have been investigated for lithium-battery applications including polyether copolymers,[71,72,74,75] acrylate polymers,[77,86,87] and polyurethane network polymers.[78] Selected examples of PEO-based cross-linked SPEs are shown in Table 1.4.

Watanabe and co-workers reported a conductivity value of 2×10^{-5} S/cm at 20 °C for a network poly(ethylene oxide)-*co*-poly(propylene oxide) copolymer with LiTFSI salt.[71] Armand and co-workers observed conductivity of 1×10^{-5} S/cm at 25 °C for their PEO based network polymer electrolytes (Table 1.4, entry 2).[74] Several acrylate based network polymer electrolytes have also been tested and have shown superior mechanical properties compared to polyether network polymers. Mono methacrylate- and di methacrylate- functionalized EO oligomers were employed to build polymeric networks of varied crosslinking density and tunable thermal

properties.[77,87] However, the use of polymers containing extremely reactive acrylate moieties in conjunction with lithium metal anode still remains questionable.

Table 1.4 Cross-linked polymer electrolytes

Entry	Polymer	Lithium Salt	Chemical Structure	Conductivity (S/cm) @ Temperature	Reference
1	Network polyether copolymer	LiTFSI	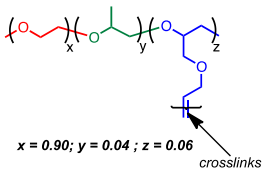	5.0×10^{-4} 30 °C	88
2	Network poly(ethylene oxide) polymer	LiTFSI	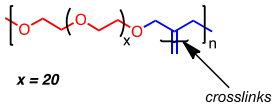	1.0×10^{-5} 20 °C	74
3	Network poly(ethylene oxide)/poly(meth acrylate) copolymers	$LiCF_3SO_3$	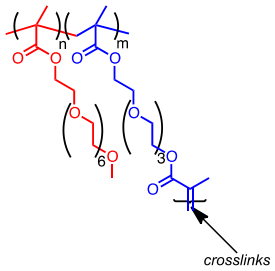	1.5×10^{-6} 20 °C	87
4	Cross-linked inorganic-organic gel polymer electrolytes	$LiCF_3SO_3$	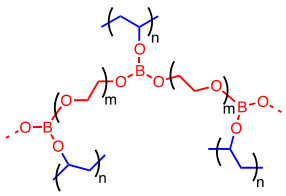	8.9×10^{-5} 20 °C	89

While all of these PEO-based cross-linked polymers demonstrate a significant advancement in the field of SPEs for LMP batteries, none of these have been tested quantitatively to demonstrate their ability to prevent lithium dendrite growth on the anode. There are only two reports of poly(methyl methacrylate)[90] and poly(acrylonitrile)[91] based cross-linked gel polymer electrolytes that have shown to inhibit the dendrite growth qualitatively using optical microscopy; however, these systems contain flammable organic solvents.

1.5.1.3 Single-Ion Conductors

In addition to good chemical and electrochemical stability, superior transport properties are required for an ideal polymer electrolyte. Binary lithium salts containing polymer electrolytes (e.g. LiX in a dissociating medium) have an ionic contribution from both the anion (≈2/3) and Li^+ cation (≈1/3). As the electrodes only exchange Li^+ with the electrolyte, a salt concentration gradient is established during operation with very deleterious effects. The growth of lithium metal dendrites is believed to occur when the anion concentration goes to zero near the interface.[42] One way to improve the transport properties and minimize the concentration gradients is by using single-ion conductors (SICs), which have $t_{Li+} \sim 1$. SICs are synthesized by the immobilization of the counter-anion to either a polymer backbone,[76,92-95] or nanoscale inorganic particle.[96-98]

The nature of the anions tethered to the polymer backbone plays a crucial role in delocalization of the negative change and reducing the ion-pairing interaction with the lithium ions, which affects the ionic conductivity. Cowie and co-workers synthesized a fluoroalkylsulfonate comb branch copolymers and compared their

Table 1.5 Single-ion conductors as solid polymer electrolytes

Entry	Polymer	Chemical Structure	Conductivity (S/cm) @Temperature	Reference
1	Poly(styrene trifluoromethanesulfonylimide of lithium-*b*-ethylene oxide-*b*-styrene trifluoromethanesulfsonylimide of lithium)	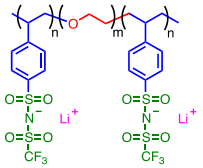	1.3×10^{-5} @60 °C	92
2	Poly[4(styrenesulfonyl)(trifluoro methanesulfonyl)imide] anion	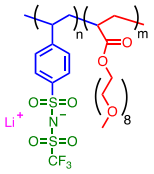	$\sigma = 7.65 \times 10^{-6}$ @25 °C	93
3	Polysiloxane single-ion conductor	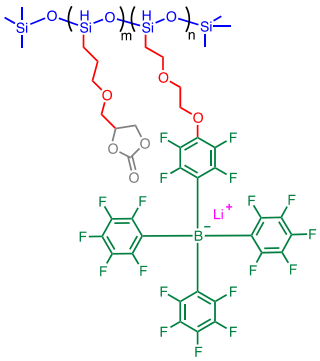	$\sigma = 10^{-7}$ @25 °C	94
4	Polysiloxane-trifluoromethylsulfonamide polyelectrolytes	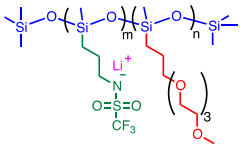	1.3×10^{-6} @25 °C	50

conductivities to the analogous non-fluorinated polymers.[99] The results of their studies demonstrated that fluoropolymers showed higher ionic conductivities than the non-fluorinated analogues due to electron withdrawing properties of the fluorine, which provides a facile release of the Li ion for conduction. Fluorinated anions, such as fluoroalkylsulfonate,[99] trifluoromethylsulfonylimide,[92,93,100-102] and perfluorinatedphenylborate[94] have been utilized in the literature to increase the ionic conductivity of these SICs. Selected recent examples of Li-ion conducting SIC are shown in Table 1.5. Armand and co-workers reported P(STFSILi)-*b*-PEO-*b*-P(STFSILi) (Table 1.5, entry 1) single-ion electrolytes that demonstrated reasonable ionic conductivity (1.3×10^{-5} S/cm at 60 °C), high Li^+ ion transference number (~0.85), and enhanced electrochemical stability compared to LiTFSI-doped PS-*b*-PEO-*b*-PS electrolytes.[93] With the aim of increasing the ionic conductivity, Colby and co-workers tethered non-coordinating anions, such as tetraphenylborate and (perfluoro)tetraphenylborate to the polysiloxane backbone (Table 1.5, entry 3) and studied their thermal and conducting properties.[94] They found that at similar ion content, the SIC with perfluorinated borate exhibited the highest conductivity, although the conductivity values were still low (10^{-7} S/cm at 25 °C). The electrochemical stability and the transport properties of these ionomers were not reported. While all of these SICs exhibit better transport properties and electrochemical properties compared to binary lithium salt-doped polymer electrolytes, their ambient and medium temperature conductivities are too low, typically 10^{-7}–10^{-6} S/cm at 25 °C.

Although SIC polymer electrolytes have shown promise in terms of superior

electrochemical properties for lithium battery applications, considerable amount of research is still needed in this area for making a practical lithium-based device operational at ambient or moderate temperature. Most of the current research efforts are focused on developing ionomers with better Li-ion conductivity. Significant contributions from both theoretical and experimental scientists are needed to develop a better understanding of structure-property relationships, and improve the properties of current SIC membranes for battery applications.

1.5.2 Plasticized Polymer Electrolytes

Unplasticized SPEs have shown promising ionic conductivity values only at elevated temperature (>70 °C) and hence the batteries equipped with these SPEs cannot be cycled at lower temperature. In contrast to the unplasticized SPEs, plasticized polymer electrolytes can achieve higher ionic conductivity at ambient temperature. Commonly used plasticizers are polar organic carbonate liquids, low molecular weight oligomers of PEG, and ionic liquids; some examples of these plasticizers are shown in Table 1.6. The plasticizers are known to increase the free energy volume and lower the glass transition temperature of the polymers. While organic carbonates are flammable, oligomers of PEG and ionic liquids are less/non-flammable.

Polymers doped with high dielectric organic solvents such as ethylene carbonate, dimethyl carbonate, propylene carbonate, etc., are generally known as gel polymer electrolytes (GPEs). In these systems, the polymer provides a strong matrix to hold the organic liquid solvent, and the polar solvents mainly promote the Li-ion conduction by increasing the dissociation of lithium salt and lithium ion mobility.

Plasticization of high molecular weight PEO-LiX electrolytes has been reported to deteriorate the mechanical properties, although these GPEs displayed ionic conductivity values as high as 10^{-3} S/cm at room temperature.[103] To achieve good dimensional stability for GPEs, various researchers have used cross-linking methods to trap the liquid plasticizer in the cross-linked polymer matrix. Polyacrylonitrile (PAN)[104-106] and poly(vinylidene fluoride) (PVdF)[107,108] polymers have been investigated to a far greater extent compared to PEO as the matrix to hold the liquid plasticizer in the GPEs. Zaghib and co-workers synthesized a GPE by cross-linking PEO using electron-beam radiation and plasticized it with EC and γ-butyrolactone.[109] These $LiBF_4$-doped GPEs exhibited high reversible capacity (345 mAh/g) and high coulombic efficiency (91%).

Low molecular weight PEG compounds have also been used as the plasticizers to improve the electrochemical performance of dry PEO-based SPEs at ambient temperature. Mastragostino and coauthors developed a PEG (M_n 500) -doped PEO based polyurethane network polymer that showed conductivity of 10^{-5} S/cm at 25 °C; however, they did not see a significant increase in conductivity upon addition of plasticizer.[110] Park and co-workers reported an interesting plasticized SPE, wherein they incorporated PEG (M_n 250) and PEO based cross-linked electrolyte inside the pores of a PE non-woven matrix. The resulting SPE containing 20 wt.% crosslinking agent and 80 wt.% non-volatile plasticizer displayed conductivity of 3.1×10^{-4} S/cm at room temperature.[111] Kang and co-workers recently reported a multi-armed

Table 1.6 Additives used for the plasticized polymer electrolytes

Additive	Chemical Structure	Flash Point (°C)	Melting Point (°C)	Boiling Point (°C)	Dielectric Constant	Dipole moment (Debye)
Organic Carbonates (OC)						
Ethylene carbonate (EC)		150	36	248	89.8	4.61
Propylene carbonate (PC)		132	−49	242	64.5	4.81
Dimethyl carbonate (DMC)		17	5	91	3.11	0.76
Diethyl carbonate (DEC)	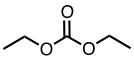	25	−74	126	2.81	0.96
Ethyl methyl carbonate (EMC)	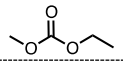	24	−53	110	2.96	0.89
Poly(ethylene glycol) (PEG)						
Dimethoxy PEG	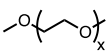	156	-	>250	-	-
Multi-arm PEG	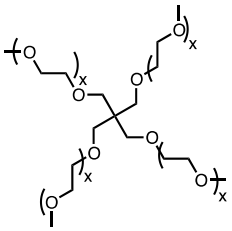	-	-	-	-	-
Ionic Liquids (IL)						
1-Ethyl-3-methylimidazolium bis(trifluoromethylsulfonyl)imide (EMI-TFSI)	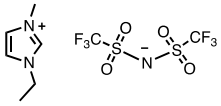	-	−17	>250	-	-
1-Butyl-3-methylimidazolium bis(trifluoromethylsulfonyl)imide (BMI-TFSI)	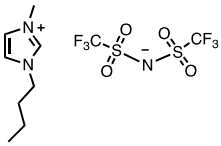	-	−4	>250	-	-
N-butyl-N-methylpyrrolidinium bis(trifluoromethylsulfonyl)imide (BMP-TFSI)	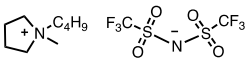	-	−50	>250	-	-

plasticizer-doped PEO- and siloxane-based cross-linked polymer, which exhibited the conductivity value of 10^{-4} S/cm at 25 °C.[112] While all these plasticized SPEs reported in the literature are major advances in the conductivity enhancement of solid polymer electrolytes, none of these systems have been tested for dendrite growth inhibition using Li-metal as the anode, and their effective use in a LMP battery remains

unknown.

Ionic liquids (IL) are salts or mixture of salts that melt at low temperature, often below room temperature; they typically consist of an asymmetric bulky organic cation and an inorganic anion. These ILs have attracted considerable interest as an alternative to organic liquid electrolytes because of several advantages, such as negligible vapor pressure, high chemical and thermally stability, non-flammability, and in some cases high electrochemical stability and hydrophobicity.[113,114] Passerini and co-workers reported an ionic liquid (N-butyl-N-methylpyrrolidinium bis (trifluoromethanesulfonyl)imide (BMP-TFSI); chemical structure is shown in Table 1.6) -doped ternary composites PEO/IL/LiTFSI that demonstrated higher conductivity compared to the neat PEO/LiTFSI polymer electrolytes due to an increase in number of charge carriers.[115] However, the mechanical properties became poor when the weight% of the ionic liquid was increased beyond a certain value. Cross-linking has been widely used as one of the strategies to obtain highly conducting IL-doped polymer composites, while still retaining good mechanical properties.[116-118] Recently, Hillmyer and co-workers reported an ionic liquid (1-Butyl-3-methylimidazolium bis(trifluoromethylsulfonyl)imide (BMI-TFSI)) -doped cross-linked polystyrene and PEO copolymers, which exhibited ionic conductivity greater than 1 mS/cm with a modulus value approaching 1 GPa at 25 °C.[118] Interestingly, certain ionic liquids have also shown to enhance the uniform lithium deposition on the lithium metal anode, thus reducing the lithium dendrite growth.[37]

In contrast to SPEs, GPEs (plasticized polymer electrolytes containing polar organic solvents) have proved their potential for commercial applications because of

higher ionic conductivity. Bellcore commercialized the first GPE based Li-ion battery, the so-called "polymer Li-ion (PLion) cells". This innovative technology made use of PVdF polymers as the matrix to hold liquid electrolyte in the PLion batteries.[119] While these PLion cells are relatively light and have energy density comparable to the Li-ion batteries, they still contain significant weight fraction of the liquid electrolytes and hence are flammable. Unlike GPE based technologies, the immediate application of plasticized polymers based on PEG and ionic liquids in any commercial electrochemical device still remains a challenge.

1.5.3 Polymer-Ceramic Composites

The introduction of nanometer-sized ceramic powders, such as Al_2O_3,[120,121] TiO_2,[41,122,123] SiO_2,[124] and ZrO_2[125] to a polymer matrix has been shown to improve the mechanical properties, increase the ionic conductivity, and decrease the interfacial resistance. Although the mechanism of the effect of these nanoparticles on the ionic conductivity is not clearly understood, it has been proposed that these nanoparticles reduce the polymer crystallinity.[126] The concept of incorporating inorganic fillers in the polymer matrix was first demonstrated by Weston and Steele,[127] and since then there have been numerous reports on improving the electrochemical properties of the polymer electrolyte by doping it with nanoparticles. Bruce and co-workers reported PEO-$LiClO_4$ electrolytes doped with nanometer sized TiO_2 and Al_2O_3 powders that showed ionic conductivity values of 1.3×10^{-5} S/cm at 30 °C, which is approximately an order of magnitude higher than the unplasticized PEO electrolytes.[122] Furthermore, unlike liquid plasticizers that lead to deterioration of mechanical properties of the SPE, the nano-sized filler particles (solid plasticizers) improved the mechanical properties

of these SPEs. Balsara and co-workers reported that a TiO_2-doped PS-*b*-PEO electrolyte containing 24 wt% TiO_2 nanoparticles exhibited enhanced dendrite growth resistance relative to the neat block copolymer electrolyte.[41] Additionally, both tensile and shear moduli of the electrolytes were non-monotonic functions of TiO_2 particle concentration.

In summary, polymer-ceramic composite electrolytes are a promising area for additional research due to their high ionic conductivities, improved mechanical properties, and superior interfacial stability. However, very few literature reports have investigated their use in electrochemical cells, suggesting that additional studies are still needed for application in commercial devices.

1.6 Conclusions

Next generation batteries that have theoretical energy densities comparable to gasoline – Li-sulfur and Li-O_2 – are based on a lithium metal anode. One of the key impediments to commercializing these high specific energy batteries is the development of an ideal solid polymer electrolyte that not only exhibits high ionic conductivity at ambient temperature, but also prevents dendrite growth at the anode. Although a large number of studies have been directed towards increasing the ionic conductivity of the SPEs, very few experimental papers have addressed the lithium dendrite growth issue.[37-41] Moreover, the polymer electrolyte field is mainly reliant on the theoretical predictions for understanding the dendrite growth at the polymer-electrolyte interface.[42,43] While some SPEs have demonstrated their viability for high temperature Li-metal battery applications (>70 °C), none of the SPEs have so far shown promise for lower temperature applications. For these reasons, the development of high performance SPEs has been very challenging. An in-depth knowledge of structure-property relationships, improved theoretical models, and an interdisciplinary approach to polymer design and electrochemical testing will likely be necessary to achieve a breakthrough SPE technology.

REFERENCES

(1) Armand, M.; Tarascon, J. M. *Nature* **2008**, *451*, 652–657.

(2) Tarascon, J. M.; Armand, M. *Nature* **2001**, *414*, 359–367.

(3) Scrosati, B.; Garche, J. *J. Power Sources* **2010**, *195*, 2419–2430.

(4) Yoshimatsu, I.; Hirai, T.; Yamaki, J. *J. Electrochem. Soc.* **1988**, *135*, 2422–2427.

(5) Bouchet, R.; Lascaud, S.; Rosso, M. *J. Electrochem. Soc.* **2003**, *150*, A1385–A1389.

(6) Scrosati, B.; Vincent, C. A. *MRS Bull.* **2000**, *25*, 28–30.

(7) https://web.ornl.gov/ccsd_registrations/battery/presentations/Session7-1100-Balsara.pdf.

(8) Dias, F. B.; Plomp, L.; Veldhuis, J. B. J. *J. Power Sources* **2000**, *88*, 169–191.

(9) Fenton, D. E.; Parker, J. M.; Wright, P. V. *Polymer* **1973**, *14*, 589–589.

(10) Armand, M. B. C., J. M.; Duclot, N. J. *Fast Ion Transport in Solids: Electrodes, and Electrolytes;* Lake Geneva, Wisconsin, U.S.A., May 21−25, 1979; Vashishta, P.; Mundy, J. N.; Shenoy, G. K., Eds; North Holland: New York, 1979.

(11) Mullerplathe, F.; Vangunsteren, W. F. *J. Chem. Phys.* **1995**, *103*, 4745–4756.

(12) Meyer, W. H. *Adv. Mater.* **1998**, *10*, 439–448.

(13) Tammann, G.; Hesse, W. *Z Anorg. Allg. Chem*. **1926**, *156,* 245–247.

(14) Vogel, H. *Phys. Z* **1921**, *22*, 645–646.

(15) Fulcher, G. S. *J. Am. Ceram. Soc.* **1925**, *8*, 789–794.

(16) Sylla, S.; Sanchez, J. Y.; Armand, M. *Electrochim. Acta* **1992**, *37*, 1699–1701.

(17) Xia, Y. Y.; Fujieda, T.; Tatsumi, K.; Prosini, P. P.; Sakai, T. *J. Power Sources* **2001**, *92*, 234–243.

(18) Cheung, I. W.; Chin, K. B.; Greene, E. R.; Smart, M. C.; Abbrent, S.; Greenbaum, S. G.; Prakash, G. K. S.; Surampudi, S. *Electrochim. Acta* **2003**, *48*, 2149–2156.

(19) EinEli, Y.; Howard, W. F. *J. Electrochem. Soc.* **1997**, *144*, L205–L207.

(20) Wolfenstine, J.; Allen, J. *J. Power Sources* **2004**, *136*, 150–153.

(21) Kita, F.; Sakata, H.; Sinomoto, S.; Kawakami, A.; Kamizori, H.; Sonoda, T.; Nagashima, H.; Nie, J.; Pavlenko, N. V.; Yagupolskii, Y. L. *J. Power Sources* **2000**, *90*, 27–32.

(22) Schmidt, M.; Heider, U.; Kuehner, A.; Oesten, R.; Jungnitz, M.; Ignat'ev, N.; Sartori, P. *J. Power Sources* **2001**, *97-8*, 557–560.

(23) Von Cresce, A.; Xu, K. *J. Electrochem. Soc.* **2011**, *158*, A337–A342.

(24) Von Cresce, A.; Xu, K. *ECS Trans.* **2012**, *41*, 17–22.

(25) Watanabe, Y.; Kinoshita, S.; Wada, S.; Hoshino, K.; Morimoto, H.; Tobishima, S. *J. Power Sources* **2008**, *179*, 770–779.

(26) Xu, K.; Angell, C. A. *J. Electrochem. Soc.* **1998**, *145*, L70–L72.

(27) Xu, M.; Dalavi, S.; Lucht, B. L.; John Wiley & Sons, Inc.: 2013, p 71–87.

(28) Zhu, Y.; Casselman, M. D.; Li, Y.; Wei, A.; Abraham, D. P. *J. Power Sources* **2014**, *246*, 184–191.

(29) Tsujioka, S. T., H.; Takahashi, M.; Sugimoto, H.; Koide, M. ; US Patent 6,787,267 (2004).

(30) Abu-Lebdeh, Y.; Davidson, I. *J. Electrochem. Soc.* **2009**, *156*, A60–A65.

(31) Aurbach, D. In *27th International Battery Seminar and Exhibit* Fort Lauderdale, Florida, 2010.

(32) Ishikawa, M.; Kawasaki, H.; Yoshimoto, N.; Morita, M. *J. Power Sources* **2005**, *146*, 199–203.

(33) Zhamu, A.; Chen, G. R.; Liu, C. G.; Neff, D.; Fang, Q.; Yu, Z. N.; Xiong, W.; Wang, Y. B.; Wang, X. Q.; Jang, B. Z. *Energ. Environ. Sci.* **2012**, *5*, 5701–5707.

(34) Gireaud, L.; Grugeon, S.; Laruelle, S.; Yrieix, B.; Tarascon, J. M. *Electrochem. Commun.* **2006**, *8*, 1639–1649.

(35) Mogi, R.; Inaba, M.; Jeong, S. K.; Iriyama, Y.; Abe, T.; Ogumi, Z. *J. Electrochem. Soc.* **2002**, *149*, A1578–A1583.

(36) Ota, H.; Wang, X. M.; Yasukawa, E. *J. Electrochem. Soc.* **2004**, *151*, A427–A436.

(37) Liu, S.; Imanishi, N.; Zhang, T.; Hirano, A.; Takeda, Y.; Yamamoto, O.; Yang, J. *J. Electrochem. Soc.* **2010**, *157*, A1092–A1098.

(38) Liu, S.; Imanishi, N.; Zhang, T.; Hirano, A.; Takeda, Y.; Yamamoto, O.; Yang, J. *J. Power Sources* **2010**, *195*, 6847–6853.

(39) Liu, S.; Wang, H.; Imanishi, N.; Zhang, T.; Hirano, A.; Takeda, Y.; Yamamoto, O.; Yang, J. *J. Power Sources* **2011**, *196*, 7681–7686.

(40) Stone, G. M.; Mullin, S. A.; Teran, A. A.; Hallinan, D. T., Jr.; Minor, A. M.; Hexemer, A.; Balsara, N. P. *J. Electrochem. Soc.* **2012**, *159*, A222–A227.

(41) Gurevitch, I.; Buonsanti, R.; Teran, A. A.; Gludovatz, B.; Ritchie, R. O.; Cabana, J.; Balsara, N. P. *J. Electrochem. Soc.* **2013**, *160*, A1611–A1617.

(42) Chazalviel, J. N. *Phys. Rev. A* **1990**, *42*, 7355–7367.

(43) Monroe, C.; Newman, J. *J. Electrochem. Soc.* **2005**, *152*, A396–A404.

(44) Gray, F.; Armand, M. *Handbook of Battery Materials*; Wiley-VCH: Wenheim.

(45) http://www.bathium.com/.

(46) Frech, R.; Manning, J.; Teeters, D.; Black, B. E. *Solid State Ionics* **1988**, *28*, 954–957.

(47) Cowie, J. M. G.; Cree, S. H. *Annu. Rev. Phys. Chem.* **1989**, *40*, 85–113.

(48) Hooper, R.; Lyons, L. J.; Mapes, M. K.; Schumacher, D.; Moline, D. A.; West, R. *Macromolecules* **2001**, *34*, 931–936.

(49) Khan, I. M.; Yuan, Y. X.; Fish, D.; Wu, E.; Smid, J. *Macromolecules* **1988**, *21*, 2684–2689.

(50) Siska, D. P.; Shriver, D. F. *Chem. Mater.* **2001**, *13*, 4698–4700.

(51) Spindler, R.; Shriver, D. F. *Macromolecules* **1988**, *21*, 648–654.

(52) Spindler, R.; Shriver, D. F. *J. Am. Chem. Soc.* **1988**, *110*, 3036–3043.

(53) Zhou, G. B.; Khan, I. M.; Smid, J. *Macromolecules* **1993**, *26*, 2202–2208.

(54) Fish, D.; Khan, I. M.; Smid, J. *Makromol. Chem. Rapid Commun.* **1986**, *7*, 115.

(55) Allcock, H. R.; Kuharcik, S. E.; Reed, C. S.; Napierala, M. E. *Macromolecules* **1996**, *29*, 3384–3389.

(56) Allcock, H. R.; OConnor, S. J. M.; Olmeijer, D. L.; Napierala, M. E.; Cameron, C. G. *Macromolecules* **1996**, *29*, 7544–7552.

(57) Blonsky, P. M.; Shriver, D. F.; Austin, P.; Allcock, H. R. *J. Am. Chem. Soc.* **1984**, *106*, 6854–6855.

(58) Blonsky, P. M.; Shriver, D. F.; Austin, P.; Allcock, H. R. *Solid State Ionics* **1986**, *18-9*, 258–264.

(59) Harris, C. S.; Shriver, D. F.; Ratner, M. A. *Macromolecules* **1986**, *19*, 987–989.

(60) Epps, T. H.; Bailey, T. S.; Waletzko, R.; Bates, F. S. *Macromolecules* **2003**, *36*, 2873–2881.

(61) Giles, J. R. M.; Gray, F. M.; Maccallum, J. R.; Vincent, C. A. *Polymer* **1987**, *28*, 1977–1981.

(62) Jannasch, P. *Chem. Mater.* **2002**, *14*, 2718–2724.

(63) Kishimoto, K.; Yoshio, M.; Mukai, T.; Yoshizawa, M.; Ohno, H.; Kato, T. *J. Am. Chem. Soc.* **2003**, *125*, 3196–3197.

(64) Kosonen, H.; Valkama, S.; Hartikainen, J.; Eerikainen, H.; Torkkeli, M.; Jokela, K.; Serimaa, R.; Sundholm, F.; ten Brinke, G.; Ikkala, O. *Macromolecules* **2002**, *35*, 10149–10154.

(65) Niitani, T.; Shimada, M.; Kawamura, K.; Kanamura, K. *J. Power Sources* **2005**, *146*, 386–390.

(66) Ruzette, A. V. G.; Soo, P. P.; Sadoway, D. R.; Mayes, A. M. *J. Electrochem. Soc.* **2001**, *148*, A537–A543.

(67) Singh, M.; Odusanya, O.; Wilmes, G. M.; Eitouni, H. B.; Gomez, E. D.; Patel, A. J.; Chen, V. L.; Park, M. J.; Fragouli, P.; Iatrou, H.; Hadjichristidis, N.; Cookson, D.; Balsara, N. P. *Macromolecules* **2007**, *40*, 4578–4585.

(68) Soo, P. P.; Huang, B. Y.; Jang, Y. I.; Chiang, Y. M.; Sadoway, D. R.; Mayes, A. M. *J. Electrochem. Soc.* **1999**, *146*, 32–37.

(69) Wang, C. X.; Sakai, T.; Watanabe, O.; Hirahara, K.; Nakanishi, T. *J. Electrochem. Soc.* **2003**, *150*, A1166–A1170.

(70) Young, W. S.; Kuan, W. F.; Epps, T. H. *J. Polym. Sci. Pol. Phys.* **2014**, *52*, 1–16.

(71) Kono, M.; Hayashi, E.; Watanabe, M. *J. Electrochem. Soc.* **1998**, *145*, 1521–1527.

(72) Watanabe, M.; Nishimoto, A. *Solid State Ionics* **1995**, *79*, 306–312.

(73) Aihara, Y.; Kuratomi, J.; Bando, T.; Iguchi, T.; Yoshida, H.; Ono, T.; Kuwana, K. *J. Power Sources* **2003**, *114*, 96–104.

(74) Alloin, F.; Sanchez, J. Y.; Armand, M. *J. Electrochem. Soc.* **1994**, *141*, 1915–1920.

(75) Nishimoto, A.; Agehara, K.; Furuya, N.; Watanabe, T.; Watanabe, M. *Macromolecules* **1999**, *32*, 1541–1548.

(76) Sun, X. G.; Kerr, J. B.; Reeder, C. L.; Liu, G.; Han, Y. B. *Macromolecules* **2004**, *37*, 5133–5135.

(77) Snyder, J. F.; Wetzel, E. D.; Watson, C. M. *Polymer* **2009**, *50*, 4906–4916.

(78) Laik, B.; Legrand, L.; Chausse, A.; Messina, R. *Electrochim. Acta* **1998**, *44*, 773–780.

(79) Boden, N.; Leng, S. A.; Ward, I. M. *Solid State Ionics* **1991**, *45*, 261–270.

(80) Niitani, T.; Shimada, M.; Kawamura, K.; Dokko, K.; Rho, Y. H.; Kanamura, K. *Electrochem. Solid St.* **2005**, *8*, A385–A388.

(81) Epps, T. H.; Bailey, T. S.; Pham, H. D.; Bates, F. S. *Chem. Mater.* **2002**, *14*, 1706–1714.

(82) Young, W. S.; Epps, T. H. *Macromolecules* **2012**, *45*, 4689–4697.

(83) Hallinan, D. T.; Mullin, S. A.; Stone, G. M.; Balsara, N. P. *J. Electrochem. Soc.* **2013**, *160*, A464–A470.

(84) Lenest, J. F.; Callens, S.; Gandini, A.; Armand, M. *Electrochim. Acta* **1992**, *37*, 1585–1588.

(85) Armand, M. *Solid State Ionics* **1983**, *9-10*, 745–754.

(86) Snyder, J. F.; Carter, R. H.; Wetzel, E. D. *Chem. Mater.* **2007**, *19*, 3793–3801.

(87) Wingert, M.; Kjell, M. H.; Jacques, E.; Behm, M.; Lindbergh, G.; Johansson, M. *Eur. Polym. J.* **2011**, *47*, 2372–2378.

(88) Nishio, H. O., H.; Fuji, Y. US Patent 6,894,143 (2005).

(89) Aydin, H.; Bozkurt, A. *J. Appl. Polym. Sci.* **2012**, *124*, 1193–1199.

(90) Tatsuma, T.; Taguchi, M.; Oyama, N. *Electrochim. Acta* **2001**, *46*, 1201–1205.

(91) Tatsuma, T.; Taguchi, M.; Iwaku, M.; Sotomura, T.; Oyama, N. *J. Electroanal. Chem.* **1999**, *472*, 142–146.

(92) Bouchet, R.; Maria, S.; Meziane, R.; Aboulaich, A.; Lienafa, L.; Bonnet, J. P.; Phan, T. N. T.; Bertin, D.; Gigmes, D.; Devaux, D.; Denoyel, R.; Armand, M. *Nat. Mater.* **2013**, *12*, 452–457.

(93) Feng, S. W.; Shi, D. Y.; Liu, F.; Zheng, L. P.; Nie, J.; Feng, W. F.; Huang, X. J.; Armand, M.; Zhou, Z. B. *Electrochim. Acta* **2013**, *93*, 254–263.

(94) Liang, S. W.; Choi, U. H.; Liu, W. J.; Runt, J.; Colby, R. H. *Chem. Mater.* **2012**, *24*, 2316–2323.

(95) Sun, X. G.; Kerr, J. B. *Macromolecules* **2006**, *39*, 362–372.

(96) Choi, N. S.; Lee, Y. M.; Lee, B. H.; Lee, J. A.; Park, J. K. *Solid State Ionics*

2004, *167*, 293–299.

(97) Schaefer, J. L.; Yanga, D. A.; Archer, L. A. *Chem. Mater.* **2013**, *25*, 834–839.

(98) Sun, J.; Bayley, P.; MacFarlane, D. R.; Forsyth, M. *Electrochim. Acta.* **2007**, *52*, 7083–7090.

(99) Cowie, J. M. G.; Spence, G. H. *Solid State Ionics* **1999**, *123*, 233–242.

(100) Meziane, R.; Bonnet, J. P.; Courty, M.; Djellab, K.; Armand, M. *Electrochim. Acta* **2011**, *57*, 14–19.

(101) Geiculescu, O. E.; Yang, J.; Zhou, S.; Shafer, G.; Xie, Y.; Albright, J.; Creager, S. E.; Pennington, W. T.; DesMarteau, D. D. *J. Electrochem. Soc.* **2004**, *151*, A1363–A1368.

(102) Watanabe, M.; Tokuda, H.; Muto, S. *Electrochim. Acta* **2001**, *46*, 1487–1491.

(103) Chintapalli, S.; Frech, R. *Solid State Ionics* **1996**, *86-8*, 341–346.

(104) Huang, B. Y.; Wang, Z. X.; Chen, L. Q.; Xue, R. J.; Wang, F. S. *Solid State Ionics* **1996**, *91*, 279–284.

(105) Huang, B. Y.; Wang, Z. X.; Li, G. B.; Huang, H.; Xue, R. J.; Chen, L. Q.; Wang, F. S. *Solid State Ionics* **1996**, *85*, 79–84.

(106) Yang, C. R.; Perng, J. T.; Wang, Y. Y.; Wan, C. C. *J. Power Sources* **1996**, *62*, 89–93.

(107) Croce, F.; Appetecchi, G. B.; Slane, S.; Salomon, M.; Tavarez, M.; Arumugam, S.; Wang, Y.; Greenbaum, S. G. *Solid State Ionics* **1996**, *86-8*, 307–312.

(108) Jiang, Z.; Carroll, B.; Abraham, K. M. *Electrochim. Acta* **1997**, *42*, 2667–2677.

(109) Zaghib, K.; Striebel, K.; Guerfi, A.; Shim, J.; Armand, M.; Gauthier, M. *Electrochim. Acta* **2004**, *50*, 263–270.

(110) Borghini, M. C.; Mastragostino, M.; Zanelli, A. *Electrochim. Acta* **1996**, *41*, 2369–2373.

(111) Lee, Y. M.; Ko, D.-H.; Lee, J. Y.; Park, J.-K. *Electrochim. Acta* **2006**, *52*, 1582–1587.

(112) Lee, J. I.; Kim, D. W.; Lee, C.; Kang, Y. *J. Power Sources* **2010**, *195*, 6138–6142.

(113) Galinski, M.; Lewandowski, A.; Stepniak, I. *Electrochim. Acta* **2006**, *51*, 5567–5580.

(114) Armand, M.; Endres, F.; MacFarlane, D. R.; Ohno, H.; Scrosati, B. *Nat. Mater.* **2009**, *8*, 621–629.

(115) Shin, J. H.; Henderson, W. A.; Passerini, S. *Electrochem. Commun.* **2003**, *5*, 1016–1020.

(116) Gerbaldi, C.; Nair, J. R.; Ahmad, S.; Meligrana, G.; Bongiovanni, R.; Bodoardo, S.; Penazzi, N. *J. Power Sources* **2010**, *195*, 1706–1713.

(117) Rupp, B.; Schmuck, M.; Balducci, A.; Winter, M.; Kern, W. *Eur. Polym. J.* **2008**, *44*, 2986–2990.

(118) Schulze, M. W.; McIntosh, L. D.; Hillmyer, M. A.; Lodge, T. P. *Nano Lett.* **2014**, *14*, 122–126.

(119) Tarascon, J. M.; Gozdz, A. S.; Schmutz, C.; Shokoohi, F.; Warren, P. C. *Solid State Ionics* **1996**, *86-8*, 49–54.

(120) Jayathilaka, P. A. R. D.; Dissanayake, M. A. K. L.; Albinsson, I.; Mellander,

B. E. *Electrochim. Acta* **2002**, *47*, 3257–3268.

(121) Krawiec, W.; Scanlon, L. G.; Fellner, J. P.; Vaia, R. A.; Giannelis, E. P. *J. Power Sources* **1995**, *54*, 310–315.

(122) Croce, F.; Appetecchi, G. B.; Persi, L.; Scrosati, B. *Nature* **1998**, *394*, 456–458.

(123) Jeon, J. D.; Kim, M. J.; Kwak, S. Y. *J. Power Sources* **2006**, *162*, 1304–1311.

(124) Raghaven, P.; Choi, J. W.; Ahn, J. H.; Cheruvally, G.; Chauhan, G. S.; Ahn, H. J.; Nah, C. *J. Power Sources* **2008**, *184*, 437–443.

(125) Panero, S.; Scrosati, B.; Sumathipala, H. H.; Wieczorek, W. *J. Power Sources* **2007**, *167*, 510–514.

(126) Capuano, F.; Croce, F.; Scrosati, B. *J. Electrochem. Soc.* **1991**, *138*, 1918–1922.

(127) Weston, J. E.; Steele, B. C. H. *Solid State Ionics* **1982**, *7*, 75–79.

CHAPTER 2

Suppression of Lithium Dendrite Growth Using Cross-Linked Polyethylene/ Poly(ethylene oxide) Polymer Electrolytes: A New Approach for Building Practical Li-Metal Batteries

Reprinted with permission from

Journal of the American Chemical Society **2014**, *136*, 7395–7402.

CHAPTER 2

Suppression of Lithium Dendrite Growth Using Cross-Linked Polyethylene/ Poly(ethylene oxide) Polymer Electrolytes: A New Approach for Building Practical Li-Metal Batteries

2.1 Abstract

Solid polymer electrolyte (SPE) membranes are a critical component for high specific energy rechargeable Li-metal polymer (LMP) batteries. SPEs are less flammable and thus increase the safety of Li-based batteries compared to current state-of-the-art Li-ion batteries that use flammable organic solvents as electrolytes. However, most SPEs exhibit low ionic conductivity at room temperature and often allow the growth of lithium dendrites that short-circuit the batteries. Both of these deficiencies are significant barriers to the commercialization of LMP batteries. Herein we present a cross-linked SPE with both high ionic conductivity (>1.0×10^{-4} S/cm at 25 °C) and excellent dendrite growth resistance. It has been proposed that SPEs with high shear storage modulus ($G' > 1.0 \times 10^{9}$ Pa) could be used to suppress lithium dendrite growth, leading to increased lifetime and safety for LMP batteries. In contrast to the theoretical predictions, the low modulus ($G' \sim 1.0 \times 10^{5}$ Pa) cross-linked SPEs reported herein exhibit remarkable dendrite growth resistance. These results suggest that a high modulus SPE is not required for dendrite growth prevention.

2.2 Introduction

Current rechargeable Li-ion batteries (LIBs) are important constituents of telecommunication devices, laptop computers, portable electronics, stationary grid-energy storage components, hybrid electric vehicles, and electric vehicles.[1-3] LIB technologies have enabled the transformation of consumer electronics market since their launch in 1991 by the Sony Corporation; however these LIBs contain flammable organic liquids as an electrolyte component that raises safety concerns.[4] Several incidents including the recent fires in the LIB unit of Tesla Model S and a Boeing 787 Dreamliner airplane have raised questions about the safety of using LIB for transport applications.[5] Furthermore, the specific energy density of current state-of-the-art LIBs is below the US Department of Energy Vehicle Technologies Program's long-term target for the secondary batteries.[6] Replacing flammable electrolytes and enhancing the energy density of Li-based battery technologies are at the forefront of research in both academia and industry.[3,7,8]

A rechargeable Li-metal based battery is considered to be one of the most promising technologies for energy storage devices due to its high theoretical storage capacity, which is facilitated by the use of lithium (Li) metal, instead of lithiated graphite (3800 $mAhg^{-1}$ compared to 380 $mAhg^{-1}$, respectively).[9] Despite these attractive features, the use of Li metal in conjunction with liquid electrolytes is currently limited by the formation of irregular Li electrodeposits (dendrites) during repeated charge-discharge cycles.[10] These dendrites can ultimately span the inter-electrode space, short circuit the cell and cause over-heating and thermal run-away. Many approaches have been proposed in the literature to delay dendrite nucleation,

including alloying Li anodes with other metals[11,12] and using additives to improve the uniformity at the solid electrolyte interface (SEI).[13-16] Although these strategies are promising, the performance suffers due to a reduced anode capacity, and durability is lowered by consumption of additives during the formation of the SEI films during successive charge-discharge cycles. An important scientific goal is the development of a solid polymer electrolyte (SPE) that inhibits dendrite growth. There are two main theoretical frameworks for understanding dendrite nucleation and propagation in an electrolyte. The Chazalviel model proposes that dendrites arise from dissimilar transport of cations and anions in an electrolyte. Specifically, anion depletion is predicted to produce large electric fields near the lithium electrode that leads to enhanced electrodeposition causing dendrites to grow. Electrolytes with higher ionic conductivity and reduced anion mobility will delay dendrite nucleation by mitigating anion depletion near the electrode-electrolyte interface.[17] Rosso and co-workers demonstrated agreement between the Chazalviel model and measured short-circuit lifetimes of lithium metal cells employing poly(ethylene oxide) (PEO) electrolytes.[18] In addition, a second framework due to Newman and Monroe considers the effect of physical forces such as electrolyte/separator modulus and surface tension on the kinetics of lithium electrodeposition. A prediction from this model is that SPEs with high shear modulus ($G' > 7$ GPa) Newman and Monroe have proposed that solid polymer electrolytes (SPEs) with high shear modulus ($G' > 6$ GPa) could be used to suppress the dendrite growth.[19] Balsara and co-workers reported mechanically rigid microphase separated polystyrene-*b*-poly(ethylene oxide) (PS-*b*-PEO) block copolymers that showed high resistance to Li dendrite growth, supporting the high

modulus theory.[20] Due to the semi-crystallinity of the PEO phase, the PS-*b*-PEO block polymers exhibited high ionic conductivities (>1.0 × 10^{-4} S/cm) above 90 °C.[21] Inspired by this important advance in dendrite resistance, we anticipated there might be SPE architectures that simultaneously exhibit higher ionic conductivities at room temperature without sacrificing resistance to Li dendrite growth.

Electrolyte membranes incorporating poly(ethylene oxide) (PEO) with a lithium salt have long been proposed as a viable candidate for LMP batteries.[22,23] However, such SPEs have poor conductivities at room temperature due to the crystallinity of PEO. Cross-linking is one of the many ways to suppress the crystallization of PEO; it increases the amount of amorphous phase in the polymer and gives the polymer rubber-like characteristics.[24,25] To date, numerous PEO based cross-linked polymers have been investigated for lithium-battery applications including polyether copolymers,[26-30] acrylate polymers,[31,32] and polyurethane network polymers.[33] Although these network polymers are mechanically rigid, low ionic conductivities at room temperature (~1.0 × 10^{-5} S/cm) limit their application. To increase the conductivity of network polymers, researchers have studied various plasticized SPEs that contain additives such as ionic liquids[34-37] and low molecular weight methoxy-terminated poly(ethylene glycol).[38-41] While all of these systems improve LMP battery performance, none of them meet all the required standards, i.e. lasting resistance to dendrite growth and high ionic conductivity of the freestanding polymer film at ambient temperature. Moreover, none of these PEO-based cross-linked SPEs have been tested quantitatively to demonstrate their ability to prevent lithium dendrite growth on the anode. To the best of our knowledge, there are only

two reports of poly(methyl methacrylate)[42] and poly(acrylonitrile)[43] based cross-linked gel polymer electrolytes that have been shown, using qualitative optical microscopy experiments, to inhibit dendrite growth; however, even these systems had to be plasticized with flammable non-aqueous electrolyte solvents, which partially defeats the purpose of using a SPE to enhance cell safety.

Herein, we report our work on a new family of Li-ion conducting SPEs comprised of stiff polyethylene (PE) chains covalently cross-linked by poly(ethylene oxide) (PEO) segments. Our synthetic route to these unique SPE structures offer the advantage of tunability of the PEO segment lengths, which provide precise control of the thermal transitions that affect ionic conductivity. Most importantly, these polymer electrolytes display both high ionic conductivity and excellent dendrite growth suppression than any other reported SPE.

2.3 Results and Discussion

We recently reported the synthesis of high performance cross-linked alkaline anion exchange membranes for fuel cell applications using ring opening metathesis polymerization (ROMP) route.[44] We expected that a similar synthesis strategy could be used to create a PEO based Li-ion conducting polymer electrolyte that could also act as an effective separator in the lithium-battery. We designed a SPE that is cross-linked with PEO segments and contains a polyethylene (PE) backbone using an orthogonal-tandem catalysis approach[45] (Figure 2.1). Constraining the PEO chains by incorporating them into a cross-linker reduces the crystallinity of PEO in the copolymers. Poly(ethylene oxide) cross-linker, **PEOX** (**1**) was readily synthesized from inexpensive starting materials in excellent yields.[46] Cyclooctene (**COE**) was

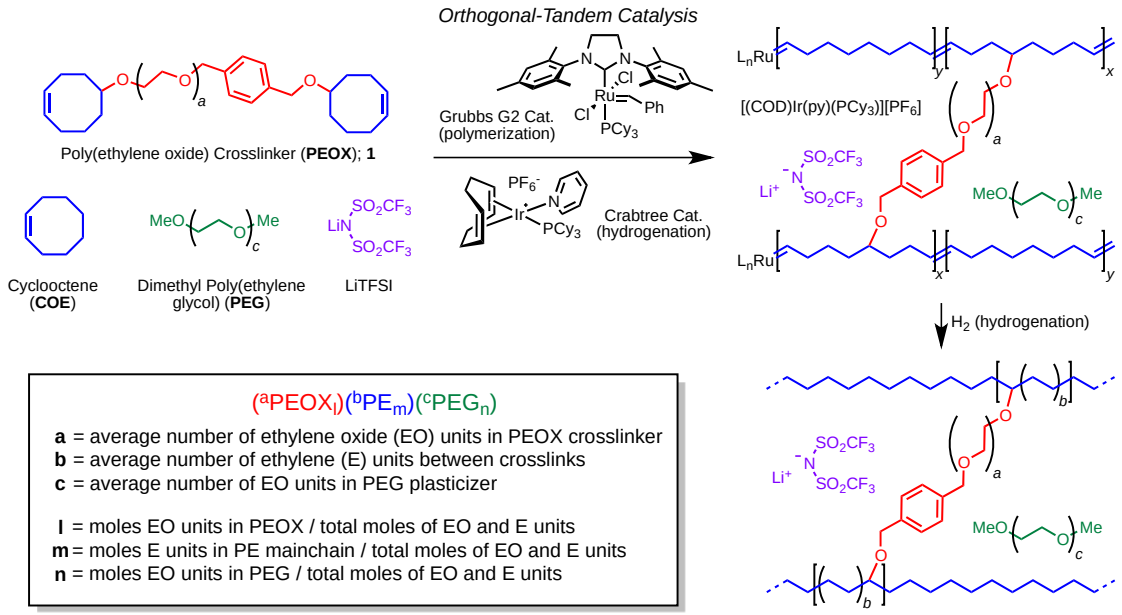

Figure 2.1 Polyethylene/poly(ethylene oxide) solid polymer electrolyte (SPE) synthesis and nomenclature.

copolymerized with **1** in the presence of Grubbs' second-generation catalyst (G2 catalyst) in THF in a fluoropolymer-lined dish.[47] After slow evaporation of the solvent at 50 °C, thin translucent films were obtained. Upon hydrogenation of these unsaturated films catalyzed by the iridium catalyst trapped within the amorphous crosslinked matrix, the mechanical strength of membranes greatly improved, and they were further examined by electrochemical tests.[48] Some of the SPEs were designed to include controlled fractions of free methoxy-terminated polyethylene glycol (**PEG**) oligomers as plasticizers to assess their effect on conductivity and mechanical properties of the membranes. To gain better understanding of this PE-PEO cross-linked solid polymer electrolyte system, a variety of polymer electrolyte samples were prepared by varying the cross-linker length, [**COE**]:[**1**] ratio, and weight percentage (wt%) of the plasticizer. To evaluate the effect of cross-linker length on the ionic

conductivity of SPEs, three **PEOX** cross-linkers with 33, 76, and 123 ethylene oxide (EO) repeat units were synthesized (Table 2.1). Nine different dry SPEs were prepared using three different cross-linkers and at three different [**COE**]:[**1**] ratios (Table 2.2). The nomenclature used for these SPEs is described in Figure 2.1; each component in the SPE is given a symbol (e.g. **PEOX** for the PEO in the cross-linker), the number of repeat units for each of the components are shown in the superscripts, and the mole fractions in the subscripts.

The compositions and thermal properties of all the cross-linked PE-PEO based SPEs are listed in Table 2.2. The SPEs containing the cross-linker with 33 EO units (^{33}PEOX: entries 1–3), showed no melting transition (T_m) of the PEO segments, indicating that the PEO domains of the cross-linked SPE are essentially amorphous. Interestingly, electrolytes with 76 EO units in the cross-linker (^{76}PEOX: entries 4–6), exhibited glass transition temperatures (T_gs) of about −49 °C which are lower than the T_gs observed for ^{33}PEOX SPEs (T_g ~ −44 °C), suggesting moderately enhanced

Table 2.1 PEO functionalized cross-linker

entry	EO units in the cross-linker[a]	M_n (NMR)[a] kg/mol	M_n (GPC)[b] kg/mol	PDI[b]	T_m[c] (°C)	ΔH_{fus}[c] (J/g)
1	33	1.8	1.3	1.1	34	124.9
2	76	3.7	3.5	1.1	47	132.4
3	123	5.8	5.4	1.1	52	153.7

[a]Determined by ^{1}H NMR spectroscopy. [b]Determined by THF gel permeation chromatography calibrated with polystyrene standards at 30 °C. [c]Determined by differential scanning calorimetry analysis of the second heat cycle.

Table 2.2 Compositions and DC ionic conductivities of unplasticized PE-PEO cross-linked SPEs[a]

entry	Unplasticized SPE	[COE]:[1] ratio	PE Segments[b]		PEO Segments[c]				DC Ionic Conductivity at 25 °C[e] (S/cm)
			T_m[d] (°C)	ΔH_{fus}[d] (J/g)	T_g[d] (°C)	T_c[d] (°C)	T_m[d] (°C)	ΔH_{fus}[d] (J/g)	
1	($^{33}PEOX_{0.32}$)($^{34}PE_{0.68}$)	15:1	89	20.0	−45	n.d.[f]	n.d.[f]	n.d.[f]	5.2×10^{-6}
2	($^{33}PEOX_{0.40}$)($^{24}PE_{0.60}$)	10:1	82	14.8	−45	n.d.[f]	n.d.[f]	n.d.[f]	9.0×10^{-6}
3	($^{33}PEOX_{0.47}$)($^{18}PE_{0.53}$)	7:1	61	6.4	−43	n.d.[f]	n.d.[f]	n.d.[f]	8.3×10^{-6}
4	($^{76}PEOX_{0.51}$)($^{34}PE_{0.49}$)	15:1	94	11.8	−49	−20	23	5.4	2.3×10^{-5}
5	($^{76}PEOX_{0.60}$)($^{24}PE_{0.40}$)	10:1	88	10.1	−50	−19	26	9.4	2.8×10^{-5}
6	($^{76}PEOX_{0.66}$)($^{18}PE_{0.34}$)	7:1	74	2.9	−48	−14	25	5.6	3.1×10^{-5}
7	($^{123}PEOX_{0.64}$)($^{34}PE_{0.36}$)	15:1	111	10.1	−38	n.d.[f]	39	18.6	8.2×10^{-6}
8	($^{123}PEOX_{0.72}$)($^{24}PE_{0.28}$)	10:1	103	1.2	−39	n.d.[f]	37	12.6	8.4×10^{-6}
9	($^{123}PEOX_{0.77}$)($^{18}PE_{0.23}$)	7:1	97	1.1	−38	n.d.[f]	38	16.1	7.4×10^{-6}

[a]All films had [EO]:[Li] composition of 20:1; where EO means ethylene oxide units in the PEOX cross-linker. [b]PE segments: Polyethylene domains in the polymer electrolyte. [c]PEO segments: Polyethylene oxide domains in the polymer electrolyte. [d]Glass transition temperature (T_g), cold crystallization temperature (T_c), and melting temperature (T_m) were determined by differential scanning calorimetry of the second heat cycle. [e]Determined by dielectric spectroscopy measurements. See Experimental Section for more details. [f]Not detected.

segmental motion of the PEO in ^{76}PEOX electrolytes. Furthermore, ^{76}PEOX SPEs exhibited both a cold crystallization temperatures (T_cs) and T_ms near room temperature in the PEO segments during the heating cycle of the DSC, while no crystallization temperature was observed in the cooling cycle on DSC. This can be attributed to the low cross-linking density of the network polymers, allowing the PEO chains to rearrange and crystallize in the network when enough energy is provided in the heating cycle during DSC.[49] For the SPEs containing 123 EO units (^{123}PEOX: entries 7–9), T_ms of around 38 °C were observed and the T_gs were much higher than those of polymer electrolytes containing 33 and 76 EO units in the cross-linker, suggesting that the PEO functionalized cross-linker length was too large to prevent the crystallization of PEO in the network structure. Furthermore, among the polymer electrolytes with different cross-linker lengths and the same ratio of [**COE**]:[**1]** (e.g. comparison of entries 1, 4, and 7), ^{33}PEOX polymer electrolytes had the smallest polyethylene (PE) crystallites in the network (lowest T_m), which could be explained by the relatively higher cross-linking density in these SPEs that inhibited the PE crystallization in the network. Also, for polymer electrolytes having the same cross-linker length (e.g. entries 1–3), higher [**COE**]:[**1]** ratios yielded materials with better mechanical integrity.

The ionic conductivities of the unplasticized SPEs were tested and the values are shown in Figure 2.2. It is clear that there is a significant effect of **PEOX** length on the ionic conductivity of the polymer electrolytes (e.g. comparison of ionic conductivities of entries 1, 4, and 7 at constant [**COE**]:[**1**] ratio). However, no substantial changes in ionic conductivities were observed when the number of

ethylene repeat units between the cross-links was changed by varying the [**COE**]:[**1**] ratio (e.g. comparison of ionic conductivities of ^{76}PEOX electrolytes: entries 4, 5, and 6). Although PEO domains in the ^{33}PEOX SPEs were completely amorphous (no T_m) and ^{76}PEOX electrolytes had crystalline PEO domains in the network structure, ^{76}PEOX electrolytes exhibited the highest ionic conductivities of 2.7×10^{-5} S/cm, which are roughly three times more than that observed for the ^{33}PEOX and ^{123}PEOX electrolytes ($<10^{-5}$ S/cm) and more than four times higher than the PEO-LiTFSI (σ of 7.2×10^{-6} S/cm at [EO]:[Li] 18:1 and 25 °C). We postulate that the surprisingly high ionic conductivity of the ^{76}PEOX electrolytes is a direct consequence of the low T_g of these SPEs, allowing enhanced segmental motion of PEO in the amorphous domains thus facilitating lithium-ion conduction. Among the ^{76}PEOX electrolytes tested,

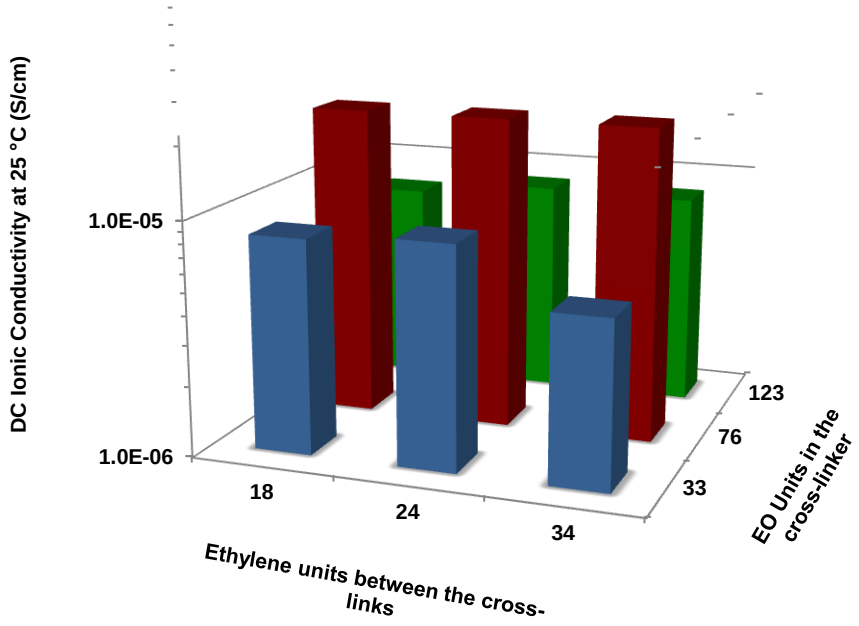

Figure 2.2 Ambient temperature DC ionic conductivities of unplasticized cross-linked PE/PEO SPEs.

($^{76}PEOX_{0.66}$)($^{18}PE_{0.34}$) exhibited maximum ionic conductivity (3.1×10^{-5} S/cm at 25 °C), which is comparable to those reported by other research groups for amorphous PEO network polymers. For instance, Watanabe and co-workers reported the conductivity value of 2×10^{-5} S/cm at 20 °C for a network poly(ethylene oxide)-co-poly(propylene oxide) copolymer with LiTFSI salt.[26] Armand and co-workers observed conductivity of 1×10^{-5} S/cm at 25 °C for their PEO based network polymer electrolytes.[28] Even though the ionic conductivity values of these PE-PEO cross-linked SPEs are similar to the other PEO-based unplasticized network polymers reported in the literature, we hypothesized that our unique polymer electrolyte design could prove advantageous for a LMP separator, because these network SPEs have mechanically strong and electrochemically stable polyethylene segments, which chemically resemble commercially available separators.[50]

It has been proposed that ionic conductivities greater than 1×10^{-4} S/cm are necessary for SPEs to function in commercial batteries that require ambient temperature operation.[1] However, PEO polymers exhibit low conductivity ($<1 \times 10^{-4}$ S/cm) at room temperature due to the crystalline domains.[51] Recently, Hawker and co-workers reported a copolymer of ethylene oxide and allyl glycidyl ether that showed an ionic conductivity of 5×10^{-5} S/cm at 25 °C.[52] We were able to achieve similar ionic conductivities for some PEO-based cross-linked SPEs (Table 2.2, entries 4–6), while still retaining good mechanical properties. Once the unplasticized SPE with the highest ionic conductivity was identified (2.7×10^{-5} S/cm at 25 °C for ^{76}PEOX SPEs), poly(ethylene glycol) dimethylether (**PEG;** M_n 275 Da and flash point 156 °C) was

Table 2.3 Compositions of plasticized PE-PEO cross-linked SPEs[a]

entry	Plasticized SPE	Weight% of the plasticizer	PE Segments[b]		PEO Segments[c]			
			T_m[d] (°C)	ΔH_{fus}[d] (J/g)	T_g[d] (°C)	T_c[d] (°C)	T_m[d] (°C)	ΔH_{fus}[d] (J/g)
1[e]	$(^{70}PEOX_{0.50})(^{34}PE_{0.50})$	0	94	11.8	−49	−20	23	5.4
2[e]	$(^{70}PEOX_{0.43})(^{34}PE_{0.43})(^{5}PEG_{0.14})$	17	91	14.8	−54	−22	15	8.3
3[e]	$(^{70}PEOX_{0.39})(^{34}PE_{0.39})(^{5}PEG_{0.22})$	25	97	19.5	−57	−22	16	12.8
4[e]	$(^{70}PEOX_{0.34})(^{34}PE_{0.35})(^{5}PEG_{0.31})$	32	95	20.1	−61	−26	18	14.9
5[e]	$(^{70}PEOX_{0.30})(^{34}PE_{0.31})(^{5}PEG_{0.39})$	40	96	14.8	−65	−29	14	11.6
6[f]	$(^{5}PEG_{1.00})$	100	n.a.[g]	n.a.[g]	−88	n.d.[h]	n.d.[h]	n.d.[h]

[a]All films had [EO]:[Li] composition of 20:1; where EO includes ethylene oxide units contained both in the PEOX cross-linker and PEG plasticizer. [b]PE segments: Polyethylene domains in the polymer electrolyte. [c]PEO segments: Polyethylene oxide domains in the polymer electrolyte. [d]Glass transition temperature (T_g), cold crystallization temperature (T_c), and melting temperature (T_m) were determined by differential scanning calorimetry of the second heat cycle. [e]All films had 80 EO units in the cross-linker and [**COE**]:[**1**] loading of 15:1. [f]Sample $^{5}PEG_{1.00}$: Dimethyl poly(ethylene glycol), M_n 250 Da with [EO]:[Li] composition of 20:1 for comparison purposes. [g]Not applicable. [h]Not detected.

added as a plasticizer to improve the ionic conductivity and support higher charge/discharge rates. Since the (^{76}PEOX$_{0.51}$)(^{34}PE$_{0.49}$) sample had better mechanical properties (qualitative tests), samples of this framework were prepared with varying amounts of **PEG** (16, 24, 31, and 39 wt%) to obtain plasticized cross-linked SPEs.[53] Compositions and thermal characteristics of the plasticized samples are reported in Table 2.3. Addition of plasticizer led to a significant decrease in T_g from −47 °C (0 wt% PEG) to −65 °C (31 wt% PEG). Also, a significant decrease in the T_c and T_m corresponding to the PEO segments in the plasticized SPEs (entries 1–5) was observed indicating that the PEO crystallization is hindered by incorporating small PEG oligomers into the cross-linked network. The temperature dependent ionic

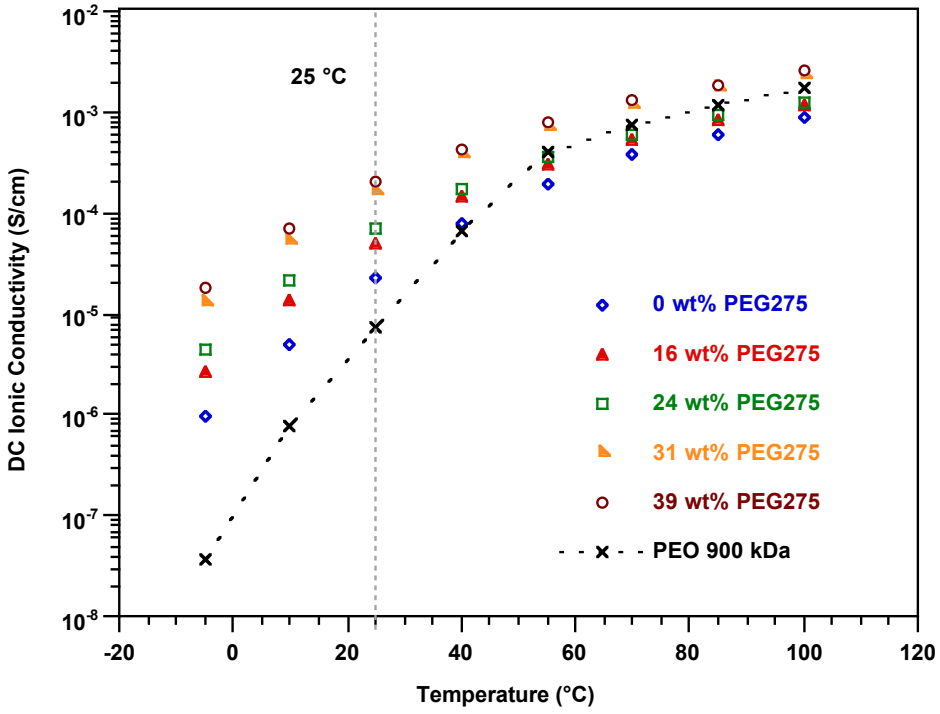

Figure 2.3 Plot of DC ionic conductivity as a function of temperature for ^{70}PEOX electrolytes having different weight percent of PEG275 plasticizer. All films had [COE]:[**1**] ratio of 15:1 and [EO]:[Li] composition of 18:1. The conductivity of a PEO 900 kDa sample with [EO]:[Li] ratio of 18:1 is also shown for comparison purposes.

conductivities of these cross-linked plasticized SPEs at various wt% of **PEG** (16, 24, 31, 39 wt%) are shown in Figure 2.3. Notably, SPE with 39 wt% **PEG** (entry 5) showed an ionic conductivity value of 2.0×10^{-4} S/cm, which is an order of magnitude higher than the unplasticized SPE (0 wt% plasticizer; entry 1). By comparison, Mastragostino and coauthors developed a **PEG** (M_n 500) doped PEO based polyurethane network polymer that showed conductivity of 10^{-5} S/cm at 25 °C; however, they did not see a significant increase in conductivity upon addition of plasticizer.[40] Park and co-workers reported an interesting plasticized SPE, wherein they incorporated **PEG** (M_n 250) and PEO based cross-linked electrolyte inside the pores of a PE non-woven matrix. The resulting SPE with 20 wt% crosslinking agent and 80 wt% non-volatile plasticizer displayed conductivity of 3.1×10^{-4} S/cm at room temperature.[54] Kang and co-workers recently reported a multi-armed plasticizer doped PEO/siloxane-based cross-linked polymer, which exhibited a conductivity value of 1.0×10^{-4} S/cm at 25 °C.[38] While all of these plasticized SPEs reported in the literature offer major improvements in conductivity for solid polymer electrolytes, none have been tested for the ability to influence lithium dendrite nucleation and growth in a battery.

Inspired by the dendrite studies reported by Balsara and co-workers,[20] we performed galvanostatic lithium plate/strip electrochemical cycling measurements in symmetric Li/SPE/Li cell to quantify the effect of our PE-PEO cross-linked SPEs on the lifetime of lithium-metal based batteries. Measurements were performed at variable current densities, *J*, using a three hour lithium plating followed by a three

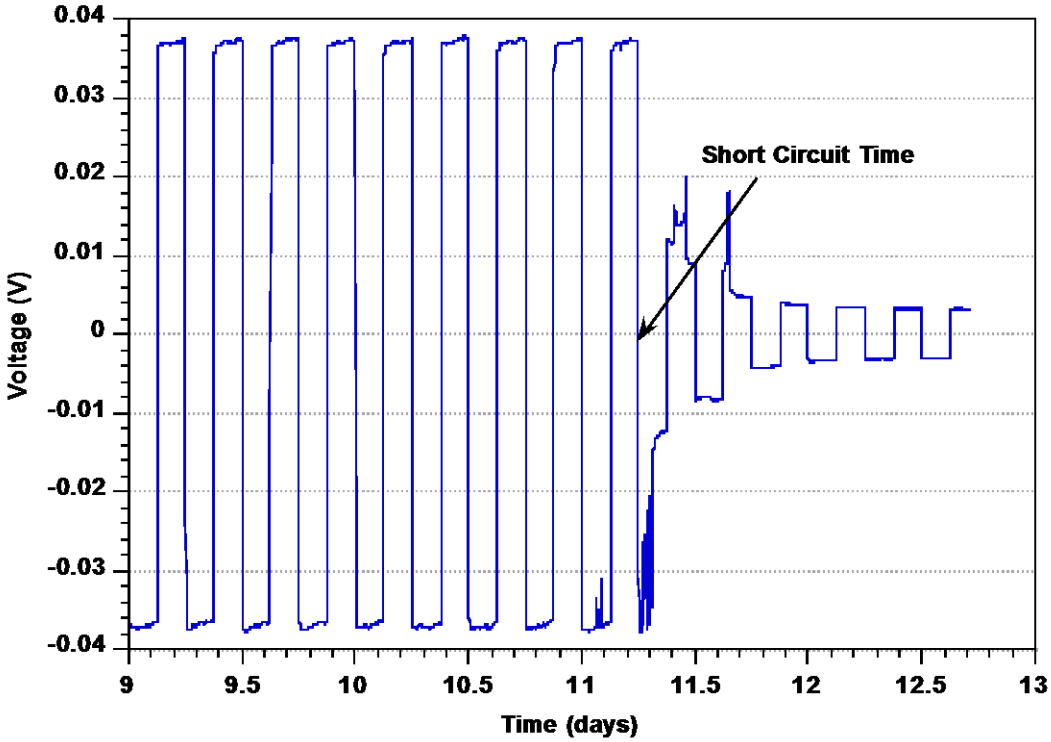

Figure 2.4 Galvanostatic cycling curve obtained for ($^{70}PEOX_{0.34}$)($^{34}PE_{0.35}$)($^{5}PEG_{0.31}$) at fixed current density of 0.65 mA/cm^2 and 90 °C. The short circuit time (t_{sc}) is labeled; C_d value is 645 C/cm^2.

hour lithium stripping routine until a sudden drop in voltage was observed. This large decline in voltage was attributed to the formation of dendrite short. The representative example for the cycling results is shown in Figure 2.4. The SPE's resistance to dendrite growth is here quantified in terms of total charge passed, C_d, at the time of cell failure by dendrite-induced short-circuits. At a current density of 0.5 mA/cm^2 and measurement temperature of 90 °C the unplasticized solid polymer electrolyte, ($^{70}PEOX_{0.50}$)($^{34}PE_{0.50}$) with only a modest shear modulus ($G' \sim 10^5$ Pa at 90 °C), displays an order of magnitude higher C_d value (1185 C/cm^2 at J = 0.50 mA/cm^2 and 90 °C) than reported for high modulus PS-*b*-PEO block copolymers (105 C/cm^2 at J =

0.26 mA/cm^2 and 90 °C).[20] Our finding demonstrates that a separator exhibiting high shear storage modulus is not a requirement to inhibit dendrite growth. Since it took about a month to short-circuit this cell operating near the upper threshold of current density allowed by the unplasticized SPE, we selected one sample, (^{70}PEOX$_{0.34}$)(^{34}PE$_{0.35}$)(^{5}PEG$_{0.31}$), a plasticized SPE (31 wt% **PEG**) with high ionic conductivity ($\sigma \sim 1.6 \times 10^{-4}$ S/cm at 25 °C) and reasonable storage modulus ($G \sim 1.0 \times 10^5$ Pa at 90 °C), to measure C_d at variable current densities (0.26 mA/cm^2–1.0 mA/cm^2) and 90 °C.

Figure 2.5 reports C_d values as a function of current density for a high molar mass PEO standard (M_n 900 kDa), PS-*b*-PEO, and (^{70}PEOX$_{0.34}$)(^{34}PE$_{0.35}$)(^{5}PEG$_{0.31}$). The PE-PEO cross-linked SPE displayed significantly higher C_d values than observed for PEO (M_n 900 kDa) sample at all the measured current density values. Notably, it displayed a C_d value of 1790 C/cm^2 that is more than an order of magnitude greater than reported for PS-*b*-PEO block copolymers (C_d value of 105 C/cm^2) under the same testing conditions (0.26 mA/cm^2 and 90 °C).[55] At higher current density values (>0.26 mA/cm^2), the cells short-circuit faster and C_d values are consequently lower. Significantly, even under these harsher measurement conditions (cells cycled at significantly higher current density), the PE-PEO cross-linked SPE displayed a higher C_d value (156 C/cm^2 at J = 1.30 mA/cm^2 and 90 °C) compared to PS-*b*-PEO block copolymer (105 C/cm^2 at J = 0.26 mA/cm^2 and 90 °C). Recently, Balsara and co-workers reported TiO_2-doped PS-*b*-PEO block copolymer, that showed better dendrite growth suppression than the PS-*b*-PEO block copolymers (C_d value of 1766 C/cm^2 compared to 374 C/cm^2 at 0.17 mA/cm^2 and 90 °C).[56,57] The SPE reported

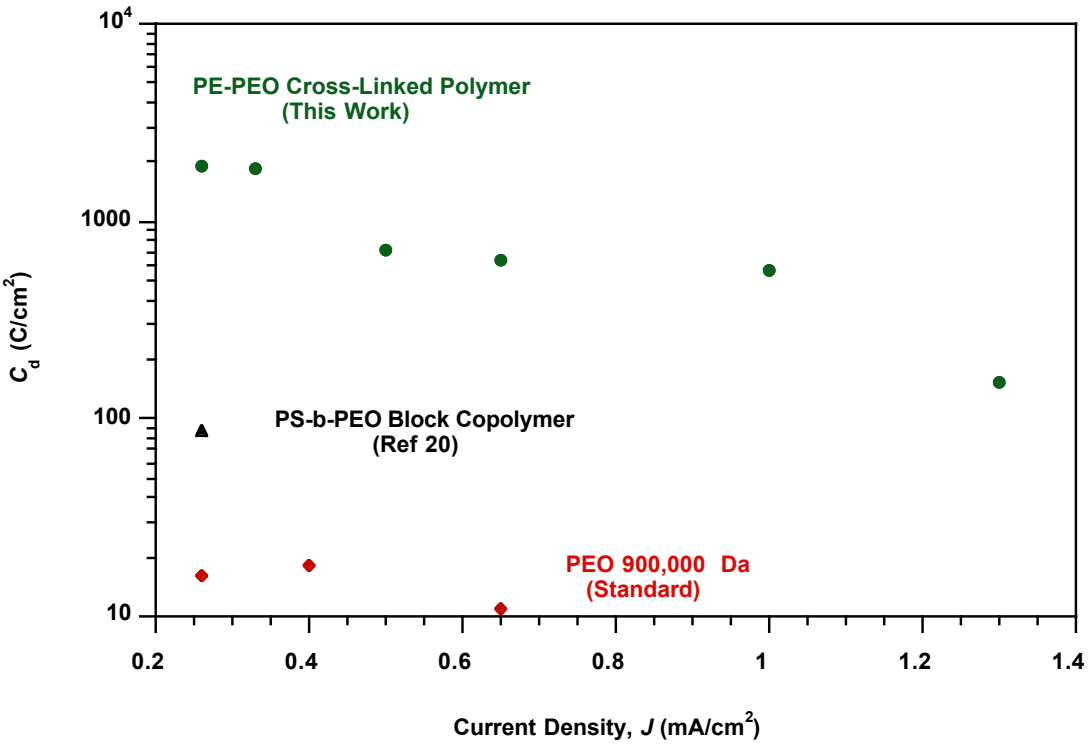

Figure 2.5 Galvanostatic cycling tests. The cycling data showing C_d as a function of current density at 90 °C for ($^{70}PEOX_{0.34}$)($^{34}PE_{0.35}$)($^{5}PEG_{0.31}$) polymer electrolyte (●), PS-*b*-PEO polymer (▲), and PEO 900 kDa (◆). The cells were cycled at constant current density with each half cycle of 3 h until a short circuit was observed.

herein, i.e. ($^{70}PEOX_{0.34}$)($^{34}PE_{0.35}$)($^{5}PEG_{0.31}$) displayed a C_d value (1790 C/cm^2 at 0.26 mA/cm^2 and 90 °C; 3 hour charge-discharge cycle) comparable to those exhibited by TiO_2-doped PS-*b*-PEO block copolymer (1766 C/cm^2 at 0.17 mA/cm^2 and 90 °C; 4 hour charge- discharge cycle). This result is notable because the dendrite tests for PE-PEO cross-linked copolymer were conducted at higher current density compared to TiO_2-doped PS-*b*-PEO block copolymer (0.26 mA/cm^2 for PE-PEO cross-linked copolymer compared to 0.17 mA/cm^2 for TiO_2-doped PS-*b*-PEO block copolymer).

To further demonstrate the application of these PE-PEO cross-linked SPEs at lower temperatures, galvanostatic cycling tests were also performed at 55 °C. The

(^{70}PEOX$_{0.34}$)(^{34}PE$_{0.35}$)(^{5}PEG$_{0.31}$) polymer electrolyte exhibited C_d values of 564 C/cm^2 and 544 C/cm^2 at 0.40 mA/cm^2 and 0.65 mA/cm^2, respectively. These results are of significant interest because the high C_d values of these SPEs indicate their ability to inhibit dendrite growth, and the high ionic conductivity value of 7.0×10^{-4} S/cm at 55 °C supports their application for moderate temperature Li-metal battery operation. We are currently investigating the origins of the unique ability of our PE-PEO cross-linked SPEs to resist the proliferation of lithium dendrites in secondary batteries using metallic lithium anodes. Judging from the chemistry and shear mechanical properties of our PE-PEO cross-linked electrolytes, it is likely that Li^+ ions see a tortuous nanoporous network of the conducting PEO phase as it migrates through the electrolyte. Such a network would facilitate migration of Li^+ ions, but could frustrate growth of micron-sized Li dendrites,[58] perhaps explaining the superior performance of our materials. Clearly significant amount of research is needed to more concretely relate the unique structure of our materials to their ability to retard dendrite growth.

Dendrite resistance of selected SPEs was also examined using more conventional, but much harsher galvanostatic polarization conditions. In this approach the voltage response in a symmetric Li/SPE/Li cell is studied during continuous one direction plating at a prescribed current density. In these measurements, the Li/SPE/Li symmetric cells were polarized at current densities in the range 0.26–1.0 mA/cm^2 at 90 °C until the voltage drop was observed. These tests were conducted to investigate the efficiency of lithium plating from the cross-linked polymer electrolyte. A typical polarization curve at current density (0.65 mA/cm^2) and 90 °C is shown in Figure 2.6.

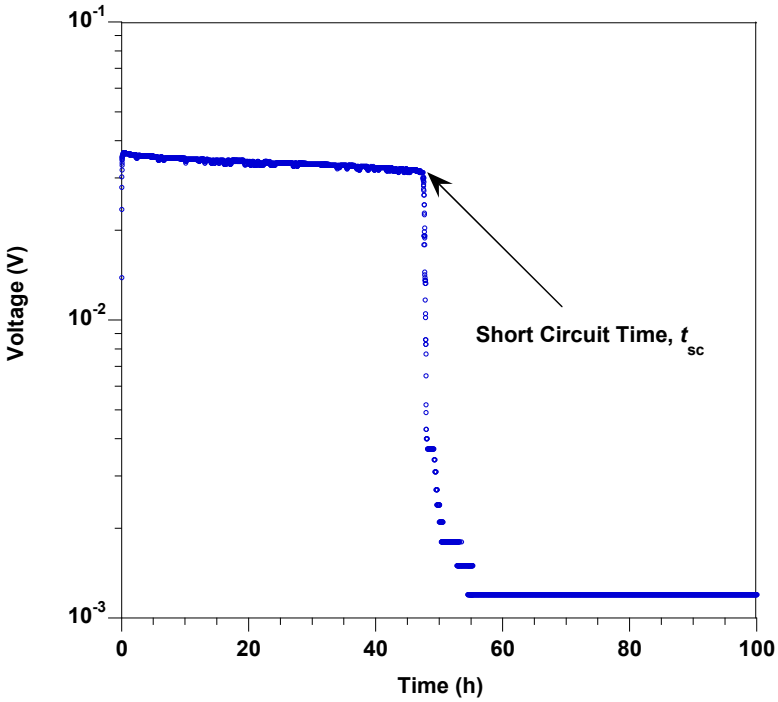

Figure 2.6 Galvanostatic polarization curve obtained for (^{70}PEOX$_{0.34}$)(^{34}PE$_{0.35}$)(^{5}PEG$_{0.31}$) at fixed current density of 0.65 mA/cm^2 and 90 °C. The short circuit time (t_{sc}) is indicated in the plot.

Remarkably, we found that cells galvanostatically polarized at current densities of less than or equal to 0.26 mA/cm^2 were able to plate the entire Li electrode without short circuit; in these cases, divergence of the potential halted testing. This finding means that a lithium battery operated under these conditions would not fail by dendrite-induced short circuits. To characterize the short circuit times (t_{sc}) at 0.26 mA/cm^2, it was necessary to laminate multiple Li foil layers (thickness ~ 800 μm) to increase the amount of source Li in the electrode being stripped. Figure 2.7 shows the variation of the measured cell short circuit time, t_{sc}, with current density (0.26 mA/cm^2–1.0 mA/cm^2) for the cross-linked SPEs at 90 °C. Duplicate measurements were performed for two cross-linked samples at a specified current density value and the results were

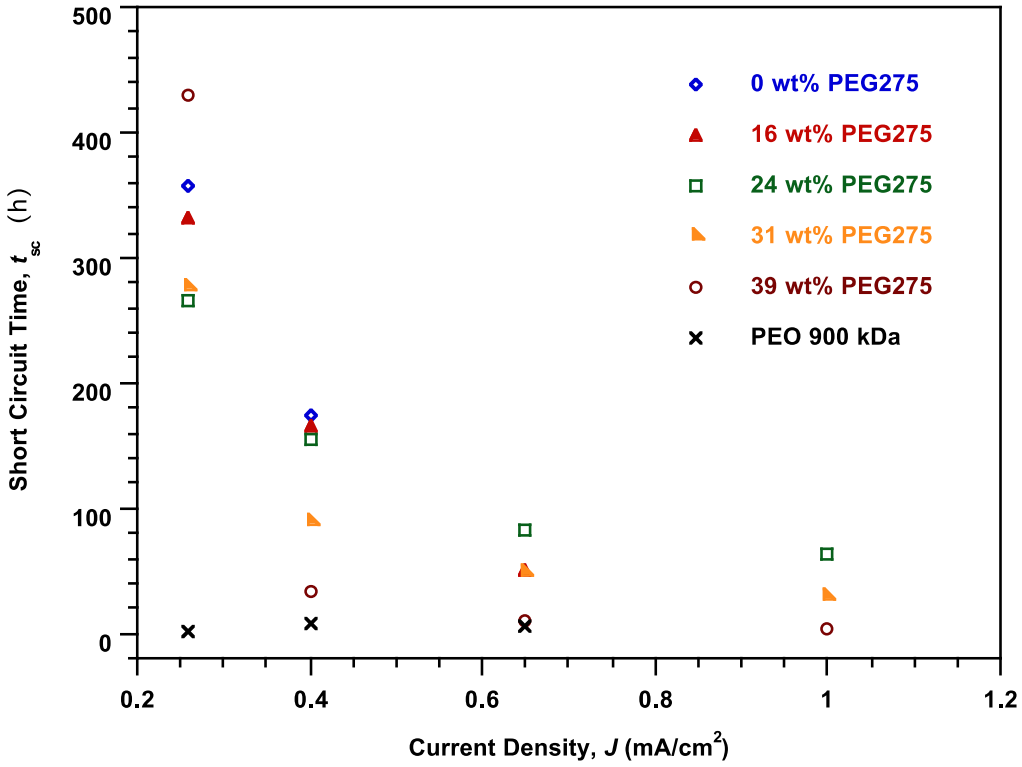

Figure 2.7 Galvanostatic polarization tests. Plot of short-circuit time as a function of current density at 90 °C for various [70]PEOX electrolytes having different weight% (wt%) of the plasticizer (PEG275). A PEO 900 kDa sample is also shown for comparison purposes.

found to be within 5% error. Since the tests were time consuming, we performed only single measurements for rest of the cross-linked SPEs and the results are shown in Figure 2.7. The short circuit times of the SPEs (Table 2.3, entries 1–5) are significantly higher than those seen for the high molar-mass PEO-LiTFSI samples (M_n 900 kDa) made in our laboratory and all other reported SPEs to date.[18,60–62]

Rosso and co-workers reported that the onset of the dendrite growth and the growth velocity of the dendrites for PEO-LiTFSI electrolytes were in agreement with the prediction of the Chazalviel model.[18] However, while we find $t_{sc} \sim J^{-2}$, consistent

with transported-limited dendrite growth assumed in the Chazalviel model, our experimental t_{sc} values are an order of magnitude or more higher than expected t_{sc} values based on this theory for most compositions.[59] We conclude that there are additional physical features present in the PE-PEO cross-linked SPEs that provide enhanced retardation of dendrites than expected. Regardless of the dendrite growth inhibition mechanism, these PE-PEO cross-linked SPEs exhibit superior capacity to inhibit dendrite growth compared to all current materials over the entire range of current densities studied. In particular, at 0.26 mA/cm^2 and 90 °C, we observed t_{sc} values of 357 h and 430 h for the unplasticized SPE (Table 2.3, entry 1) and 39 wt% plasticized SPE (entry 5) respectively. In terms of C_d, these values are equivalent to 334 C/cm^2 and 403 C/cm^2, though the test method is much more severe than galvanostatic cycling. By comparison, Rosso and co-workers reported a t_{sc} of 2 h at 0.25 mA/cm^2 and 90 °C for PEO-LiTFSI polymer electrolytes.[18] Liu and co-workers doped silica nanofillers[60] and ionic liquids[61] in the PEO-LiTFSI polymer electrolytes, and observed t_{sc} of 90 h and 135 h respectively at 0.25 mA/cm^2 and 60 °C. They were able to increase the short circuit time to 168 h by doping it with both nano-SiO_2 and ionic liquid;[62] however, their reported short-circuit times (tests conducted at 60 °C) are still two times lower than our best PE-PEO cross-linked SPEs (tests conducted at 90 °C) reported herein. Note that all of the above referenced SPEs measure the short-circuit time using visualization cells with the inter-electrode distance of 1 mm, instead of Li/polymer/Li symmetric coin cells used for our tests.[18,60-62] Due to much larger inter-electrode separation distance, the dendrites will short these visualization cells slower than coin cells, suggesting that the reported short-circuit times in these reports

are larger than expected in an actual cell. This suggests that the ability to resist the dendrite growth using the PE-PEO cross-linked SPEs disclosed herein is significantly higher than any other SPE reported in the literature to date.

2.4 Conclusions

In summary, we have developed a facile synthetic approach for the synthesis of a PE-PEO cross-linked SPE system that displays both high conductivity (>10^{-4} S/cm at 25 °C) and exceptional dendrite growth resistance. The cross-linked polymer electrolyte reported herein exhibits unprecedented levels of lithium dendrite growth resistance (demonstrated by highest C_d value and longest short circuit time reported to date). The combination of excellent dendrite growth resistance and high conductivity will allow the use of these SPEs in rechargeable LMP battery technology for high energy density applications. In addition, they are also potential electrolyte components for next generation high energy density Li battery technologies, lithium-sulfur and lithium-air batteries, which utilize Li metal as an anode material. We are currently studying the performance of these electrolytes in battery devices using a lithium-metal anode and standard $LiCoO_2$ cathode material. We believe that our unique polymer electrolyte design will spur investigation in the scientific community regarding the potential mechanisms of dendrite growth inhibition.

2.5 Experimental

2.5.1 General Considerations

All reactions and manipulations of air and moisture sensitive compounds were carried out under dry nitrogen using a Braun UniLab drybox or standard Schlenk line techniques unless otherwise specified. ^{1}H NMR spectra were collected in deuterated

solvents on a Varian INOVA 500 spectrometer and referenced with residual non-deuterated solvent shifts ($CHCl_3$ = 7.26 ppm) and are reported relative to tetramethylsilane (δ = 0 ppm). ^{13}C NMR spectra were recorded on Varian INOVA (^{13}C, 125 MHz) spectrometer and referenced to chloroform (δ 77.23 ppm). High-resolution mass spectrometry (HRMS) analyses were performed at the Mass Spectrometry Laboratory at the University of Illinois at Urbana-Champaign.

Gel permeation chromatography (GPC) analyses were carried out using an Agilent PL-GPC 50 integrated system, equipped with UV and refractive index detectors, and 2 PL gel Mini-MIX C columns (5 micron, 4.6 mm ID). The GPC columns were eluted with tetrahydrofuran at 30 °C at 0.3 mL/min and were calibrated with monodisperse polystyrene standards. Differential scanning calorimetry (DSC) analyses of polymer samples were performed on a TA Instruments Q1000 instrument equipped with liquid nitrogen cooling system. Polymer samples were made in aluminum pans and heated under nitrogen from −100 °C to 180 °C at a rate of 10 °C per minute and then cooled to −100 °C at a rate of 10 °C per minute, followed heating to 180 °C at a rate of 10 °C per minute. The glass transition temperature (T_g) and the melting temperature (T_m) were recorded from the second heating run.

The thickness of the cross-linked solid polymer electrolytes for all measurement purposes was 200 ± 30 μm. The conductivity data of the polymer electrolytes was obtained over a range of frequencies (0.1 to 3 × 10^6 Hz) and temperature (−5 °C to 100 °C) using a Novocontrol Dielectric Broadband Spectrometer fitted with a Quatro temperature control system. Conductivity measurements were performed using blocking/solid polymer electrolyte

(SPE)/blocking cell orientation, using gold plated stainless steel electrodes. Symmetric lithium coin cells (Li/SPE/Li) for short-circuit measurements were prepared in an argon filled MBraun glovebox using Hohsen components, size 2032, with 9.9 mm diameter lithium electrodes and a 12.7 mm diameter cross-linked electrolyte sample. Coin cell crimping was performed with a MTI electric crimping machine to ensure uniformity. Lithium/SPE/Stainless Steel (Li/SPE/SS) coin cells were prepared in an argon filled MBraun glovebox using Hohsen components, size 2032, with 9.9 mm diameter lithium electrodes and a 12.7 mm diameter cross-linked electrolyte sample. The cyclic voltammetric measurements were performed on Li/SPE/SS coin cells using a VersaStat 3 potentiostat (Princeton Applied Research) controlled by VersaStudio software. The potential was scanned from −0.2 V to 4.5 V at 1 mV/s sweep rate and 22 °C. Galvanostatic cyclic short-circuit measurements were performed on Li/SPE/Li symmetric coin cells using a Neware CT-3008 battery tester with wiring into (Fisher Scientific and VWR) convection ovens to maintain T = 90°C. The cells were cycled at constant current density with each half cycle of 3 h until a sudden drop in voltage was observed. Galvanostatic polarization measurements were performed on Li/SPE/Li symmetric coin cells using a Neware CT-3008 battery tester. The storage $G'(\omega)$ and loss $G''(\omega)$ moduli were quantified using small amplitude oscillatory shear measurements. Anton Paar Physica MCR 301 rheometer with 10 mm diameter parallel plates was used for rheological measurements. The ac impedance spectroscopy measurements were made using Li/SPE/Li symmetric coin cells prepared in an argon filled MBraun glovebox, using a Novocontrol Broadband Dielectric Spectrometer fitted with a Quatro temperature control system at frequency ranging from 2 KHz to

900 MHz and at an amplitude of 10 mV.

2.5.2 Materials

Sodium hydride (95%), 1,5-cyclooctadiene, *cis*-cyclooctene (95%), *meta*-chloroperoxybenzoic acid, Grubbs' 2nd Generation catalyst (Cl_2(iMes)(PCy_3)Ru=CHPh), and Crabtree's catalyst [(COD)Ir(py)(PCy_3)]PF_6 were purchased from Sigma-Aldrich and used as received. Bis(trifluoromethane)sulfonimide lithium salt, LiTFSI (99.95% trace metals basis) was purchased from Sigma-Aldrich and dried *in vacuo* at 90 °C for 24 h and transferred directly into the glove box. Ethylene oxide was purchased from Sigma-Aldrich and dried over *n*-BuLi before use. Dimethyl poly(ethylene glycol), PEG275 (M_n (NMR) = 275 Da; M_n (Sigma-Aldrich label) = 250 Da) was bought from Sigma-Aldrich, dried over activated 3 Å sieves for 48 hours, and degassed by three freeze pump thaw cycles before use. Dibromo-*p*-xylene (97%) was purchased from Alfa Aesar and used as received. Sodium hydroxide and sodium chloride were purchased from Mallinckrodt and used as received. HPLC grade tetrahydrofuran was purchased from Fisher Scientific and dried over an alumina column and degassed by three freeze pump thaw cycles before use. Chloroform was dried over P_2O_5 and distilled prior to use. Hydrogen (99.99%) was purchased from Airgas. $CDCl_3$ was purchased from Cambridge Isotope Laboratories (CIL) and used as received.

Following a literature procedure,[63] 5-hydroxy-1-cyclooctene was prepared, dried over activated 3 Å sieves, and degassed by three freeze pump thaw cycles before use. Potassium naphthalenide in THF was prepared from naphthalene and potassium at a concentration of 0.59 M (titrated with a standard benzoic acid solution until a

persistent green color was observed as an end-point of the titration) and degassed by three freeze pump thaw cycles before use.

2.5.3 Synthesis

2.5.3.1 Synthesis of the PEO Functionalized Cross-linker

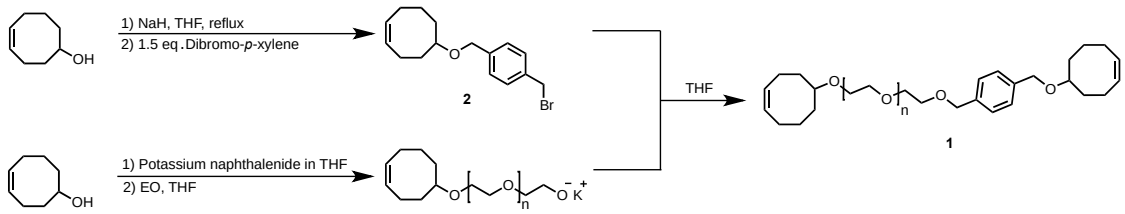

Scheme 1 General scheme for the synthesis of cross-linker **1**.

Preparation of (Z)-5-((4-(bromomethyl)benzyl)oxy)cyclooct-1-ene (2): A suspension of NaH (2.65 g, 105 mmol) in anhydrous THF (150 mL) was treated dropwise with 5-hydroxycyclooct-1-ene (8.65 g, 68.5 mmol) and heated to 70 °C under N_2 for 16 h. This solution was cooled to room temperature and dropwise cannula transferred to the solution of α,α′-dibromo-*p*-xylene (27.5 g, 104 mmol) in anhydrous THF (150 mL) at 22 °C under N_2, which led to the instantaneous precipitation of salts in a bright yellow solution. The resulting solution was stirred at 22 °C for 16 h and quenched with minimum amount of ethanol until the effervescence ceased. The solution was filtered and the filtrate was concentrated on a rotary evaporator to yield a colorless oil. Hexanes were added (~150 mL) to the crude reaction mixture to recrystallize out excess dibromo-*p*-xylene. Dibromo-*p*-xylene was filtered and the filtrate was concentrated on rotary evaporator to yield colorless oil, which was further purified by column chromatography on silica using 1:1 CH_2Cl_2/hexanes. Desired product was isolated as colorless oil (7.1 g, 34%). ^{1}H NMR

(500 MHz, $CDCl_3$) δ 7.43 – 7.28 (m, 4H), 5.79 – 5.52 (m, 2H), 4.57 – 4.36 (m, 4H), 3.54 – 3.40 (m, 1H), 2.59 – 1.18 (m, 10H). ^{13}C NMR (126 MHz, $CDCl_3$) δ 139.71, 136.84, 130.19, 129.50, 129.14, 127.85, 80.32, 69.85, 34.32, 33.57, 33.33, 25.87, 25.68, 22.78. HRMS (ESI) m/z calculated for $C_{16}H_{21}ONaBr$ ($M + Na^+$) 331.0673, found 331.0681.

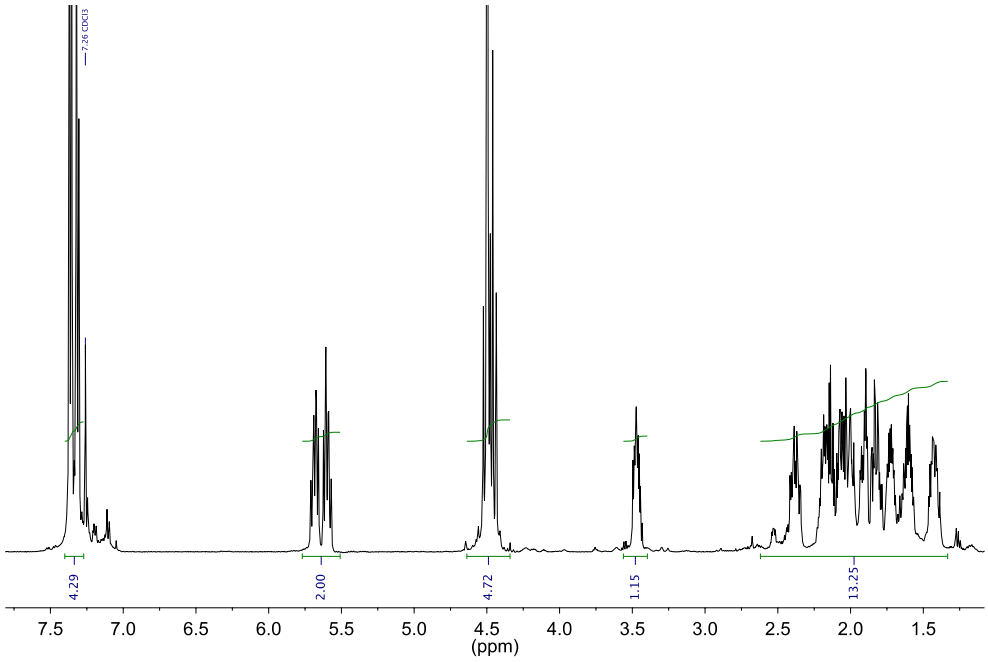

Figure 2.8 ^1H NMR spectrum of (*Z*)-5-((4-(bromomethyl)benzyl)oxy)cyclooct-1-ene (**2**). Signal at 7.26 ppm is the residual $CHCl_3$.

Preparation of the PEO functionalized cross-linker (1): In a N_2 glovebox, a Fischer-Porter bottle was charged with 5-hydroxycyclooct-1-ene (144 mg, 1.14 mmol) solution in THF (2.0 mL). 0.59 M THF solution of potassium naphthalenide (1.9 mL, 1.1 mmol) was added to the alcohol solution dropwise resulting in a dark green solution. The vessel was sealed with the reactor head and the apparatus was removed from the box and stirred at 22 °C for 1 h. The solution was cooled to −78 °C and ethylene oxide (3.58 g, 81.3 mmol) was then condensed into it. The solution was allowed to warm to room temperature over 16 h. After 16 h, the living alkoxide end group was capped with **2** (0.43 g, 1.4 mmol), which resulted in immediate precipitation of white KBr salt. The reaction mixture was stirred at 50 °C for 5 h and then allowed to warm to room temperature. The salts formed were filtered over a Celite plug and the filtrate was partially concentrated on rotary evaporator. PEO functionalized cross-linker was then precipitated in ~200 mL hexanes. The resulting white powder (3.3 g, 84%) was dried in vacuum at 30 °C for several hours until its mass was constant. ^{1}H NMR (500 MHz, $CDCl_3$) δ 7.26 (m, 4H), 5.70 – 5.46 (m, 4H), 4.61 – 4.32 (m, 4H), 3.61 (s, 305H), 3.32 (ddd, *J* = 9.9, 7.8, 4.3 Hz, 1H), 2.71 – 1.29 (m, 20H). ^{13}C NMR (126 MHz, $CDCl_3$) δ 138.39, 137.17, 129.95, 129.88, 129.26, 129.21, 127.59, 127.31, 80.75, 79.77, 72.85, 72.35, 70.42, 69.78, 69.18, 67.51, 61.49, 34.10, 33.99, 33.23, 33.06, 25.65, 25.61, 25.47, 25.41, 22.55, 22.51.

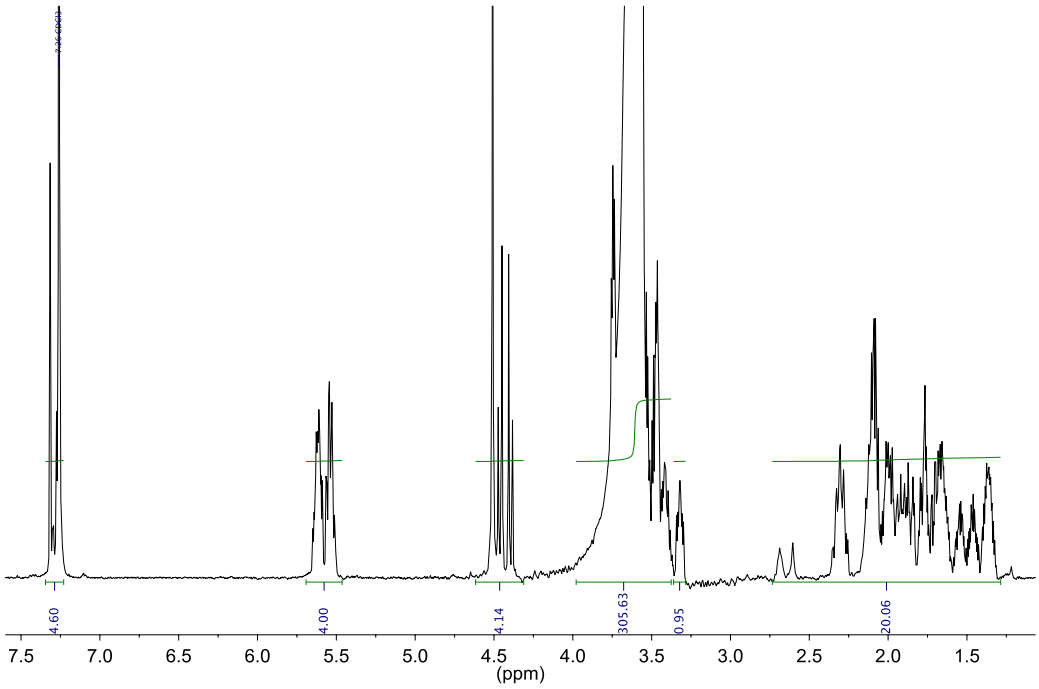

Figure 2.9 ^{1}H NMR Spectrum of PEO functionalized cross-linker (**1**) of molecular weight 3.7 kg/mol. Signal at 7.26 ppm is the residual $CHCl_3$.

2.5.3.2 Synthesis of Cross-Linked Solid Polymer Electrolytes (SPEs)

I. Unplasticized Cross-Linked SPE

General Scheme for the Synthesis of Unplasticized Cross-Linked SPE

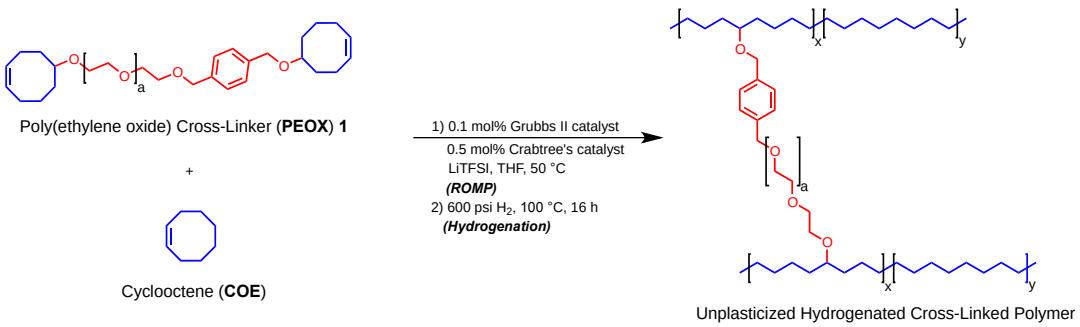

Scheme 2.2 General scheme for the synthesis of unplasticized cross-linked SPE.

Nomenclature of Unplasticized Cross-Linked SPE

(^{a}PEOX$_{l}$)(^{b}PE$_{m}$)

where

PEOX: PEO in the cross-linker; **PE**: Polyethylene**; a**: average number of ethylene oxide (EO) units in PEOX cross-linker; **b**: average number of ethylene (E) units between the crosslinks; **l**: moles of EO units in the PEOX/ total moles of EO and E units; **m**: moles E units in the PE mainchain/ total moles of EO and E units; **l + m** = 1

Calculations for l, m, and n

l′ = (mmoles of PEOX) × a

m′ = [(mmoles of COE) × 4] + [(mmoles of PEOX) × 8]

$$\mathbf{l} = \frac{\mathbf{l'}}{\mathbf{l'} + \mathbf{m'}}$$

$$\mathbf{m} = \frac{\mathbf{m'}}{\mathbf{l'} + \mathbf{m'}}$$

Sample Procedure for the Synthesis of Unplasticized Cross-Linked SPE, (^{33}PEOX$_{0.32}$)(^{34}PE$_{0.68}$): Cross-linker **1** (156 mg, 0.0872 mmol) with 33 EO units in the cross-linker and COE (179 μL, 1.37 mmol) were combined and dissolved in 1.5 mL of THF. Grubbs' 2nd generation catalyst (1.2 mg, 0.0015 mmol) dissolved in 0.5 mL of THF was added to the monomer mixture, followed by addition of LiTFSI (45 mg, 0.16 mmol). Crabtree's catalyst (6.0 mg, 0.0075 mmol) dissolved in 0.5 mL $CHCl_3$ was then added to the resultant solution and shaken vigorously for a minute. It was then transferred to a metal dish (fluoropolymer-lined, diameter of 5.25 cm and depth of 3.0 cm) placed in a volume glass chamber bearing two Kontes glass valves on top. The chamber was placed on top of the hot plate equipped with a metal plate to ensure uniform heating and film was casted under N_2 flow at 50 °C (set-up is shown in Figure 2.10) for 3 h. After the solvent evaporated off, the Kontes valves were closed and the glass chamber was taken in the glove box. Hexane was added to the metal dish in order to release the film from the dish. The film was dried in vacuum at 22 °C for 24 h and then placed in a Parr reactor and sealed. It was pressurized to 600 psig with hydrogen and then vented down to 50 psig. This process was repeated twice more to purge the reactor of air, then pressurized to 600 psig and heated to 100 °C. After 16 h, it was cooled, vented and the hydrogenated film was dried under vacuum at 22 °C.

Figure 2.10 Experimental set-up for the synthesis of SPE under inert conditions.

II. Plasticized Cross-Linked SPEs

General Scheme for the Synthesis of Plasticized Cross-Linked SPE

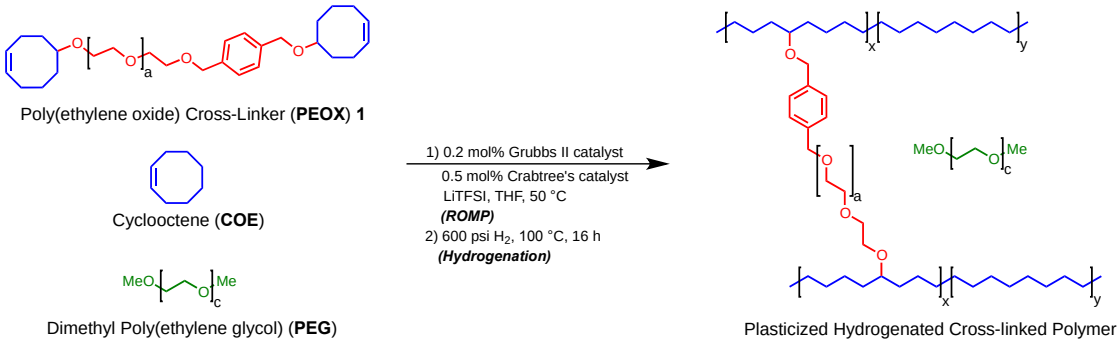

Scheme 2.3 General scheme for the synthesis of plasticized cross-linked SPE.

Nomenclature of Plasticized Cross-Linked SPE

(^{a}PEOX$_{l}$)(^{b}PE$_{m}$)(^{c}PEG$_{n}$)

where

PEOX: PEO in the cross-linker; **PE**: Polyethylene; **PEG**: Dimethyl poly(ethylene glycol); **a**: average number of ethylene oxide (EO) units in PEOX cross-linker; **b**: average number of ethylene (E) units between the crosslinks; **c**: average number of EO units in PEG plasticizer; **l**: moles EO units in PEOX/ total moles of EO and E units; **m**: moles E units in PE mainchain/ total moles of EO and E units; **n**: moles EO units in PEG/ total moles of EO and E units; **l** + **m** + **n** = 1.

Calculations for l, m, and n

l′ = [(mmoles of PEOX) × a]

m′ = [(mmoles of COE) × 4] + [(mmoles of PEOX) × 8]

$$\mathbf{n' = [(mmoles\ of\ PEG) \times 5]}$$

$$\mathbf{l} = \frac{\mathbf{l'}}{\mathbf{l' + m' + n'}}$$

$$\mathbf{m} = \frac{\mathbf{m'}}{\mathbf{l' + m' + n'}}$$

$$\mathbf{n} = \frac{\mathbf{n'}}{\mathbf{l' + m' + n'}}$$

Sample procedure for the Synthesis of Plasticized Cross-Linked SPE with the Optimized EO units in the Cross-linker, (^{70}PEOX$_{0.34}$)(^{34}PE$_{0.35}$)(^{5}PEG$_{0.31}$): Cross-linker **1** (121 mg, 0.0352 mmol) with 70 EO units in the cross-linker and COE (73 μL, 0.56 mmol) were combined and dissolved in 1.5 mL of THF. Grubbs' 2nd generation catalyst (1.2 mg, 0.0015 mmol) dissolved in 0.5 mL of THF was added to the monomer mixture, followed by addition of LiTFSI (79 mg, 0.28 mmol) and PEG275 (120 mg, 0.436 mmol). Crabtree's catalyst (2.8 mg, 0.0075 mmol) dissolved in 0.5 mL $CHCl_3$ was added to the resultant solution and shook vigorously for a minute. It was then transferred to a metal dish (fluoropolymer-lined, diameter of 5.25 cm and depth of 3.0 cm) and solution casted in the similar manner to the dry film as described above. The film was dried *in* vacuum at 22 °C for 24 h and then placed in a Parr reactor equipped with an overhead stirrer and sealed. It was pressurized to 600 psig with hydrogen and then vented down to 50 psig. This process was repeated twice more to purge the reactor of air, then pressurized to 600 psig and heated to 100 °C. After 16 h, Parr reactor was cooled, vented and the plasticized SPE was dried under vacuum at 22 °C for 24 h.

2.5.4 Control Experiments

I. Testing the activity of Grubbs' second generation catalyst in the presence of additives

The activity of Grubbs' second-generation catalyst (G2 catalyst) in the presence of additives (LiTFSI and Crabtree's catalyst) was examined by doing control experiments. The cross-linked SPE films discussed above are insoluble and hence cannot be analyzed using NMR and GPC techniques. To gauge the activity of G2 catalyst for the cross-linked system, we studied a solvent processable model copolymer system. COE was copolymerized with PEG-grafted COE[64] using G2 catalyst in the absence and presence of additives to obtain unsaturated copolymers (**3**), which were analyzed by GPC to determine the activity of the G2 catalyst (Scheme 2.4).

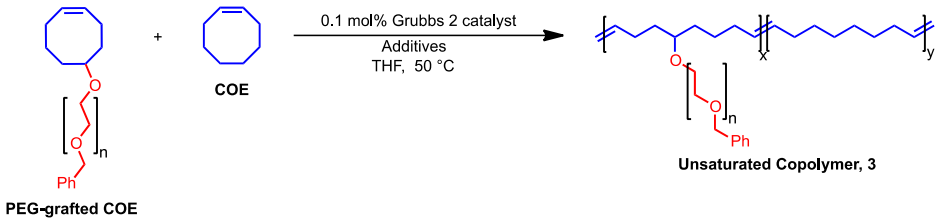

Scheme 2.4 Copolymerization of COE with PEG-grafted COE.

Sample procedure for the synthesis of copolymers of COE and PEG-grafted COE without any additive: PEG-grafted COE (34 mg, 0.051 mmol) with 10 EO units in the graft and COE (85 mg, 0.77 mmol) were combined in a 5 mL scintillation vial and dissolved in 1.0 mL of THF. G2 catalyst (0.7 mg, 0.0008 mmol) dissolved in 0.5 mL

of THF was added to the monomer mixture. The reaction mixture was heated at 50 °C for 3 h, cooled to room temperature, and concentrated under reduced pressure to yield a light brown polymer. The polymer thus obtained was further analyzed by GPC analysis.

Results and discussion

Ring opening metathesis polymerization (ROMP) experiments were done to determine the activity of G2 catalyst in the presence and absence of LiTFSI and Crabtree's catalyst (Table 2.4, entries 1-3). The GPC results indicate that the molecular weights of the unsaturated copolymers change upon addition of LiTFSI and Crabtree's catalyst to the monomer mixture. However, the G2 catalyst was still very active in the presence of these additives, implying that the ROMP should have proceeded efficiently for the PE-PEO cross-linked polymer system as well.

Table 2.4 Control experiments to estimate Grubbs' 2nd catalyst activity for the cross-linked system

Entry No.	LiTFSI (mmol)	Crabtree's catalyst (mol%)	M_n[a] (kg/mol)	M_w/M_n[a]
1	-	-	60	1.8
2	0.038	-	96	1.6
3	0.038	0.5	83	1.4

[a]Number average molecular weight (M_n) and weight average molecular weight (M_w) were determined by THF gel permeation chromatography calibrated with polystyrene standards at 30 °C.

II. Testing the activity of Crabtree's catalyst in the polymer film

To estimate the activity of the hydrogenation catalyst (Crabtree's catalyst), a PEG-grafted COE comonomer was used instead of the PEOX cross-linker (**1**) to obtain soluble hydrogenated copolymer that could be analyzed using ^{1}H NMR spectroscopy. COE was copolymerized with PEG-grafted COE using G2 catalyst in the presence of LiTFSI and Crabtree's catalyst to yield the unsaturated polymer film (Figure 2.11). The unsaturated polymer film was hydrogenated under the same conditions as the cross-linked system to obtain soluble hydrogenated copolymer (**4**). The hydrogenated polymer was analyzed by ^{1}H NMR spectroscopy to determine percent conversion of the hydrogenation reaction.

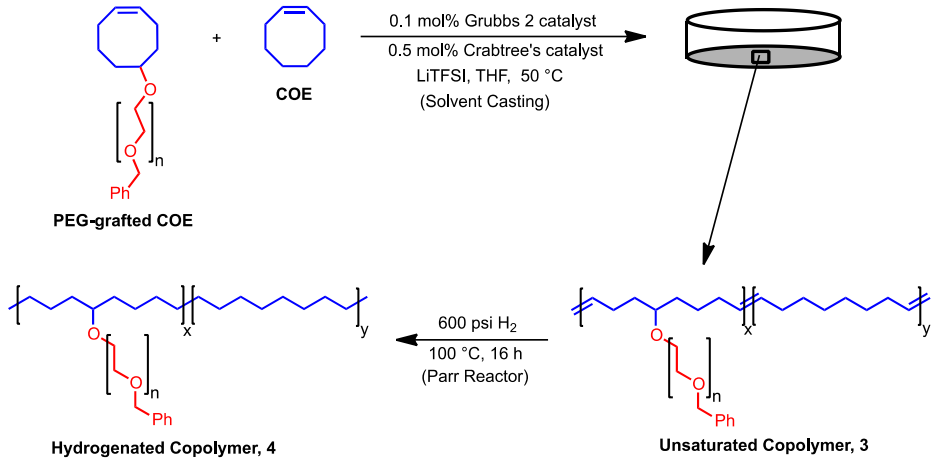

Figure 2.11 Synthesis of soluble hydrogenated copolymer.

Experimental procedure: PEG-grafted COE (66 mg, 0.14 mmol) with 6 EO units in the graft and COE (245 mg, 2.10 mmol) were combined and dissolved in 1.5 mL of THF. G2 catalyst (2.0 mg, 0.0024 mmol) dissolved in 0.5 mL of THF was added to the monomer mixture, followed by addition of LiTFSI (22 mg, 0.070 mmol).

Crabtree's catalyst (9.5 mg, 0.012 mmol) dissolved in 0.5 mL $CHCl_3$ was added to the resultant solution and shaken vigorously for a minute. It was then transferred to a metal dish (fluoropolymer-lined, diameter of 5.25 cm and depth of 3.0 cm) and solution cast in the similar manner to the dry film as described for the cross-linked system. The sticky polymer film was dried in vacuum at 22 °C for 24 h and then placed in a Parr reactor equipped with an overhead stirrer and sealed. It was pressurized to 600 psig with hydrogen and then vented down to 50 psig. This process was repeated twice more to purge the reactor of air, then pressurized to 600 psig and heated to 100 °C. After 16 h, the Parr reactor was cooled to room temperature, vented, and the polymer film was dried under vacuum at 22 °C for 24 h.

Analysis of the soluble hydrogenated copolymer (4)

The hydrogenated polymer was analyzed using ^{1}H NMR spectroscopy measurements. The ^{1}H NMR spectra of the unsaturated copolymer and the hydrogenated copolymer are shown in Figure S5. The integrations of the multiplet signal at δ 5.5 ppm (corresponding to the alkene protons in the polymer backbone and highlighted in the Figure 2.12) were analyzed compared to the integrations of the signal at δ 4.6 ppm (corresponding to the benzylic hydrogens) to determine the percent hydrogenation of unsaturated copolymer. ^{1}H NMR analysis indicated 95% conversion, confirming that the activity of Crabtree's catalyst was still very good in the solid polymer film. This result demonstrated that the catalyst was able to diffuse through the polymer domains of the unsaturated copolymer film and hydrogenate the double bonds along the backbone.

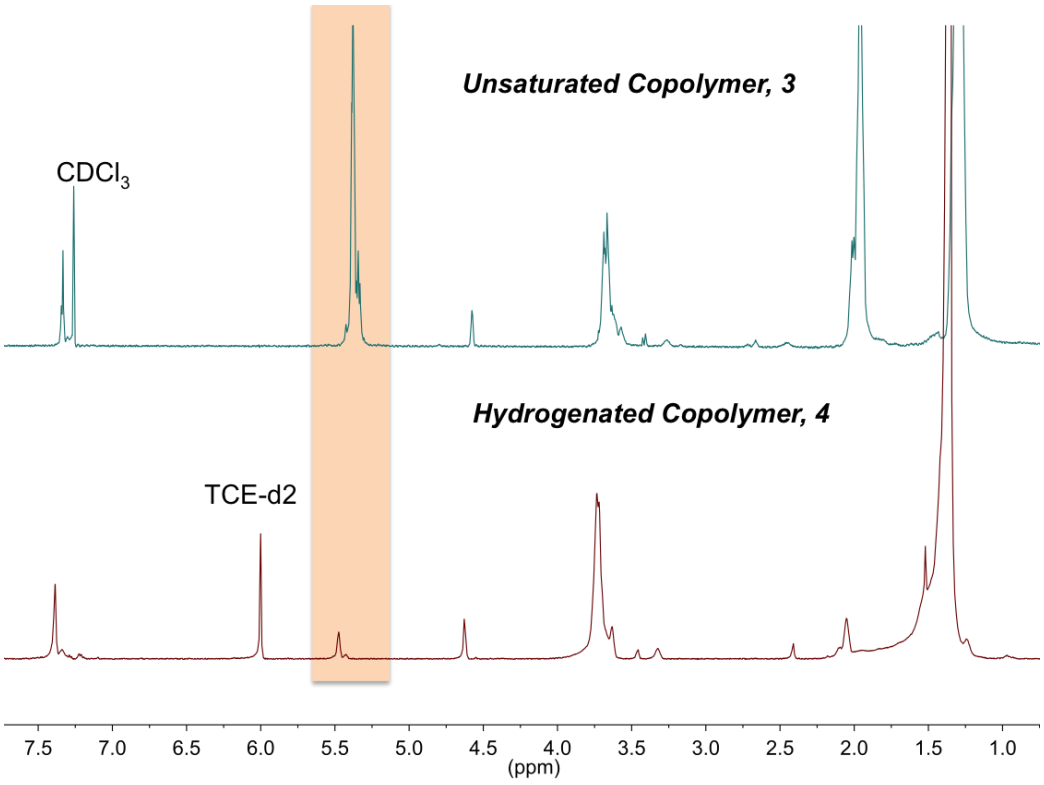

Figure 2.12 ^{1}H NMR spectra of the unsaturated copolymer, **3** (top) and the hydrogenated copolymer, **4** (bottom). The ^{1}H NMR spectrum for **3** was acquired in $CDCl_3$ at 22 °C and the signal at 7.26 ppm in the top spectrum is the residual $CHCl_3$. The ^{1}H NMR spectrum for **4** was acquired in 1,1,2,2-tetrachloroethane-d_2 (TCE-d_2) at 130 °C and the signal at 6.00 ppm in the bottom spectrum is the residual TCE-d_1.

2.5.5 Differential Scanning Calorimetry (DSC)

DSC analysis was performed using a TA Instruments Q1000 instrument equipped with liquid nitrogen cooling system and automated sampler. Typical DSC samples were made in aluminum pans and the method used was 10 °C/ min ramp, with one cycle of heating, cooling, and heating again. The DSC data of the second heat cycle for the unplasticized samples with variable EO units in the PEOX cross-linker (33, 76, and 123) and at [**COE**]:[**1**] loading of 15:1 is shown in Figure 2.13. Electrolytes containing 76 EO units in the **PEOX** cross-linker exhibited the lowest T_g values suggesting that ^{76}PEOX electrolytes had moderately better segmental motion of PEO chains in the SPEs.

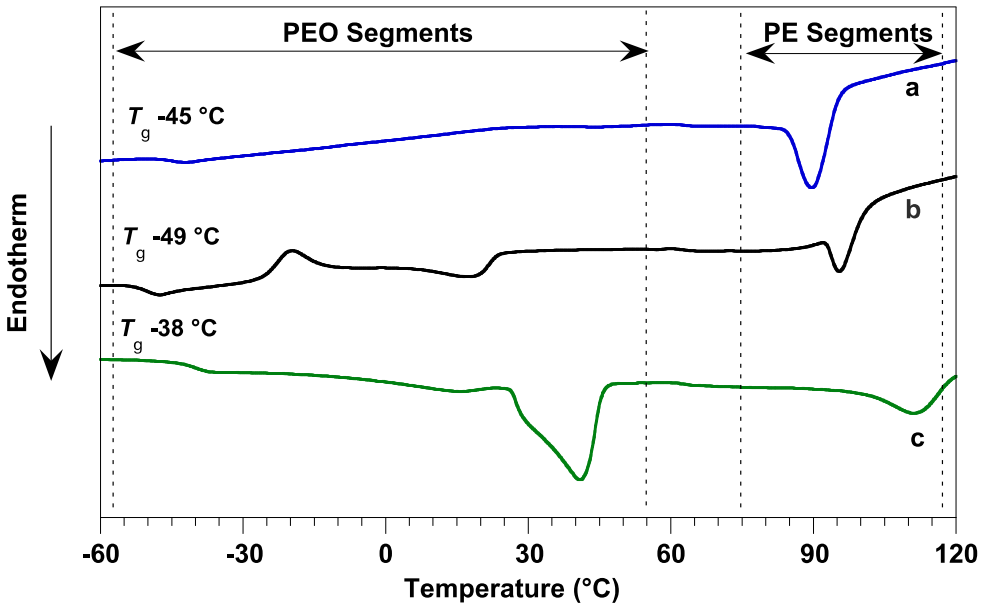

Figure 2.13 DSC traces of the second heat cycle for unplasticized crosslinked solid polymer electrolytes with variable EO units in the cross-linker, **1**. All films had [**COE**]:[**1**] loading of 15:1, and [EO]: [Li] composition of 18:1. a) 33, b) 76, and c) 123 EO units in the cross-linker.

With the aim of increasing the ionic conductivity of these polymer electrolytes, varied amounts of PEG275 plasticizer were added to the polymer framework with the optimized EO units. For the plasticized sample set, a new batch of PEOX cross-linker was synthesized to obtain approximately 76 EO units. Since it is challenging to control the exact amount of EO, the PEOX cross-linker with 70 EO units (^{70}PEOX) was employed instead of ^{76}PEOX cross-linker. DSC traces of the second heat cycle for the ^{70}PEOX electrolytes having different weight% of the PEG275 plasticizer are shown in Figure 2.14.

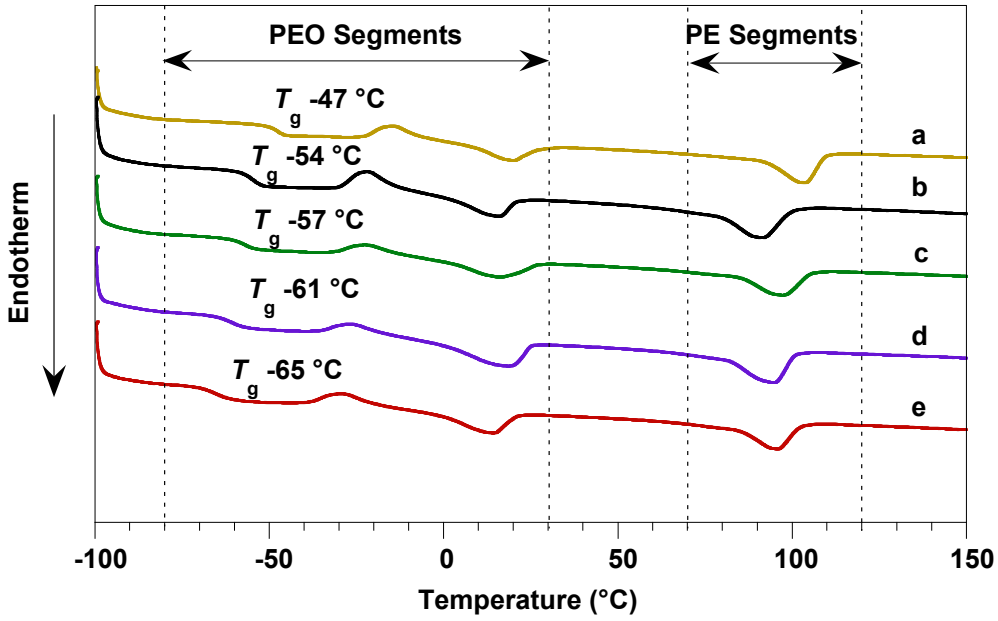

Figure 2.14 DSC traces of second heat cycle of ^{70}PEOX electrolytes having different weight% of the plasticizer. All films had [**COE**]:[**1**] ratio of 15:1 and [EO]:[Li] composition of 18:1. a) 0 wt%, b) 16 wt%, c) 24 wt%, d) 31 wt%, and e) 39 wt% PEG275 plasticizer in the cross-linked films.

2.5.6 DC Ionic Conductivity

The DC ionic conductivity at each temperature was determined from the plateau value of the plot of real part of the conductivity as a function of frequency, as described in seminal work by Jonscher.[65] A sample plot of Re[conductivity] vs. frequency is shown in Figure 2.15. The inset shows a plot of Re[conductivity], Im[conductivity], and tan(delta) at variable frequency for the representative sample at 25 °C.

Conductivity measurements are estimated to be accurate to ±5%, the accuracy of determining the film thicknesses. The DC ionic conductivity values of unplasticized SPEs at variable temperatures are given in Table 2.5. ^{76}PEOX electrolytes exhibited highest ionic conductivity values of around 2.7×10^{-5} S/cm (entries 4–6) at room temperature. This is presumably due to better segmental motion of PEO chains in the ^{76}PEOX SPEs as suggested by the lowest T_g of these ^{76}PEOX electrolytes. At higher temperatures (above 50 °C), the crystalline PEO domains in the ^{123}PEOX electrolytes melted, and hence the conductivity values of ^{76}PEOX and ^{123}PEOX are similar in magnitude. Variable temperature DC ionic conductivity values of plasticized ^{70}PEOX electrolytes with different weight% of PEG275 plasticizer are reported in Table 2.6. The ionic conductivity values for PEO-LiTFSI sample (entry 6) at different temperature are also listed. Below the melting temperature of PEO (<50 °C), all the ^{70}PEOX electrolytes (entries 1–5) showed higher conductivity values than PEO-LiTFSI sample due to the highly crystalline PEO domains in PEO-LiTFSI sample. Most importantly, samples with 31 and 39 wt% of the PEG275 plasticizer (entries 4 and 5) showed conductivity values greater than 1.0×10^{-4} S/cm at ambient

temperature.

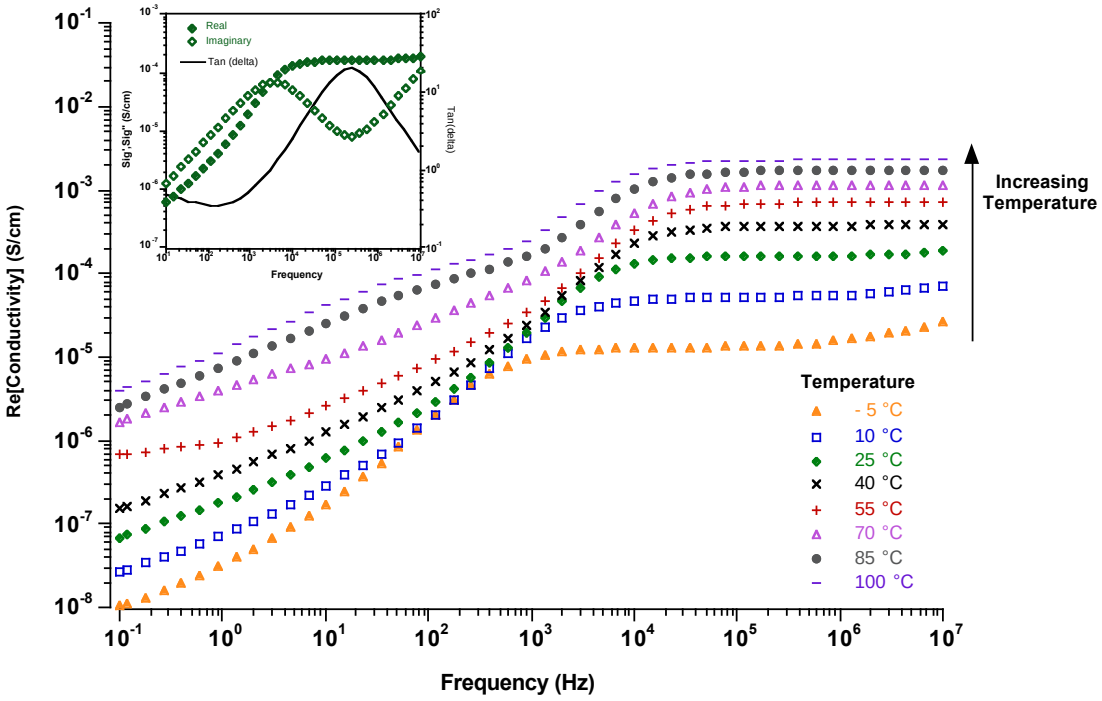

Figure 2.15 Real part of the ionic conductivity vs. frequency plot for (^{70}PEOX$_{0.34}$)(^{34}PE$_{0.35}$)(^{5}PEG$_{0.31}$) sample at variable temperatures. Inset shows the real conductivity (Sig′), imaginary conductivity (Sig″), and tan(delta) vs. frequency plot for (^{70}PEOX$_{0.34}$)(^{34}PE$_{0.35}$)(^{5}PEG$_{0.31}$) electrolyte at 25 °C.

Table 2.5 DC ionic conductivities of unplasticized solid polymer electrolytes[a]

Entry	Sample Name	DC Ionic Conductivity (S/cm)[b]							
		−5 °C	**10 °C**	**25 °C**	**40 °C**	**55 °C**	**70 °C**	**85 °C**	**100 °C**
1	$(^{33}PEOX_{0.32})(^{34}PE_{0.68})$	1.3×10^{-7}	1.1×10^{-6}	5.2×10^{-6}	1.8×10^{-5}	4.5×10^{-5}	9.3×10^{-5}	1.7×10^{-4}	2.5×10^{-4}
2	$(^{33}PEOX_{0.40})(^{24}PE_{0.60})$	1.9×10^{-7}	1.7×10^{-6}	9.0×10^{-6}	3.2×10^{-5}	8.3×10^{-5}	1.8×10^{-4}	3.2×10^{-4}	4.8×10^{-4}
3	$(^{33}PEOX_{0.47})(^{18}PE_{0.53})$	2.0×10^{-7}	1.7×10^{-6}	8.3×10^{-6}	2.8×10^{-5}	7.3×10^{-5}	1.5×10^{-4}	2.6×10^{-4}	4.0×10^{-4}
4	$(^{76}PEOX_{0.51})(^{34}PE_{0.49})$	1.0×10^{-6}	5.0×10^{-6}	2.3×10^{-5}	7.7×10^{-5}	1.9×10^{-4}	3.7×10^{-4}	6.1×10^{-4}	9.0×10^{-4}
5	$(^{76}PEOX_{0.60})(^{24}PE_{0.40})$	2.2×10^{-7}	2.5×10^{-6}	2.8×10^{-5}	1.0×10^{-4}	2.3×10^{-4}	4.6×10^{-4}	7.6×10^{-4}	1.1×10^{-3}
6	$(^{76}PEOX_{0.66})(^{18}PE_{0.34})$	1.3×10^{-6}	8.5×10^{-6}	3.1×10^{-5}	1.1×10^{-4}	2.3×10^{-4}	3.8×10^{-4}	5.3×10^{-4}	7.1×10^{-4}
7	$(^{123}PEOX_{0.64})(^{34}PE_{0.36})$	5.1×10^{-8}	7.8×10^{-7}	8.2×10^{-6}	5.5×10^{-5}	2.0×10^{-4}	4.4×10^{-4}	7.5×10^{-4}	1.1×10^{-3}
8	$(^{123}PEOX_{0.72})(^{24}PE_{0.28})$	4.8×10^{-8}	7.6×10^{-7}	8.4×10^{-6}	5.6×10^{-5}	2.1×10^{-4}	4.0×10^{-4}	6.7×10^{-4}	1.0×10^{-3}
9	$(^{123}PEOX_{0.77})(^{18}PE_{0.23})$	5.2×10^{-8}	7.4×10^{-7}	7.4×10^{-6}	6.2×10^{-5}	2.2×10^{-4}	4.1×10^{-4}	6.7×10^{-4}	1.0×10^{-3}

[a]All films had [EO]:[Li] composition of 18:1; where EO means ethylene oxide units in the PEOX cross-linker. [b]Determined by dielectric spectroscopy measurements.

Table 2.6 DC ionic conductivities of plasticized solid polymer electrolytes[a]

Entry	Sample Name	DC Ionic Conductivity (S/cm)[b]							
		−5 °C	**10 °C**	**25 °C**	**40 °C**	**55 °C**	**70 °C**	**85 °C**	**100 °C**
1[c]	$(^{70}PEOX_{0.50})(^{34}PE_{0.50})$	1.2×10^{-6}	7.6×10^{-6}	3.1×10^{-5}	8.8×10^{-5}	1.8×10^{-4}	3.1×10^{-4}	4.5×10^{-4}	6.1×10^{-4}
2[c]	$(^{70}PEOX_{0.43})(^{34}PE_{0.43})(^{5}PEG_{0.14})$	2.6×10^{-6}	1.4×10^{-5}	5.1×10^{-5}	1.4×10^{-4}	3.1×10^{-4}	5.5×10^{-4}	8.6×10^{-4}	1.2×10^{-3}
3[c]	$(^{70}PEOX_{0.39})(^{34}PE_{0.39})(^{5}PEG_{0.22})$	4.4×10^{-6}	2.1×10^{-5}	7.0×10^{-5}	1.7×10^{-4}	3.6×10^{-4}	6.1×10^{-4}	9.2×10^{-4}	1.2×10^{-3}
4[c]	$(^{70}PEOX_{0.34})(^{34}PE_{0.35})(^{5}PEG_{0.31})$	1.3×10^{-5}	5.2×10^{-5}	1.6×10^{-4}	3.7×10^{-4}	7.0×10^{-4}	1.2×10^{-3}	1.7×10^{-3}	2.3×10^{-3}
5[c]	$(^{70}PEOX_{0.30})(^{34}PE_{0.31})(^{5}PEG_{0.39})$	1.8×10^{-5}	7.1×10^{-5}	2.0×10^{-4}	4.3×10^{-4}	7.9×10^{-4}	1.3×10^{-3}	1.8×10^{-3}	2.6×10^{-3}
6[d]	PEO (900 kDa)	3.6×10^{-8}	7.5×10^{-7}	7.2×10^{-6}	6.6×10^{-5}	3.9×10^{-4}	7.6×10^{-4}	1.2×10^{-3}	1.8×10^{-3}

[a]All films had [EO]:[Li] composition of 18:1; where EO includes ethylene oxide units contained both in the PEOX cross-linker and PEG plasticizer. [b]Determined by dielectric spectroscopy measurements. [c]All films had 70 EO units in the cross-linker and [**COE**]:[**1**] loading of 15:1. [d]Sample PEO (900 kDa) is poly(ethylene oxide), M_n 900 kDa polymer doped with LiTFSI salt having [EO]:[Li] composition of 18:1 for comparison purposes.

2.5.7 Cyclic Voltammetry Measurements

The electrochemical stability window of the SPE was determined by cyclic voltammetry. The cyclic voltammogram of ($^{70}PEOX_{0.34}$)($^{34}PE_{0.35}$)($^{5}PEG_{0.31}$) is shown in Figure 2.16. The cross-linked SPE is stable up to 4.0 V versus Li^{+}/Li, which is in agreement with the previously reported electrochemical stability of PEO-LiTFSI polymer electrolytes.[66]

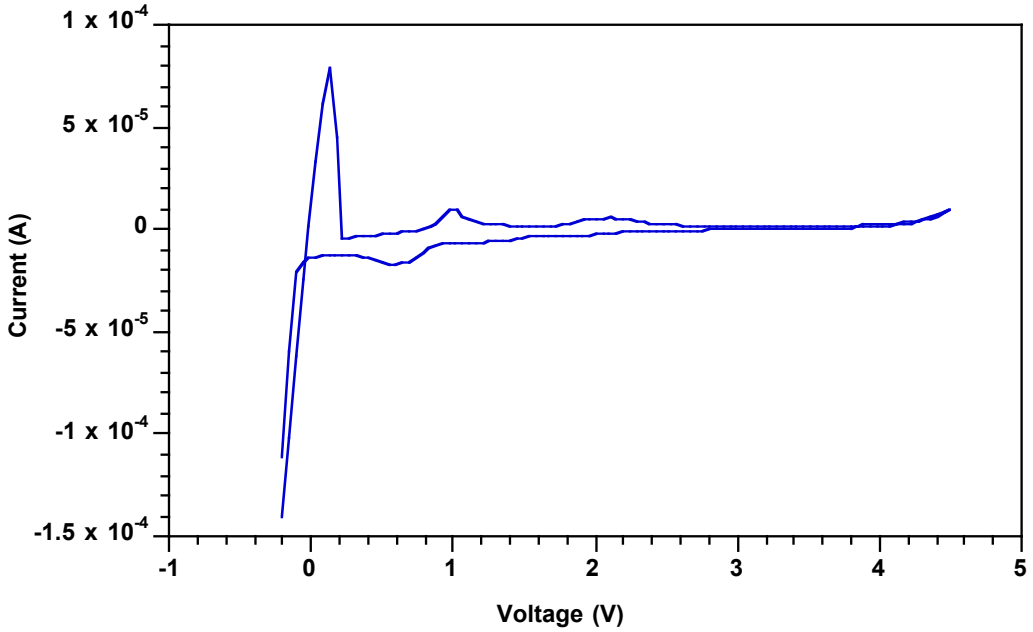

Figure 2.16 Cyclic voltammogram obtained for ($^{70}PEOX_{0.34}$)($^{34}PE_{0.35}$)($^{5}PEG_{0.31}$) at 1.0 mV/s and 22 °C.

2.5.8 Galvanostatic Cycling Measurements

Galvanostatic cycling short-circuit measurements were performed on Li/SPE/Li symmetric coin cells using a Neware CT-3008 battery tester with wiring into (Fisher Scientific and VWR) convection ovens to maintain T = 90 °C. Repeated three hour charge and three hour discharge cycles were performed at the specified current density value, with no rest periods, following an initial 24 hour period of three

hour charge and three hour discharge cycling at a lower current density (10% of the final value). The cells were cycled at constant current density with each half cycle of 3 h until a sudden drop in voltage was observed. This large decline in voltage was attributed to the formation of dendrite short.

2.5.9 Galvanostatic Polarization Measurements

Galvanostatic polarization measurements were performed on Li/SPE/Li symmetric coin cells using a Neware CT-3008 battery tester. These tests were conducted to investigate the efficiency of lithium plating from the cross-linked polymer electrolyte.

Calculation of the predicted short-circuit time via the Chazalviel model

When a cell containing a binary electrolyte undergoes polarization at high current densities, the concentration of anions approaches zero at the deposition interface and a divergence in the potential occurs at Sand's time, τ_s. Chazalviel predicted that the onset time of the dendrite growth for cells containing dilute, binary, monovalent electrolytes operating at high current density follows a power law as a function of the current density, very similar to the Sand's law given by[17]:

$$\tau_s = \pi D \left(\frac{eC_0}{2Jt_a}\right)^2 \quad (1)$$

where τ_s is the Sand's time, D is the ambipolar diffusion coefficient (m^2/s), e is the elementary charge (C), C_0 is the ion concentration ($\#/m^3$), J is the applied current density (A/m^2), and t_a is the anion transference number (non-dimensional).

Previous reports[18,67,68] find that the dendrite nucleation time of symmetric lithium cells containing a PEO-LiTFSI electrolyte undergoing galvanostatic polarization at high current density values is roughly equal to Sand's time and thus fit

the Chazalviel's model. Experimental work has shown that dendrite onset occurs at this timescale even at low current densities, when finite anion concentrations are predicted at the interface and a stable potential exists in cells being galvanostatically polarized at steady-state.[18]

Optical measurements[69] have indicated that the dendrite front advances at the same rate as the anion depletion zone retreats across the cell, at a speed

$$v = \mu_a E \tag{2}$$

where μ_a is the anion mobility ($m^2/V/s$) and the electric field $E = J/\sigma$ (V/m), where σ is the DC ionic conductivity (S/m), at moderate fields, also as predicted by Chazalviel.[5] The time required for dendrites to traverse the distance L between electrodes can therefore be approximated as

$$t_g = \frac{\sigma L}{\mu_a J} \tag{3}$$

where t_g is the dendrite growth time and L is the interelectrode distance. Therefore, the predicted short circuit time, t_{sc} according to the Chazalviel model is

$$t_{sc\ predicted} \approx \tau_s + t_g = \pi D \left(\frac{eC_0}{2Jt_a}\right)^2 + \frac{\sigma L}{\mu_a J} \tag{4}$$

where t_g is the dendrite growth time and τ_s is the Sand's time (dendrite onset time). The short circuit time has been shown by optical measurements to be equivalent to the drop-off in the potential observed during galvanostatic polarization experiments. No immediate drop in the cell potential is observed before the dendrite spans the interelectrode space and short circuits the cell.[68]

Knowledge of the mobile ion concentration in conjuction with ionic conductivity data allows the ambipolar diffusion coefficient D to be calculated using

the Nernst-Einstein equation:

$$D = \frac{\lambda kT}{C_0 q^2} \quad (5)$$

where λ is the molar DC ionic conductivity (S-m^2/mol), k is the Boltzmann constant (J/K), T is temperature (K), and q is the charge of the diffusing species (C). The molar DC ionic conductivity, λ, is related to the measured DC ionic conductivity (σ) *via* the following relationship:

$$\lambda = {}^{\sigma}/_{n} \quad (6)$$

where n is the molar ion concentration (mol/m^3) and .

For the purposes of this publication, C_o of a given electrolyte is calculated by determining the relative volume fractions of the PE and PEO domains by considering the weight fraction of PE and PEO in the copolymer, and assuming that the density of PE is 0.90 g/cm^3, the density of the PEO is 1.1 g/cm^3, and the density of the PEO/LiTFSI domain is 1.38 g/cm^3. PEO doped with LiTFSI to a concentration of 1:18 Li:EO is calculated to have $n = 1.17$ M, assuming an ideal mixture. It is also assumed that all of the LiTFSI is dissociated, contributing to the effective C_0 and to the ionic conductivity, as has been found experimentally for other PEO-LiTFSI electrolytes.[70]

The lithium transference number, t_{Li+}, of electrolyte (^{70}PEOX$_{0.34}$)(^{34}PE$_{0.35}$)(^{5}PEG$_{0.31}$) was measured via the Bruce-Scrosati method[71] to be 0.16 ± 0.01 at 90 °C. Therefore, the anion transference number for this sample is as follows: t_a = 1 - t_{Li+}= 0.84 ± 0.01 at 90 °C. The anion transference number of the other samples under consideration was assumed to be equivalent to this value.

The interelectrode distance, L, was assumed to be equal to the average electrolyte film thickness, 200 μm. Finally, the anion mobility, μ_a, was computed from the Einstein relation as

$$\mu_a = \frac{qDt_a}{kT} \quad (7)$$

The predicted short circuit times ($t_{\text{sc predicted}}$) for the ^{70}PEOX electrolytes with different weight% of the plasticizer were calculated according to the Chazalviel model as given by equation 4. Table 2.7 displays the computed parameters that were used to calculate $t_{sc\ predicted}$ at 90 °C and variable current density values (0.25 – 1.0 mA/cm^2). The representative values of the predicted short-circuit times at 0.26 mA/cm^2 are also shown in Table 2.7.

Table 2.7 Predicted short-circuit times for ^{70}PEOX electrolytes using Chazalviel model[a]

Entry	Sample Name	Sigma, σ (S/cm)	C_o (#/m^3)	D (m^2/s)	μ_a (m^2/V/s)	0.26 mA/cm^2 Current Density		
						τ_s (h)	t_g (h)	$t_{sc\ pred}$ (h)
1	(^{70}PEOX$_{0.50}$)(^{34}PE$_{0.50}$)	5.0×10^{-4}	3.6×10^{26}	2.8×10^{-11}	7.4×10^{-10}	4.1	1.5	5.6
2	(^{70}PEOX$_{0.43}$)(^{34}PE$_{0.43}$)(^{5}PEG$_{0.14}$)	9.6×10^{-4}	4.1×10^{26}	4.6×10^{-11}	1.2×10^{-9}	8.9	1.7	11
3	(^{70}PEOX$_{0.39}$)(^{34}PE$_{0.39}$)(^{5}PEG$_{0.22}$)	1.0×10^{-3}	4.3×10^{26}	4.6×10^{-11}	1.2×10^{-9}	10	1.8	12
4	(^{70}PEOX$_{0.34}$)(^{34}PE$_{0.35}$)(^{5}PEG$_{0.31}$)	1.9×10^{-3}	4.6×10^{26}	8.1×10^{-11}	2.2×10^{-9}	20	1.9	22
5	(^{70}PEOX$_{0.30}$)(^{34}PE$_{0.31}$)(^{5}PEG$_{0.39}$)	2.1×10^{-3}	4.9×10^{26}	8.3×10^{-11}	1.0×10^{-9}	23	2.0	25

[a]All films had 70 EO units in the cross-linker and [**COE**]:[**1**] loading of 15:1. The composition of [EO]:[Li] in each of the sample is 18:1; where EO includes ethylene oxide units contained both in the PEOX cross-linker and PEG plasticizer.

The experimentally observed t_{sc} values were compared to the $t_{sc\ predicted}$ values for the ^{70}PEOX SPEs at variable current density values, and the data are shown in Figure 2.17. We observed an order of magnitude higher t_{sc} values than predicted by Chazalviel model for most compositions of the PE-PEO cross-linked SPEs. While the absolute values of the short-circuit times are well above the t_{sc} values predicted by the model, the functional dependence of the t_{sc} with respect to the applied current density is similar to that predicted by the model.

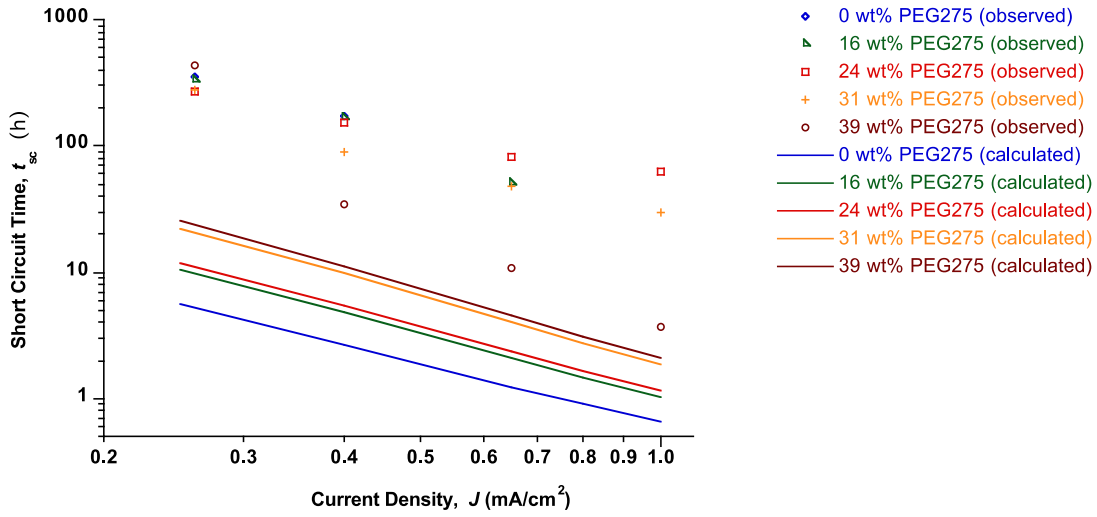

Figure 2.17 Comparison of measured t_{sc} with the predicted short-circuit times for ^{70}PEOX electrolytes having different weight% of the plasticizer at 90 °C. All films had [**COE**]:[**1**] ratio of 15:1 and [EO]:[Li] composition of 18:1. The observed t_{sc} values are shown with hollow symbols and the calculated values as predicted by Chazalviel model are shown as solid lines.

2.5.10 Rheology

The storage $G'(\omega)$ and loss $G''(\omega)$ moduli were quantified using small amplitude oscillatory shear measurements. An Anton Paar Physica MCR 301 rheometer with 10 mm diameter parallel plates was used for rheological measurements. The properties were measured as a function of applied angular frequency at low strain (0.1%) and 90 °C. The shear rheology for the ^{70}PEOX electrolytes (Table 2.3) is displayed in Figure 2.18. Both the unplasticized (0 wt% PEG275) and plasticized polymer electrolytes (16, 24, 31 and 39 wt% PEG275) exhibit solid-like properties, as evident by the frequency independent moduli. Also, the $G'(\omega)$ of these SPEs is an order of magnitude higher than $G''(\omega)$, suggesting that these electrolytes act as an elastic solids. The storage moduli, G' of these PE-PEO cross-linked polymer electrolytes is ~ 10^5 Pa at 90 °C.

The shear rheology measurement for PEO 900 kDa sample at 90 °C was also performed and the data is shown in Figure 2.19. The frequency dependent moduli of PEO sample indicate that it has fluid-like properties as opposed to the PE-PEO cross-linked samples. The storage moduli, G' of the PEO sample was observed to be ~ 4 × 10^4 Pa at 10 rad/s, 0.1% strain and 90 °C.

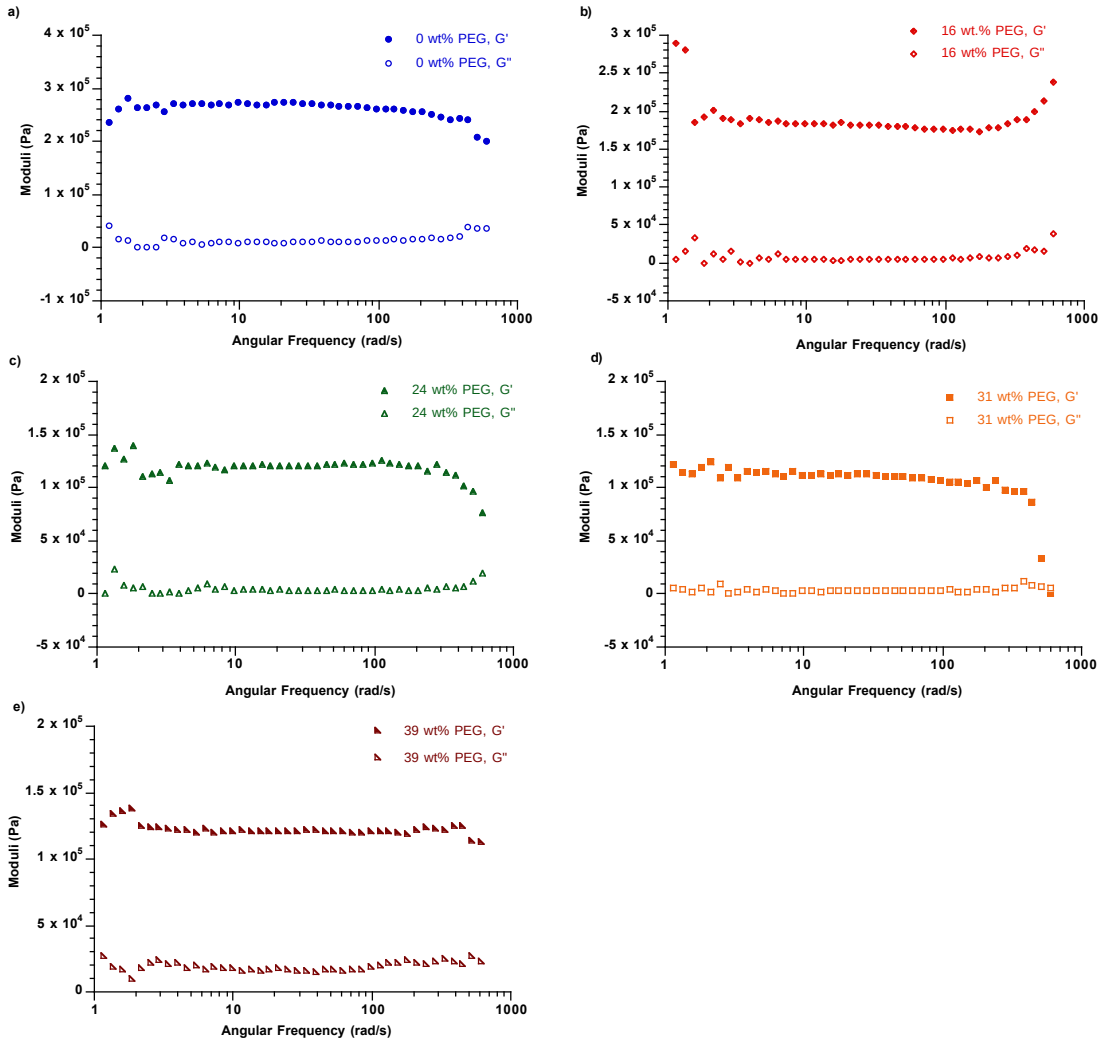

Figure 2.18 Rheological measurements on ^{70}PEOX electrolytes having different weight% of the plasticizer at 90 °C. All films had [**COE**]:[**1**] ratio of 15:1 and [EO]:[Li] composition of 18:1. Storage modulus $G'(\omega)$ is shown with filled symbols, and the loss modulus $G''(\omega)$ is shown with hollow symbols. a) 0 wt%, b) 16 wt%, c) 24 wt%, d) 31 wt%, and e) 39 wt% PEG275 plasticizer in the cross-linked films.

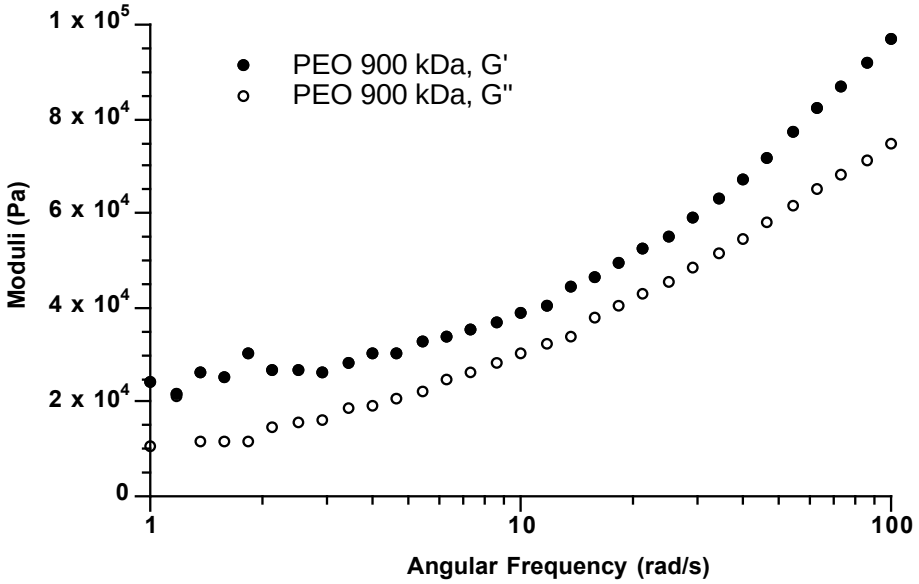

Figure 2.19 Rheological measurements on PEO 900 kDa sample with [EO]:[Li] composition of 18:1 at 90 °C. Storage modulus $G'(\omega)$ is shown with filled symbols, and the loss modulus $G''(\omega)$ is shown with hollow symbols.

2.5.11 Electrochemical Impedance Spectroscopy (EIS)

The ac impedance spectroscopy measurements were made using Li/SPE/Li symmetric coin cells prepared in an argon filled MBraun glovebox, using a Novocontrol Broadband Dielectric Spectrometer fitted with a Quatro temperature control system at frequency ranging from 2 KHz to 900 MHz and at an amplitude of 10 mV. Impedance spectra for the ^{70}PEOX electrolytes were measured as a function of wt% of the plasticizer at 18 °C (Figure 2.20a). The bulk resistance (R_b) of the polymer electrolytes decreases significantly with the increase in the amount of PEG275 in the SPEs, while interfacial resistance (R_i) remains relatively constant. The variable temperature impedance spectra for ($^{70}PEOX_{0.34}$)($^{34}PE_{0.35}$)($^{5}PEG_{0.31}$) are shown in Figure 2.20b. The electrolyte exhibit low interfacial resistance (~10 Ω/cm^2) in contact with lithium metal at 90 °C. Notably, at elevated temperatures the measured interfacial

resistance is lower than that of the bulk resistance.

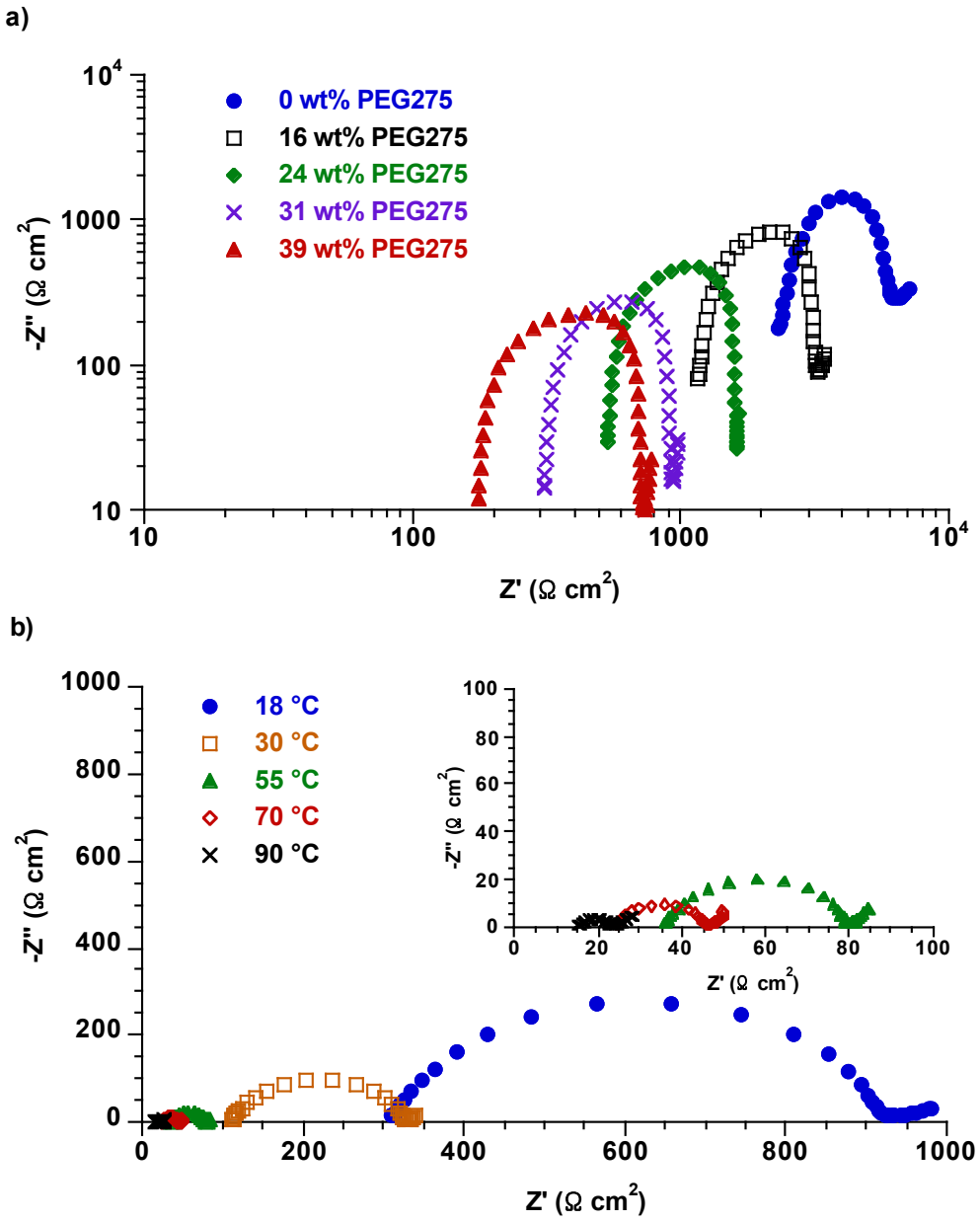

Figure 2.20 a) Impedance spectra for ^{70}PEOX electrolytes with varied plasticizer weight at 18 °C. All films had [**COE**]:[**1**] ratio of 15:1 and [EO]:[Li] composition of 18:1. b) Impedance spectra for ($^{70}PEOX_{0.34}$)($^{34}PE_{0.35}$)($^{5}PEG_{0.31}$) at variable temperature.

2.5.12 Scanning Electron Microscopy

Figure 2.21 displays representative SEM images of the lithium electrodes post-deposition and short-circuiting. In general, the plated lithium electrode after the galvanostatic polarization tests was mostly flat; small areas were observed with finger-like dendrites as shown in Figure 2.22. In contrast, the lithium electrodes post-galvanostatic cycling appeared to have a dense layer of mossy dendrites. This suggests that dendrites did not form immediately prior to short-circuit of the cycling cells, but likely grew through the electrolyte film over a period of multiple plating/stripping cycles.

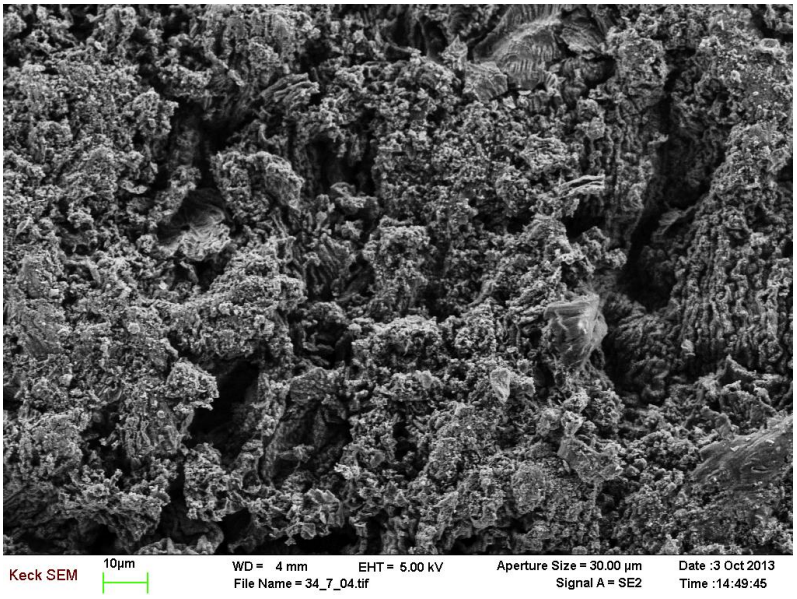

Figure 2.21 Scanning electron micrographs of the plated lithium electrodes for $(^{70}PEOX_{0.34})(^{34}PE_{0.35})(^{5}PEG_{0.31})$ electrolyte after short-circuit from galvanostatic cycling at 0.4 mA/cm^2 and 90 °C.

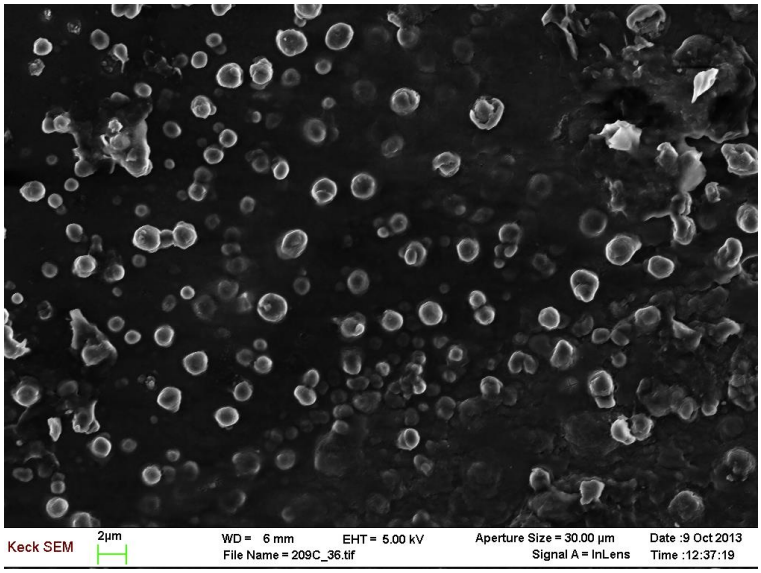

Figure 2.22 Scanning electron micrographs of the plated lithium electrodes for ($^{70}PEOX_{0.34}$)($^{34}PE_{0.35}$)($^{5}PEG_{0.31}$) electrolyte after short-circuit from galvanostatic polarization at 0.2 mA/cm^2 and 90 °C.

2.5.12 Small Angle X-Ray Scattering Data

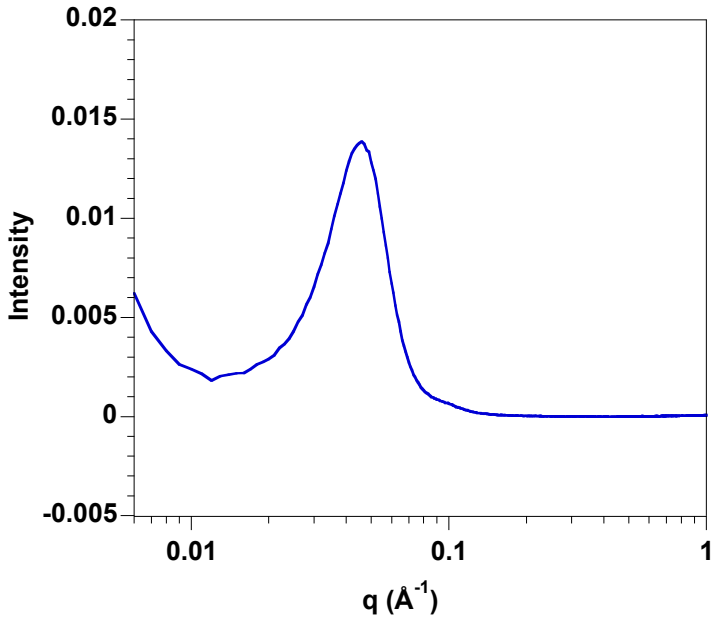

Figure 2.23 Small Angle X-ray Scattering (SAXS) profiles of scattering angle intensity as a function of wavevector (q) for ($^{70}PEOX_{0.34}$)($^{34}PE_{0.35}$)($^{5}PEG_{0.31}$) electrolyte.

REFERENCES

(1) Tarascon, J. M.; Armand, M. *Nature* **2001**, *414*, 359–367.

(2) Goodenough, J. B.; Park, K. S. *J. Am. Chem. Soc.* **2013**, *135*, 1167–1176.

(3) Goodenough, J. B.; Kim, Y. *Chem. Mater.* **2010**, *22*, 587–603.

(4) Xu, K. *Chem. Rev.* **2004**, *104*, 4303–4417.

(5) Jacoby, M. *Chem. Eng. News* **2013**, *91(6)*, 33–37.

(6) Vehicle Technology Program, U. D. Multi-year program plan, 2011–2015. http://www1.eere.energy.gov/vehiclesandfuels/pdfs/program/vt_mypp_2011-2015.pdf.

(7) Armand, M.; Tarascon, J. M. *Nature* **2008**, *451*, 652–657.

(8) Scrosati, B.; Garche, J. *J. Power Sources* **2010**, *195*, 2419–2430.

(9) Zu, C. X.; Li, H. *Energ. Environ. Sci.* **2011**, *4*, 2614–2624.

(10) Yoshimatsu, I.; Hirai, T.; Yamaki, J. *J. Electrochem. Soc.* **1988**, *135*, 2422–2427.

(11) Ishikawa, M.; Kawasaki, H.; Yoshimoto, N.; Morita, M. *J. Power Sources* **2005**, *146*, 199–203.

(12) Stark, J. K.; Ding, Y.; Kohl, P. A. *J. Electrochem. Soc.* **2011**, *158*, A1100–A1105.

(13) Zhamu, A.; Chen, G. R.; Liu, C. G.; Neff, D.; Fang, Q.; Yu, Z. N.; Xiong, W.; Wang, Y. B.; Wang, X. Q.; Jang, B. Z. *Energ. Environ. Sci.* **2012**, *5*, 5701–5707.

(14) Gireaud, L.; Grugeon, S.; Laruelle, S.; Yrieix, B.; Tarascon, J. M. *Electrochem. Commun.* **2006**, *8*, 1639–1649.

(15) Mogi, R.; Inaba, M.; Jeong, S. K.; Iriyama, Y.; Abe, T.; Ogumi, Z. *J. Electrochem. Soc.* **2002**, *149*, A1578–A1583.

(16) Ota, H.; Wang, X. M.; Yasukawa, E. *J. Electrochem. Soc.* **2004**, *151*, A427–A436.

(17) Chazalviel, J. N. *Phys. Rev. A* **1990**, *42*, 7355–7367.

(18) Rosso, M.; Gobron, T.; Brissot, C.; Chazalviel, J. N.; Lascaud, S. *J. Power Sources* **2001**, *97-8*, 804–806.

(19) Monroe, C.; Newman, J. *J. Electrochem. Soc.* **2005**, *152*, A396–A404.

(20) Stone, G. M.; Mullin, S. A.; Teran, A. A.; Hallinan, D. T., Jr.; Minor, A. M.; Hexemer, A.; Balsara, N. P. *J. Electrochem. Soc.* **2012**, *159*, A222–A227.

(21) Singh, M.; Odusanya, O.; Wilmes, G. M.; Eitouni, H. B.; Gomez, E. D.; Patel, A. J.; Chen, V. L.; Park, M. J.; Fragouli, P.; Iatrou, H.; Hadjichristidis, N.; Cookson, D.; Balsara, N. P. *Macromolecules* **2007**, *40*, 4578–4585.

(22) Fenton, D. E.; Parker, J. M.; Wright, P. V. *Polymer* **1973**, *14*, 589–589.

(23) Armand, M. B.; Chabagno, J. M.; Duclot, N. J. *Fast Ion Transport in Solids: Electrodes, and Electrolytes*; Lake Geneva, Wisconsin, U.S.A., May 21−25,1979; Vashishta, P.; Mundy, J. N.; Shenoy, G. K., Eds; North Holland: New York, 1979.

(24) Lenest, J. F.; Callens, S.; Gandini, A.; Armand, M. *Electrochim. Acta* **1992**, *37*, 1585–1588.

(25) Armand, M. *Solid State Ionics* **1983**, *9-10*, 745–754.

(26) Kono, M.; Hayashi, E.; Watanabe, M. *J. Electrochem. Soc.* **1998**, *145*, 1521–1527.

(27) Watanabe, M.; Nishimoto, A. *Solid State Ionics* **1995**, *79*, 306–312.

(28) Alloin, F.; Sanchez, J. Y.; Armand, M. *J. Electrochem. Soc.* **1994**, *141*, 1915–1920.

(29) Aihara, Y.; Kuratomi, J.; Bando, T.; Iguchi, T.; Yoshida, H.; Ono, T.; Kuwana, K. *J. Power Sources* **2003**, *114*, 96–104.

(30) Nishimoto, A.; Agehara, K.; Furuya, N.; Watanabe, T.; Watanabe, M. *Macromolecules* **1999**, *32*, 1541–1548.

(31) Snyder, J. F.; Carter, R. H.; Wetzel, E. D. *Chem. Mater.* **2007**, *19*, 3793–3801.

(32) Sun, X. G.; Reeder, C. L.; Kerr, J. B. *Macromolecules* **2004**, *37*, 2219–2227.

(33) Laik, B.; Legrand, L.; Chausse, A.; Messina, R. *Electrochim. Acta* **1998**, *44*, 773–780.

(34) Kim, G. T.; Appetecchi, G. B.; Carewska, M.; Joost, M.; Balducci, A.; Winter, M.; Passerini, S. *J. Power Sources* **2010**, *195*, 6130–6137.

(35) Rupp, B.; Schmuck, M.; Balducci, A.; Winter, M.; Kern, W. *Eur. Polym. J.* **2008**, *44*, 2986–2990.

(36) Matsumoto, K.; Endo, T. *J. Polym. Sci., Part A: Polym. Chem.* **2011**, *49*, 3582–3587.

(37) Schulze, M. W.; McIntosh, L. D.; Hillmyer, M. A.; Lodge, T. P. *Nano Lett.* **2014**, *14*, 122–126.

(38) Lee, J. I.; Kim, D. W.; Lee, C.; Kang, Y. *J. Power Sources* **2010**, *195*, 6138–6142.

(39) Wang, L.; Li, N.; He, X. M.; Wan, C. R.; Jiang, C. Y. *Electrochim. Acta* **2012**, *68*, 214–219.

(40) Borghini, M. C.; Mastragostino, M.; Zanelli, A. *Electrochim. Acta* **1996**, *41*, 2369–2373.

(41) Morita, M.; Fukumasa, T.; Motoda, M.; Tsutsumi, H.; Matsuda, Y. *J. Electrochem. Soc.* **1990**, *137*, 3401–3404.

(42) Tatsuma, T.; Taguchi, M.; Oyama, N. *Electrochim. Acta* **2001**, *46*, 1201–1205.

(43) Tatsuma, T.; Taguchi, M.; Iwaku, M.; Sotomura, T.; Oyama, N. *J. Electroanal. Chem.* **1999**, *472*, 142–146.

(44) Robertson, N. J.; Kostalik, H. A.; Clark, T. J.; Mutolo, P. F.; Abruña, H. D.; Coates, G. W. *J. Am. Chem. Soc.* **2010**, *132*, 3400–3404.

(45) Shindoh, N.; Takemoto, Y.; Takasu, K. *Chem.—Eur. J.* **2009**, *15*, 12168–12179.

(46) The non-symmetrical design results in higher purity than the symmetrical coupling COE-O$(CH_2CH_2O)_n^-$ anions with p-dibromoxylene. For a related structure that was used to create capsules *via* ROMP, see Emrick, T. S.; Brietenkamp, K. US Patent 7,598,313 (2009).

(47) The reaction mixture for polymer casting also contained hydrogenation catalyst (Crabtree's catalyst) and lithium bis(trifluoromethanesulfonyl)imide (LiTFSI) ([EO]:[Li] = 18:1). The activity of the Grubbs G2 catalyst in the presence of TFSI anion and Crabtree's catalyst was confirmed by control experiments. COE was copolymerized with PEG-grafted COE using Grubbs' G2 catalyst in the presence and absence of additives to obtain copolymers, and the number average molecular weights (M_ns) of these polymers were determined using GPC. The activity of the Grubbs' G2 catalyst was found to be comparable with

or without the presence of additives. See Experimental Section for more details.

(48) The efficiency of hydrogenation step of the cross-linked unsaturated SPE films was confirmed by a control experiment. COE (**1**) was copolymerized with mono-COE terminated PEG in the presence of lithium bis(trifluorosulfonyl) imide (LiTFSI) ([EO]:[Li] = 18:1) using Grubbs' G2 catalyst to obtain a non-crosslinked, unsaturated film. The film was subsequently hydrogenated in the same manner as the cross-linked films. The hydrogenation reaction occured with 95% reduction of main-chain alkenes, as confirmed by ^{1}H NMR spectroscopy. See Experimental Section for details. Similar solid state hydrogenation reactions have been previously reported using Crabtree's catalyst for polystyrene-*b*-polybutadiene-*b*-polystyrene block copolymer. For details, see: Gilliom, L. R.; Honnell, K. G. Macromolecules **1992**, *25*, 6066–6068.

(49) He and co-workers observed similar cold crystallization peaks for PEO-$LiClO_4$ network polymer electrolytes in the presence of star plasticizers. See reference 39 for more details.

(50) Arora, P.; Zhang, Z. M. *Chem. Rev.* **2004**, 104, 4419–4462.

(51) Berthier, C.; Gorecki, W.; Minier, M.; Armand, M. B.; Chabagno, J. M.; Rigaud, P. *Solid State Ionics* **1983**, 11, 91–95.

(52) Barteau, K. P.; Wolffs, M.; Lynd, N. A.; Fredrickson, G. H.; Krarner, E. J.; Hawker, C. J. *Macromolecules* **2013**, 46, 8988–8994.

(53) For the plasticized sample set, a new sample of PEOX cross-linker was

synthesized to obtain approximately 76 EO units. Since it is challenging to control the exact amount of EO, the PEOX cross-linker with 70 EO units (^{70}PEOX) was employed instead of ^{76}PEOX cross-linker. .

(54) Lee, Y. M.; Ko, D. H.; Lee, J. Y.; Park, J. K. *Electrochim. Acta* **2006**, 52, 1582–1587.

(55) Cycling tests for ($^{70}PEOX_{0.34}$)($^{34}PE_{0.35}$)($^{5}PEG_{0.31}$) polymer electrolyte were performed on two different symmetric coin cells at 0.26 mA/cm^2 and 90 °C; C_d values of 1707 C/cm^2 and 1881 C/cm^2 were recorded for these cells and the average value is reported in the text.

(56) Gurevitch, I.; Buonsanti, R.; Teran, A. A.; Gludovatz, B.; Ritchie, R. O.; Cabana, J.; Balsara, N. P. *J. Electrochem. Soc.* **2013**, *160*, A1611–A1617.

(57) The charge-discharge cycle used in the latest report was different than their previous studies on PS-*b*-PEO block copolymers (4 hours compared to 3 hours in the previous report).

(58) Tu, Z. Y.; Kambe, Y.; Lu, Y. Y.; Archer, L. A. *Adv. Energy Mater.* **2014**, *4*, 1300654/1−1300654/6.

(59) See Experimental Section for details.

(60) Liu, S.; Imanishi, N.; Zhang, T.; Hirano, A.; Takeda, Y.; Yamamoto, O.; Yang, J. J. Power Sources **2010**, 195, 6847–6853.

(61) Liu, S.; Imanishi, N.; Zhang, T.; Hirano, A.; Takeda, Y.; Yamamoto, O.; Yang, J. *J. Electrochem. Soc.* **2010**, *157*, A1092–A1098.

(62) Liu, S.; Wang, H.; Imanishi, N.; Zhang, T.; Hirano, A.; Takeda, Y.; Yamamoto, O.; Yang, J. *J. Power Sources* **2011**, *196*, 7681–7686.

(63) Hillmyer, M. A.; Laredo, W. R.; Grubbs, R. H. *Macromolecules* **1995**, *28*, 6311–6316.

(64) PEG-grafted COE was prepared using a living anionic polymerization method, which is similar to the procedure descibed above for the preparation of the PEO-functionalized cross-linker (**1**). Benzyl bromide was used as a capping agent for the preparation of PEG-grafted COE instead of **2** for the synthesis of cross-linker **1**.

(65) Jonscher, A. K. *Nature* **1977**, *267*, 673–679.

(66) Cheung, I. W.; Chin, K. B.; Greene, E. R.; Smart, M. C.; Abbrent, S.; Greenbaum, S. G.; Prakash, G. K. S.; Surampudi, S. *Electrochim. Acta* **2003**, *48*, 2149–2156.

(67) Brissot, C.; Rosso, M.; Chazalviel, J. N.; Lascaud, S. *J. Power Sources* **1999**, *81*, 925–929.

(68) Rosso, M.; Brissot, C.; Teyssot, A.; Dolle, M.; Sannier, L.; Tarascon, J. M.; Bouchetc, R.; Lascaud, S. *Electrochim. Acta* **2006**, *51*, 5334–5340.

(69) Brissot, C.; Rosso, M.; Chazalviel, J. N.; Lascaud, S. *J. Electrochem. Soc.* **1999**, *146*, 4393–4400.

(70) Johansson, A.; Gogoll, A.; Tegenfeldt, J. *Polymer* **1996**, *37*, 1387–1393.

(71) Bruce, P. G.; Evans, J.; Vincent, C. A. *Solid State Ionics* **1988**, *28*, 918–922.

CHAPTER 3

Binary Salt-Doped Tetraphenylborate Tethered Li-Ion Conducting Ionomers: Synthesis, Characterization, and Applications for Lithium Metal Batteries

CHAPTER 3

Binary Salt-Doped Tetraphenylborate Tethered Li-Ion Conducting Ionomers: Synthesis, Characterization, and Applications for Lithium Metal Batteries

3.1 Abstract

We report a new class of 'binary salt-doped single-ion conductor (mixed SIC)' electrolytes for Li-ion conduction. These mixed SICs were synthesized using ring opening metathesis polymerization chemistry and evaluated as electrolytes for lithium battery applications. A weakly coordinating tetraphenylborate anion was covalently attached to a rigid polyethylene backbone in a polyethylene/poly(ethylene oxide) (PE/PEO) cross-linked polymer, and further doped with a binary lithium salt ($LiBPh_4$) to develop these mixed SICs. A systematic investigation of the effect of different fractions of immobilized borate anions on the thermal properties, electrochemical stability, and ionic conductivities of the electrolytes is reported. At similar Li^+ ion concentration, the increase in binary salt content in the mixed SIC system led to a significant increase in ionic conductivity values. However, the electrochemical stability of the single-ion electrolyte was observed to decrease upon doping with the binary lithium salt. The results reported in this study demonstrate that these modular mixed SICs are an interesting platform to obtain high ionic conductivities and tunable electrochemical stabilities.

3.2 Introduction

Reducing greenhouse gas emissions and achieving a sustainable energy supply have been long-standing goals for mankind. Rechargeable batteries are considered an excellent means of storing and supplying large amounts of energy for sustainable transportation options, like electric vehicles and hybrid-electric vehicles, and grid energy storage applications.[1-3] Li-ion batteries (LIBs) have gained notable attention for automotive applications due to their high energy density compared to other battery technologies.[4-6] However, the inherent flammability of their liquid electrolyte components raises safety concerns. In contrast to liquid electrolytes, solid polymer electrolytes (SPEs) are less flammable and therefore considered to be safer alternatives to their liquid counterparts in LIBs.[7] Additionally, these SPEs allow the miniaturization of devices, allowing higher energy density values. However, like the liquid electrolytes, most of the lithium salt-doped SPEs have low lithium-ion transference numbers (t_{Li+}), unacceptably low ionic conductivities at room temperature, and unsatisfactory electrochemical performance.[8,9] The poor electrochemical performance is proposed to arise from the ionic concentration gradients within the cell, which produce physical and chemical changes at the electrode/electrolyte interface that lead to high internal and interfacial resistance (Figure 3.1a).[10]

Single-ion conductors (SICs), in which anions are tethered to the polymer backbone have long been proposed as an ideal candidate to achieve superior battery performance (Figure 3.1b).[8] Single-ion conductors offer number of advantages, such as t_{Li+} approaching unity and the absence of concentration polarization effects.[9,11] Despite these attractive features, their practical applications are limited due to low

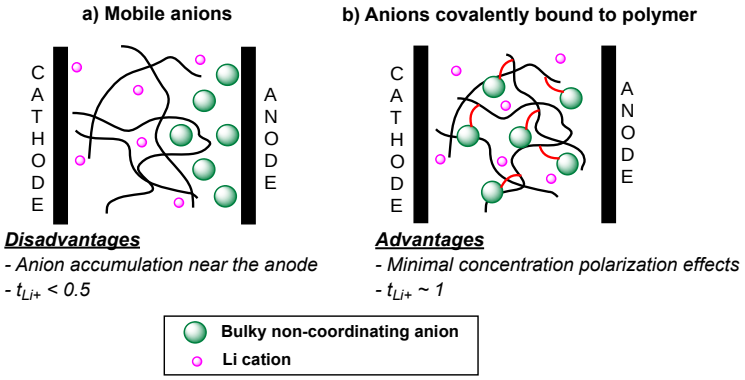

Figure 3.1 Li-ion conduction during charge in polymer electrolytes. a) Polymer electrolytes containing mobile anions. b) Single-ion conductors with anions covalently bound to the polymer.

room temperature ionic conductivity ($<10^{-4}$ S/cm at 25 °C). Ionic conductivity of the SICs is strongly influenced by the nature of the anions tethered to the polymer backbone. Numerous anions such as carboxylate,[12] alkyl sulfonate,[13,14] bis(allylmalonato)borate,[15-17] and trifluoromethylsulfonimide[18-22] have been anchored to the polymer backbone to obtain Li^+ conducting polyelectrolytes. To increase the Li^+ ion mobility and improve the battery performance, current research efforts are focused on developing new anions, which facilitate better delocalization of negative charge, decrease the ion-pair dissociation energy and thus increase the concentration of mobile Li^+ ions. Theoretical calculations have suggested that trifluoromethylsulfonimide ($N(SO_2CF_3)_2^-$; TFSI) and tetraphenylborate (BPh_4^-; TPB) anions have relatively low ion-dissociation energy.[23] While a variety of TFSI tethered single-ion electrolytes have been investigated in the literature,[18-22] only few SIC reports have examined the effect of covalently bound BPh_4^- anions on the electrolyte's properties.[24,25] Moreover, TFSI anions are known to corrode the aluminum current collector in a lithium based battery device.[26] We were interested in exploring the effect

of weakly coordinating BPh_4^- anion in the SIC electrolyte because of their non-toxic and hydrolytically stable nature.[27] Previously, Colby and co-workers reported TPB containing SICs in which the BPh_4^- anions were tethered on a low T_g polysiloxane backbone.[24,25] Although these poly(ethylene glycol) (PEG; M_n 600 Da)-doped and TPB tethered polysiloxane ionomers exhibited reasonable ionic conductivity at ambient temperature ($10^{-5.2}$ S/cm for the 70 wt% PEG-doped composition at 25 °C),[24] the mechanical properties of the polysiloxane ionomers are expected to be extremely poor, preventing their use as a separator in a battery device. In contrast to the previously reported ionomers, we aimed to tether these weakly coordinating BPh_4^- anions on a mechanically rigid polyethylene (PE) backbone in a polyethylene/poly(ethylene oxide) (PE/PEO) framework. The specific PE/PEO framework used in the study was also selected based on their unprecedented lithium dendrite growth resistance in high energy Li-metal batteries (LMB) reported in our previous study.[28]

Recently, Tikekar et al. proposed a theoretical model, which suggests that the lifetime of a LMB may be improved by use of a mixed conducting system, e.g. doping of a single-ion conducting electrolyte containing immobilized anions with a free lithium salt.[29] Significantly, their calculations predicts that the presence of even a low fraction of immobilized anions (10%) should decrease the potential at the electrode/electrolyte interface, and thereby increase the stability of lithium electrodeposits compared to conventional liquid electrolytes. Inspired by this theory, we sought to develop binary lithium salt-doped single-ion conductors with variable fractions of immobilized anions. Beyond the benefits anticipated from the theory, we

anticipate that in these binary lithium salt-doped polyelectrolytes, the immobilized anions would serve to decrease the detrimental ionic concentration gradients, and the free lithium salt would increase the conductivity of the electrolyte.

Although there have been previous reports on lithium-ion conducting SICs, none of these SIC electrolytes have been doped with a binary lithium salt. Our specific interest in this first study is two-fold. First, to quantify and study the effect of different fractions of immobilized anion on the electrochemical properties of the polymer electrolyte. And, second to evaluate the effect of the binary salt content in the electrolyte on ionic conductivity and electrochemical stability of the SICs. We prepared a series of binary salt-doped SICs containing varying fractions of covalently bound anions to the polymer backbone. Tetraphenylborate anions were selected due to their weakly coordinating nature,[27] and were immobilized on the mechanically rigid polyethylene backbone. A binary lithium salt, namely lithium tetraphenylborate ($LiBPh_4$) was also added during the preparation of these electrolyte formulations. These ionomers were synthesized using ring opening metathesis chemistry and further tested as Li-ion conducting electrolytes for LMB applications.

3.3 Results and Discussion

3.3.1 Single-Ion Conductors (SICs)

To enhance Li^+ ion mobility, increase the Li^+ ion transport number, achieve higher conductivity, and minimize concentration polarization effects, we sought to develop a lithium-ion conducting ionomer with bulky non-coordinating anions, namely tetraphenylborate anions tethered to the polyethylene backbone. Previously, we reported a polyethylene/poly(ethylene oxide) (PE/PEO) cross-linked solid polymer

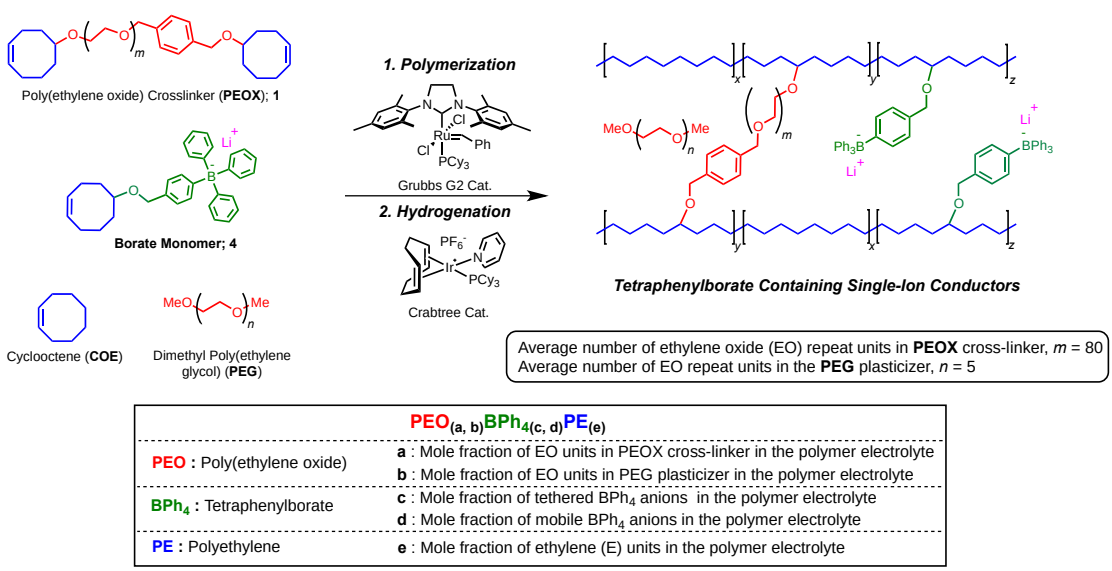

Figure 3.2 Synthesis and nomenclature of tetraphenylborate containing network polyethylene/ poly(ethylene oxide) single-ion conductors.

electrolyte (SPE), which was synthesized using ring opening metathesis polymerization (ROMP).[28] This unique demonstrated high ionic conductivity and excellent dendrite growth resistance at the lithium metal anode. In the current investigation, a similar ROMP strategy was used to synthesize tetraphenylborate containing polymer electrolytes, wherein the borate anion was tethered to the polyethylene (PE) backbone and the SPE was chemically cross-linked by poly(ethylene oxide) (PEO) segments (Figure 3.2) Previous studies on the unplasticized PE/PEO cross-linked system suggested that the number of ethylene oxide (EO) units in the cross-links played a crucial role in affecting the segmental motion of the PEO chains.[28] Therefore, in the current study, we synthesized the SICs with the optimum cross-linker length (80 EO units in the cross-linker), as shown in Figure 3.2. Furthermore, inspired by the higher ionic conductivities reported by Colby and co-workers for the plasticized polysiloxane ionomers compared to the host

ionomer,[24] we incorporated 31 weight% (wt%) of a non-volatile plasticizer, poly(ethylene glycol) with M_n = 275 Da in our PE/PEO cross-linked ionomers.

Due to the functional group tolerance of the Grubbs' second-generation (G2) catalyst, we chose to employ a ROMP strategy to polymerize functional comonomers, such as poly(ethylene oxide) cross-linker (PEOX; **1)** and borate monomer (**4**). The cross-linker **1** was synthesized using anionic polymerization in excellent yields, and the borate monomer (**4**) was prepared *via* the reaction of a Grignard reagent with triphenylborane.[30] The copolymerization of cyclooctene (COE) with comonomers **1** and **4** using G2 catalyst in a Teflon-lined dish at 50 °C led to the formation of thin polymer films (~150 μm). These polymer films were subsequently hydrogenated in the solid state using Crabtree's catalyst to yield mechanically strong tetraphenylborate containing single-ion conductors (SICs).[31]

To obtain the optimum borate ion content for the Li^+ ion conductivity in these SICs, polyelectrolytes with variable ion contents were prepared by changing the [COE]:[**4**] ratios, while keeping the cross-linking density of the network SIC similar for all the compositions, i.e. [**1**]: ([COE]+[**4**]) loading of 1:15. To gain better understanding of these SICs, the thermal properties of these electrolytes were studied using differential scanning calorimetry (DSC) and the data are summarized in Table 3.1. The crystallization of the PEO domains in the polymer was completely inhibited when the weight% of **4** in the ionomers was increased from 15 wt% (Table 3.1, entry 1) to 31 wt% (Table 3.1, entry 5). We hypothesize that this is due to increase in the concentration of dissociated Li^+ ion at higher weight% of the borate monomer, which leads to higher concentration of solvated Li^+ ion in the PEO domains, thereby

Table 3.1 Compositions and thermal transitions of PE/PEO single-ion conductors[a]

Entry	Single-Ion Conductor Sample	[COE]: [4]	Weight% of the Borate Monomer	[EO]: [Li] ratio[b]	PE Segments[c]		PEO Segments[d]			
					T_m[e] (°C)	ΔH_{fus}[e] (J/g)	T_g[e] (°C)	T_c[e] (°C)	T_m[e] (°C)	ΔH_{fus}[e] (J/g)
1	PEO $_{(0.394,\ 0.283)}$ $BPh_{4\ (0.015,\ 0)}$ PE $_{(0.308)}$	3.4	15	44	70	6.8	−55	−23	28	25.1
2	PEO $_{(0.384,\ 0.294)}$ $BPh_{4\ (0.020,\ 0)}$ PE $_{(0.302)}$	2.3	19	34	57	1.9	−52	−5	26	3.3
3	PEO $_{(0.378,\ 0.303)}$ $BPh_{4\ (0.023,\ 0)}$ PE $_{(0.296)}$	1.8	22	29	n.d.[f]	n.d.[f]	−44	n.d.[f]	n.d.[f]	n.d.[f]
4	PEO $_{(0.373,\ 0.318)}$ $BPh_{4\ (0.028,\ 0)}$ PE $_{(0.281)}$	1.2	25	25	n.d.[f]	n.d.[f]	−42	n.d.[f]	n.d.[f]	n.d.[f]
5	PEO $_{(0.358,\ 0.338)}$ $BPh_{4\ (0.037,\ 0)}$ PE $_{(0.267)}$	0.6	31	19	n.d.[f]	n.d.[f]	−33	n.d.[f]	n.d.[f]	n.d[f]

[a]All films had 80 EO units in the PEOX cross-linker, [**1**]: ([COE]+[**4**]) loading of 1:15, and 31 wt% PEG275. [b]EO means ethylene oxide units contained both in the PEOX cross-linker and PEG plasticizer. [c]PE segments: Polyethylene domains in the polymer electrolyte. [d]PEO segments: Polyethylene oxide domains in the polymer electrolyte. [e]Glass transition temperature (T_g), cold crystallization temperature (T_c), and melting temperature (T_m) were determined by differential scanning calorimetry of the second heat cycle. [f]Not detected.

reducing the crystallinity. Additionally, a significant increase in the glass transition temperature (T_g) of the PEO domains was observed when the borate ion content was increased in the ionomer (Figure 3.3a). The higher T_g of the SICs at higher ion content may be explained by the ion aggregation at higher ion content. Colby and co-workers observed similar increase in T_g values for polyester ionomers.[32,33] The borate monomer incorporation in the polymer membrane also had a significant effect on the crystallization of PE chains in the network electrolyte. Notably, the PE crystallization was completely inhibited in the SIC compositions with higher weight% of the borate monomer (>19 wt%), suggesting that the tethered borate anions inhibited the alignment of the PE chains, leading to lower crystallinity in PE domains.

The DC ionic conductivities of the borate containing single-ion conductors were measured using dielectric spectroscopy measurements,[30] and the data for the samples with varying weight% of the ionic monomer (Table 3.1, entries 1–5) are shown in Figure 3.3b. A steep decrease in the ionic conductivity was observed for the SIC composition with ethylene oxide to lithium ratio ([EO]:[Li]) of 44 (Table 3.1, entry 1) below 60 °C, due to higher degree of crystallinity of PEO in the polymer network, as evident by higher enthalpy of fusion for the PEO domains (ΔH_{fus} = 6.8 J/g). However, at higher weight% of the borate monomer (Table 3.1, entries 2–5), the drop in the conductivity is not as sharp. The maximum ionic conductivity value of 1.3×10^{-6} S/cm was observed for the SIC composition with [EO]:[Li] ratio of 34 at 25 °C. At higher wt% of the borate monomer (Table 3.1, entries 3–5), the PEO domains were observed to be completely amorphous, but the ionic conductivity values were lower compared to the composition with 19 wt% borate monomer (Table 3.1, entry 2). This

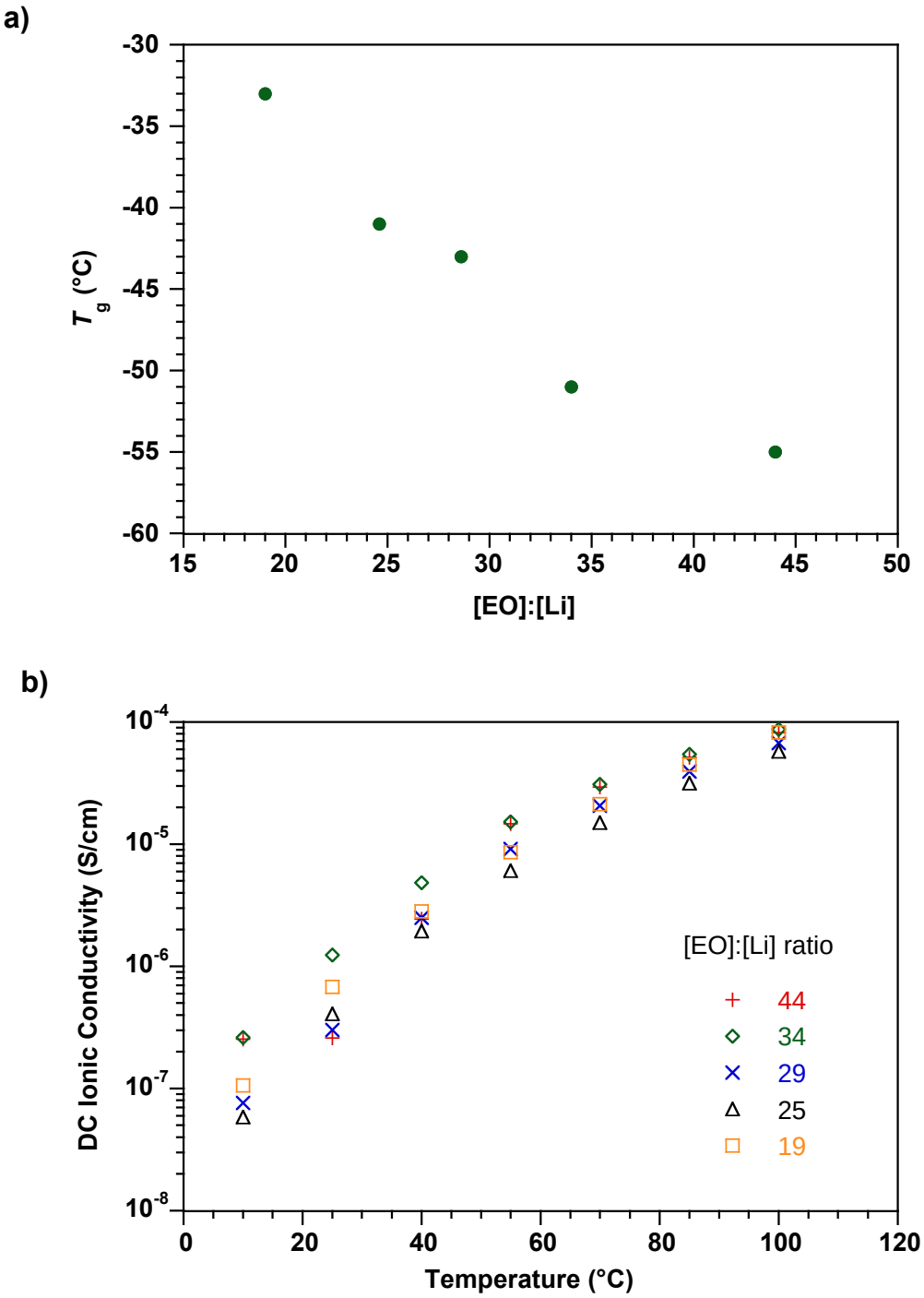

Figure 3.3 PE/PEO single-ion conductors containing tetraphenylborate anions. a) Glass transition temperature (T_g) as a function of [EO]:[Li] ratio. b) Variable temperature DC ionic conductivity of SICs at variable [EO]:[Li] ratios.

drop in conductivity values could be attributed to ion aggregation in the polymer electrolytes at higher ionic content, which leads to higher T_g and thus poor segmental motion of the PEO chains causing lower ionic conductivity.

To evaluate the electrochemical stability of these tetraphenylborate containing PE/PEO SICs, cyclic voltammetry measurements were performed on the SICs using Li/SPE/stainless steel coin cells at 1 mV/s scan rate and 22 °C. The cyclic voltammetry results for the SIC composition with the highest ionic conductivity are shown in Figure 3.4. For comparison, the results obtained for a LiTFSI-doped PE/PEO electrolyte are also shown. The tetraphenylborate containing SIC demonstrated electrochemical stability up to 5.5 V versus Li, which is approximately 1.5 V higher

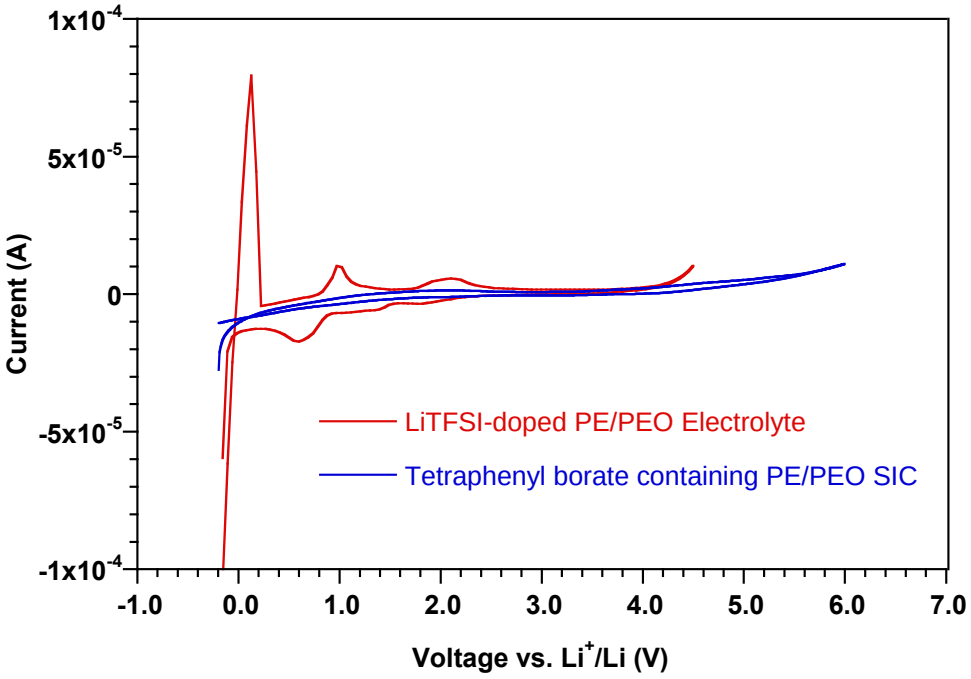

Figure 3.4 Cyclic voltammograms of LiTFSI-doped cross-linked PE/PEO electrolyte (red) and tetraphenylborate containing PE/PEO single-ion conductors (blue) at 1 mV/s scan rate and 22 °C.

than the binary lithium salt-doped PE/PEO electrolyte. This result is of significant interest because it shows that in contrast to the previously investigated LiTFSI-doped PE/PEO electrolytes,[28] the tetraphenylborate containing SICs could be used as electrolytes for high-voltage batteries, which use 5.0 V cathode materials.

3.3.2 Binary Salt-Doped Mixed Single-Ion Conductors (Mixed SIC)

Once the polyelectrolyte composition with the highest ionic conductivity was identified (Table 3.1, entry 2: [EO]:[Li] ratio of 34), lithium tetraphenylborate ($LiBPh_4$) was added to this electrolyte composition to develop new binary lithium salt-doped SICs. These binary salt-doped SICs are referred to as mixed SICs (Figure 3.5) in the text. To gain a better understanding of this mixed SIC system, ionomer compositions with variable fractions of the immobilized borate monomer were developed. The compositions of the mixed SIC electrolytes are summarized in Table 3.2.[34] For all the SPE compositions, the [EO]:[Li] ratio was kept constant in order to achieve similar Li^+ ion concentrations, whereas the [COE]:[**4**] ratio was varied.

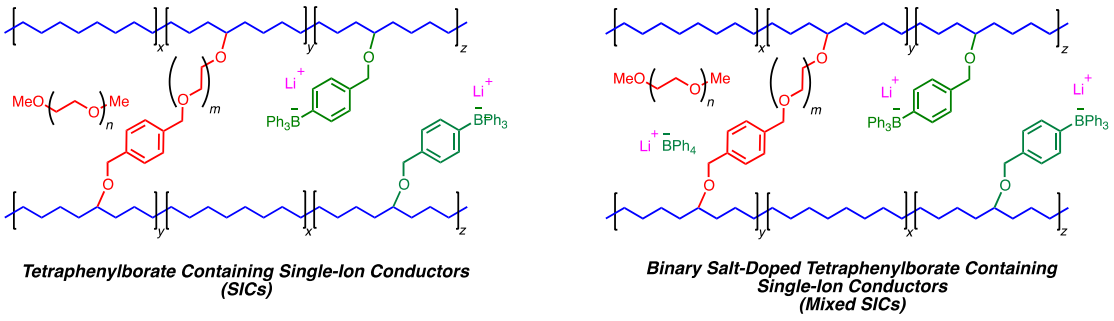

Figure 3.5 Left: Tetraphenylborate containing single-ion conductors (SICs). Right: Lithium tetraphenylborate salt doped-SICs (mixed SICs). The mobile Li^+ ions are shown in pink color.

Table 3.2 Compositions and thermal transitions of binary salt-doped PE/PEO single-ion conductors

Entry	Mixed Single-Ion Conductor Sample	% immobilized borate[c]	[COE]:[4]	PE Segments[d]		PEO Segments[e]			
				T_m^f (°C)	ΔH_{fus}^f (J/g)	T_g^f (°C)	T_c^f (°C)	T_m^f (°C)	ΔH_{fus}^f (J/g)
1[a]	$PEO_{(0.384,\ 0.294)}\ BPh_{4\ (0.020,\ 0)}\ PE_{(0.302)}$	100	2.3	57	1.9	−52	−5	26	3.3
2[b]	$PEO_{(0.369,\ 0.290)}\ BPh_{4\ (0.015,\ 0.005)}\ PE_{(0.321)}$	75	3.7	67	7.7	−52	−11	20	11.4
3[b]	$PEO_{(0.364,\ 0.298)}\ BPh_{4\ (0.010,\ 0.010)}\ PE_{(0.318)}$	50	5.8	76	19.7	−47	−5	25	15.6
4[b]	$PEO_{(0.360,\ 0.307)}\ BPh_{4\ (0.005,\ 0.015)}\ PE_{(0.313)}$	25	12.8	83	17.3	−43	−9	24	5.3
5[b]	$PEO_{(0.356,\ 0.311)}\ BPh_{4\ (0.002,\ 0.018)}\ PE_{(0.313)}$	10	33.3	88	15.4	−40	n.d.[g]	n.d.[g]	n.d.[g]

[a]Single-ion conductor. This film had 80 EO units in the cross-linker, [**1**]:([COE]+[**4**]) loading of 1:15, and 31wt% PEG275 plasticizer. [EO]:[Li] composition was 34, where EO means ethylene oxide units contained both in the PEOX cross-linker and PEG plasticizer. [b]$LiBPh_4$-doped SICs (mixed SICs). All the films had 70 EO units in the cross-linker, [**1**]:([COE]+[**4**]) loading of 1:15, and 31wt% PEG275 plasticizer. [EO]:[Li] composition was 34, where EO means ethylene oxide units contained both in the PEOX cross-linker and PEG plasticizer and Li means lithium from both the borate monomer and $LiBPh_4$. [c]% immobilized borate = [(mmoles of **4**)/ {(mmoles of **4**) + (mmoles of $LiBPh_4$)}] × 100. [d]PE segments: Polyethylene domains in the polymer electrolyte. [e]PEO segments: Polyethylene oxide domains in the polymer electrolyte. [f]Glass transition temperature (T_g), cold crystallization temperature (T_c), and melting temperature (T_m) were determined by differential scanning calorimetry of the second heat cycle. [g]Not detected.

The thermal properties of the mixed SIC system were studied using differential scanning calorimetry (DSC) measurements and the data are summarized in Table 3.2. The glass transition temperatures of the PEO were considerably influenced by the incorporation of $LiBPh_4$ salt in the SICs (Figure 3.6a). As the binary salt concentration was increased from 0 (Table 3.2, entry 1) to 90% (Table 3.2, entry 5), the T_g of the PEO segments increased from −52 °C to −40 °C. This result suggests that the flexibility of PEO chain is significantly affected by doping the SICs with a binary salt. In other words, for the mixed SIC compositions (Table 3.2, entries 2–5), average ion aggregation is stronger than the Li^+ ion solvation by the PEO chains, causing an increase in T_g. In contrast, for the undoped SIC composition (100% immobilized; Table 3.2, entry 1), the weakly coordinating tetraphenylborate anions are covalently attached to the polymer backbone and hence the ion aggregation (cation-anion interactions) is less of an issue. As a result, at similar Li^+ ion concentrations ([EO]:[Li] ratio of 34), the Li^+ ion is solvated to a greater extent by PEO in an undoped SIC composition compared to the mixed SIC compositions (Table 3.2, entries 2–5), leading to a lower T_g value in the undoped composition.

Furthermore, for the mixed SIC compositions with similar cross-linking density values but different [COE]:[**4**] ratios, the PE crystallization was significantly affected. Among the tested mixed SICs, the compositions with higher [COE]:[**4**] ratios demonstrated higher melting point of PE due to longer PE chains between the grafted units in these compositions. For example, the composition with the highest [COE]:[**4**] ratio of 33.3 (Table 3.2, entry 5; 10% immobilized borate monomer) exhibited a T_m value of 88 °C, whereas the mixed SIC with the lowest ratio (Table 3.2, entry 1; 100%

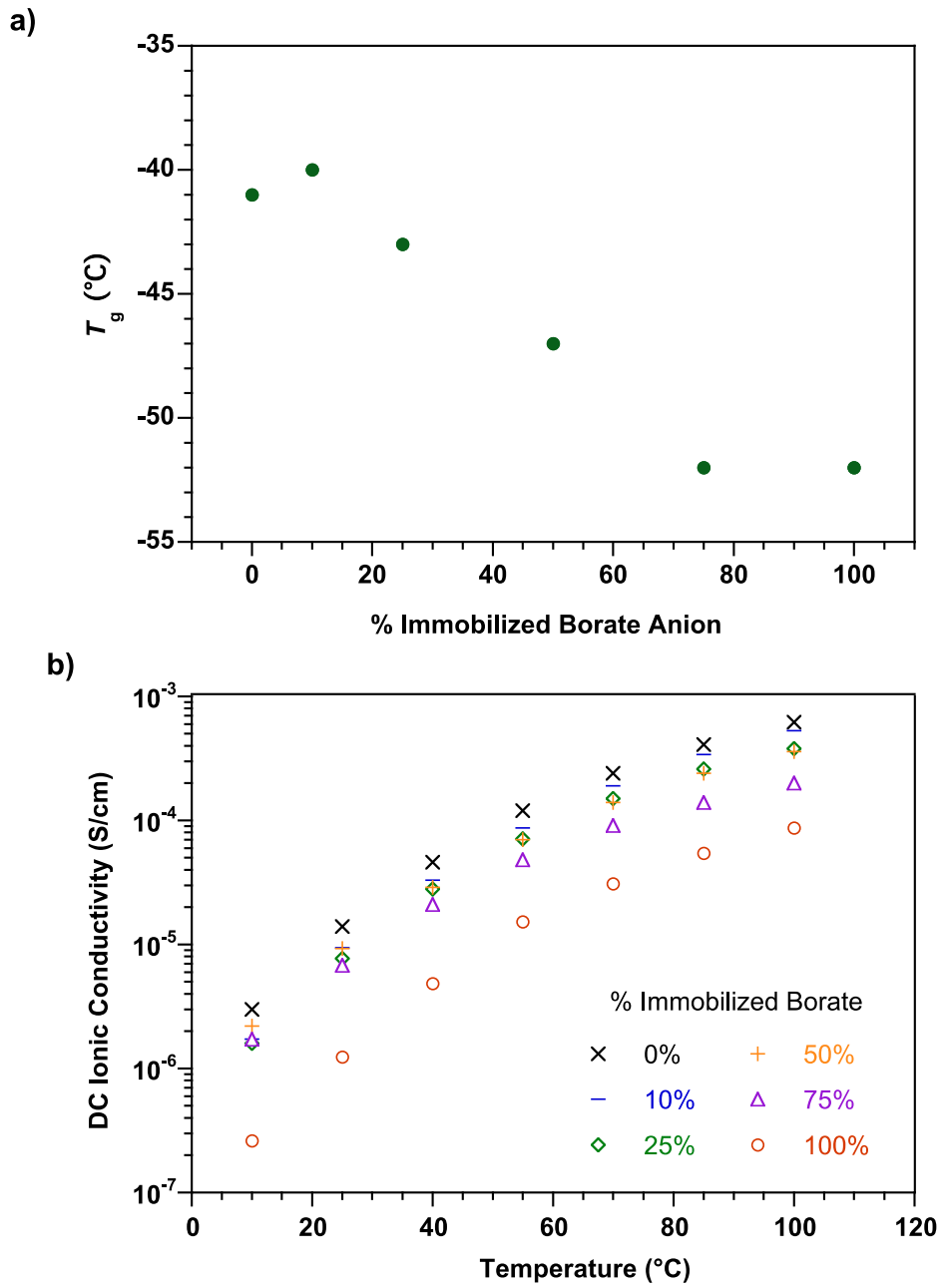

Figure 3.6 Mixed single ion conductors. a) Glass transition temperature (T_g) as a function of % immobilized borate. d) Variable temperature ionic conductivities of $LiBPh_4$ salt-doped PE/PEO single-ion conductors containing different fractions of immobilized tetraphenylborate anions. All films had 80 EO units in the cross-linker, [**1**]:([COE]+[**4**]) loading of 1:15 and 31wt% PEG275 plasticizer, and [EO]:[Li] composition of 34. The sample composition containing 100% immobilized borate is an SIC without any free $LiBPh_4$ salt. The data for a $LiBPh_4$ salt-doped PE/PEO electrolyte (0% immobilized) is also shown for comparison purposes.

immobilized borate monomer) showed the lowest melting temperature of 57 °C for the PE segments.

Figure 3.6b shows the variable temperature ionic conductivity of mixed SICs that contain variable amounts of immobilized borate anions. The conductivity data for a $LiBPh_4$ salt-doped SPE (i.e. 0% immobilized borate anion) is also shown in the plot for comparison purposes. The $LiBPh_4$-doped electrolyte composition (0% immobilized borate) demonstrated the highest ionic conductivity values at temperatures measured (10-100 °C). Of the tested mixed SICs (Table 3.2, entries 2–5), the compositions with lower fractions of immobilized borate anions in the electrolyte showed relatively higher ionic conductivity values at all temperatures tested. For example, the electrolyte compositions with 75% and 10% immobilized borate anions showed ionic conductivity values of 4.8×10^{-5} S/cm and 8.7×10^{-5} S/cm at 55 °C, respectively. Notably, the ionic conductivity values of some of these mixed SICs are almost an order of magnitude higher than the state-of-the-art triblock polyelectrolytes reported in the literature (1.3×10^{-5} S/cm at 60 °C).[18] It has been proposed that in the salt-doped PEO electrolytes, the ion-transport is strongly influenced by the segmental motion of the polymer chains.[35] Hence, one would expect that the electrolytes with a lower T_g should exhibit higher ionic conductivity. Despite the increased T_gs of the mixed SICs (Table 3.2, entries 2–5) compared to the undoped SIC composition (Table 3.2, entry 1), higher ionic conductivities were observed for these mixed SIC compositions. These results are unexpected and imply that the ion mobility for these mixed SICs is not only dictated by the segmental motion of the PEO chain, but also by the ion hopping. Since this is the first report of a binary salt-doped SIC and ion conduction is a complex

phenomenon, it is unclear at this point as to what mechanism is causing facile ion conduction in these mixed SICs. Nonetheless, the modular mixed SICs reported herein provide access to a new family of polyelectrolyte system that display promising ionic conductivity values for Li-metal battery operation.

To investigate the effect of binary lithium salt in the mixed SIC compositions on the electrochemical stability of the SPEs, cyclic voltammetry measurements were performed at 22 °C. The electrochemical stability results for the mixed SICs with 10% and 75% immobilized borate anion are shown in Figure 3.7. For comparison, the results for the undoped composition (100% immobilized borate) are also shown. The 100% immobilized sample is stable up to 5.5 V at 22 °C. The electrochemical stability of the electrolytes drops significantly upon addition of $LiBPh_4$ salt to the SICs. The observed trend could be rationalized on the basis of the oxidative instability of the anions at higher voltages.[36] Notably, the mixed SIC composition with maximum binary salt content (10% immobilized borate) shows oxidative stability only up to 4.2 V, which is 1.3 V lower than the undoped composition. In contrast, the composition with lesser binary salt content (75% immobilized borate anion) shows less anodic decomposition than the 10% immobilized system, as shown in the Figure 3.7. This result demonstrates that these mixed SIC systems are of significant interest due to their high ionic conductivity and tunable electrochemical stability. Galvanostatic lithium plating experiments are currently underway to determine the effect of the immobilized borate anions on the short-circuit time.

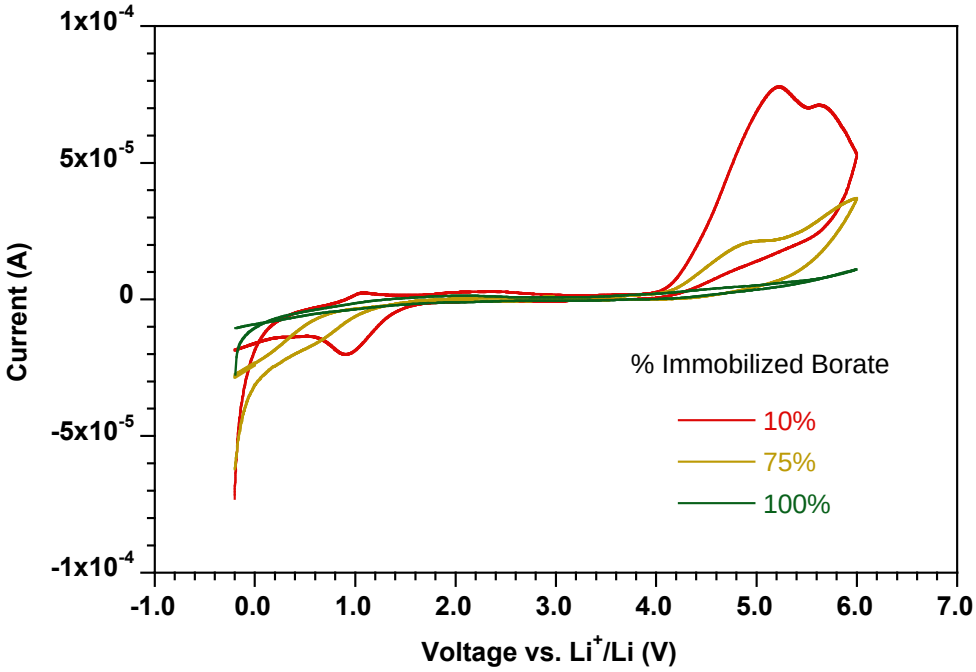

Figure 3.7 Cyclic voltammetry results for $LiBPh_4$-doped single-ion conductors with varied fractions of immobilized borate anions; 10% immobilized borate (red) and 75% immobilized borate (yellow). The undoped SIC composition, i.e. 100% immobilized borate (green) is also shown for comparison purposes.

3.4 Conclusions

We successfully developed a facile synthetic protocol for new Li-ion conducting SICs that contain immobilized tetraphenylborate anions. Due to the non-coordinating nature of these borate anions, the high ionic conductivity value of 1.5×10^{-5} S/cm at 55 °C was observed for the SIC without any binary salt. Upon doping the SICs with a binary salt, mixed SICs were obtained and ionic conductivities were found to increase substantially. In particular, the mixed SIC composition with 10% immobilized borate anion demonstrated the highest ionic conductivity (~10^{-4} S/cm at 55 °C). These mixed SICs also provided access to a modular electrolyte system with

tunable electrochemical stability. The correlation of the fraction of the immobilized borate anion to the dendrite growth resistance in an LMB battery is currently under investigation in our laboratory. We believe that these mixed SICs are an interesting class of polymer electrolytes and the structure-function correlations of this system will provide useful insights for the design of superior electrolyte formulations.

3.5 Experimental

3.5.1 General

All reactions and manipulations of air and moisture sensitive compounds were carried out under dry nitrogen using a Braun UniLab drybox or standard Schlenk line techniques unless otherwise specified. ^{1}H NMR spectra were collected in deuterated solvents on a Varian INOVA 400 or Varian INOVA 500 spectrometer and referenced with residual non-deuterated solvent shifts ($CHCl_3$ = 7.24 ppm) and are reported relative to tetramethylsilane (δ = 0 ppm). ^{13}C NMR spectra were recorded on a Varian INOVA (^{13}C, 100 MHz) or Varian INOVA (^{13}C, 125 MHz) spectrometer and referenced to chloroform (δ 77.23 ppm). ^{11}B NMR were recorded on a Bruker ARX 300 (96 MHz) and referenced to an external standard ($BF_3{\cdot}Et_2O$). High-accuracy mass data were obtained using MALDI and ESI sources. MALDI mass spectra were obtained on a Waters Micro MX MALDI-TOF mass spectrometer using negative ion mode and a reflectron detector. Samples were prepared by depositing the analyte dissolved in a saturated dithranol solution onto a stainless steel sample plate. The plate was dried in air before loading it into the instrument. HRMS (ESI) analyses were performed at the Mass Spectrometry Laboratory at the University of Illinois at Urbana-Champaign.

Gel permeation chromatography (GPC) analyses were carried out using an Agilent PL-GPC 50 integrated system, equipped with UV and refractive index detectors, and 2 PL gel Mini-MIX C columns (5 micron, 4.6 mm ID). The GPC columns were eluted with tetrahydrofuran at 30 °C at 0.3 mL/min and were calibrated with monodisperse polystyrene standards. Differential scanning calorimetry (DSC) analyses of polymer samples were performed on a TA Instruments Q1000 instrument equipped with liquid nitrogen cooling system. Polymer samples were loaded in aluminum pans and heated under nitrogen from −100 °C to 180 °C at a rate of 10 °C per minute and then cooled to −100 °C at a rate of 10 °C per minute, followed heating to 180 °C at a rate of 10 °C per minute. The glass transition temperature (T_g) and the melting temperature (T_m) were recorded from the second heating run. Thermogravimetric analysis (TGA) from 20-1000 °C was carried out on a TA Instruments Q500 Thermogravimetric Analyzer in nitrogen atmosphere using a 10 °C/min ramp without equilibration delay.

The conductivity data of the polymer electrolytes was obtained over a range of frequencies (0.1-3×10^6 Hz) and temperatures (−5 °C to 100 °C) using a Novocontrol Dielectric Broadband Spectrometer fitted with a Quatro temperature control system. Conductivity measurements were performed using blocking/solid polymer electrolyte/blocking cell orientation, using gold plated stainless steel electrodes. Symmetric lithium coin cells for short-circuit measurements were prepared in an argon filled MBraun glovebox using Hohsen components, size 2032, with 9.9 mm diameter lithium electrodes and a 12.7 mm diameter cross-linked electrolyte sample. Coin cell crimping was performed with a MTI electric crimping machine to ensure uniformity.

Lithium/SPE/Stainless Steel (Li/SPE/SS) coin cells were prepared in an argon filled MBraun glovebox using Hohsen components, size 2032, with 9.9 mm diameter lithium electrodes and a 12.7 mm diameter cross-linked electrolyte sample. The cyclic voltammetric measurements were performed on Li/SPE/SS coin cells using a Solartron (Model 1470) Potentiostat/Galvanostat. The potential was scanned from −0.2 V to 6.0 V at 1 mV/s sweep rate and 22 °C.

3.5.2 Materials

Sodium hydride (95%), 1,5-cyclooctadiene, *cis*-cyclooctene (95%), 4-bromobenzyl bromide (98%), 1,2-dibromoethane, *meta*-chloroperoxybenzoic acid, lithium carbonate (>99%), Grubbs' 2nd Generation catalyst (Cl_2(iMes)(PCy_3)Ru=CHPh), and Crabtree's catalyst [(COD)Ir(py)(PCy_3)]PF_6 were purchased from Sigma-Aldrich and used as received. Lithium tetraphenylborate tris(1,2-dimethoxyethane), $LiBPh_4$·3DME (98%) was purchased from Sigma-Aldrich and dried *in vacuo* at 90 °C for 24 h and transferred directly into the glove box. Ethylene oxide was purchased from Sigma-Aldrich and dried over *n*-BuLi before use. Triphenylborane, 95% (Strem Chemicals), magnesium turnings (Strem Chemicals), anhydrous sodium sulfate (Mallinckrodt), and dibromo-*p*-xylene, 97% (Alfa Aesar) were used as received. HPLC grade tetrahydrofuran was purchased from Fisher Scientific and dried over an alumina column and degassed by three freeze pump thaw cycles before use. Chloroform was dried over P_2O_5 and distilled prior to use. Hydrogen (99.99%) was purchased from Airgas. NMR solvents ($CDCl_3$ and acetone-d_6) were purchased from Cambridge Isotope Laboratories (CIL) and used as received.

Following a literature procedure,[37] 5-hydroxy-1-cyclooctene was prepared, dried over activated 3 Å sieves for three days, and degassed by three freeze pump thaw cycles before use. Potassium naphthalenide in THF was prepared from naphthalene and potassium at a concentration of 0.35 M (titrated with a standard benzoic acid solution until a persistent green color was observed as an end-point of the titration) and degassed by three freeze pump thaw cycles before use.

3.5.3 Synthesis

3.5.3.1 Synthesis of the PEO Functionalized Cross-linker

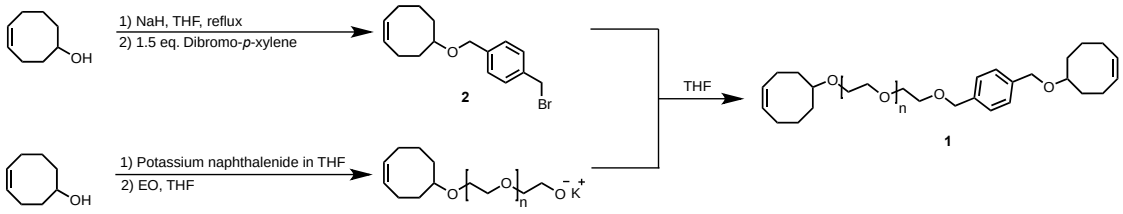

Scheme 3.1 General scheme for the synthesis of cross-linker **1**.

For the synthesis and characterization of **2**, see Section 2.5.3.1.

For the synthesis and characterization of the PEO functionalized cross-linker (**1**), see Section 2.5.3.1.

3.5.3.2 Synthesis of Tetraphenylborate Functionalized Cyclooctene Monomer (4)

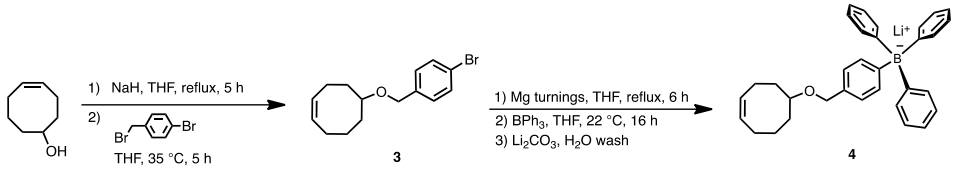

Scheme 3.2 Synthesis of tetraphenylborate functionalized cyclooctene monomer.

Preparation of (*Z*)-5-((4-bromobenzyl)oxy)cyclooct-1-ene (3): A suspension of NaH (0.722 g, 28.6 mmol) in anhydrous THF (25 mL) was treated dropwise with 5-hydroxycyclooct-1-ene (2.32 g, 18.4 mmol) and heated to 70 °C under N_2 for 16 h. After cooling to room temperature, a solution of *p*-bromobenzyl bromide (4.83 g, 19.3 mmol) dissolved in anhydrous THF (25 mL) was added to the alkoxide solution under standard Schlenk conditions at 22 °C. The resulting solution was stirred at 35 °C for 2 h, cooled to room temperature, and quenched with ethanol. The resultant suspension was filtered through a pad of celite and the filtrate was concentrated on a rotary evaporator. Dichloromethane was added (~150 mL) to the crude reaction mixture and the organic phase was washed with saturated brine, then dried over anhydrous sodium sulfate, filtered, and concentrated under reduced pressure to yield a colorless oil, which was further purified by column chromatography on silica using 1:1 CH_2Cl_2/hexanes. The desired product was isolated as colorless oil (4.3 g, 80%). ^{1}H NMR (500 MHz, $CDCl_3$) δ 7.49 – 7.41 (m, 2H), 7.24 – 7.17 (m, 2H), 5.76 – 5.50 (m, 2H), 4.54 – 4.31 (m, 2H), 3.44 (dddd, *J* = 9.9, 7.3, 4.1, 1.5 Hz, 1H), 2.44 – 1.32 (m, 10H). ^{13}C NMR (125 MHz, $CDCl_3$) δ 138.28, 131.46, 130.13, 129.52, 129.15, 80.30,

69.52, 34.29, 33.34, 25.87, 25.68, 22.74. HR-MS (ESI) *m/z* calculated for ($M + H^+$) 294.0619, found 294.0615.

Preparation of Lithium (*Z*)-(4-((cyclooct-4-en-1-yloxy)methyl)phenyl) triphenyl borate (4): A three-neck 100 ml round bottom flask equipped with a reflux condenser was charged with magnesium turnings (130 mg, 5.34 mmoles). A few drops of dibromoethane were added to the flask under N_2 flow to activate the magnesium surface. A solution of **3** (1.03 g, 3.52 mmoles) in 20 mL dry THF was slowly added to the magnesium *via* cannula (initially only 25% of the bromide solution was added). The resultant solution was heated with a heat gun to gently reflux the reaction mixture. After a gentle reflux began, the remaining solution of **3** in THF was added to the flask and the reaction mixture was refluxed for 6 hours. The resultant Grignard reagent was cooled to room temperature and cannula transferred to a solution of triphenylborane (0.843 g, 3.48 mmoles) in 5 mL of dry THF under standard Schlenk conditions. The resultant pale yellow solution was stirred for 16 h at room temperature and then concentrated under reduced pressure to yield a pale yellow powder. The yellow crystalline powder was redissolved in 25 mL of ethyl acetate and poured into 10 mL of saturated lithium carbonate aqueous solution to allow the ion exchange. The resultant biphasic solution was stirred for 24 hours, followed by the extraction of aqueous layer with ethyl acetate (3×20 mL). The organic phases were combined, dried over activated 3Å molecular sieves for 6 hours, and subsequently concentrated under reduced pressure to yield a light brown powder (1.1 g, 67%). ^{1}H NMR (400 MHz, Acetone-d_6) δ 7.42 – 7.24 (m, 8H), 6.96 – 6.88 (m, 8H), 6.78 (dddd, J = 9.0, 6.5, 1.6, 0.9 Hz, 3H), 5.73 – 5.48 (m, 2H), 4.42 – 4.27 (m, 2H), 3.46 (dddd, J = 9.6, 7.7, 4.1, 1.0 Hz, 1H),

2.40 – 2.27 (m, 1H), 2.23 – 2.09 (m, 2H), 2.02 – 1.09 (m, 1H). ^{13}C NMR (126 MHz, Acetone-d_6) δ 165.51, 165.11, 164.72, 164.33, 136.98, 136.97, 136.96, 136.95, 136.73, 136.72, 136.71, 136.70, 135.42, 132.69, 131.04, 129.89, 125.97, 125.95, 125.93, 125.91, 125.89, 122.18, 79.61, 71.79, 35.16, 33.72, 26.29, 26.17, 23.31. ^{11}B NMR (96 MHz, Acetone-d_6) δ −5.99. HR-MS (ESI) *m/z* calculated for (M^-) 457.2708, found 457.2702.

3.5.3.2 Synthesis of polymer electrolytes

3.5.3.2.1 Single-Ion Conductors

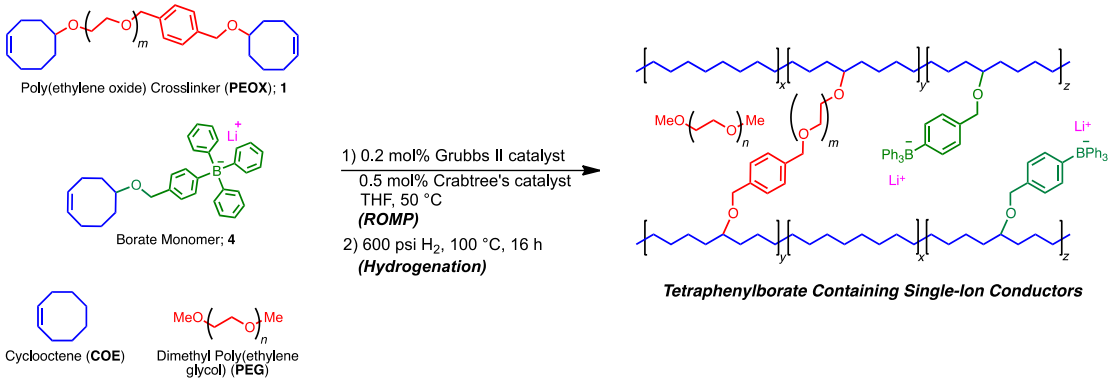

Scheme 3.3 Synthesis of tetraphenylborate containing PE/PEO network single-ion conductors.

Sample Procedure for the Synthesis of Tetraphenylborate containing Single-Ion Cross-Linked SPE, [EO]:[Li] = 34 (Table 3.1, entry 2): In a glove box, the PEOX cross-linker **1** (128 mg, 0.0320 mmol) with 83 EO units in the cross-links, compound **4** (64 mg, 0.14 mmol), and COE (42 µL, 0.32 mmol) were combined and dissolved in 2.5 mL of dry THF. Grubbs' 2nd generation catalyst (1.0 mg, 0.0012 mmol) dissolved in 0.5 mL of THF was added to the monomer mixture, followed by addition of PEG275 (112 mg, 0.407 mmol). Crabtree's catalyst (2.2 mg, 0.0027 mmol) dissolved

in 0.5 mL $CHCl_3$ was then added to the resultant solution and shaken vigorously for one minute. It was then transferred to a metal dish (fluoropolymer-lined, diameter of 5.25 cm and depth of 3.0 cm) placed in a volume glass chamber bearing two Kontes glass valves on top. The chamber was placed on top of the hot plate equipped with a metal plate to ensure uniform heating and film was casted under N_2 flow at 50 °C for 3 h. After the solvent evaporated off, the Kontes valves were closed and the glass chamber was taken into the glove box. Hexane (3 mL) was added to the metal dish in order to release the film from the dish. The film was dried in vacuum at 22 °C for 24 h and then placed in a Parr reactor and sealed. It was pressurized to 600 psig with hydrogen and then vented down to 50 psig. This process was repeated twice more to purge the reactor of air, then pressurized to 600 psig and heated to 100 °C. After 16 h, it was cooled, vented and the hydrogenated film was dried under vacuum at 22 °C for 24 h.

3.5.3.2.2 Binary Salt-Doped Single Ion Conductors

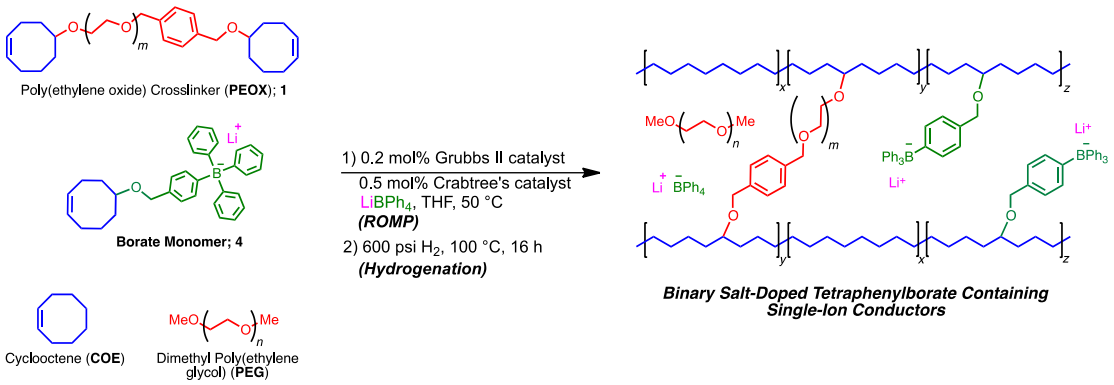

Scheme 3.4 Synthesis of $LiBPh_4$ salt-doped PE/PEO single-ion conductors.

Sample Procedure for the Synthesis of Lithium Tetraphenylborate Binary Salt containing Single-Ion Cross-Linked SPE, 50% Immobilized Borate on the Polymer Backbone (Table 3.2, entry 3): In a glove box, cross-linker **1** (123 mg, 0.0318 mmol) with 67 EO units in the cross-linker, compound **4** (32 mg, 0.069 mmol), and COE (52 μL, 0.40 mmol) were combined and dissolved in 2.5 mL of dry THF. Grubbs' 2nd generation catalyst (1.0 mg, 0.0012 mmol) dissolved in 0.5 mL of dry THF was added to the monomer mixture, followed by addition of $LiBPh_4$.3DME (40 mg, 0.067 mmol) and PEG275 (112 mg, 0.407 mmol). Crabtree's catalyst (2.2 mg, 0.0027 mmol) dissolved in 0.5 mL $CHCl_3$ was then added to the resultant solution and shaken vigorously for one minute. It was then transferred to a metal dish (fluoropolymer-lined, diameter of 5.25 cm and depth of 3.0 cm) placed in a volume glass chamber bearing two Kontes glass valves on top. The chamber was placed on top of the hot plate equipped with a metal plate to ensure uniform heating and film was casted under N_2 flow at 50 °C for 3 h. After the solvent evaporated off, the Kontes valves were closed and the glass chamber was taken into the glove box. Hexane (~ 3 mL) was added to the metal dish in order to release the film from the dish. The film was dried in vacuum at 22 °C for 24 h and then placed in a Parr reactor and sealed. It was pressurized to 600 psig with hydrogen and then vented down to 50 psig. This process was repeated twice more to purge the reactor of air, then pressurized to 600 psig and heated to 100 °C. After 16 h, it was cooled, vented and the hydrogenated film was dried under vacuum at 22 °C for 24 h.

3.5.4 MALDI Data

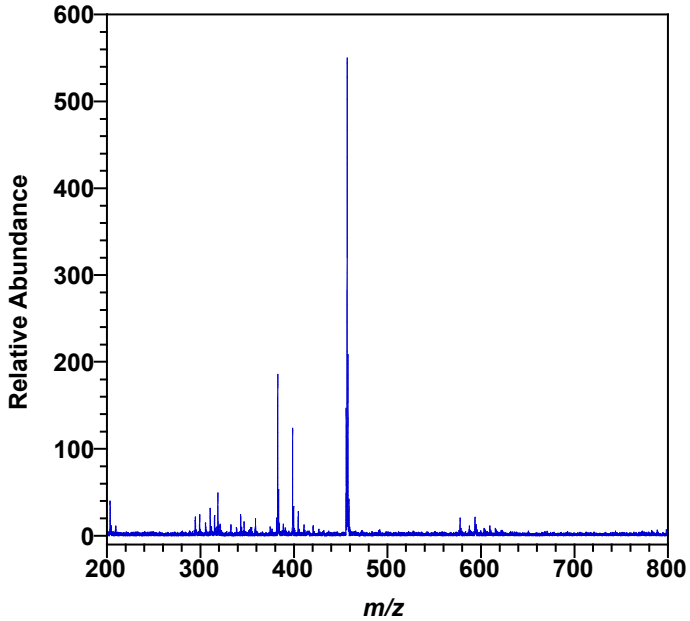

Figure 3.8 MALDI spectrum of lithium (*Z*)-(4-((cyclooct-4-en-1-yloxy)methyl) phenyl)triphenylborate (**4**). *m/z* calculated for (M^-) 457.2708, found 457.8013.

3.5.5 Thermal Gravimetric Analysis (TGA)

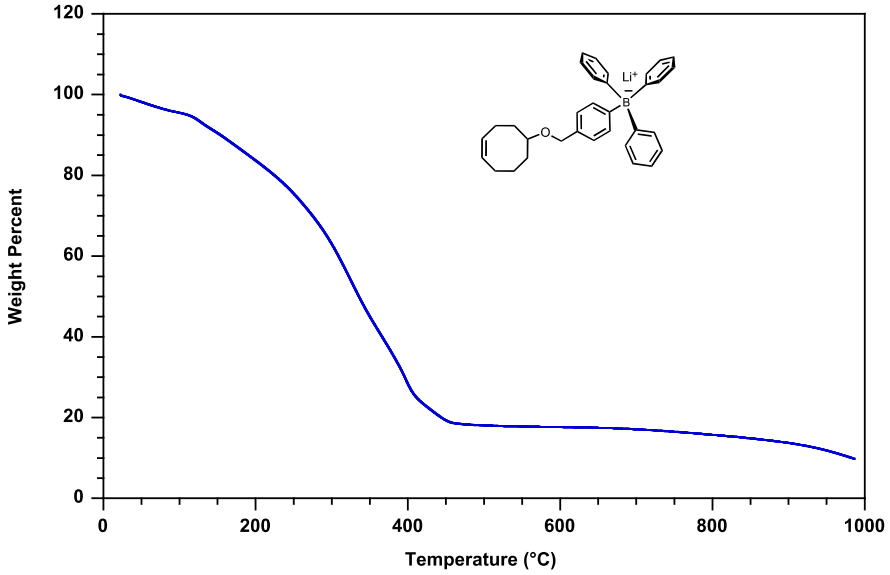

Figure 3.9 TGA trace of lithium (*Z*)-(4-((cyclooct-4-en-1-yloxy)methyl)phenyl) triphenylborate (**4**).

The thermal decomposition data for the tetraphenylborate functionalized cyclooctene monomer (compound **4**) is shown in Figure 3.9. The onset decomposition temperature for this precursor was observed to be in the vicinity of 200 °C, which is significantly higher than the operating temperature of a lithium-based battery.

3.5.6 Differential Scanning Calorimetry

3.5.6.1 Single-Ion Conductors

DSC analysis was performed using a TA Instruments Q1000 instrument equipped with liquid nitrogen cooling system and automated sampler. Typical DSC samples were made in aluminum pans and the method used was 10 °C/ min ramp, with one cycle of heat, cool, and heat again. The DSC data of the second heat cycle for the single-ion samples with variable composition of [EO]:[Li] units in the network polymer electrolyte are shown in Figure 3.10. The segmental motion of the PEO chains was significantly affected by the ionic content in the ionomers. For example, a 20 °C increase in the glass transition temperature was observed when the weight% of the borate monomer was increased from 16 wt% ([EO:[Li] = 44) to 31 wt% ([EO:[Li] = 19). Furthermore, the PEO crystallization was completely inhibited when higher weight% of the borate monomer was incorporated in the Li-ion conducting ionomers.

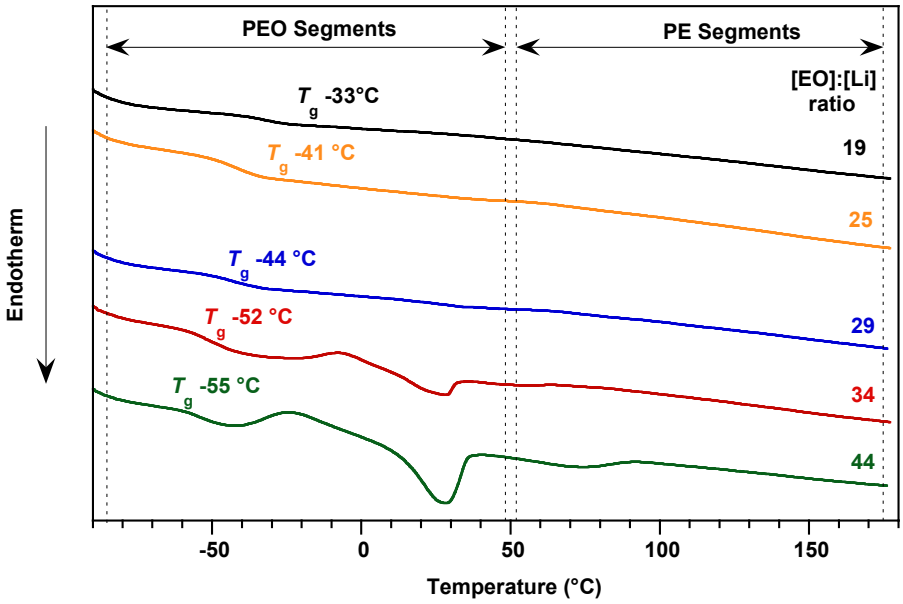

Figure 3.10 DSC traces of the second heat cycle for the tetraphenylborate containing SICs with varying [EO]:[Li] ratio.

3.5.6.2 Binary Salt-Doped SICs

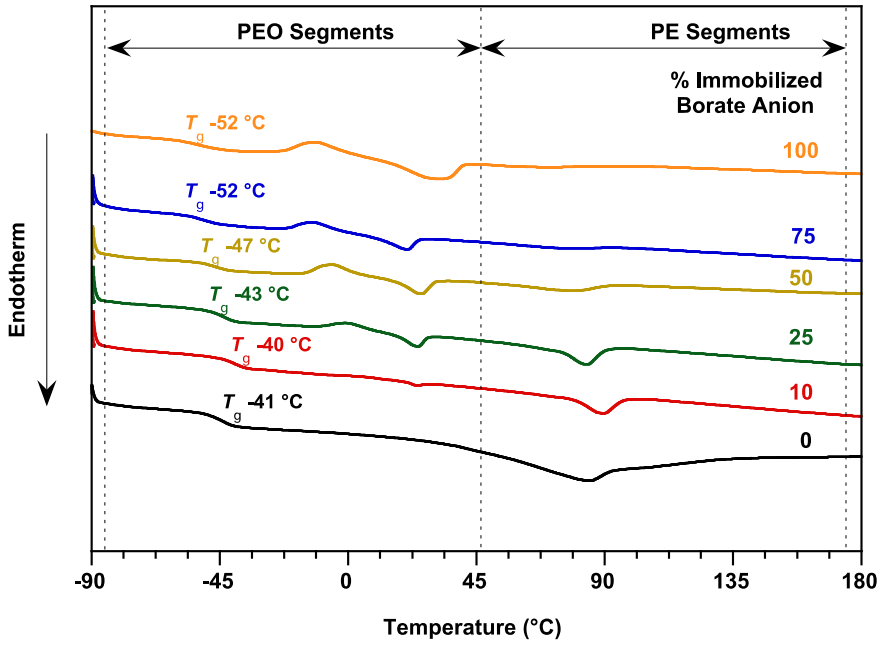

Figure 3.11 DSC traces of the second heat cycle for the lithium tetraphenylborate-doped SICs containing variable % of immobilized borate.

3.5.7 DC Ionic Conductivities

3.5.7.1 Single-Ion Conductors (SICs)

The DC ionic conductivity at each temperature was determined from the plateau value of the plot of real part of the conductivity (Sig′) as a function of frequency, as described in seminal work by Jonscher.[38] A representative plot of Sig′ vs. frequency for the SIC composition with [EO]:[Li] ratio of 34 (Table 3.1, entry 2) at variable temperatures is shown in Figure 3.12.

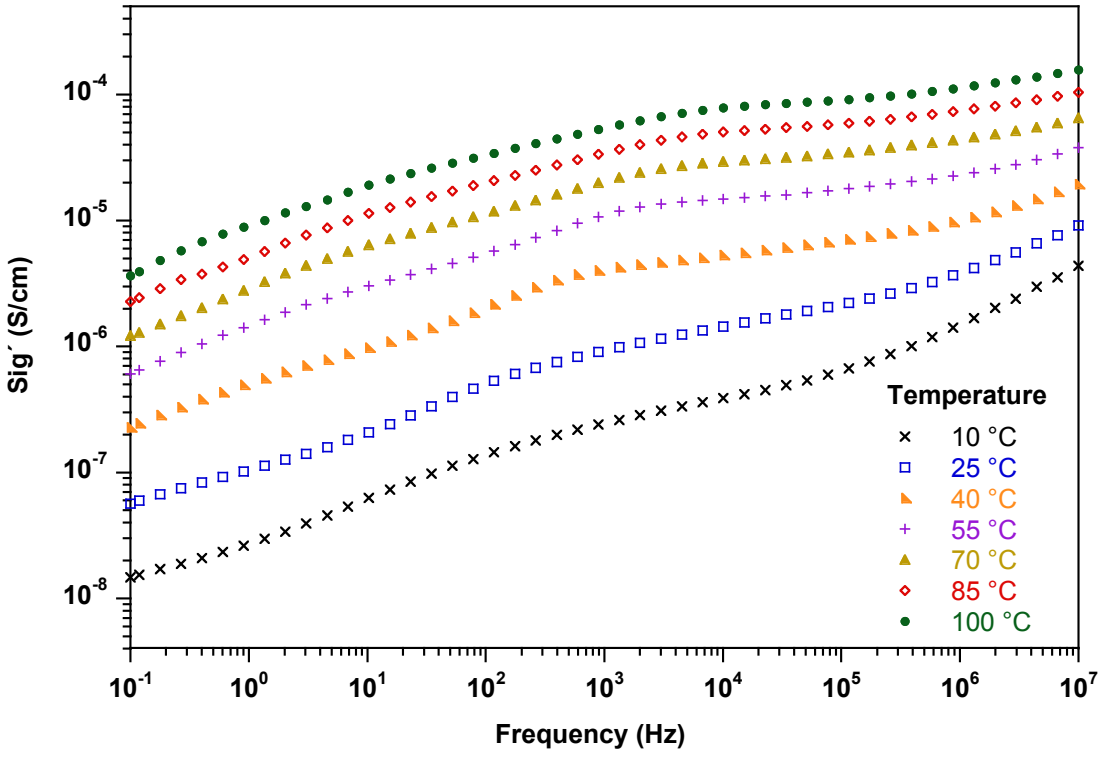

Figure 3.12 Real part of the ionic conductivity vs. frequency plot for the SIC electrolyte with [EO]:[Li] composition of 34 at variable temperatures.

Table 3.3 DC ionic conductivities of tetraphenylborate containing single-ion conductors[a]

entry	Weight% of the borate monomer	[COE]:[4]	[EO]:[Li] ratio[b]	DC Ionic Conductivity (S/cm)[c]						
				10 °C	25 °C	40 °C	55 °C	70 °C	85 °C	100 °C
1	15	3.4	44	2.5×10^{-7}	2.6×10^{-7}	2.4×10^{-6}	1.5×10^{-5}	2.9×10^{-5}	5.2×10^{-5}	8.2×10^{-5}
2	19	2.3	34	2.6×10^{-7}	1.2×10^{-6}	4.9×10^{-6}	1.5×10^{-5}	3.1×10^{-5}	5.5×10^{-5}	8.7×10^{-5}
3	22	1.8	29	7.6×10^{-8}	3.0×10^{-7}	2.5×10^{-6}	9.1×10^{-6}	2.1×10^{-5}	3.9×10^{-5}	6.7×10^{-5}
4	25	1.2	25	5.8×10^{-8}	4.1×10^{-7}	1.9×10^{-6}	6.1×10^{-6}	1.5×10^{-5}	3.2×10^{-5}	5.8×10^{-5}
5	31	0.6	19	1.1×10^{-7}	6.8×10^{-6}	2.8×10^{-6}	8.6×10^{-6}	2.1×10^{-5}	4.5×10^{-5}	8.2×10^{-5}

[a]All films had 80 EO units in the PEOX cross-linker, [**1**]: ([COE]+[**4**]) loading of 1:15, and 31 wt% PEG275. [b]EO means ethylene oxide units contained both in the PEOX cross-linker and PEG plasticizer. [c]Determined by dielectric spectroscopy measurements.

Table 3.4 DC ionic conductivities of binary salt-doped PE/PEO single-ion conductors

entry	% immobilized borate monomer[d]	[COE]:[4]	DC Ionic Conductivity (S/cm)[e]						
			10 °C	25 °C	40 °C	55 °C	70 °C	85 °C	100 °C
1[a]	0	n.a.[f]	3.0×10^{-6}	1.4×10^{-5}	4.6×10^{-5}	1.2×10^{-4}	2.4×10^{-4}	4.1×10^{-4}	6.2×10^{-4}
2[b]	10	33.3	1.7×10^{-6}	9.4×10^{-6}	3.3×10^{-5}	8.7×10^{-5}	1.9×10^{-4}	3.4×10^{-4}	5.3×10^{-4}
3[b]	25	12.8	1.6×10^{-6}	7.7×10^{-6}	2.8×10^{-5}	7.1×10^{-5}	1.5×10^{-4}	2.6×10^{-4}	3.8×10^{-4}
4[b]	50	5.8	2.2×10^{-6}	9.3×10^{-6}	2.9×10^{-5}	7.0×10^{-5}	1.4×10^{-4}	2.4×10^{-4}	3.6×10^{-4}
5[b]	75	3.7	1.7×10^{-6}	6.8×10^{-6}	2.1×10^{-5}	4.8×10^{-5}	9.1×10^{-5}	1.4×10^{-4}	2.0×10^{-4}
6[c]	100	2.3	2.6×10^{-7}	1.2×10^{-6}	4.9×10^{-6}	1.5×10^{-5}	3.1×10^{-5}	5.5×10^{-5}	8.7×10^{-5}

[a] $LiBPh_4$-doped PE/PEO cross-linked electrolyte. This film had 80 EO units in the cross-linker, [**1**]:([COE]) loading of 1:15, and 31wt% PEG275 plasticizer. [EO]:[Li] composition was 34, where EO means ethylene oxide units contained both in the PEOX cross-linker and PEG plasticizer. [b] $LiBPh_4$-doped SICs (mixed SICs). All the films had 80 EO units in the cross-linker, [**1**]:([COE]+[**4**]) loading of 1:15, and 31wt% PEG275 plasticizer. [EO]:[Li] composition was 34, where EO means ethylene oxide units contained both in the PEOX cross-linker and PEG plasticizer, and Li means lithium from both the borate monomer and $LiBPh_4$. [c] Single-ion conductor. This film had 80 EO units in the cross-linker, [**1**]:([COE]+[**4**]) loading of 1:15, and 31wt% PEG275 plasticizer. [EO]:[Li] composition is 34, where EO means ethylene oxide units contained both in the PEOX cross-linker and PEG plasticizer. [d] % immobilized borate = [(mmoles of **4**)/ {(mmoles of **4**) + (mmoles of $LiBPh_4$)}] × 100. [e] Determined by dielectric spectroscopy measurements. [f] Not applicable.

3.5.8 Cyclic Voltammetry Measurements

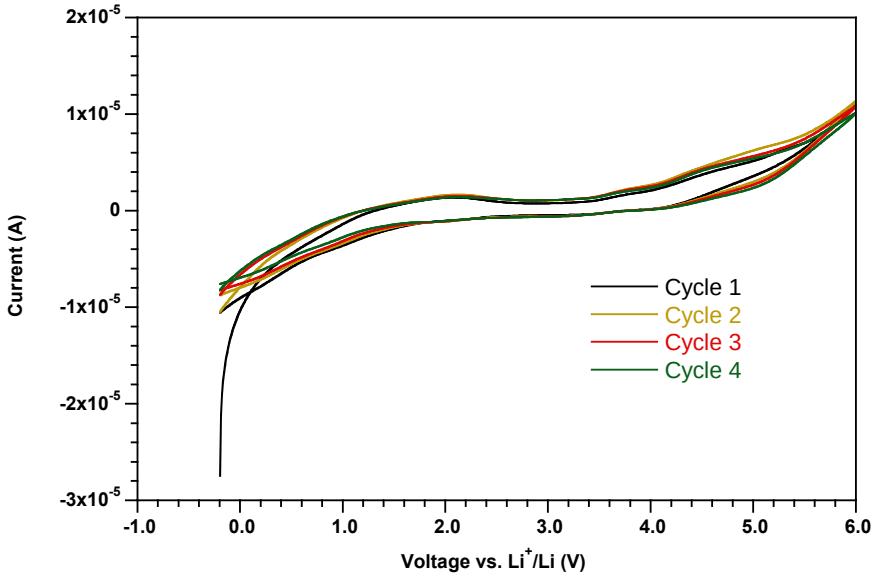

Figure 3.13 Cyclic voltammogram of the tetraphenylborate containing single-ion conductor having [COE]:[**4**] ratio of 2.3 and [EO:[Li] composition of 34 (Table 3.2, entry 1).

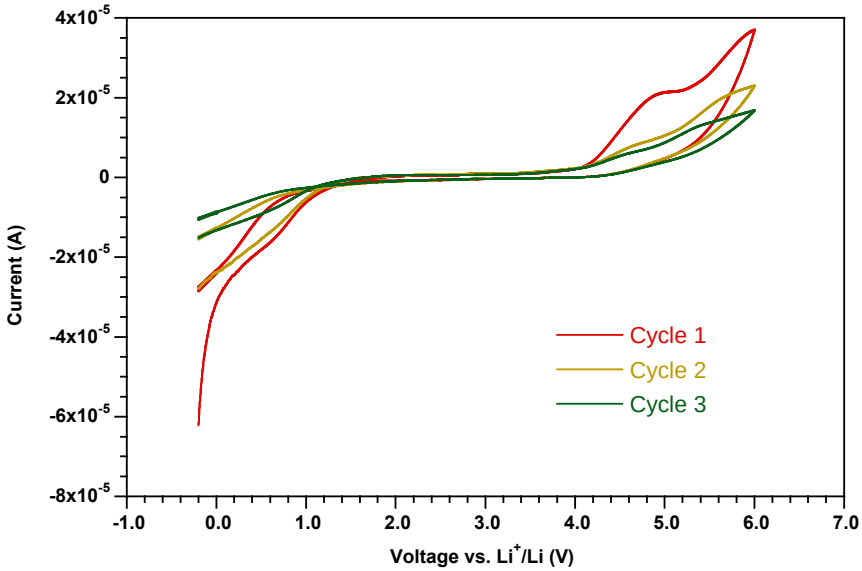

Figure 3.14 Cyclic voltammogram of $LiBPh_4$-doped single-ion conductor having 75% immobilized borate, [COE]:[**4**] ratio of 3.7, and [EO]:[Li] composition of 34 (Table 3.2, entry 2).

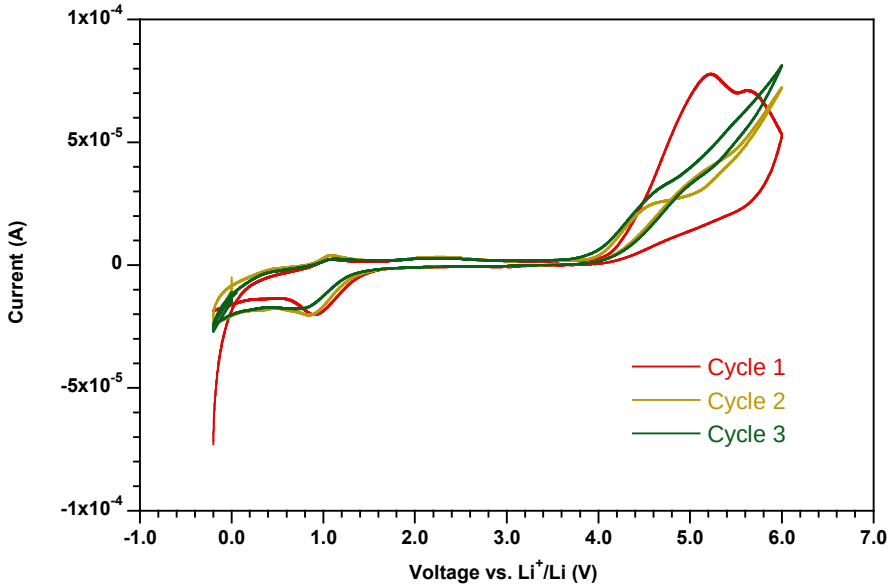

Figure 3.15 Cyclic voltammogram of the $LiBPh_4$-doped single-ion conductor having 10% immobilized borate, [COE]:[**4**] ratio of 33.3, and [EO]:[Li] composition of 34 (Table 3.2, entry 5).

3.5.9 NMR Spectra

(*Z*)-5-((4-(bromomethyl)benzyl)oxy)cyclooct-1-ene (2)

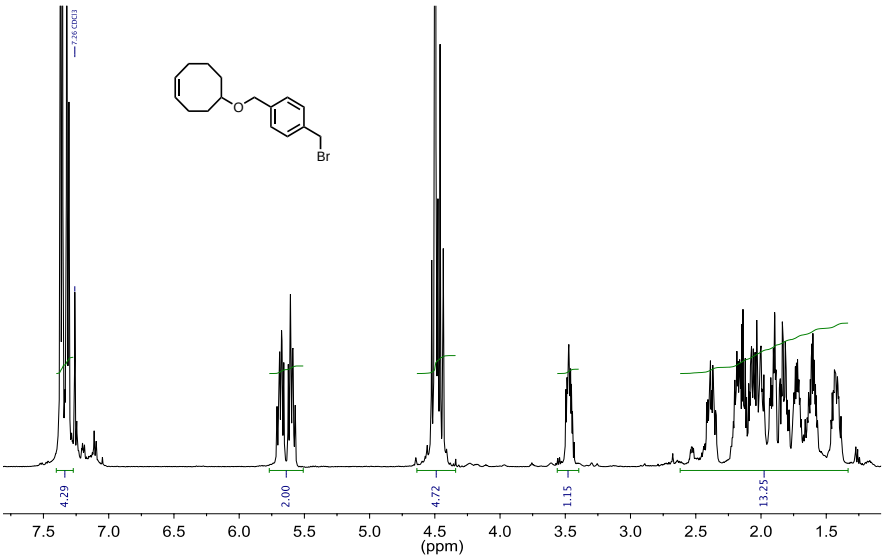

Figure 3.16 ^{1}H NMR Spectrum of (*Z*)-5-((4-(bromomethyl)benzyl)oxy)cyclooct-1-ene (**2**). Signal at 7.26 ppm is residual $CHCl_3$.

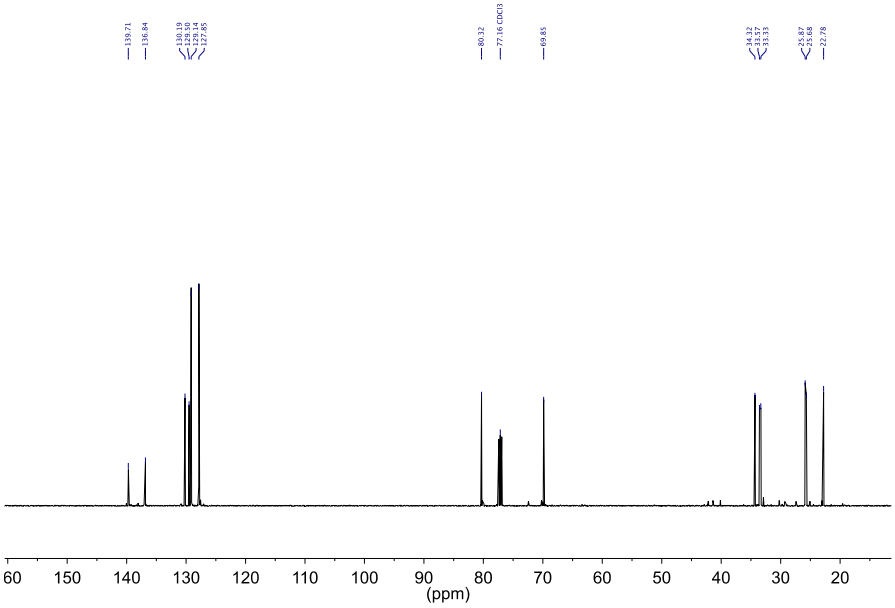

Figure 3.17 ^{13}C NMR Spectrum of (*Z*)-5-((4-(bromomethyl)benzyl)oxy)cyclooct-1-ene (**2**). Signal at 77.16 ppm is residual $CDCl_3$.

PEO functionalized cross-linker (1)

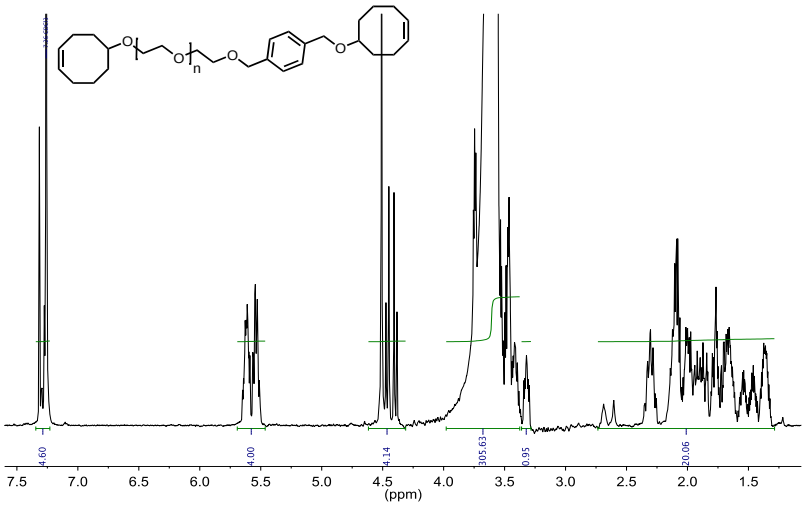

Figure 3.18 ^{1}H NMR Spectrum of PEO functionalized cross-linker (**1**) of molecular weight 3.7 kDa. Signal at 7.26 ppm is residual $CHCl_3$.

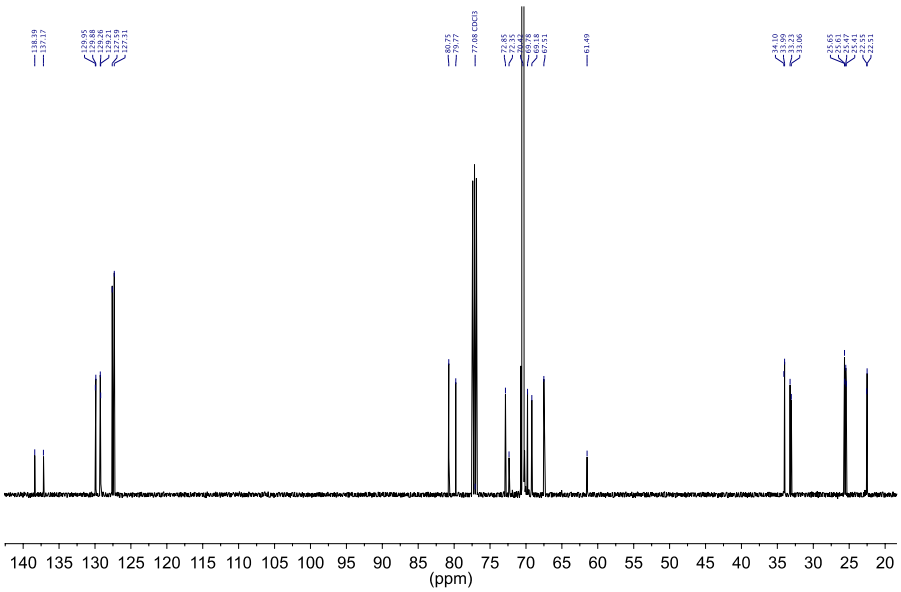

Figure 3.19 ^{13}C NMR Spectrum of PEO functionalized cross-linker (**1**) of molecular weight 3.7 kDa. Signal at 77.16 ppm is residual $CDCl_3$.

(*Z*)-5-((4-bromobenzyl)oxy)cyclooct-1-ene (3)

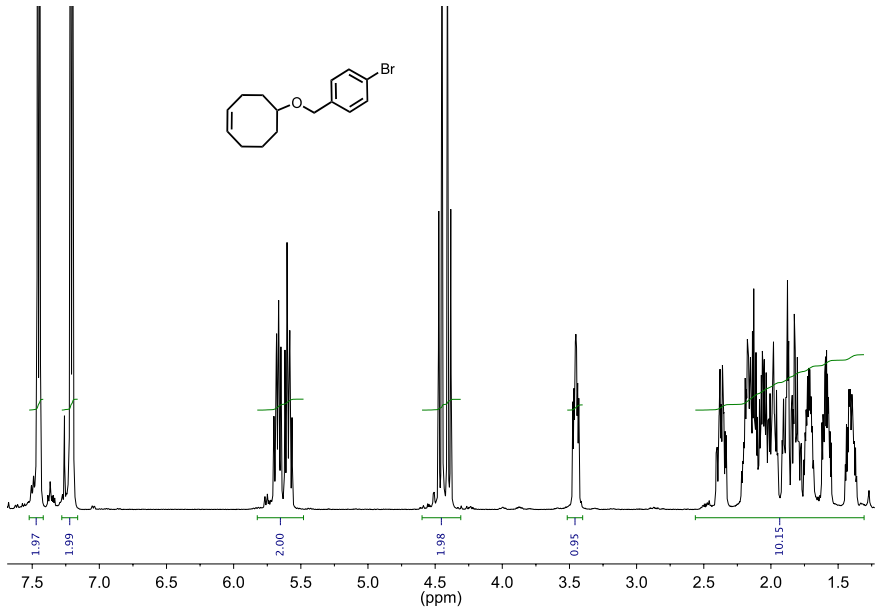

Figure 3.20 ^{1}H NMR Spectrum of (*Z*)-5-((4-bromobenzyl)oxy)cyclooct-1-ene (**3**). Signal at 7.24 ppm is residual $CHCl_3$.

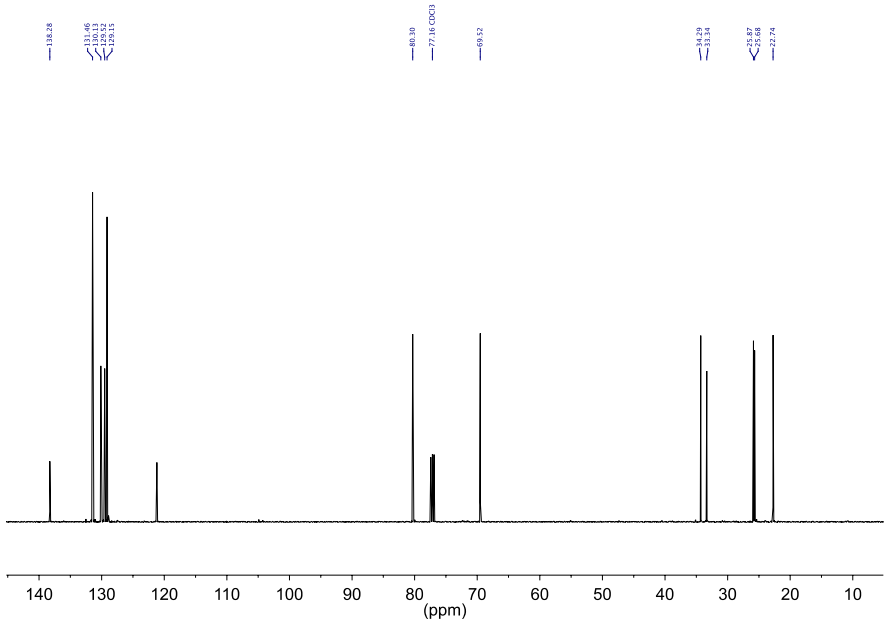

Figure 3.21 ^{13}C NMR Spectrum of (*Z*)-5-((4-bromobenzyl)oxy)cyclooct-1-ene (**3**). Signal at 77.16 ppm is residual $CDCl_3$.

Lithium (*Z*)-(4-((cyclooct-4-en-1-yloxy)methyl)phenyl)triphenylborate (4)

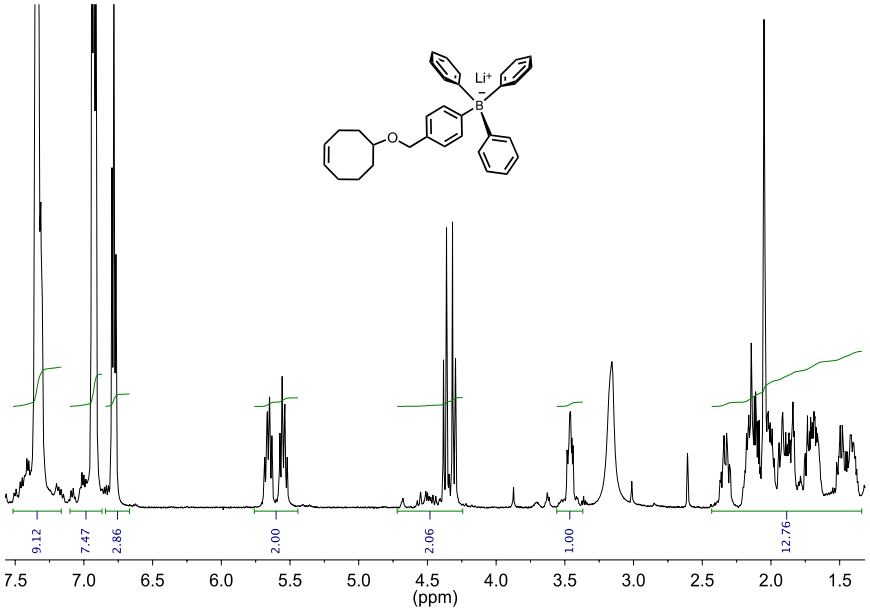

Figure 3.22 ^{1}H NMR Spectrum of lithium (*Z*)-(4-((cyclooct-4-en-1-yloxy)methyl)phenyl)triphenylborate (**4**). Signal at 2.05 ppm is residual signal from acetone.

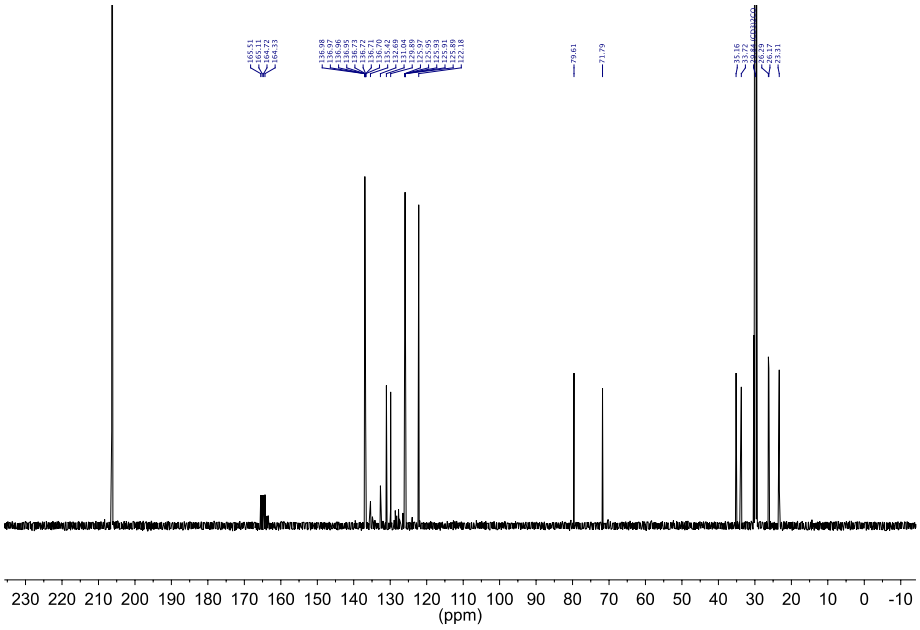

Figure 3.23 ^{13}C NMR Spectrum of lithium (*Z*)-(4-((cyclooct-4-en-1-yloxy)methyl)phenyl)triphenylborate (**4**). Signals at 29.84 and 206.3 ppm are the residual signals from acetone.

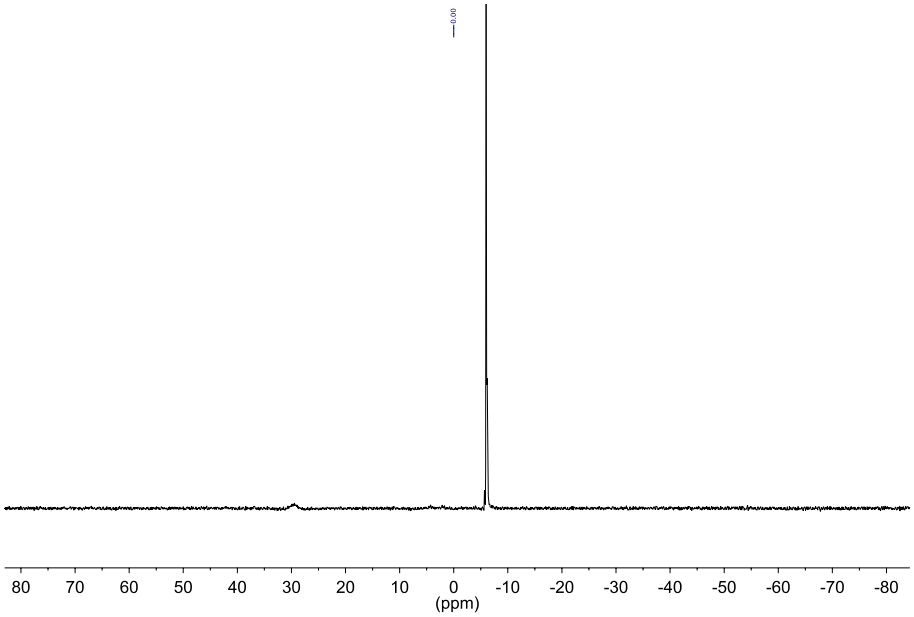

Figure 3.24 ^{11}B NMR Spectrum of lithium (*Z*)-(4-((cyclooct-4-en-1-yloxy)methyl)phenyl)triphenylborate (**4**). Spectrum was referenced externally to $BF_3{\cdot}Et_2O$ ($\delta = 0$ ppm).

REFERENCES

(1) Yang, Z. G.; Zhang, J. L.; Kintner-Meyer, M. C. W.; Lu, X. C.; Choi, D. W.; Lemmon, J. P.; Liu, J. *Chem. Rev.* **2011**, *111*, 3577–3613.

(2) Armand, M.; Tarascon, J. M. *Nature* **2008**, *451*, 652–657.

(3) Scrosati, B.; Garche, J. *J. Power Sources* **2010**, *195*, 2419–2430.

(4) Goodenough, J. B.; Kim, Y. *Chem. Mater.* **2010**, *22*, 587–603.

(5) Goodenough, J. B.; Park, K. S. *J. Am. Chem. Soc.* **2013**, *135*, 1167–1176.

(6) Tarascon, J. M.; Armand, M. *Nature* **2001**, *414*, 359–367.

(7) Dias, F. B.; Plomp, L.; Veldhuis, J. B. J. *J. Power Sources* **2000**, *88*, 169–191.

(8) Thomas, K. E.; Sloop, S. E.; Kerr, J. B.; Newman, J. *J. Power Sources* **2000**, *89*, 132–138.

(9) Wright, P. V. *MRS Bull.* **2002**, *27*, 597–602.

(10) Chazalviel, J. N. *Phys. Rev. A* **1990**, *42*, 7355–7367.

(11) Kerr, J. B. In *Science and Technology of Lithium Batteries*; Kluwer Academic: Boston, 2003, pp 575–622.

(12) Kobayashi, N.; Uchiyama, M.; Tsuchida, E. *Solid State Ionics* **1985**, *17*, 307–311.

(13) Cowie, J. M. G.; Spence, G. H. *Solid State Ionics* **1999**, *123*, 233–242.

(14) Ito, K.; Ohno, H. *Solid State Ionics* **1995**, *79*, 300–305.

(15) Sun, X. G.; Kerr, J. B. *Macromolecules* **2006**, *39*, 362–372.

(16) Sun, X. G.; Kerr, J. B.; Reeder, C. L.; Liu, G.; Han, Y. B. *Macromolecules* **2004**, *37*, 5133–5135.

(17) Sun, X. G.; Reeder, C. L.; Kerr, J. B. *Macromolecules* **2004**, *37*, 2219–2227.

(18) Bouchet, R.; Maria, S.; Meziane, R.; Aboulaich, A.; Lienafa, L.; Bonnet, J. P.; Phan, T. N. T.; Bertin, D.; Gigmes, D.; Devaux, D.; Denoyel, R.; Armand, M. *Nat. Mater.* **2013**, *12*, 452–457.

(19) Feng, S. W.; Shi, D. Y.; Liu, F.; Zheng, L. P.; Nie, J.; Feng, W. F.; Huang, X. J.; Armand, M.; Zhou, Z. B. *Electrochim. Acta* **2013**, *93*, 254–263.

(20) Meziane, R.; Bonnet, J. P.; Courty, M.; Djellab, K.; Armand, M. *Electrochim. Acta* **2011**, *57*, 14–19.

(21) Allcock, H. R.; Welna, D. T.; Maher, A. E. *Solid State Ionics* **2006**, *177*, 741–747.

(22) Herath, M. B.; Creager, S. E.; Rajagopal, R. V.; Geiculescu, O. E.; DesMarteau, D. D. *Electrochim. Acta* **2009**, *54*, 5877–5883.

(23) Liu, W.; Janik, M. J.; Colby, R. H. In *Polymers for Energy Storage and Delivery: Polyelectrolytes for Batteries and Fuel Cells*; Page, K. A., Soles, C. L., Runt, J. , Eds.; American Chemical Society: Washington, DC, 2011; Chapter 2, pp 19–44.

(24) Choi, U. H.; Liang, S.; O'Reilly, M. V.; Winey, K. I.; Runt, J.; Colby, R. H. *Macromolecules* **2014**, *47*, 3145–3153.

(25) Liang, S. W.; Choi, U. H.; Liu, W. J.; Runt, J.; Colby, R. H. *Chem. Mater.* **2012**, *24*, 2316–2323.

(26) Aravindan, V.; Gnanaraj, J.; Madhavi, S.; Liu, H. K. *Chem.—Eur. J.* **2011**, *17*, 14326–14346.

(27) Krossing, I.; Raabe, I. *Angew. Chem. Int. Ed.* **2004**, *43*, 2066–2090.

(28) Khurana, R.; Schaefer, J. L.; Archer, L. A.; Coates, G. W. *J. Am. Chem. Soc.* **2014**, *136*, 7395–7402.

(29) Tikekar, M. D.; Archer, L. A.; Koch, D. L. *J. Electrochem. Soc.* **2014**, *161*, A847–A855.

(30) See Experimental Section for details.

(31) A similar solid state hydrogenation reaction has been previously reported by our group for a binary salt doped polyethylene/poly(ethylene oxide) polymer electrolyte. The efficiency of the hydrogenation step was examined by doing a control experiment. For details, see the Supporting Information of reference 28.

(32) Dou, S. C.; Zhang, S. H.; Klein, R. J.; Runt, J.; Colby, R. H. *Chem. Mater.* **2006**, *18*, 4288–4295.

(33) Fragiadakis, D.; Dou, S.; Colby, R. H.; Runt, J. *J. Chem. Phys.* **2009**, *130,* 064907(1) –064907(11).

(34) For the mixed single-ion conductor sample set, a new sample of PEOX cross-linker was synthesized to obtain approximately 80 EO units. Since it is difficult to control the exact amount of EO, the PEOX cross-linker with 70 EO units was employed instead of PEOX cross-linker containing 80 EO units.

(35) Berthier, C.; Gorecki, W.; Minier, M.; Armand, M. B.; Chabagno, J. M.; Rigaud, P. *Solid State Ionics* **1983**, *11*, 91–95.

(36) Armand, M. *Solid State Ionics* **1983**, *9-10*, 745–754.

(37) Hillmyer, M. A.; Laredo, W. R.; Grubbs, R. H. *Macromolecules* **1995**, *28*, 6311–6316.

(38) Jonscher, A. K. *Nature* **1977**, *267*, 673–679.

CHAPTER 4

Development of New Solid Polymer Electrolyte Formulations: Effect of Lithium Salts and Plasticizers on Electrolyte Performance

CHAPTER 4

Development of New Solid Polymer Electrolyte Formulations: Effect of Lithium Salts and Plasticizers on Electrolyte Performance

4.1 Abstract

We report new solid polymer electrolyte (SPE) formulations for lithium metal batteries. These formulations were developed by varying the lithium salts and plasticizers in cross-linked polyethylene/poly(ethylene oxide) (PE/PEO) SPEs. The impact of these additives upon the electrochemical performance of the electrolyte was investigated. The counter anions of the lithium salts had a significant effect on the ionic conductivity and electrochemical stability of the SPE's performance. Specifically, lithium bis(oxalato)borate containing SPE shows an electrochemical stability up to 4.6 V, which is 0.7 V higher than the SPE containing lithium bis(trifluoromethanesulfonyl)imide salt. In addition, the effects of various plasticizers on the cross-linked PE/PEO electrolyte's performance were also examined. Different plasticizers containing poly(ethylene glycol) oligomers and cyclic carbonate moieties were synthesized and tested for their influence on the SPE's properties. In particular, SPE formulations with cyclic carbonate plasticizers show relatively low ionic conductivity.

4.2 Introduction

Electrolyte formulation is crucial for successful operation of a Li-based rechargeable battery over wide range of temperatures and operating voltage.[1] A mixture of 1.0 M solution of $LiPF_6$ in ethylene carbonate/dimethyl carbonate (1:1, v/v) is widely accepted as an optimum electrolyte composition for 3.6 V Li-ion batteries (LIB). However, no electrolyte composition has so far been proven to be effective enough to allow for the commercialization of high voltage (5.0 V) LIBs due to the oxidative instability of these electrolytes against high cathode materials. Furthermore, the use of these liquid electrolytes in conjunction with high energy Li-metal batteries (LMBs) is currently limited by the formation of irregular lithium structures (also called as dendrites) on the Li-metal anode over repeated charge-discharge cycles.[2,3] In contrast, some of the solid polymer electrolyte (SPE) formulations have shown promise for the rechargeable LMB technology by delaying the lithium dendrite growth and nucleation.[4,5] The development of a Li-ion conducting SPE formulation, which is stable against Li-metal anode and is electrochemically stable at high voltages is thus an area of significant interest.

One of the essential components of the electrolyte is a Li-ion conducting salt. For the successful operation of a rechargeable lithium battery, an ideal lithium salt should have the following properties: a) high Li^+ ion conductivity, b) good electrochemical stability (high decomposition voltage), c) high thermal stability, d) non-toxicity, e) good solubility in the polar organic solvent (or polymer matrix in the case of polymer electrolyte), f) low cost, g) formation of a stable and less resistive solid-electrolyte-interface (SEI) layer at the electrolyte-electrode interface, and g)

chemical stability towards the electrode components.[6] It has been observed that lithium salts play a crucial role in the conducting properties and electrochemical stability of the electrolyte in LIBs containing polar organic solvents.[6-9] Kita and co-workers investigated the structural effects of fluoroorganic lithium salts on the conductivity, electrochemical stability, aluminum corrosion at high voltage, and cell performance of a Li-ion battery.[7] They found that among a lithium salt series, the anions with longer fluoroalkyl chains showed higher oxidation potential. For example, the oxidation potentials for CF_3SO_3Li, $C_4F_9SO_3Li$, and $C_8F_{17}SO_3Li$ were determined to be 4.8, 6.0, and 6.5 V, respectively in propylene carbonate electrolyte. In another instance, Tsujioka *et al.* examined the electrolytes containing different lithium salts and found that the electrolyte compositions containing a mixture of lithium borate and lithium imide salts demonstrated high capacity retention during charge-discharge cycles of a Li-ion battery.[8]

While many researchers have explored the effects of different lithium salts for the LIB technologies, only a few literature reports have discussed the effects of lithium salt in a SPE formulation for LMBs.[10,11] Greenbaum and co-workers investigated the effect of three different salts namely $LiClO_4$, CF_3SO_3Li, and LiTFSI, for the PEO/Al_2O_3 composite SPEs on the electrochemical performance of these electrolytes.[10] Among the salts investigated, the SPEs containing LiTFSI showed the highest conductivity. Furthermore, they observed that PEO-LiTFSI electrolytes showed significantly lower electrochemical stability when compared to PEO-CF_3SO_3Li SPE at 40 °C. It is clear that the counter anions in the lithium salt play a significant role in the ionic conductivity and electrochemical stability of polymer

electrolytes.

SPEs are desired to have high ionic conductivity values (>1.0 × 10^{-4} S/cm at 25 °C) to allow the efficient charge-discharge of the batteries at room temperature.[12,13] PEO polymers are the most extensively studied polymer electrolytes for Li-battery applications due to their high chemical and electrochemical stability, ability to dissolve lithium salts, low cost, and non-toxicity.[14] Unfortunately, lithium-salt doped PEO polymers have low ionic conductivities at ambient temperature, due to their high crystallinity.[15] Addition of a plasticizer has been used as one of the many strategies to increase their ionic conductivity.[16-20] McBreen and co-workers listed the following criteria for plasticizer selection: a) ability to decrease the glass transition temperature of the polymer host allowing better segmental motion for Li-ion conduction, b) high dielectric constant to increase the lithium salt dissociation, c) ability to suppress the crystallinity of the polymer host, c) good miscibility with the polymer, d) low volatility, and e) inertness towards the electrode materials.[18] Numerous plasticizers have been used to improve the conductivity of SPEs, including oligomers of poly(ethylene glycol) (PEG),[20,21] cyclic carbonates,[18,22,23] and ionic liquids.[24-26] Cyclic carbonates have high dielectric constant values, which cause greater lithium salt dissociation, leading to higher ionic conductivity. It has been shown that higher ionic conductivities (>10^{-4} S/cm at 25 °C) could be obtained for PEO-$LiCF_3SO_3$ polymer electrolytes at higher weight percentages (~ 150 wt%) of propylene carbonate (PC).[22] However, the mechanical properties of these PC-doped polymer electrolytes deteriorate upon plasticization. Most importantly, these cyclic carbonates are flammable, which raises safety concerns. In contrast to cyclic carbonate plasticizers,

PEG oligomers and ionic liquids are less/non-flammable, and hence they are safer alternatives to the flammable cyclic carbonate plasticizers.

To formulate a SPE composition that supports high voltage cathode material and is stable with a lithium metal anode, we investigated the effects of changing counter anions of the lithium salt on the electrochemical properties of the electrolyte. For some SPE formulations, we used a use of mixture of two different salts to investigate their effects on electrochemical performance. In addition, we also examined the effects of various plasticizers on the conductivity of an optimized SPE composition.

4.3 Results and Discussion

In Chapter 2, we reported cross-linked polyethylene/poly(ethylene oxide) (PE/PEO) solid polymer electrolytes (SPEs), comprised of mechanically strong polyethylene (PE) chains covalently cross-linked by Li-ion conducting poly(ethylene oxide) (PEO) segments. The cross-linked polymer framework of PE/PEO electrolytes is shown in Figure 4.1. We studied different sample compositions by varying the number of EO units in the cross-links, cross-linking density, and weight% of the plasticizer. After testing large number of samples, we found an optimum SPE composition (^{80}PEOX: ~80 ethylene oxide units in the cross-links, 34 PE units between the cross-links, 31 wt% PEG275 as the plasticizer, and lithium bis(trifluoromethanesulfonyl)imide (LiTFSI) as the salt). The optimized formulation exhibited high ionic conductivity (>1.0×10^{-4} S/cm at 25 °C) and excellent resistance to lithium dendrite growth. These optimized LiTFSI-doped SPE formulations are potential candidates for 4.0 V Li-metal batteries (LMBs), as demonstrated by cyclic

voltammetry measurements.[27] However, they cannot be employed for LMBs equipped with 5.0 V cathode materials due to electrochemical decomposition of the electrolyte at high voltages against the cathode.

4.3.1 Effect of lithium salts

To enhance the electrochemical stability of the cross-linked PE/PEO polymer electrolytes for high voltage applications, we investigated the effect of varying the counter anions of the lithium salts for the optimized SPE formulation (^{80}PEOX) on the electrochemical stability. The cross-linked polymer framework and the structures of the lithium salts are shown in Figure 4.1. Eight different lithium salts were developed by employing four lithium salts; four formulations contained a single lithium salt (Table 4.1, entries 1, 2, 7, 8) and the remaining four SPE formulations were comprised of a mixture of two lithium salts, LiTFSI and lithium bis(oxalato)borate (LiBOB) in varied ratios (Table 4.1, entries 3–6). The DSC traces of plasticized SPEs containing different lithium salts are shown in Figure 4.2. The SPE composition with LiTFSI salt exhibited the lowest glass transition temperature (T_g) value of −61 °C, while the SPEs containing sulfonate salts, namely $C_4F_9SO_3Li$ (entry 7) and CF_3SO_3Li (entry 8)

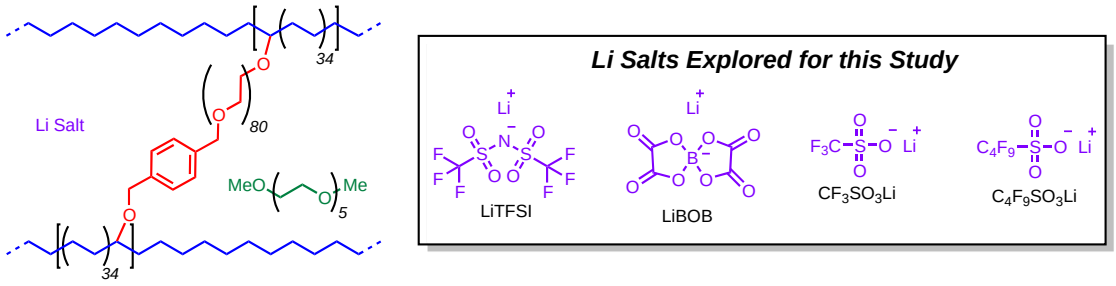

Figure 4.1 Polyethylene/poly(ethylene oxide) polymer electrolytes with different lithium salts. Left: Polymer framework. Right: Lithium salts tested for various formulations.

Table 4.1 Compositions and thermal properties of plasticized PE/PEO cross-linked SPEs with different lithium binary salts[a]

Entry	Lithium Salt	PE Segments[b]		PEO Segments[c]			
		T_m[d] (°C)	ΔH_{fus}[d] (J/g)	T_g[d] (°C)	T_c[d] (°C)	T_m[d] (°C)	ΔH_{fus}[d] (J/g)
1	LiTFSI	95	20.1	−61	−26	18	14.9
2	LiBOB	97	28.3	−50	n.d.[f]	n.d.[f]	n.d.[f]
3	LiTFSI/LiBOB (80:20)	97	26.5	−56	−14	14	3.3
4	LiTFSI/LiBOB (70:30)	98	28.8	−57	−17	14	6.7
5	LiTFSI/LiBOB (60:40)	98	27.6	−56	−15	13	5.7
6	LiTFSI/LiBOB (50:50)	86	33.7	−53	n.d.[f]	n.d.[f]	n.d.[f]
7	$C_4F_9SO_3Li$	91	27.3	−49	−21	24	19.4
8	CF_3SO_3Li	96	34.4	−36	n.d.[f]	27	29.4

[a]All films had 80 ethylene oxide (EO) units in the cross-linker, 34 polyethylene (PE) units between the cross-links, and [EO]:[Li] composition of 18:1; where EO where EO includes ethylene oxide units contained both in the cross-links and PEG plasticizer. [b]PE segments: Polyethylene domains in the polymer electrolyte. [c]PEO segments: Poly(ethylene oxide) domains in the polymer electrolyte. [d]Glass transition temperature (T_g), cold crystallization temperature (T_c), melting temperature (T_m), and ΔH_{fus} were determined by differential scanning calorimetry of the second heat cycle. [f]Not detected.

showed the highest T_g values of −49 °C and −36 °C, respectively. For the SPEs containing LiBOB salt (entry 2) and a 50:50 mixture of LiBOB and LiTFSI (entry 6), no crystallization was observed in the PEO segments, suggesting that the bis(oxalateborate) (BOB) anion played a significant role in suppressing the crystallization of PEO in the network structure. Furthermore, the SPE formulations incorporating the mixtures of LiTFSI and LiBOB (entries 3–6) exhibited glass transition temperatures which were higher than the SPE containing LiTFSI (entry 1) and lower than the composition with LiBOB (entry 2), indicating that both the anions (TFSI and BOB) influenced the segmental mobility of the PEO chain in the network polymer electrolyte.

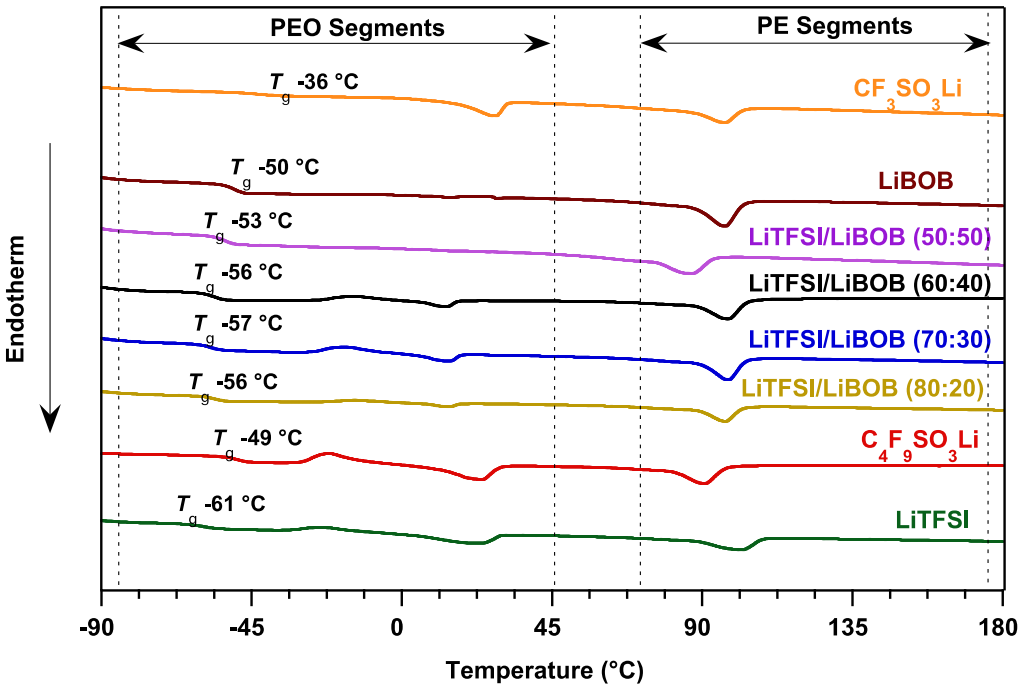

Figure 4.2 DSC traces of PE/PEO cross-linked polymer electrolytes (80 EO units in the cross-linker, 34 PE units between the cross-links, 31 wt% PEG275 plasticizer) with different lithium salts.

The ionic conductivities of the SPEs containing different lithium salts were obtained using dielectric spectroscopic measurements[28] at variable temperature (−5 to 100 °C) and the data are shown in Figure 4.3. Notably, all the SPEs showed higher ionic conductivity values than the PEO standard (M_n ~ 900 kDa) sample at low and medium temperatures (−5 to 50 °C). In addition, the data clearly shows that there is a significant effect of the electrolyte salt upon the ionic conductivity. Among the salts investigated, the SPE formulation containing LiTFSI exhibited the highest ionic conductivities at all the measured temperatures. Presumably, the high conductivity

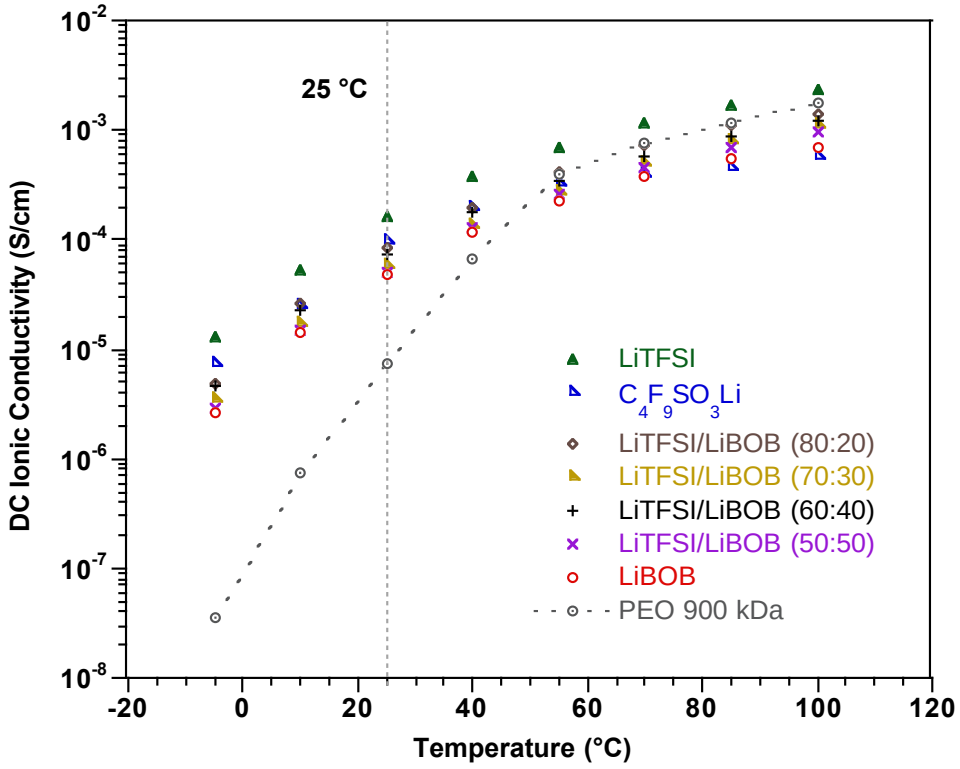

Figure 4.3 Variable temperature conductivity of PE/PEO cross-linked polymers (80 EO units in the cross-linker, 34 PE units between the cross-links, 31 wt% PEG275 plasticizer) with different lithium salts.

value of this SPE is due to its lowest glass transition temperature, allowing better segmental motion of the PEO chains in the polymer electrolyte and thus facile Li-ion conduction. Although, the PEO domains in the SPE formulation containing LiBOB were amorphous (i.e. the crystallization of PEO was completely suppressed), this SPE (Table 4.1, entry 2) exhibited the lowest ionic conductivity (4.8×10^{-5} S/cm at 25 °C) of the tested SPEs. We postulate that this conductivity drop is due to the coordination of Li^+ ion with the BOB anion, as shown in Figure 4.5. The chelation with the BOB

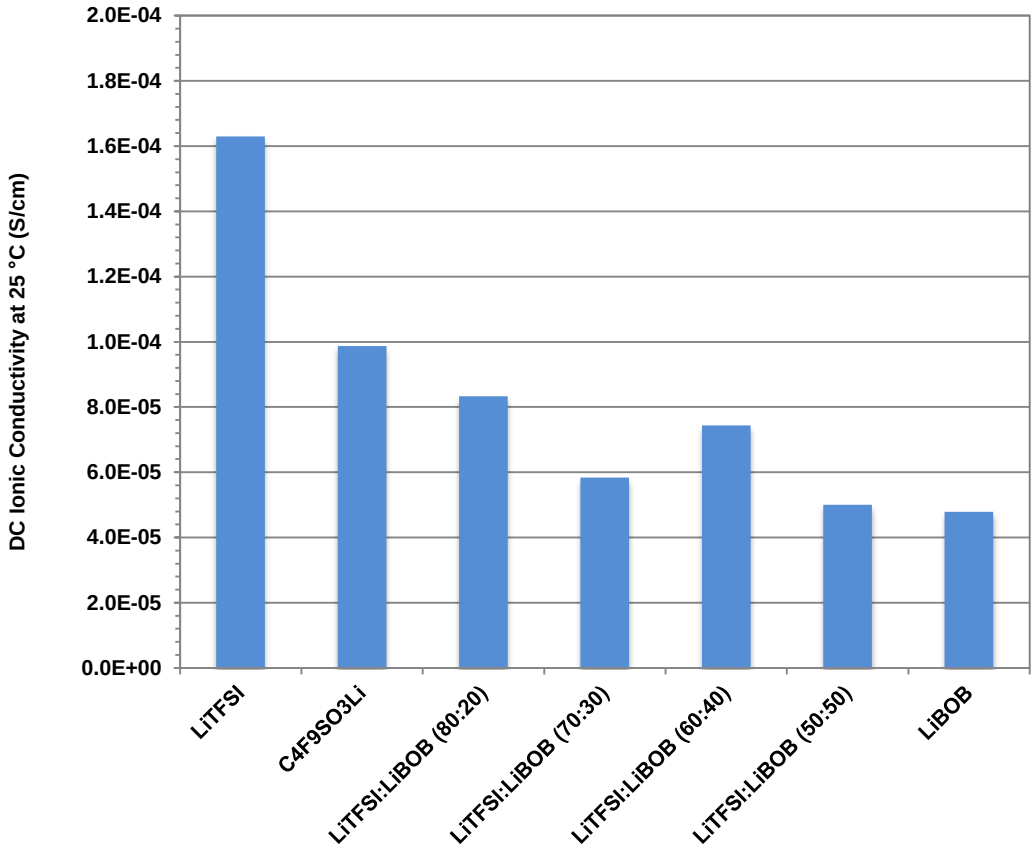

Figure 4.4 Room temperature conductivity of ^{80}PEOX electrolytes (80 EO units in the cross-linker, 34 PE units between the cross-links, 31 wt% PEG275 plasticizer) with variable lithium salts.

anion lowers the lithium ion mobility, leading to a lower ionic conductivity value. A significant effect of the Li^+-BOB^- coordination was also reflected in the ionic conductivity values for the SPE formulations containing a mixture of LiTFSI and LiBOB (Table 4.1, entries 3–6). The conductivity values dropped drastically when LiBOB was added to the SPE formulations containing LiTFSI. Even for the composition with the lowest mole fraction of LiBOB (Table 4.1, entry 3), the ionic conductivity value was observed to be 8.3×10^{-5} S/cm at 25 °C, which is two times lower than the LiTFSI-doped SPE.

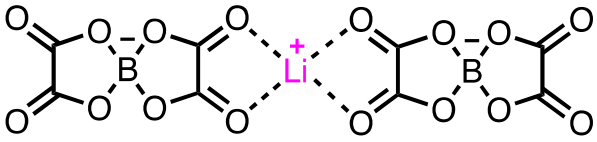

Figure 4.5 Proposed model for low ionic conductivity of LiBOB-doped SPE.

In the pursuit of finding a SPE formulation with an enhanced electrochemical stability window, we performed cyclic voltammetry (CV) measurements on the lithium salt doped SPEs (Table 4.1). The CV measurements were performed on Li/SPE/SS coin cells at 1 mV/s and 22 °C, and the data are shown in Figure 4.6. The two reversible features were observed in the CVs around 1.0 V and 2.0 V and they could be attributed to the oxide impurities in the stainless steel working electrode.[29] The oxidative instability for an SPE was gauged by an irreversible response on the cyclic voltammogram; the electrochemical stability data for the lithium salt-doped

SPE formulations are summarized in Figure 4.7. The data clearly indicate that the counter anions play a crucial role in dictating the electrochemical stability window for an SPE. While the LiTFSI-doped SPE composition displayed the voltage stability up to 3.9 V (Figure 4.6a), the oxidative stability was significantly enhanced upon addition of LiBOB to the SPE formulations. In particular, LiBOB-doped SPE showed an electrochemical stability up to 4.6 V at 22 °C (Figure 4.6b). Also, the SPE compositions containing mixtures of LiTFSI and LiBOB salts showed an enhanced electrochemical stability window when compared to LiTFSI. For the CF_3SO_3Li-doped SPE composition, the electrochemical stability window was wider than the SPE containing LiTFSI (stable up to 4.2 V compared to 3.9 V) at ambient temperature. Greenbaum and co-workers observed a similar electrochemical stability trend for LiTFSI and CF_3SO_3Li-doped PEO/Al_2O_3 composites.[10] $C_4F_9SO_3Li$-doped polymer electrolyte showed an oxidation peak around 4.5 V, which could be attributed to the unknown impurities in the commercially available $C_4F_9SO_3Li$ salt. This SPE composition (Table 4.1, entry 7) is stable up to 4.5 V, which is approximately 0.3 V higher than the CF_3SO_3Li salt-doped composition (Table 4.1, entry 8). Kita and co-workers observed similar oxidative stability increase for the liquid electrolytes containing anions of organic lithium salts with longer fluoroalkyl groups.[7]

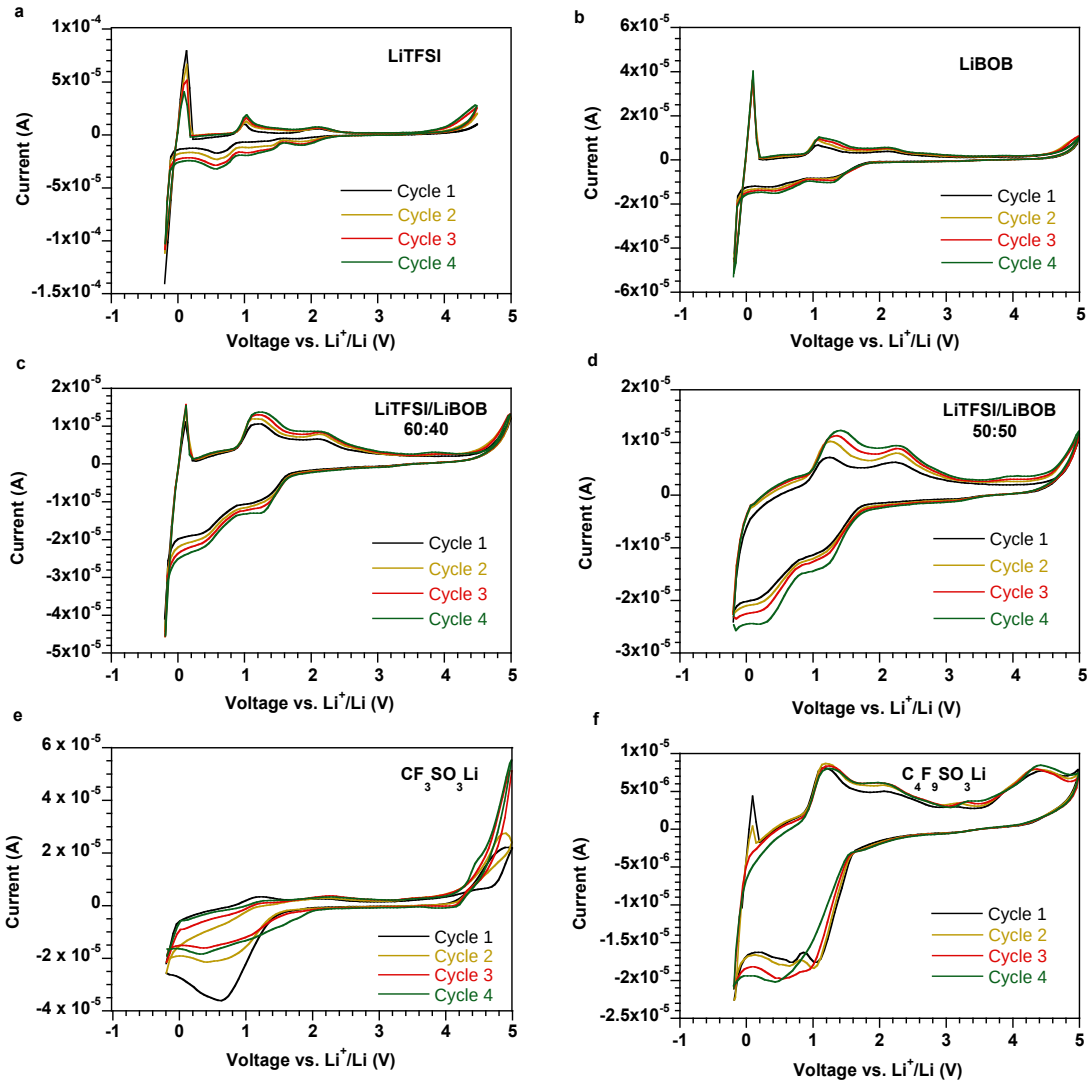

Figure 4.6 Cyclic voltammograms of cross-linked electrolytes (80 EO units in the cross-linker, 34 PE units between the cross-links, 31 wt% PEG275 plasticizer, and [EO]:[Li] ratio of 18:1) containing different lithium salts at 1 mV/s scan rate and 22 °C. a) LiTFSI, b) LiBOB, c) LiTFSI/LiBOB (60:40), d) LiTFSI/LiBOB (50:50), e) CF_3SO_3Li, and f) $C_4F_9SO_3Li$.

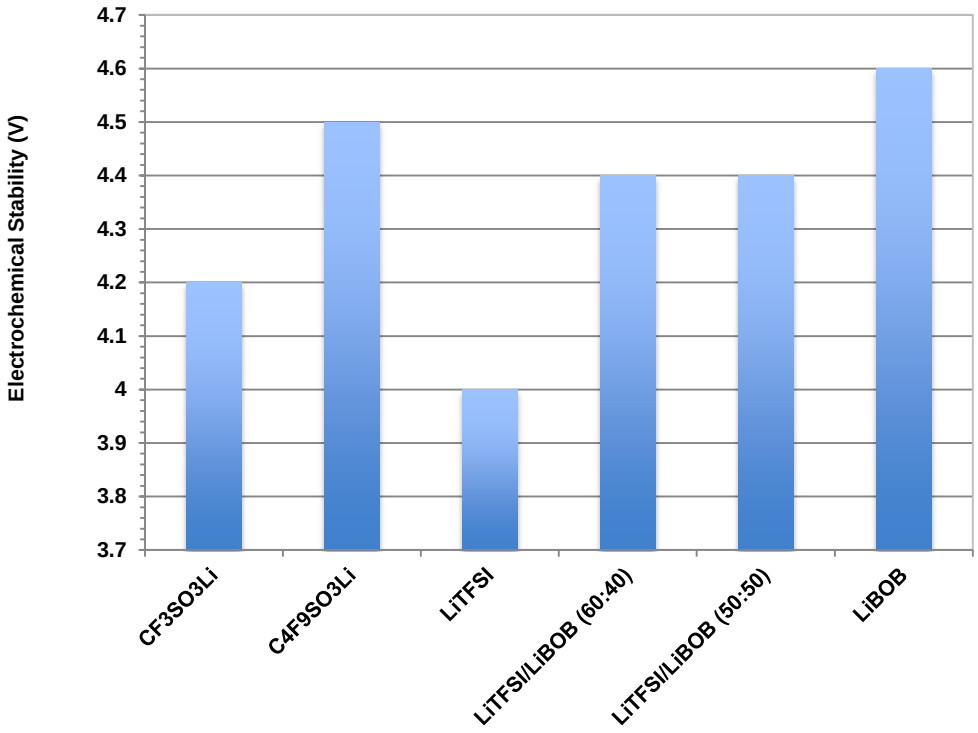

Figure 4.7 Electrochemical stability of ^{80}PEOX electrolytes (80 EO units in the cross-linker, 34 PE units between the cross-links, 31 wt% PEG275 plasticizer, and [EO]:[Li] ratio of 18:1) containing different lithium salts at 22 °C.

To summarize the effect of lithium salts in the electrolyte formulation on the properties of electrolyte – counter anions of the lithium salts were found to have a significant effect on both the ionic conductivity and the electrochemical stability of the SPE. Among the tested lithium salts, the SPE containing LiTFSI showed the highest conductivity value of 1.7×10^{-4} S/cm at 25 °C and an electrochemical stability up to 3.9 V. Although a significant improvement in the electrochemical stability was observed for the SPE compositions containing LiBOB/LiTFSI salt combinations compared to LiTFSI-doped SPEs, addition of LiBOB to the LiTFSI-doped SPE formulations led to a dramatic decrease in ionic conductivity.

4.3.2 Effect of plasticizers

In an effort to increase the conductivity of the cross-linked PE/PEO SPEs, we investigated the effects of different plasticizers in the SPE formulations. The polymer framework and the plasticizers explored in the current study are shown in Figure 4.8. Five different plasticizers were chosen for this study – dimethoxy-terminated PEG (M_n 275 Da and 500 Da), star PEG (M_n of each arm ~ 500 Da), bis(cyclic carbonate)-terminated PEG (BCC-PEG; M_n 500 Da), and tetracyclic carbonate (TCC). Star PEG, BCC-PEG, and TCC were synthesized, dried, and subsequently used as plasticizers for SPE formulations; dimethoxy-terminated PEGs were purchased from commercial sources and dried before their use as additives in the SPE formulations. The superior performance of multi-arm PEG or star PEG plasticizers at lower temperatures compared to the linear plasticizers, as reported by Kang and co-workers, inspired us to use them for the current study.[20] The high dielectric constant of the cyclic carbonates (BCC-PEG500 and TCC) and their solubility in lithium salts motivated their use as plasticizers for this study.

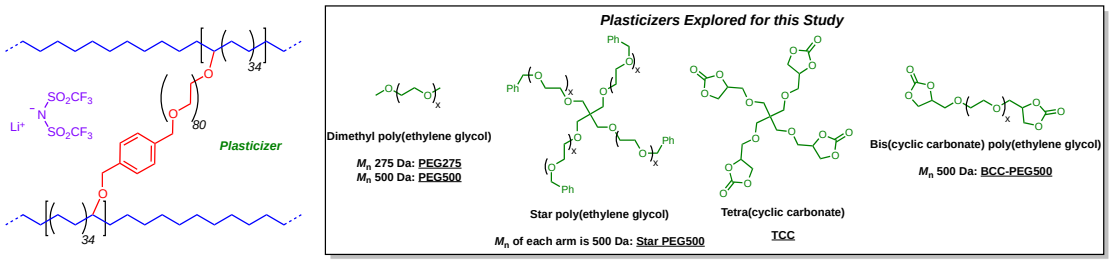

Figure 4.8 Polyethylene/poly(ethylene oxide) polymer electrolytes with different plasticizers. Left: Polymer framework. Right: Plasticizers investigated for the SPE formulations.

The compositions and the thermal data for the SPE formulations containing five different plasticizers are listed in Table 4.2. The DSC traces of these plasticized SPE formulations are shown in Figure 4.9. Among the SPE compositions with linear plasticizers (PEG275, PEG500, and BCC-PEG500), the one containing PEG275 exhibited the lowest glass transition temperature of −61 °C and had crystalline PEO domains in the network polymer. In contrast to the PEG275 formulation, the SPE containing BCC-PEG500 plasticizer (Table 4.2, entry 4) was completely amorphous in the PEO segments (i.e. no T_m was observed for the PEO segments).

Table 4.2 Compositions and thermal properties of PE/PEO cross-linked SPEs with different plasticizers[a]

Entry	Additive	PE Segments[b]		PEO Segments[c]			
		T_m[d] (°C)	ΔH_{fus}[d] (J/g)	T_g[d] (°C)	T_c[d] (°C)	T_m[d] (°C)	ΔH_{fus}[d] (J/g)
1	None	91	15.2	−47	−14	20	15.2
2	PEG275	95	20.1	−61	−26	18	14.9
3	PEG500	110	12.9	−56	n.d.[f]	29	43.6
4	BCC-PEG500	109	13.8	−42	n.d.[f]	n.d.[f]	n.d.[f]
5	Star-PEG500	101	17.6	−42	0	22	2.2
6	TCC	99	23.2	−25	n.d.[f]	n.d.[f]	n.d.[f]

[a]All films had 80 EO units in the cross-linker, 34 PE units between the cross-links, and LiTFSI salt at the [EO]:[Li] composition of 18:1; where EO includes ethylene oxide units contained both in the cross-links and the plasticizer. [b]PE segments: Polyethylene domains in the polymer electrolyte. [c]PEO segments: Poly(ethylene oxide) domains in the polymer electrolyte. [d]Glass transition temperature (T_g), cold crystallization temperature (T_c), melting temperature (T_m), and ΔH_{fus} were determined by differential scanning calorimetry of the second heat cycle. [f]Not detected.

However, BCC-PEG500 plasticizer led to a significant increase in glass transition temperature (T_g = −42 °C) compared to the unplasticized composition, which is presumably due to the inter- and intra- molecular dipole-dipole interactions of the cyclic carbonate units. Most likely, similar kinds of secondary interactions of the cyclic carbonate moiety occurred in the TCC containing formulations (Table 4.2, entry 6) and consequently a significantly higher T_g value of −25 °C was observed. Kim and co-workers observed a similar thermal transitions trend for the cyclic carbonate containing plasticizers.[19]

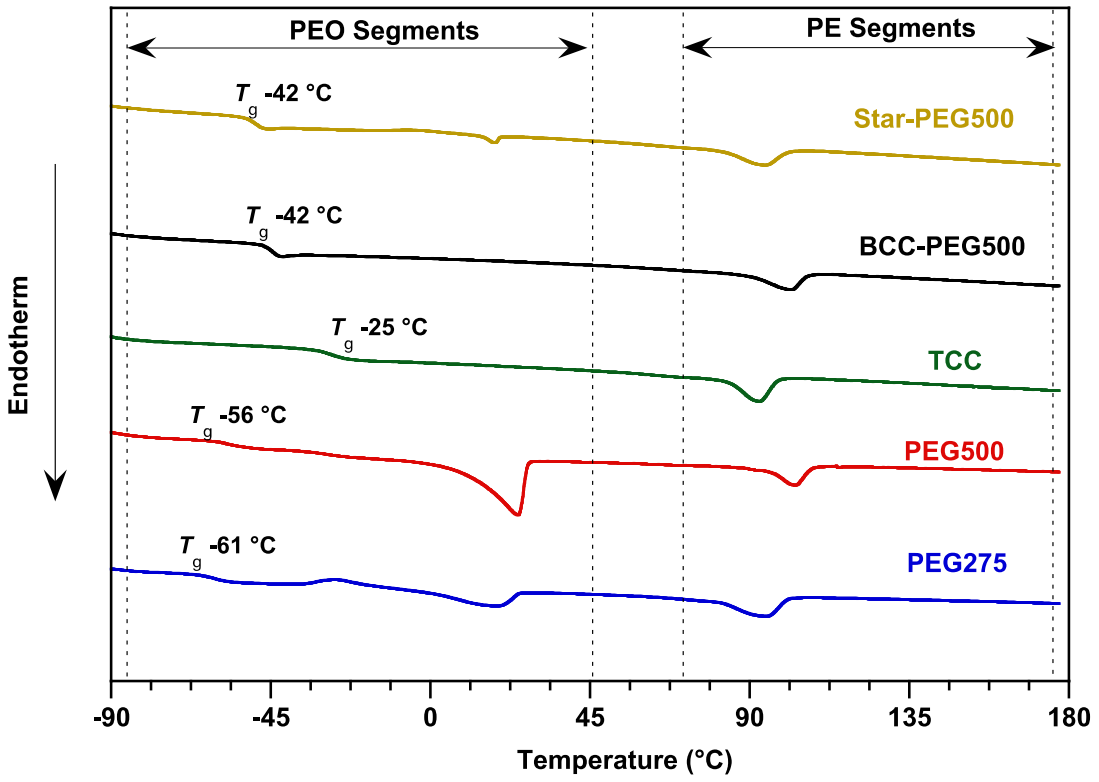

Figure 4.9 DSC traces of [80]PEOX electrolytes (80 EO units in the cross-linker, 34 PE units between the cross-links, LiTFSI salt at [EO]:[Li] composition of 18:1) with different plasticizers.

Room temperature ionic conductivity measurements were performed on the SPEs containing different plasticizers and the data are shown in Figure 4.10. The room temperature ionic conductivity of the unplasticized SPE was 1.7×10^{-4} S/cm. Upon plasticization, the conductivity of all the SPEs except the one containing TCC increased. Most likely, this is due to the strong chelation of the Li^+ ion with the four cyclic carbonate units in the TCC, which leads to low lithium ion mobility and reduced ionic conductivity. As expected, the SPE formulation with the lowest T_g (the one containing PEG275 plasticizer) showed the highest ionic conductivity value (1.7×10^{-4} S/cm at 25 °C). The molecular weight of the PEG oligomer was observed to have a significant effect on the Li^+ ion conduction. The SPE with PEG500 plasticizer exhibited 5 times lower ionic conductivity than the electrolyte composition with PEG275 (3.6×10^{-5} S/cm compared to 1.7×10^{-4} S/cm at 25 °C). Presumably, this is

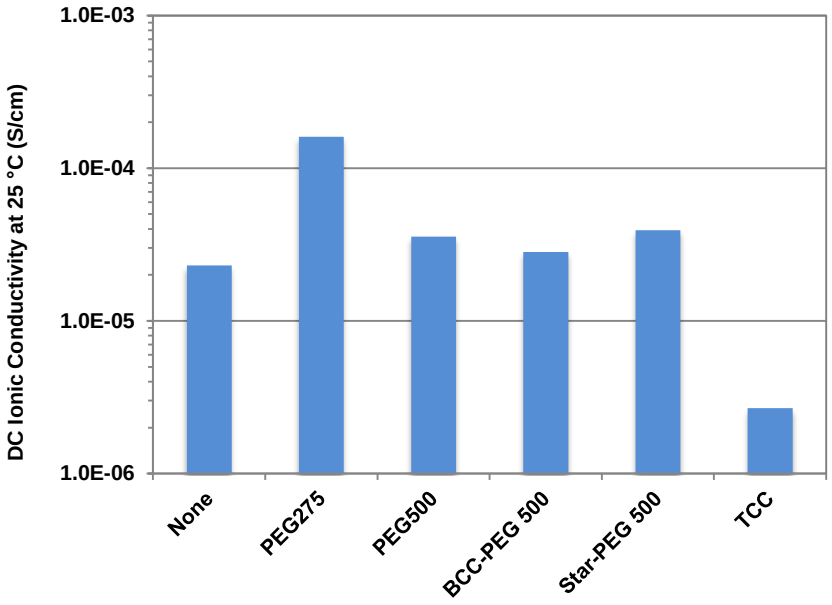

Figure 4.10 Room temperature conductivity of ^{80}PEOX electrolytes (80 EO units in the cross-linker, 34 PE units between the cross-links, and LiTFSI salt at the [EO]:[Li] composition of 18:1) containing different plasticizers.

due to the increase in viscosity of the electrolyte with increase in molecular weight of the PEG plasticizer, which ultimately leads to reduced lithium ion mobility. Kim and co-workers observed similar molecular weight effects of the PEG plasticizers upon the ionic conductivity of polymer electrolytes.[19] The connectivity of PEG chain (M_n ~ 500 Da) had little effect on the conductivity (Table 4.2, entries 3–5) suggesting that the segmental motion of the PEO chain is very similar in these SPE compositions at ambient temperature.

4.4 Conclusions

In summary, we have shown that lithium salts and plasticizers have a significant impact on the properties of the cross-linked PE/PEO electrolyte formulations. A new LiBOB-doped SPE formulation was developed that displayed 0.7 V higher electrochemical decomposition voltage than the LiTFSI-doped composition. However, the ionic conductivity of this LiBOB containing SPE was five times lower than the SPE containing LiTFSI salt. The effect of various plasticizers in LiTFSI-doped SPE formulations was also examined. Of the tested SPE compositions, the formulation with low molecular weight dimethoxy-terminated PEG (M_n = 275 Da) plasticizer exhibited the highest ionic conductivity while the SPE composition with tetracyclic carbonate plasticizer showed the lowest ionic conductivity. Current research efforts in our laboratory are focused on developing SPE formulations with different fluorinated additives to improve the electrochemical stability. Additionally, other plasticizers such as ionic liquids and crown ethers are also being explored for making new SPE compositions to improve the conductivity of the SPE.

4.5 Experimental

4.5.1 General

All reactions and manipulations of air and moisture sensitive compounds were carried out under dry nitrogen using a Braun UniLab drybox or standard Schlenk line techniques unless otherwise specified. ^{1}H NMR spectra were collected in deuterated solvents on a Varian INOVA 400 or Varian INOVA 500 spectrometer and referenced with residual non-deuterated solvent shifts ($CHCl_3$ = 7.24 ppm) and are reported relative to tetramethylsilane (δ = 0 ppm). ^{13}C NMR spectra were recorded on a Varian INOVA (^{13}C, 100 MHz) or Varian INOVA (^{13}C, 125 MHz) spectrometer and referenced to chloroform (δ 77.23 ppm). High-resolution mass spectrometry (HRMS) analyses were performed at the Mass Spectrometry Laboratory at the University of Illinois at Urbana-Champaign. MALDI mass spectra were obtained on a Waters Micro MX MALDI-TOF mass spectrometer using negative ion mode and a reflectron detector. Samples were prepared by depositing the analyte dissolved in a saturated dithranol solution onto a stainless steel sample plate. The plate was dried in air before loading it into the instrument.

Gel permeation chromatography (GPC) analyses were carried out using an Agilent PL-GPC 50 integrated system, equipped with UV and refractive index detectors, and 2 PL gel Mini-MIX C columns (5 micron, 4.6 mm ID). The GPC columns were eluted with tetrahydrofuran at 30 °C at 0.3 mL/min and were calibrated with monodisperse polystyrene standards. Differential scanning calorimetry (DSC) analyses of polymer samples were performed on either a TA Instruments Q1000 instrument equipped with liquid nitrogen cooling system or a Mettler Polymer DSC

instrument equipped with a chiller. Polymer samples on TA Instruments Q1000 instrument were made in aluminum pans and heated under nitrogen from −100 °C to 180 °C at a rate of 10 °C per minute and then cooled to −100 °C at a rate of 10 °C per minute, followed heating to 180 °C at a rate of 10 °C per minute. The glass transition temperature (T_g) and the melting temperature (T_m) were recorded from the second heating run.

The conductivity data of the polymer electrolytes was obtained over a range of frequencies (0.1 to 3 × 10^6 Hz) and temperatures (−5 °C to 100 °C) using a Novocontrol Dielectric Broadband Spectrometer fitted with a Quatro temperature control system. Conductivity measurements were performed using blocking/solid polymer electrolyte/blocking cell orientation, using gold plated stainless steel electrodes. Lithium/SPE/Stainless Steel (Li/SS/Li) coin cells were prepared in an argon filled MBraun glovebox using Hohsen components, size 2032, with 9.9 mm diameter lithium electrodes and a 12.7 mm diameter cross-linked electrolyte sample. Coin cell crimping was performed with a MTI electric crimping machine to ensure uniformity. The cyclic voltammetric measurements were performed on Li/SS/Li coin cells using a VersaStat 3 potentiostat (Princeton Applied Research) controlled by a VersaStudio software. The potential was scanned from −0.2 V to 4.5 V at 1 mV/s sweep rate and 22 °C.

4.5.2 Materials

Sodium hydride (95%), 1,5-cyclooctadiene, *cis*-cyclooctene (95%), *meta*-chloroperoxybenzoic acid (≤77%), tetrabutylammonium bromide (ACS reagent, ≥98%), allyl bromide (reagent grade, 97%), poly(ethylene glycol) digycidyl ether (M_n

~ 500 Da), Grubbs 2nd Generation catalyst (Cl_2(iMes)(PCy_3)Ru=CHPh), and Crabtree's catalyst [(COD)Ir(py)(PCy_3)]PF_6 were purchased from Sigma-Aldrich and used as received. Bis(trifluoromethane)sulfonimide lithium salt (LiTFSI; 99.95% trace metals basis), lithium bis(oxalate) borate (LiBOB), and lithium trifluoromethansulfonate ($LiCF_3SO_3$; 99.95% trace metals basis) were purchased from Sigma-Aldrich and dried in vacuum at 90 °C for 24 h and transferred directly into the glove box. Lithium 1,1,2,2,3,3,4,4,4-nonafluorobutane-1-sulfonate ($LiC_4F_9SO_3$) was obtained from TCI America and dried in vacuum at 90 °C for 24 h and transferred directly into the glove box. Ethylene oxide was purchased from Sigma-Aldrich and dried over *n*-BuLi before use. Pentaerythritol was purchased from Sigma-Aldrich and recrystallized from anhydrous DMF (>99%) before use. Dibromo-*p*-xylene (97%) and benzyl bromide (99%) was purchased from Alfa Aesar and used as received. Sodium hydroxide, sodium bicarbonate, potassium hydroxide, sodium sulfate, sodium bisulfite, and sodium chloride were purchased from Mallinckrodt and used as received. HPLC grade tetrahydrofuran was purchased from Fisher Scientific and dried over an alumina column and degassed by three freeze pump thaw cycles before use. Chloroform was dried over P_2O_5 and distilled prior to use. Hydrogen (99.99%) was purchased from Airgas. CO_2 was purchased from Airgas and passed over a column of 4Å molecular sieves before use. $CDCl_3$ was purchased from Cambridge Isotope Laboratories (CIL) and used as received.

Following a literature procedure,[30] 5-hydroxy-1-cyclooctene was prepared, dried over activated 3 Å sieves, and degassed by three freeze pump thaw cycles before use. Potassium naphthalenide in THF was prepared from naphthalene and potassium at

a concentration of 0.35 M (titrated with a standard benzoic acid solution until a persistent green color was observed as an end-point of the titration) and degassed by three freeze pump thaw cycles before use.

4.5.3 Synthesis

4.5.3.1 Synthesis of plasticizers

Preparation of star poly(ethylene glycol), A (M_n of each arm ~ 500 Da)

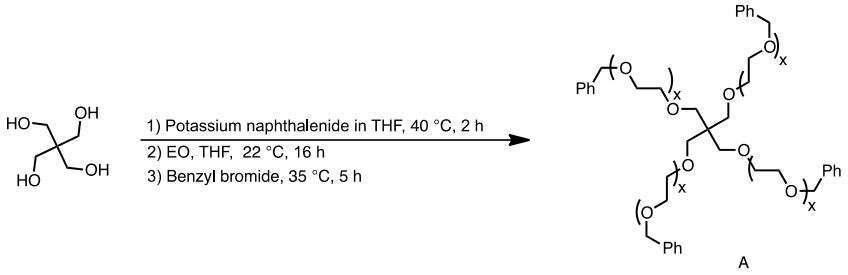

Scheme 4.1 Synthesis of star poly(ethylene glycol).

Preparation of Star PEG-500 (A): In a N_2 glovebox, a Fischer-Porter bottle was charged with pentaerythritol (173 mg, 1.27 mmol) solution in THF (2.5 mL). A solution of potassium naphthalenide (1.9 mL, 0.35 M, 5.1 mmol) in THF was added to the alcohol solution dropwise resulting in a dark green solution. The vessel was sealed with the reactor head and the apparatus was removed from the box and stirred at 40 °C for 2 h. The solution was cooled to −78 °C and ethylene oxide (2.46 g, 55.8 mmol) was then condensed into it. The solution was allowed to warm to room temperature over 16 h. After 16 h, the living alkoxide was capped with benzyl bromide (1.7 g, 9.9 mmol), which resulted in immediate precipitation of white KBr salt. The reaction mixture was stirred at 35 °C for 3 h and then allowed to cool to room temperature. The salts formed were filtered over a Celite plug and the filtrate was partially concentrated

on rotary evaporator. Star-PEG was then precipitated in ~200 mL hexanes. The hexanes was decanted and the resulting viscous polymer (1.9 g, 73%) was dried in vacuum at 30 °C for several hours until its mass was constant. ^{1}H NMR (500 MHz, Chloroform-*d*) δ 7.56 – 7.27(m, 20H), 4.67 – 4.40 (m, 8H), 3.95 – 3.26 (m, 150H). ^{13}C NMR (126 MHz, $CDCl_3$) δ 138.25, 128.33, 127.71, 127.56, 73.20, 70.55, 69.41. THF GPC: M_n 1.0 kDa and M_w/M_n 1.4.

Preparation of Tetracyclic carbonate (D)

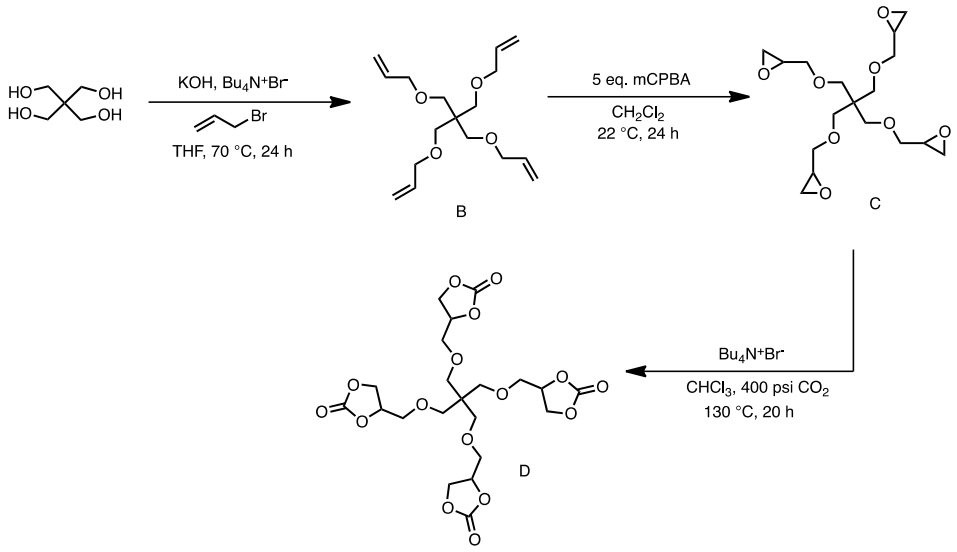

Scheme 4.2 Synthesis of tetracyclic carbonate.

Synthesis of 3-(3-(allyloxy)-2,2-bis((allyloxy)methyl)propoxy)prop-1-ene (B): Compound B was synthesized according to a modified literature procedure.[31] KOH (4.94 g, 88.1 mmol) and tetrabutyl ammonium bromide (2.91 g, 9.03 mmol) were added to a solution of pentaerythritol (1.0 g, 7.3 mmol) in 20 mL of THF under air.

Allyl bromide (7.63 mL, 88.1 mmol) was dropwise injected into the reaction mixture *via* a syringe. The resulting mixture was then refluxed for 24 hours, cooled to room temperature, and filtered. The organic layer was diluted with diethyl ether (2 × 50 mL), washed with saturated brine solution (30 mL), and dried over anhydrous sodium sulfate. The organic layer was concentrated under reduced pressure to yield the product (1.9 g, 89%). ^{1}H NMR (500 MHz, Chloroform-*d*) δ 5.87 (ddt, *J* = 17.2, 10.5, 5.3 Hz, 4H), 5.33 – 5.06 (m, 8H), 3.94 (dt, *J* = 5.4, 1.5 Hz, 8H), 3.45 (s, 8 H). ^{13}C NMR (126 MHz, $CDCl_3$) δ 135.35, 116.18, 72.36, 69.46, 45.51. HRMS (ESI) m/z calculated for $C_{17}H_{29}O_4$ (M^+) 297.2066, found 297.2070.

Synthesis of 2,2'-(((2,2-bis((oxiran-2-ylmethoxy)methyl)propane-1,3-diyl) bis(oxy)) bis(methylene))bis(oxirane) (C): A solution of mCPBA (1.8 g, 8.2 mmol) in dichloromethane (30 mL) was dropwise added to compound B (1.9 g, 6.4 mmol) *via* a addition funnel under air at 22 °C. The resulting mixture was stirred for 24 h at room temperature. The reaction mixture was filtered and washed with aqueous $NaHSO_3$ to react with the excess mCPBA. The resulting phases were separated and the aqueous layer was extracted with diethyl ether (2 × 50 mL). The organic layer was washed with saturated $NaHCO_3$ solution, dried with sodium sulfate, filtered, and concentrated under reduced pressure to yield the product (2.3 g, 94%). ^{1}H NMR (400 MHz, $CDCl_3$) δ 3.65 (dd, *J* = 11.7, 2.8 Hz, 4H), 3.50 – 3.39 (m, 8H), 3.31 (ddq, *J* = 11.6, 5.8, 0.9 Hz, 4H), 3.06 (ddt, *J* = 5.7, 4.2, 2.8 Hz, 4H), 2.72 (dd, *J* = 5.1, 4.1 Hz, 4H), 2.54 (dd, *J* = 5.1, 2.7 Hz, 4H). ^{13}C NMR (101 MHz, $CDCl_3$) δ 72.03, 69.91, 50.83, 45.73, 44.17. HRMS (ESI) m/z calculated for $C_{17}H_{29}O_8$ (M^+) 361.1862, found 361.1863.

Synthesis of 4,4'-(((2,2-bis(((2-oxo-1,3-dioxolan-4-yl)methoxy)methyl)propane-1,3-diyl)bis(oxy))bis(methylene))bis(1,3-dioxolan-2-one) (D): A glass sleeve with a magnetic stir bar was charged with tetrabutyl ammonium bromide (18 mg, 0.056 mmol), compound C (1.8 g, 4.8 mmol), and chloroform (5 mL) and placed in a Parr reactor. It was pressurized to 400 psig with CO_2 and then vented down to 100 psig. This process was repeated twice more to purge the reactor of air, then pressurized to 400 psig and heated to 130 °C. After 16 h, the Parr reactor was cooled to room temperature, vented, and the crude reaction mixture was concentrated under reduced pressure to yield the product as a light brown liquid (2.6 g, 96%). ^{1}H NMR (400 MHz, Chloroform-*d*) δ 4.88 – 4.76 (m, 4H), 4.55 – 4.29 (m, 8H), 3.70 (dtd, *J* = 10.9, 5.5, 2.2 Hz, 4H), 3.63 – 3.52 (m, 4H), 3.51 – 3.36 (m, 8H). ^{13}C NMR (126 MHz, $CDCl_3$) δ 155.38, 75.39, 70.93, 70.73, 70.52, 70.46, 69.68, 69.55, 69.48, 66.31, 45.80, 31.03. HRMS (ESI) m/z calculated for $C_{21}H_{29}O_{16}$ (M^+) 537.1456, found 537.1458.

Preparation of bis(cyclic carbonate) terminated poly(ethylene glycol) (BCC-PEG) PEG (E)

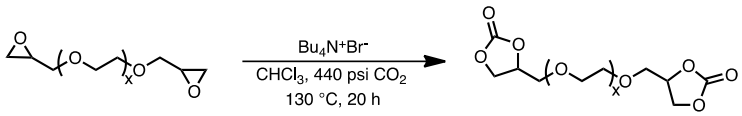

Scheme 4.3 Synthesis of bis(cyclic carbonate) terminated poly(ethylene glycol) (**E**).

Synthesis of BCC-PEG (E): A glass sleeve with a magnetic stir bar was charged with tetrabutyl ammonium bromide (75 mg, 0.23 mmol), diglycidyl polyethylene glycol (5.0 mL, 0.011 mmol; M_n 500), and chloroform (1 mL) and placed in a Parr reactor. It was pressurized to 400 psig with CO_2 and then vented down to 100 psig. This process

was repeated twice more to purge the reactor of air, then pressurized to 440 psig and heated to 130 °C. After 20 h, the Parr reactor was cooled to room temperature, vented, and the crude reaction mixture was concentrated under reduced pressure to yield the product as a pale yellow viscous liquid (6.3 g, 96%). ^{1}H NMR (400 MHz, Chloroform-*d*) δ 4.77 (ddt, *J* = 8.0, 6.1, 3.8 Hz, 2H), 4.50 – 4.39 (m, 2H), 4.38 – 4.30 (m, 2H), 3.91 – 3.42 (m, 38H). ^{13}C NMR (101 MHz, $CDCl_3$) δ 154.98, 75.13, 71.15, 70.42, 70.12, 66.22. MALDI-TOF (m/z): calculated for $C_{22}H_{38}O_{14}Na$ ($M + Na^+$) 549.2159, found 549.3552.

4.5.3.2 Synthesis of the PEO Functionalized Cross-linker

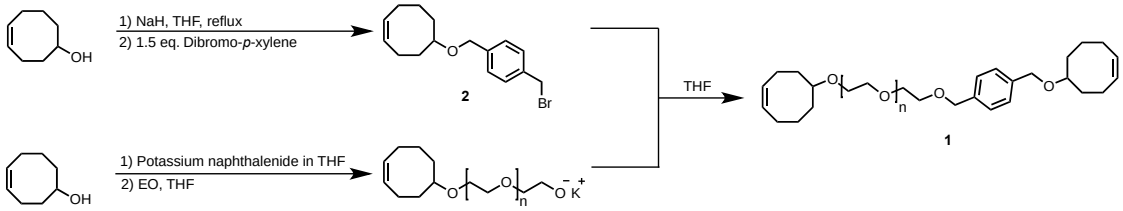

Scheme 4.4 General scheme for the synthesis of cross-linker **1**.

For the synthesis of **2**, see Section 2.5.3.1.

For the synthesis of PEO functionalized cross-linker (**1**), see Section 2.5.3.1.

4.5.3.3 Synthesis of Solid Polymer Electrolytes

Synthesis of Cross-Linked SPEs with Different Lithium Salts

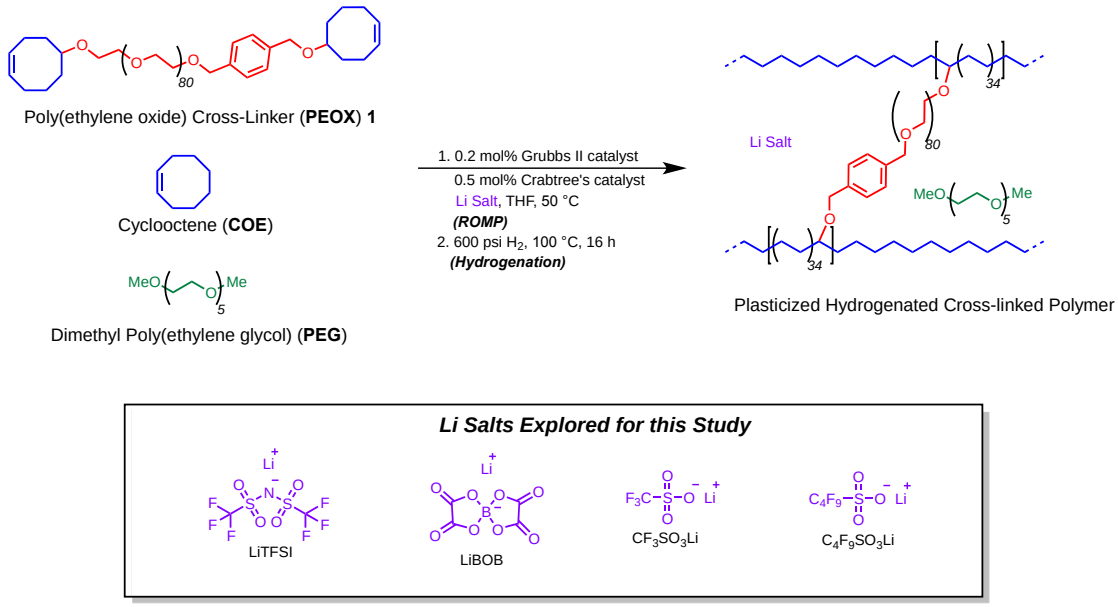

Figure 4.11 Synthesis of the cross-linked PE/PEO polymer electrolytes with different lithium salts.

Sample procedure for the synthesis of cross-linked PE/PEO electrolytes with different salts (LiBOB as the salt; Table 4.1, entry 2): Cross-linker **1** (122 mg, 0.0329 mmol) with 76 EO units in the cross-linker and COE (73 μL, 0.56 mmol) were combined and dissolved in 1.5 mL of THF. Grubbs' 2nd generation catalyst (1.0 mg, 0.0012 mmol) dissolved in 0.5 mL of THF was added to the monomer mixture, followed by addition of LiBOB (54.3 mg, 0.28 mmol) and PEG275 (120 mg, 0.436 mmol). Crabtree's catalyst (2.8 mg, 0.0035 mmol) dissolved in 0.5 mL $CHCl_3$ was added to the resultant solution and shaken vigorously for a minute. The reaction mixture was then transferred to a metal dish (fluoropolymer-lined, diameter of 5.25 cm and depth of 3.0 cm) placed in a volume glass chamber bearing two Kontes glass

valves on top. The chamber was placed on top of the hot plate equipped with a metal plate to ensure uniform heating and film was casted under N_2 flow at 50 °C for 3 h. After the solvent evaporated off, the Kontes valves were closed and the glass chamber was taken in the glove box. Hexane was added to the metal dish in order to release the film from the dish. The film was dried in vacuum at 22 °C for 24 h and then placed in a Parr reactor equipped with an overhead stirrer and sealed. It was pressurized to 600 psig with hydrogen and then vented down to 50 psig. This process was repeated twice more to purge the reactor of air, then pressurized to 600 psig and heated to 100 °C. After 16 h, the Parr reactor was cooled, vented and the plasticized SPE was dried under vacuum at 22 °C for 24 h.

Synthesis of Cross-Linked SPEs with Different Plasticizers

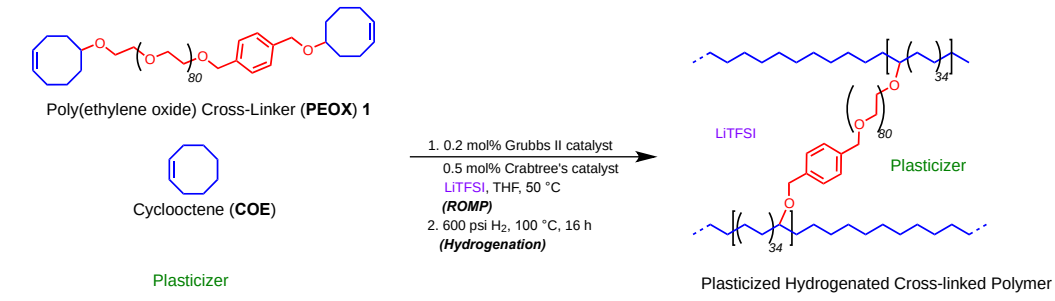

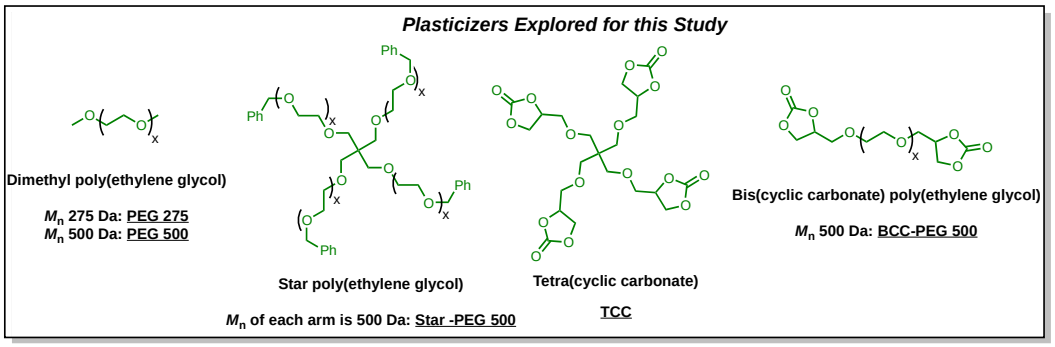

Figure 4.12 Synthesis of the cross-linked PE/PEO polymer electrolytes with different plasticizers.

Sample procedure for the synthesis of cross-linked PE/PEO electrolytes with different plasticizers (31 wt% PEG500 as the plasticizer; Table 4.2, entry 3): Cross-linker **1** (122 mg, 0.0305 mmol) with 82 EO units in the cross-linker and COE (73 μL, 0.56 mmol) were combined and dissolved in 1.5 mL of THF. Grubbs' 2nd generation catalyst (1.0 mg, 0.0012 mmol) dissolved in 0.5 mL of THF was added to the monomer mixture, followed by addition of LiTFSI (79 mg, 0.28 mmol) and PEG500 (120 mg, 0.240 mmol). Crabtree's catalyst (2.8 mg, 0.0035 mmol) dissolved in 0.5 mL $CHCl_3$ was added to the resultant solution and shaken vigorously for a minute. It was then transferred to a metal dish (fluoropolymer-lined, diameter of 5.25 cm and depth of 3.0 cm) and solution casted in the similar manner to the dry film as described above. The film was dried in vacuum at 22 °C for 24 h and then placed in a Parr reactor equipped with an overhead stirrer and sealed. It was pressurized to 600 psig with hydrogen and then vented down to 50 psig. This process was repeated twice more to purge the reactor of air, then pressurized to 600 psig and heated to 100 °C. After 16 h, the Parr reactor was cooled, vented and the plasticized SPE was dried under vacuum at 22 °C for 24 h.

4.5.4 DC Ionic Conductivity

The DC ionic conductivity at each temperature was determined from the plateau value of the plot of real part of the conductivity as a function of frequency, as described in seminal work by Jonscher.[28] For details, refer to Section 2.5.6. DC ionic conductivity values of the plasticized SPE formulations with different lithium salts at variable temperatures are given in Table 4.3.

Table 4.3 DC ionic conductivities of plasticized solid polymer electrolytes with different lithium salts[a]

Entry	Lithium Salt	DC Ionic Conductivity (S/cm)[b]							
		−5 °C	**10 °C**	**25 °C**	**40 °C**	**55 °C**	**70 °C**	**85 °C**	**100 °C**
1	LiTFSI	1.3×10^{-5}	5.2×10^{-5}	1.6×10^{-4}	3.7×10^{-4}	7.0×10^{-4}	1.2×10^{-3}	1.7×10^{-3}	2.3×10^{-3}
2	LiBOB	2.7×10^{-6}	1.4×10^{-5}	4.8×10^{-5}	1.2×10^{-4}	2.3×10^{-4}	3.8×10^{-4}	5.5×10^{-4}	6.8×10^{-4}
3	LiTFSI/LiBOB (80:20)	4.8×10^{-6}	2.6×10^{-5}	8.3×10^{-5}	2.0×10^{-4}	4.2×10^{-4}	7.3×10^{-4}	1.1×10^{-3}	1.4×10^{-3}
4	LiTFSI/LiBOB (70:30)	3.5×10^{-6}	1.7×10^{-5}	5.8×10^{-5}	1.4×10^{-4}	2.8×10^{-4}	4.9×10^{-4}	7.8×10^{-4}	1.1×10^{-3}
5	LiTFSI/LiBOB (60:40)	4.6×10^{-6}	2.3×10^{-5}	7.4×10^{-5}	1.8×10^{-4}	3.4×10^{-4}	5.8×10^{-4}	9.0×10^{-4}	1.2×10^{-3}
6	LiTFSI/LiBOB (50:50)	2.9×10^{-6}	1.5×10^{-5}	5.0×10^{-5}	1.3×10^{-4}	2.6×10^{-4}	4.5×10^{-4}	6.9×10^{-4}	9.6×10^{-4}
7	$C_4F_9SO_3Li$	7.4×10^{-6}	2.5×10^{-5}	9.9×10^{-5}	1.9×10^{-4}	3.3×10^{-4}	4.0×10^{-4}	4.6×10^{-4}	5.9×10^{-4}

[a]All films had [EO]:[Li] composition of 18:1; where EO means ethylene oxide units in the PEOX cross-linker. [b]Determined by dielectric spectroscopy measurements.

4.5.5 NMR Spectra

(*Z*)-5-((4-(bromomethyl)benzyl)oxy)cyclooct-1-ene (2)

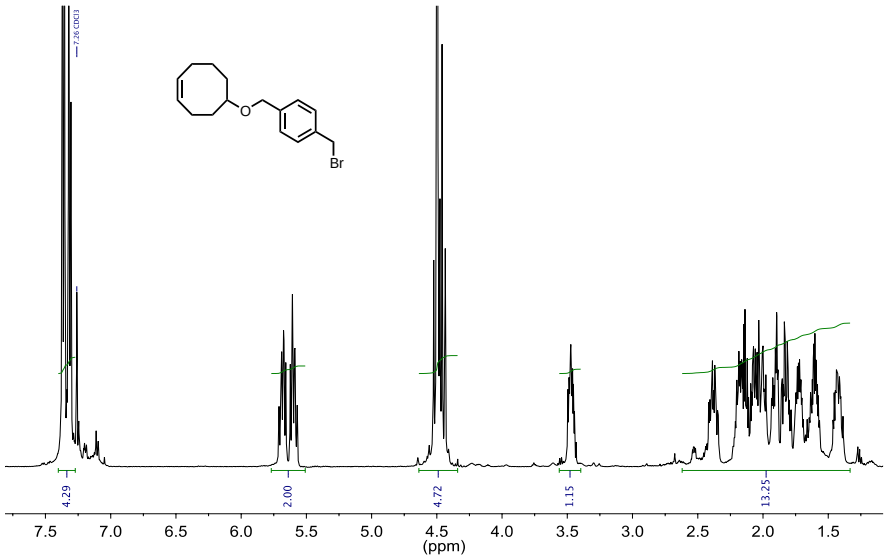

Figure 4.13 ^{1}H NMR Spectrum of (*Z*)-5-((4-(bromomethyl)benzyl)oxy)cyclooct-1-ene (**2**). Signal at 7.26 ppm is residual $CHCl_3$.

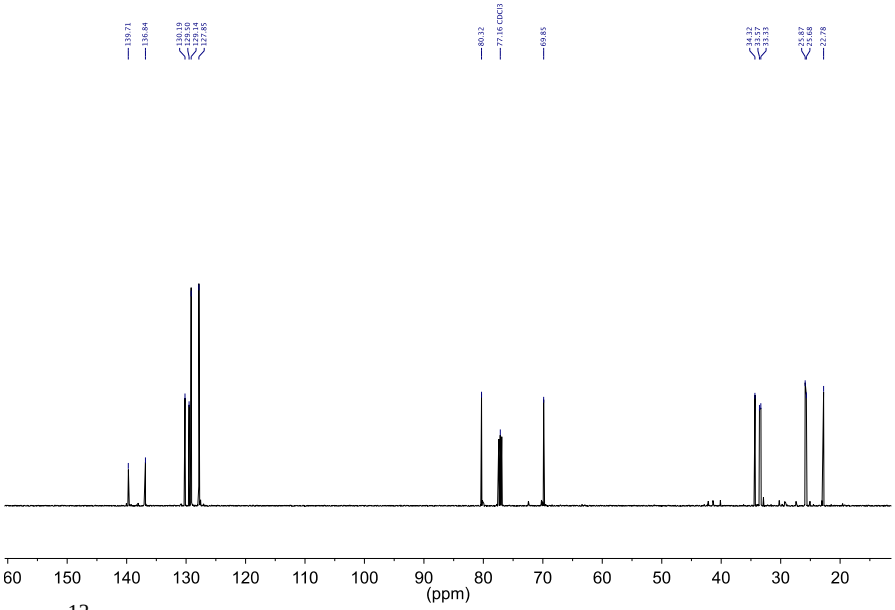

Figure 4.14 ^{13}C NMR Spectrum of (*Z*)-5-((4-(bromomethyl)benzyl)oxy)cyclooct-1-ene (**2**). Signal at 77.16 ppm is residual $CDCl_3$.

PEO functionalized cross-linker (1)

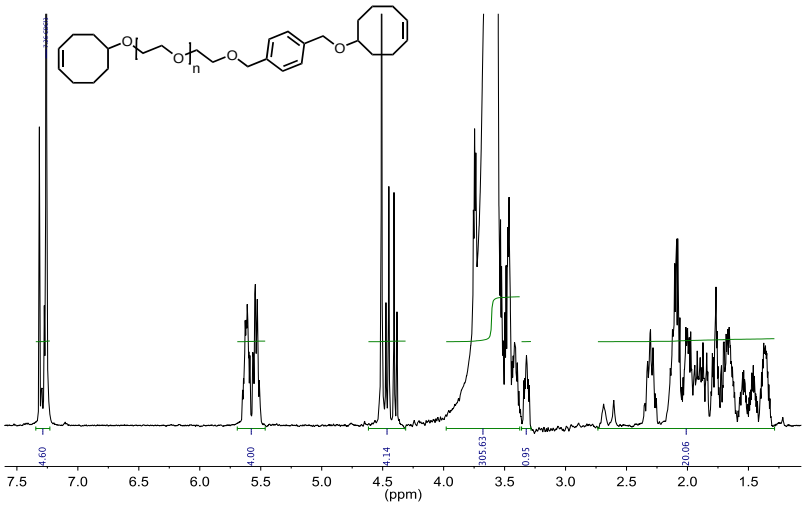

Figure 4.15 ^{1}H NMR Spectrum of PEO functionalized cross-linker (**1**) of molecular weight 3.7 kDa. Signal at 7.26 ppm is residual $CHCl_3$.

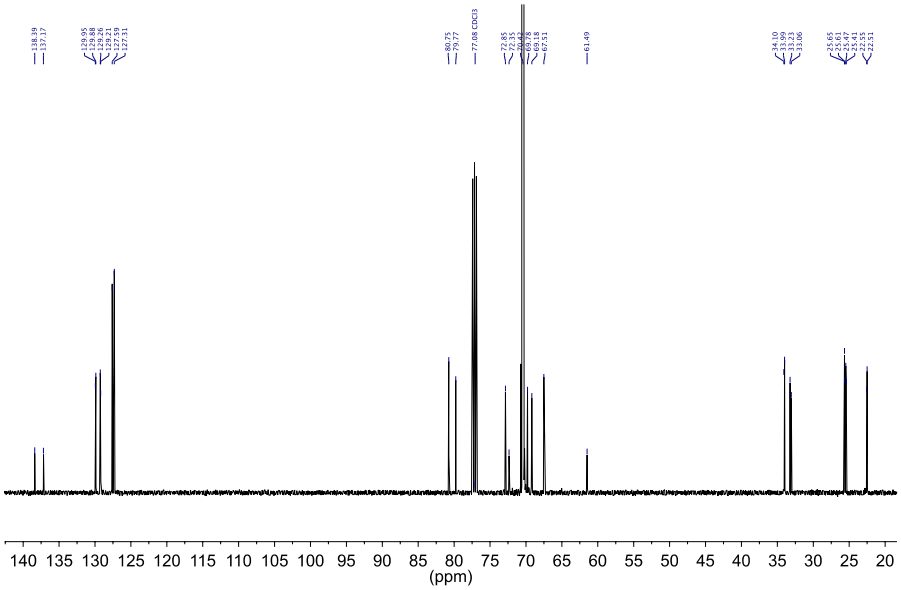

Figure 4.16 ^{13}C NMR Spectrum of PEO functionalized cross-linker (**1**) of molecular weight 3.7 kDa. Signal at 77.16 ppm is residual $CDCl_3$.

Star PEG-500 (A)

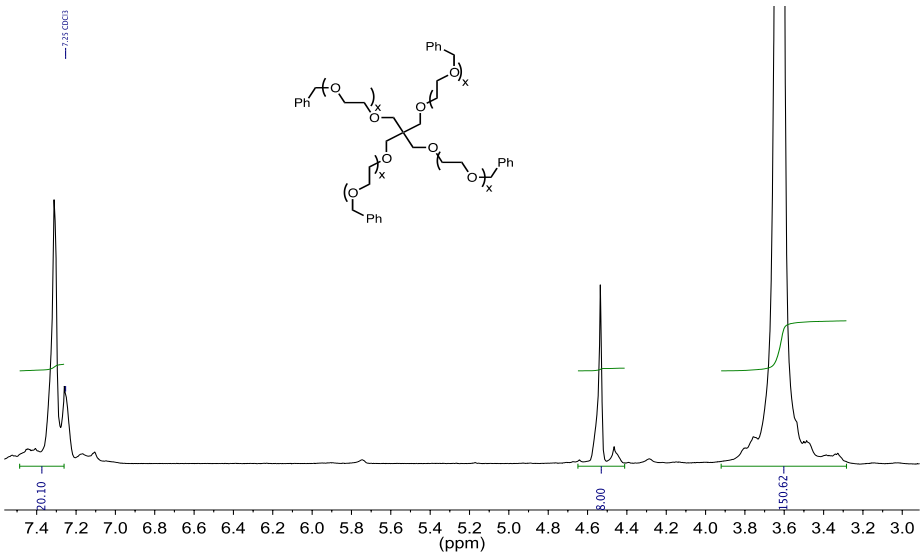

Figure 4.17 ^{1}H NMR spectrum of star poly(ethylene glycol) (PEG). The average molecular weight of each arm in the star PEG is 500 Da. Signal at 7.26 ppm is residual $CHCl_3$.

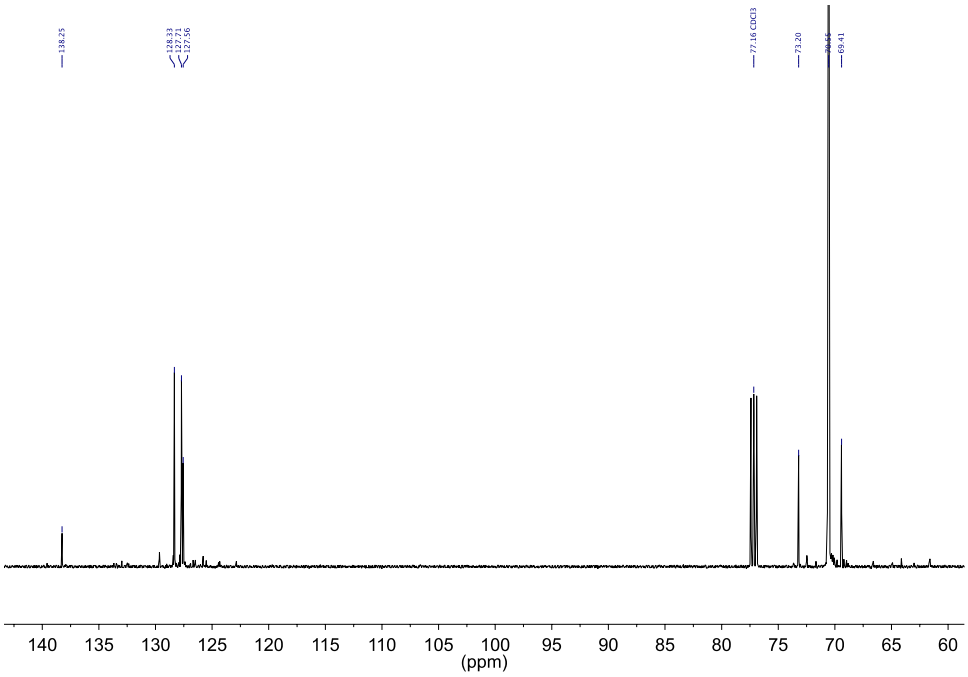

Figure 4.18 ^{13}C NMR spectrum of star poly(ethylene glycol) (PEG). The average molecular weight of each arm in the star PEG is 500 Da. Signal at 77.16 ppm is residual $CDCl_3$.

3-(3-(allyloxy)-2,2-bis((allyloxy)methyl)propoxy)prop-1-ene (B)

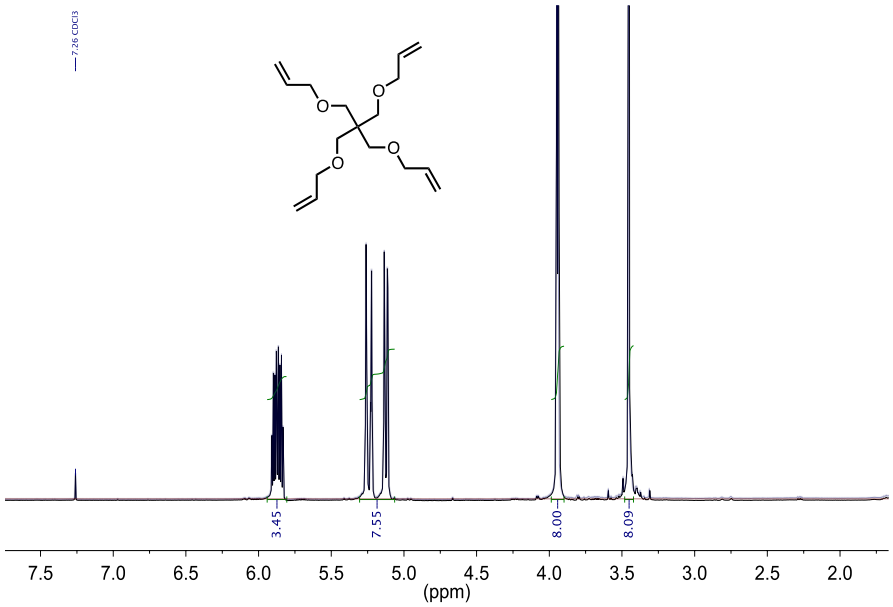

Figure 4.19 ^{1}H NMR spectrum of 3-(3-(allyloxy)-2,2-bis((allyloxy)methyl)propoxy) prop-1-ene (**B**). Signal at 7.26 ppm is residual $CHCl_3$.

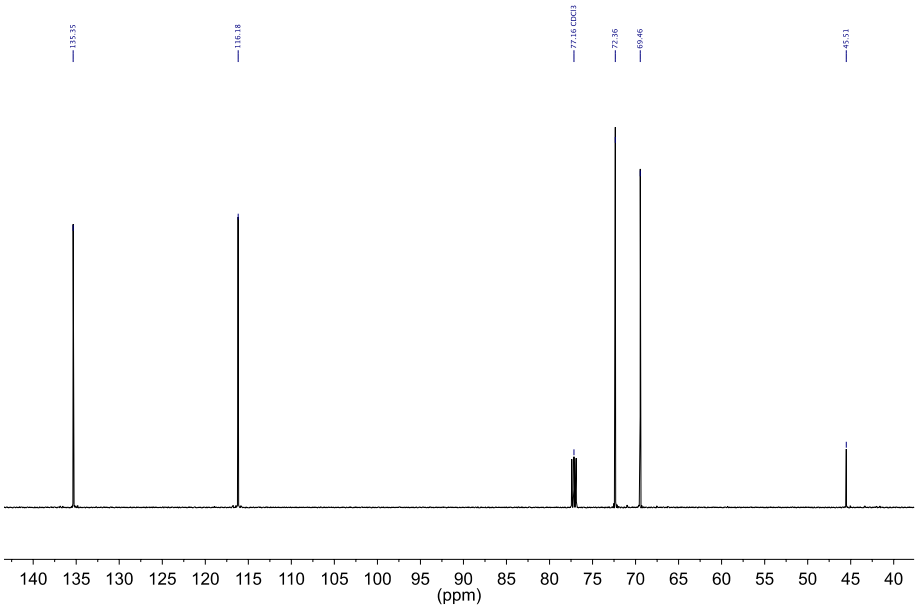

Figure 4.20 ^{13}C NMR spectrum of 3-(3-(allyloxy)-2,2-bis((allyloxy)methyl)propoxy) prop-1-ene (**B**). Signal at 77.16 ppm is residual $CDCl_3$.

2,2'-(((2,2-bis((oxiran-2-ylmethoxy)methyl)propane-1,3-diyl)bis(oxy))bis (methylene))bis(oxirane) (C)

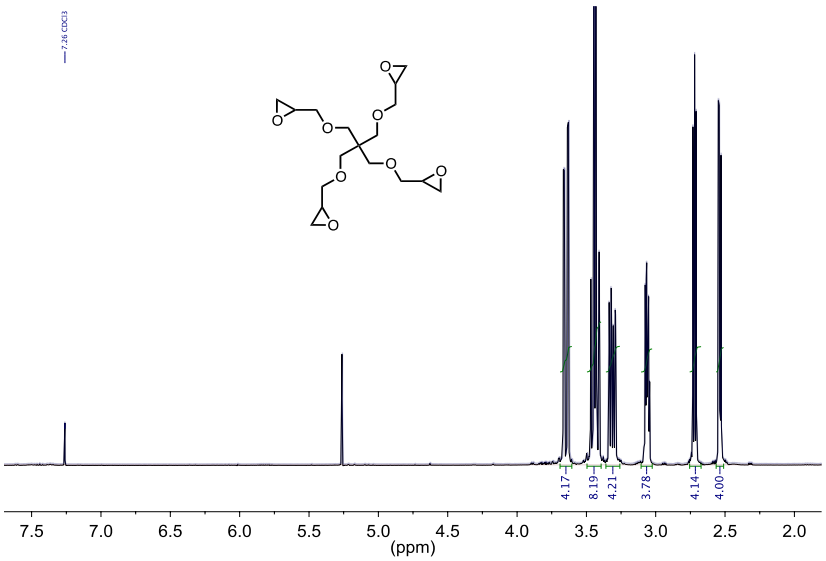

Figure 4.21 ^{1}H NMR spectrum of 2,2'-(((2,2-bis((oxiran-2-ylmethoxy)methyl) propane-1,3-diyl)bis(oxy))bis (methylene))bis(oxirane) (**C**). Signal at 7.26 ppm is residual $CHCl_3$.

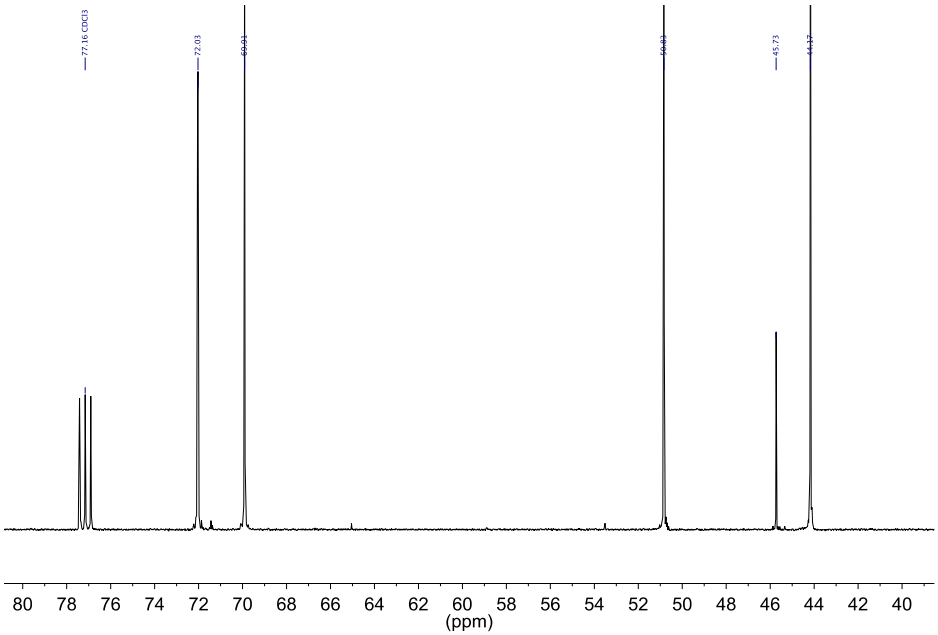

Figure 4.22 ^{13}C NMR spectrum of 2,2'-(((2,2-bis((oxiran-2-ylmethoxy)methyl) propane-1,3-diyl)bis(oxy))bis (methylene))bis(oxirane) (**C**). Signal at 77.16 ppm is residual $CDCl_3$.

4,4'-(((2,2-bis(((2-oxo-1,3-dioxolan-4-yl)methoxy)methyl)propane-1,3-diyl)bis (oxy)) bis(methylene))bis(1,3-dioxolan-2-one) (D)

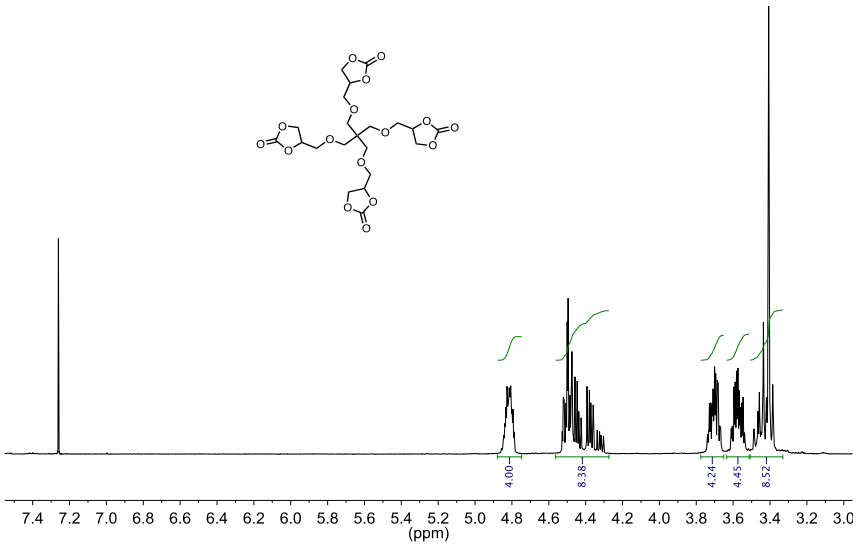

Figure 4.23 ^{1}H NMR spectrum of 4,4'-(((2,2-bis(((2-oxo-1,3-dioxolan-4-yl)methoxy) methyl)propane-1,3-diyl)bis (oxy)) bis(methylene))bis(1,3-dioxolan-2-one) (**D**). Signal at 7.26 ppm is residual $CHCl_3$.

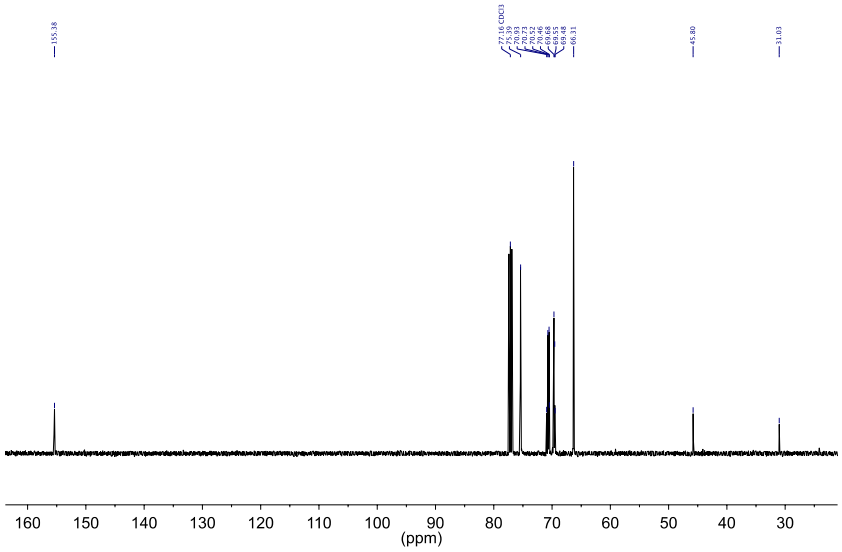

Figure 4.24 ^{13}C NMR spectrum of 4,4'-(((2,2-bis(((2-oxo-1,3-dioxolan-4-yl)methoxy) methyl)propane-1,3-diyl)bis (oxy)) bis(methylene))bis(1,3-dioxolan-2-one) (**D**). Signal at 77.16 ppm is the residual $CDCl_3$.

Bis(cyclic carbonate) poly(ethylene glycol) (BCC-PEG, E)

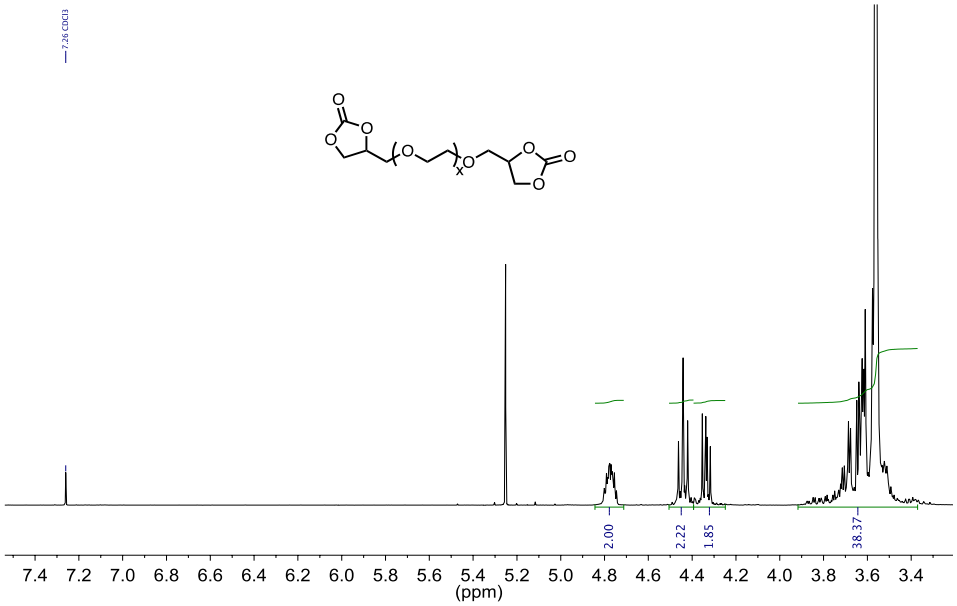

Figure 4.25 ^{1}H NMR spectrum of BCC-PEG (**E**) of molecular weight 500 Da. Signal at 7.26 ppm is residual $CHCl_3$.

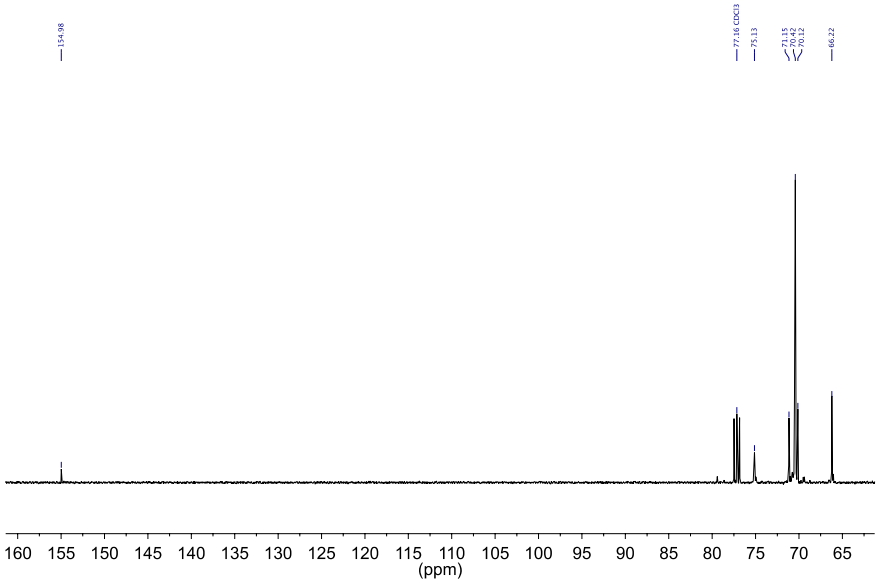

Figure 4.26 ^{13}C NMR spectrum of BCC-PEG (**E**) of molecular weight 500 Da. Signal at 77.16 ppm is the residual $CDCl_3$.

REFERENCES

(1) Xu, K. *Chem. Rev.* **2004**, *104*, 4303–4417.

(2) Yoshimatsu, I.; Hirai, T.; Yamaki, J. *J. Electrochem. Soc.* **1988**, *135*, 2422–2427.

(3) Aurbach, D.; Daroux, M. L.; Faguy, P. W.; Yeager, E. *J. Electrochem. Soc.* **1987**, *134*, 1611–1620.

(4) Stone, G. M.; Mullin, S. A.; Teran, A. A.; Hallinan, D. T., Jr.; Minor, A. M.; Hexemer, A.; Balsara, N. P. *J. Electrochem. Soc.* **2012**, *159*, A222–A227.

(5) Gurevitch, I.; Buonsanti, R.; Teran, A. A.; Gludovatz, B.; Ritchie, R. O.; Cabana, J.; Balsara, N. P. *J. Electrochem. Soc.* **2013**, *160*, A1611–A1617.

(6) Aravindan, V.; Gnanaraj, J.; Madhavi, S.; Liu, H. K. *Chem.—Eur. J.* **2011**, *17*, 14326–14346.

(7) Kita, F.; Sakata, H.; Sinomoto, S.; Kawakami, A.; Kamizori, H.; Sonoda, T.; Nagashima, H.; Nie, J.; Pavlenko, N. V.; Yagupolskii, Y. L. *J. Power Sources* **2000**, *90*, 27–32.

(8) Tsujioka, S. T., H.; Takahashi, M.; Sugimoto, H.; Koide, M. ; US Patent 678,726,7 (2004).

(9) Subadevi, R.; Sivakumar, M.; Rajendran, S.; Wu, H. C.; Wu, N. L. *J. Appl. Polym. Sci.* **2011**, *119*, 1–6.

(10) Cheung, I. W.; Chin, K. B.; Greene, E. R.; Smart, M. C.; Abbrent, S.; Greenbaum, S. G.; Prakash, G. K. S.; Surampudi, S. *Electrochim. Acta* **2003**, *48*, 2149–2156.

(11) Xu, W.; Belieres, J. P.; Angell, C. A. *Chem. Mater.* **2001**, *13*, 575–580.

(12) Tarascon, J. M.; Armand, M. *Nature* **2001**, *414*, 359–367.

(13) Goodenough, J. B.; Park, K. S. *J. Am. Chem. Soc.* **2013**, *135*, 1167–1176.

(14) Armand, M. B. C., J. M.; Duclot, N. J. *Fast Ion Transport in Solids: Electrodes, and Electrolytes*; Lake Geneva, Wisconsin, U.S.A., May 21−25, 1979; Vashishta, P.; Mundy, J. N.; Shenoy, G. K., Eds; North Holland: New York, 1979.

(15) Berthier, C.; Gorecki, W.; Minier, M.; Armand, M. B.; Chabagno, J. M.; Rigaud, P. *Solid State Ionics* **1983**, *11*, 91–95.

(16) Kumar, M.; Sekhon, S. S. *Eur. Polym. J.* **2002**, *38*, 1297–1304.

(17) Kumar, M.; Sekhon, S. S. *Ionics* **2002**, *8*, 223–233.

(18) Lee, H. S.; Yang, X. Q.; McBreen, J.; Xu, Z. S.; Skotheim, T. A.; Okamoto, Y. *J. Electrochem. Soc.* **1994**, *141*, 886–889.

(19) Park, M. K.; Kim, H. S.; An, J. H.; Kim, J. *J. Ind. Eng. Chem.* **2005**, *11*, 222–227.

(20) Lee, J. I.; Kim, D. W.; Lee, C.; Kang, Y. *J. Power Sources* **2010**, *195*, 6138–6142.

(21) Borghini, M. C.; Mastragostino, M.; Zanelli, A. *Electrochim. Acta* **1996**, *41*, 2369–2373.

(22) Chintapalli, S.; Frech, R. *Solid State Ionics* **1996**, *86-8*, 341–346.

(23) Zaghib, K.; Striebel, K.; Guerfi, A.; Shim, J.; Armand, M.; Gauthier, M. *Electrochim. Acta* **2004**, *50*, 263–270.

(24) Gerbaldi, C.; Nair, J. R.; Ahmad, S.; Meligrana, G.; Bongiovanni, R.; Bodoardo, S.; Penazzi, N. *J. Power Sources* **2010**, *195*, 1706–1713.

(25) Rupp, B.; Schmuck, M.; Balducci, A.; Winter, M.; Kern, W. *Eur. Polym. J.* **2008**, *44*, 2986–2990.

(26) Schulze, M. W.; McIntosh, L. D.; Hillmyer, M. A.; Lodge, T. P. *Nano Lett.* **2014**, *14*, 122–126.

(27) See Experimental Section for more details.

(28) Jonscher, A. K. *Nature* **1977**, *267*, 673–679.

(29) Sylla, S.; Sanchez, J. Y.; Armand, M. *Electrochim. Acta* **1992**, *37*, 1699–1701.

(30) Hillmyer, M. A.; Laredo, W. R.; Grubbs, R. H. *Macromolecules* **1995**, *28*, 6311–6316.

(31) Tomalia, D. A.; Swanson, D. R.; Huang, B.; Pulgam, V. R.; Heinzelmann, J. R.; Svenson, S.; Reyna, L. A.; Zhuravel, M. A.; Chauhan, A. S.; DeMattei, C. R. US Patent 798,542,4 (2011).

CHAPTER 5

Investigating Syndiotactic Polypropylene-*b*-Poly(ethylene oxide)-*b*-Syndiotactic Polypropylene Triblock Copolymers as Solid Polymer Electrolytes for Lithium Metal Batteries

Reprinted with permission from

Solid State Ionics **2014**, *263*, 87–94.

CHAPTER 5

Investigating Syndiotactic Polypropylene-*b*-Poly(ethylene oxide)-*b*-Syndiotactic Polypropylene Triblock Copolymers as Solid Polymer Electrolytes for Lithium Metal Batteries

5.1 Abstract

Solid block copolymer electrolytes comprised of syndiotactic polypropylene-*block*-poly(ethylene oxide)-*block*-syndiotactic polypropylene (PEOP) doped with lithium bis(trifluoromethanesulfonyl)imide (LiTFSI) were synthesized and characterized for the first time. Materials containing a semi-crystalline block as the mechanically robust phase have received relatively little attention previously in the literature. While each block exhibits high crystallinity in the neat state, the addition of LiTFSI inhibits the crystallization of the poly(ethylene oxide) (PEO) block without quantitatively affecting the crystalline nature of syndiotactic polypropylene (sPP). The block copolymers form strongly-segregated morphologies both in the absence and presence of LiTFSI that persist to high temperatures. PEOP/LiTFSI electrolytes were found to have reasonable conductivities that follow the expected Vogel-Tammen-Fulcher behavior of polymer electrolytes. Unlike previously studied block copolymer electrolytes, these PEOP/LiTFSI electrolytes exhibit an optimal conductivity at intermediate molecular weight.

5.2 Introduction

Solid polymer electrolytes (SPEs) have been demonstrated to be one of the key components for the development of next-generation high performance batteries in combination with a lithium metal anode.[1,2] Extensive work has shown that poly(ethylene oxide) (PEO) possesses good ionic conductivity when doped with organic salts.[3] Subsequent implementation of PEO in full cell battery experiments has demonstrated its potential for use as a practical SPE.[4-7] In salt-containing PEO, ionic transport is linked to the polymer chain segmental motion,[8,9] which occurs predominantly in the amorphous phase.[10,11] Thus SPE-based battery must be operated at temperatures (T) above the PEO melting temperature, $T_{m,PEO}$. However, it has been shown that the mechanical properties of PEO in the amorphous phase are insufficient to prevent short circuit due to lithium dendrite growth originating at the lithium metal anode during battery cycling.[12,13] The design of a SPE material which pairs high ionic conductivity with robust mechanical properties is clearly an area of significant interest to facilitate high-energy density batteries.

In light of the challenges associated with creating an optimal SPE, a variety of polymeric systems have been investigated. Molecular architectures such as comb-like copolymers,[14,15] cross-linked polymer networks,[16,17] graft copolymers,[18-21] and block copolymers[18,22] have been explored for use as electrolytes in an attempt to independently tune the structural and transport properties. In many cases immiscibility between the blocks induces phase separation,[23-25] producing ordered nanoscopic morphologies.[26] Typically the resulting copolymer retains the properties of each polymer, yielding a material with hard, insulating phases interspersed with soft,

ionically conductive phases.

In studies utilizing block copolymers as SPE, the archetypal mechanical phase is made of a polymer with high glass transition temperature (T_g) such as polystyrene (PS).[22,27-31] For symmetric PS-PEO diblock copolymers[28-31] (SEO), the ionic conductivity σ has been shown to increase with PEO chain length and a plateau value is reached as the molecular weight of the PEO block exceeds 100 kg/mol. In contrast, σ of PEO homopolymers decreases with increasing molecular weight, reaching a plateau as the molecular weight of the PEO block exceeds 1 kg/mol.[8] Beyond PS-based block copolymers, a wide range of different glassy polymers[32-37] have been considered for use as the structural block. Mayes, Sadoway, and co-workers notably reported a loss in conductivity associated with an increased T_g of the structural block for PEO-based graft copolymer electrolytes.[38-41] However, these arguments are inconsistent with the data previously reported in the literature.[28,42]

In contrast to the extensive work described above featuring a glassy structural block, to our knowledge only P. Jannasch has reported the use of a semi-crystalline polymer as the structural block in a block copolymer electrolyte.[43] The author studied a triblock copolymer composed of polyethylene as the outer, structural blocks, and an inner, ionically-conductive block comprising of a copolymer of PEO and poly(propylene oxide). For the solid polymer electrolyte application, the ideal molecular design contains a (semi-)crystalline block with melting temperature higher than that of the conducting block. Ionic conductivity in the range of 2×10^{-4} S / cm at 90 °C can be reached when this copolymer is doped with LiTFSI salt.

Herein we report synthesis and characterization of symmetric syndiotactic

polypropylene-*block*-poly(ethylene oxide)-*block*-syndiotactic polypropylene (PEOP) triblock copolymers that are comprised of a central PEO block and a semi-crystalline syndiotactic polypropylene (sPP) as outer blocks. The thermal and morphological properties as well as the ionic conductivity of such PEOP block copolymers when doped with LiTFSI are reported and compared to PS-based block copolymer electrolyte studied previously.

5.3 Results and Discussion

To study the effect of a semi-crystalline structural polymer, such as syndotactic polypropylene (sPP) on the properties of a Li-ion conducting poly(ethylene oxide) (PEO) polymer, we synthesized syndiotactic polypropylene-*block*-poly(ethylene oxide)-*block*-syndiotactic polypropylene (PEOP) triblock copolymers. These PEOP block copolymers were synthesized using "click" coupling reaction of azide-terminated sPP (sPP-N_3) with the dipropargyl-terminated PEO (Figure 5.1). The sPP-CH_2-CH_2-CH_2-N_3 was synthesized from allyl-terminated sPP (sPP-CH_2-CH=CH_2) in three consecutive steps in good yields.[44-46] The percent end group functionalization of sPP polymer was mainly dependent on hydroboration/oxidation conditions such as solvent, reaction time, and temperature. End group analysis of the sPP-N_3 polymers using ^{1}H NMR spectroscopy suggested that there is some proton-terminated sPP (sPP-CH_2-CH_2-CH_3) present in the sPP-N_3 polymer. The propargyl-terminated PEO was synthesized from commercially available PEO in one step using Williamson ether reaction of the deprotonated PEO with the propargyl bromide. Conversion of the hydroxyl to the propargyl-treminated PEO proceeded with high efficiency (>95%)

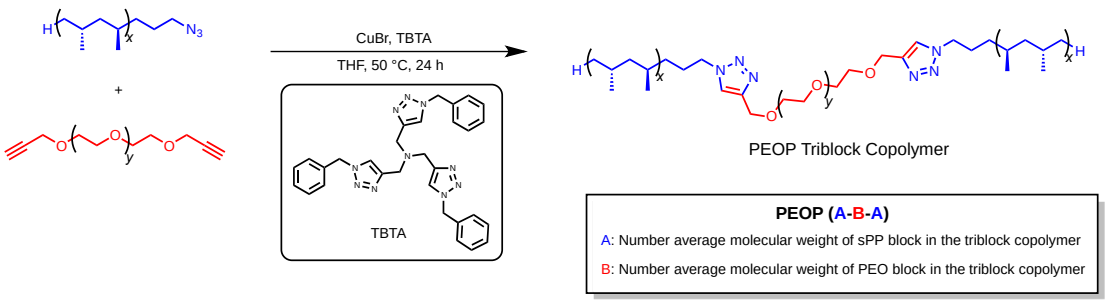

Figure 5.1 Synthesis and nomenclature of PEOP triblock copolymers.

according to the end group analysis using ^{1}H NMR spectroscopy.

Synthetic methodologies to obtain amphiphilic block copolymers, which are comprised of PEO as an ion-conducting block and a semi-crystalline polymer as a structural block, remain limited.[47,48] Recently Zhu and co-workers reported azide-alkyne "click" coupling reaction to synthesize sPP-*b*-PEO diblock copolymers.[48] We used similar "click" chemistry methods to obtain amphiphilic PEOP triblock copolymers in this work. A coupling reaction of sPP-N_3 was performed with dipropargyl-terminated PEO using Cu(I) as the catalyst and TBTA as the ligand[49] to obtain PEOP triblock copolymers. The ^{1}H NMR spectra of individual blocks and the PEOP triblock copolymer are shown in Figure 5.2. The peak corresponding to the -CH_2N$_3$ end group of sPP-N_3 polymer at δ 3.25 ppm disappeared and a new peak appeared at δ 4.31 ppm upon the triazole formation in the PEOP block copolymer. Also, once the coupling reaction occurred, the chemical shift of the signals originating from the HC≡C-CH_2O- end groups of the propargyl terminated PEO shifted from δ 4.16 ppm to δ 4.69 ppm. The presence of a characteristic peak of triazole moiety at δ 7.55 ppm also confirms the "click" reaction and formation of PEOP triblock copolymer.

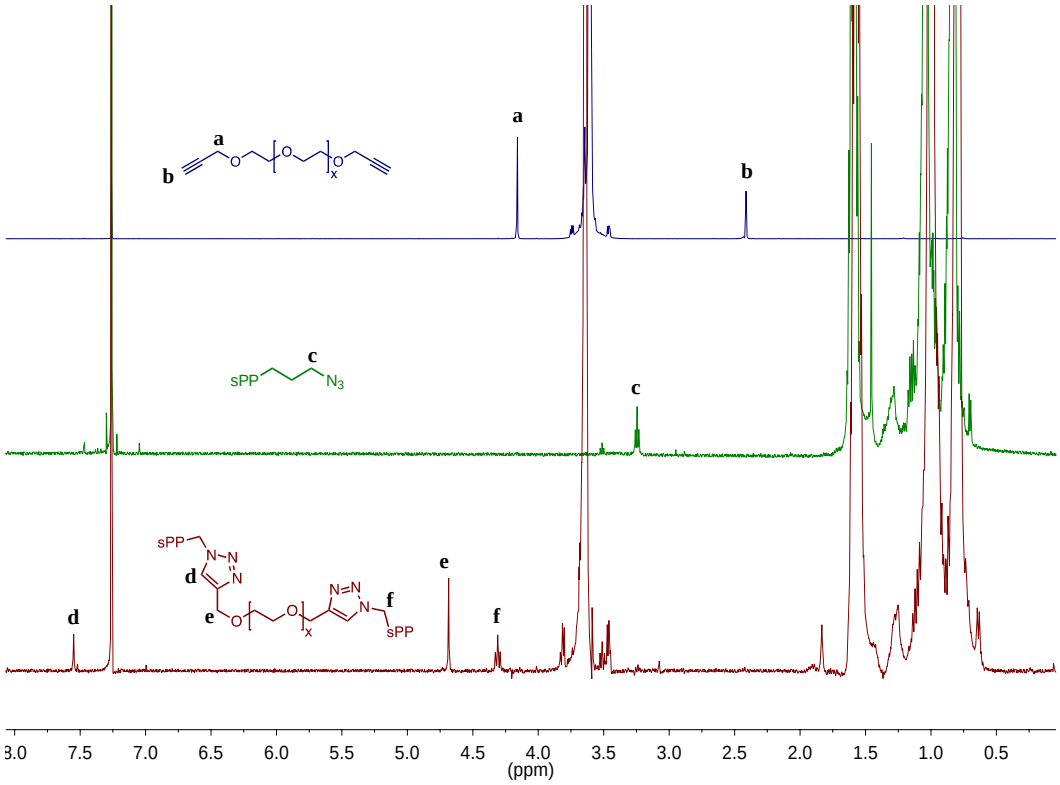

Figure 5.2 ^{1}H NMR spectra (500 MHz, $CDCl_3$, 60 °C) of CH≡C-CH_2O-PEO-CH_2O-C≡CH (blue), sPP-$(CH_2)_3$-N_3 (green), and sPP-*b*-PEO-*b*-sPP triblock copolymer (red).

The PEOP triblock copolymers synthesized for this study are listed in Table 5.1. Each of the PEOP triblock copolymer samples contained a portion of unfunctionalized sPP homopolymer that was not able to react with functionalized PEO homopolymer and could not be removed from the triblock copolymer (Table 5.1). High temperature gel permeation chromatography (GPC) analyses of PEOP triblock copolymers do not reflect a significant increase in molecular weight. Presumably, this is due to insignificant change in hydrodynamic radii of the PEOP polymer and presence of sPP homopolymer. The presence of this sPP homopolymer might influence the mechanical properties and ionic conductivity of the PEOP electrolytes.

Table 5.1 Characteristics of PEOP triblock copolymers

Polymer	$M_{n,sPP}$[a] (kg/mol)	N_{sPP}*[b]	$M_{n,PEO}$[a] (kg/mol)	N_{PEO}*[b]	ϕ_{PEO}	$\phi_{sPP,h}$[a]	ϕ_c[c]	*mol% of unfunctionalized sPP*[a]
PEOP (4-3-4)	4.1	86	3.4	53	0.24	0.17	0.27	22
PEOP (4-8-4)	4.0	84	8.5	133	0.44	0.32	0.49	49
PEOP (4-16-4)	4.0	84	15.8	247	0.60	0.24	0.64	49
PEOP (5-16-5)	5.0	105	15.8	247	0.54	0.33	0.59	56
PEOP (10-38-10)	10.5	220	37.6	589	0.57	0.43	0.62	68

[a] Determined by ^{1}H NMR spectroscopy using end group analysis. [b] The length of each block in number of repeat units, relative to a reference unit volume v_0 = 0.1 nm^3, is given as N_{sPP}^* and N_{PEO}^* (where N_i^* is defined by $M_{n,i} \cdot v_i / M_i \cdot v_0$). The propylene repeat unit is defined with respect to a dimer of the propylene monomer (*i.e.*, C_6H_{12}) by convention. M_P and M_{EO} are the repeat unit molar masses of propylene (84.16 g / mol) and ethylene oxide (44.05 g / mol), respectively. v_P and v_{EO} are the repeat unit volumes of propylene (0.176 nm^3) and ethylene oxide (0.069 nm^3), respectively, at a reference temperature of 140 °C. [c] ϕ_c is the volume fraction of the conducting phase. See the Experimental Section for more details.

Nonetheless, we used these PEOP triblock copolymers without any further purification for the thermal, morphological, and electrochemical studies described subsequently.

To understand the crystalline nature of each block in PEOP block copolymers, we performed DSC measurements to identify the location of the melting transitions in each of the polymers considered here. All samples exhibited two melting transitions in the vicinity of the melting points of syndiotactic PP and PEO homopolymers. The results of these experiments are summarized in Figure 5.3a, where T_m of each block is shown as a function of M_n. The measured $T_{m,sPP}$ for high-M_n sPP is significantly reduced compared with previously reported values for homopolymer sPP and sPP-containing block copolymers, albeit for polymers which generally possess much larger M_n than that considered here. The values for $T_{m,sPP}$ represent the maximum value for the endothermic peak observed on heating the sample. Within experimental error, $T_{m,sPP}$ was found to be independent of M_n, with an average value of 105 ± 5 °C. By comparison, thermal characterization of sPP homopolymers have shown that $T_{m,sPP}$ increases monotonically with M_n in the range 1 – 50 kg/mol, at which point it reaches a plateau value of 160 °C.[50] Block copolymers studied previously containing sPP have shown depressed $T_{m,sPP}$ as well, generally in the range of 130 – 135 °C.[51-53] In these cases, however, the M_n of the sPP blocks is again much higher than that encountered here. Another aspect that has been shown to affect the thermal transitions is the degree of syndiotacticity. De Rosa and co-workers synthesized sPP homopolymers of varying syndiotacticity and observed a reduction in $T_{m,sPP}$ with decreasing syndiotacticity.[54] In the sPP-containing block copolymers studied here, the tacticity of sPP is expected to be approximately 80% corresponding to a homopolymer melting temperature of

116 °C, based on an extrapolated linear relationship between $T_{m,sPP}$ and % [*rrrr*].[55] Thus the values of $T_{m,sPP}$ reported here seem reasonable. It is possible that the presence of a covalently-bonded PEO blocks could interfere with the sPP crystallization process, reducing both $T_{m,sPP}$ and $X_{c,sPP}$. In contrast to PP crystallization, $T_{m,PEO}$ is observed to increase monotonically with increasing M_n, from 38 to 63 °C while $M_{n,PEO}$ is increased by approximately one order of magnitude. In the inset of Figure 5.3a, $T_{m,PEO}$ is shown to have a linear dependence on 1 / $M_{n,PEO}$, which has been observed with PEO homopolymers[56] as well as PEO-polyolefin block copolymers.[47] The presence of two distinct melting endotherms found upon heating provides evidence for the existence of strongly immiscible microphases of the block copolymer.

In addition to identifying the location of T_m for each block, it is also possible to determine $X_{c,i}$ in each microphase from the DSC profiles. The results of this analysis are shown in Figure 5.3b. For the sPP blocks, similar to $T_{m,sPP}$, it is found that there is no dependence of $X_{c,sPP}$ on M_n. The samples of PEOP were found to have $X_{c,sPP}$ = 16 ± 3 % in the neat state for the sPP phases. However, the PEO phases have a much higher crystalline fractions, with $X_{c,PEO}$ = 41 ± 4 %. While $X_{c,PEO}$ has larger variation across all samples than $X_{c,sPP}$, it seems to be also M_n-independent.

DSC experiments were carried out for samples doped with LiTFSI to establish changes in the PEOP physical properties when utilized as an electrolyte. The results of these experiments are summarized in Figure 5.4. The samples were prepared at single salt concentration of r = 0.063 ± 0.006. This corresponds to a weight fraction $w_{Li/EO}$ of 0.29 ± 0.02 of LiTFSI in the PEO domains, assuming that LiTFSI is completely solubilized by the PEO chains.[31,57] When comparing $T_{m,sPP}$ for the salt-free

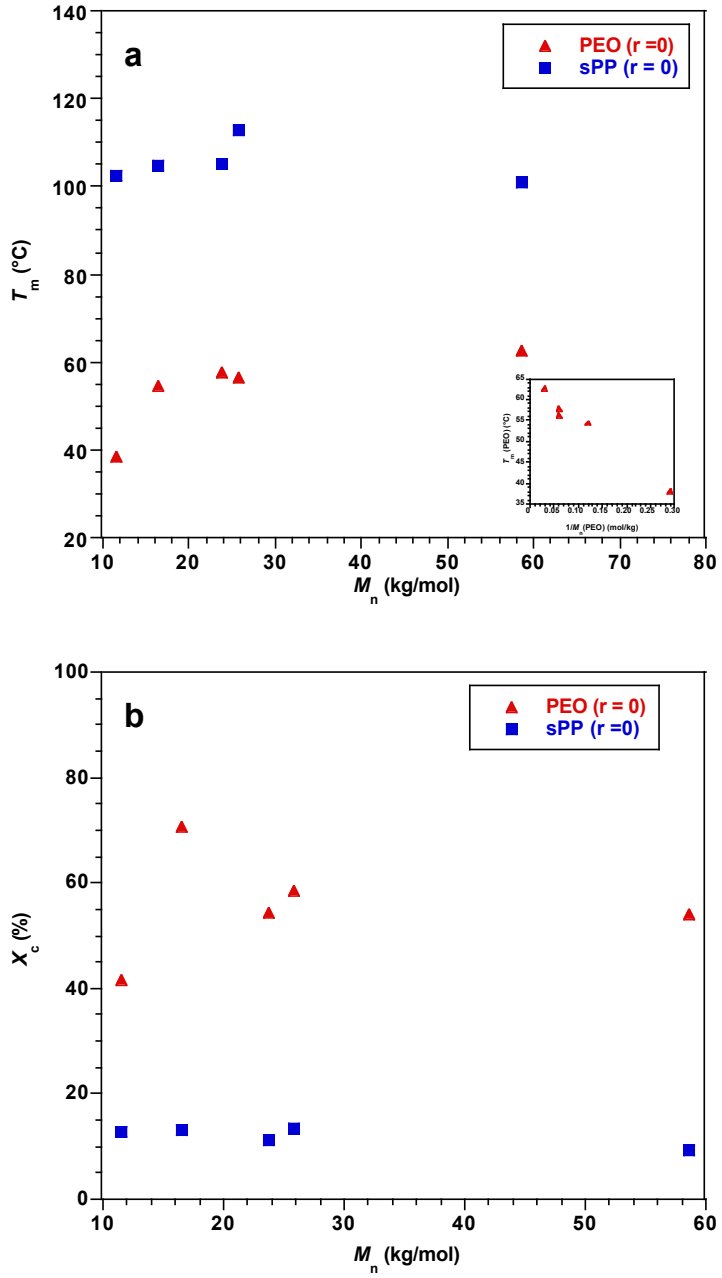

Figure 5.3 Melting temperature (a) and crystallinity (b) of sPP and PEO blocks in neat PEOP triblock copolymer as a function of total molecular weight. The inset of (a) shows linear relationship between $T_{m,PEO}$ and $M_{n,PEO}$.

and salt-doped PEOP materials, it is evident that the LiTFSI has minimal effect on the

crystalline nature of sPP, supporting the hypothesis that the salt is fully segregated to PEO domains. In the salt-containing PEOP samples, there is again no dependence of $T_{m,sPP}$ on M_n, and the samples have an average value of 107 ± 3 °C. The presence of LiTFSI also has minimal effect on $X_{c,sPP}$, which decreases slightly to a value of 12 ± 3%. Conversely, presence of LiTFSI has a significant impact on PEO crystallinity. The lowest-M_n copolymer, PEOP (4-3-4), has no measurable crystallinity when doped with LiTFSI. Signatures of PEO crystallization remained absent when the temperature scan rate was decreased to 5 °C / min, suggesting that the presence of salt completely suppresses crystallization of PEOP (4-3-4). Aside from PEOP (4-3-4), the other four other samples studied exhibited DSC peaks consistent with PEO crystallization even in the presence of LiTFSI but with a reduction in $T_{m,PEO}$ to a value that was roughly independent of M_n equal to 48 ± 3 °C. This result agrees with the findings described by Yuan *et al*.,[58] for SEO electrolytes, where low M_n electrolytes ($M_{n,PEO}$ < 8 kg / mol) show no observable crystallinity, while in the high-M_n case $T_{m,PEO}$ was in reasonable agreement with $T_{m,PEO}$ observed here for PEOP. The effect of LiTFSI on PEO crystallization is further examined by comparing $X_{c,PEO}$ for the salt-free and salt-doped PEOP materials. The average value of $X_{c,PEO}$ for the samples containing a non-zero crystalline fraction with added salt was equal to 12 ± 9 % compared to 41 ± 4 % for the salt-free PEOP polymer. This strong effect of LiTFSI on PEO crystallinity is to be expected, since PEO is well-known to solvate lithium salts *via* coordination with the ether oxygen that interferes with the ability of the chain to form crystalline structures.[11]

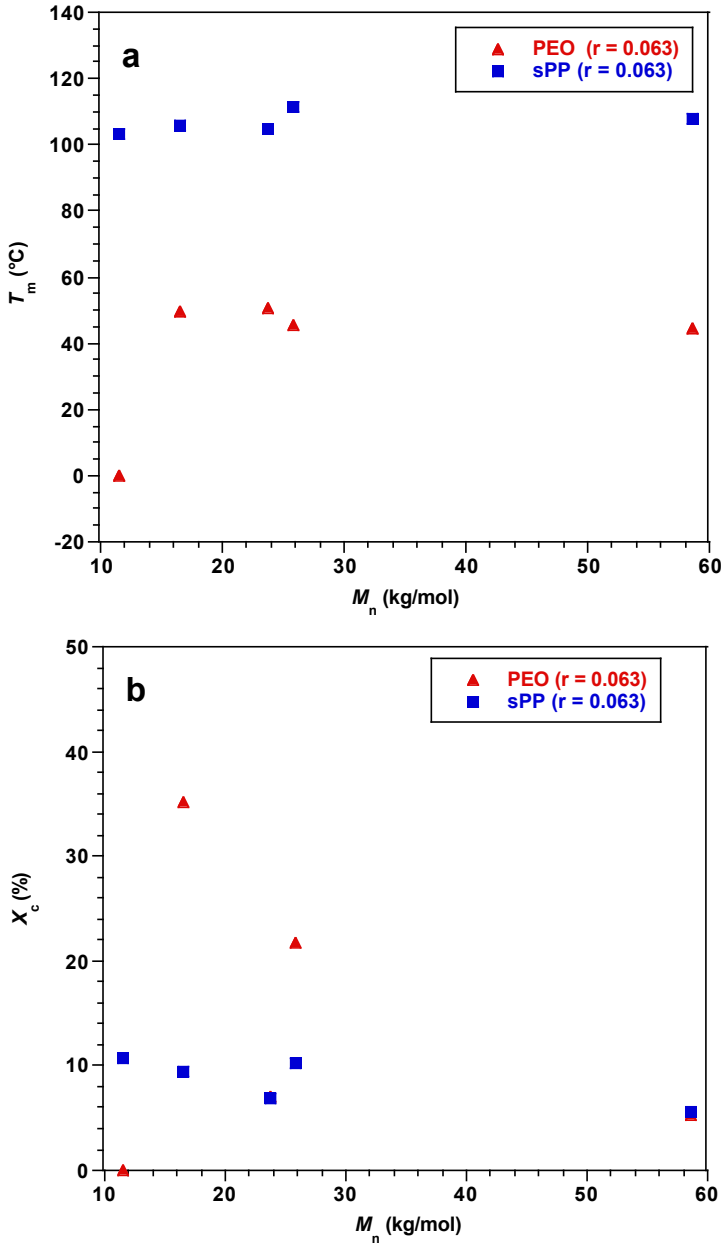

Figure 5.4 Melting temperature (a) and crystallinity (b) of sPP and PEO blocks in LiTFSI-doped PEOP triblock copolymer.

The effect of salt on the crystalline nature of the polymers can also be observed using wide angle X-ray scattering (see Experimental Section). To quantify the effect of salt on the crystallinity of each block, we can consider the change in X_c as defined in eq. 1:

$$\Delta X_{c,i} = \frac{X_{c,i,r=0} - X_{c,i,r=0.85}}{X_{c,i,r=0}} \quad (1)$$

In Figure 5.5, the values obtained for ΔX_c are plotted as a function of ϕ_{PEO}. The reduction in $X_{c,sPP}$ is linearly dependent on $\phi_{PEO} = 1 - \phi_{sPP}$. Conversely, $\Delta X_{c,PEO}$ has a non-monotonic dependence on ϕ_{PEO}, with a minimum at intermediate values of ϕ_{PEO} within the range considered here.

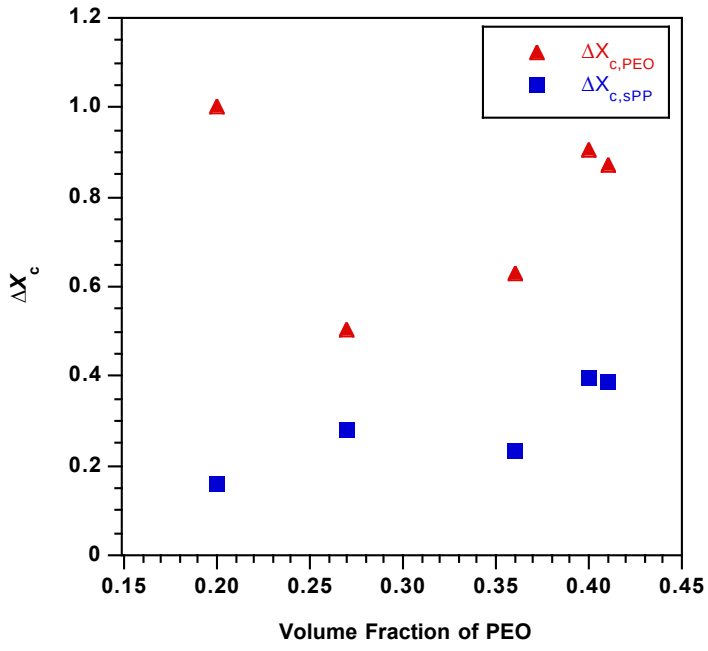

Figure 5.5 Percent change in crystallinity for sPP and PEO blocks in LiTFSI-doped PEOP block copolymers.

We performed SAXS experiments on the neat PEOP as well as LiTFSI-doped material to determine the microphase separation exhibited by these samples. Figure 5.6a shows the azimuthally-averaged SAXS profiles for neat and salt-doped PEOP in parts a and b, respectively. Each of the profiles was collected at 120 °C, well above T_m for each phase of the block copolymer, and thus represents the microphase condition at thermal equilibrium. Several observations are immediately evident. As M_n increases, there is a clear increase in d, both in the case of neat PEOP and PEOP-LiTFSI mixtures, based on decreasing values of the primary scattering peak at q^*. In Figure 5.6a it is found that d for PEOP (10-38-10) is large enough such that q^* cannot be resolved by the SAXS instrument utilized. Conversely the four PEOP samples with lower M_n have a quantifiable value of q^*, which provides measured values of d that increases from 18 nm for PEOP (4-3-4) to 56 nm for PEOP (5-16-5). Based on $q_{min,SAXS} = 0.1$ nm^{-1}, we can set a lower bound on d for PEOP (10-38-10) at 63 nm. In addition to determining the trend of d with M_n, the SAXS profiles can also be used to identify the morphology of the PEOP samples. For PEOP (4-3-4), the higher order peaks are located at q values which have ratio $q / q^* = 3^{1/2}$, $7^{1/2}$, and $9^{1/2}$, indicative of the hexagonally-packed cylindrical morphology. PEOP (4-8-4), with a larger $\phi_{PEO} = 0.27$, displayed higher order peaks at $q / q^* = 2$, 4, and 5, suggestive of lamellar morphology. Higher M_n polymers had less clearly defined morphologies. This is presumably due to slow diffusion of chains in the melt that prevents the formation of well-ordered morphologies. In spite of this, it is possible to identify probable morphologies for PEOP (4-16-4) and PEOP (5-16-5) based on the presence of "shoulder peaks", which indicate that each of these polymers form the lamellar

morphology. This is reasonable since both of these polymers are reasonably symmetric (*i.e.*, ϕ_{PEO} close to 0.5). Since q^* for PEOP (10-38-10) is not observed in this experiment, it is not possible to identify the morphology based on SAXS.

a)

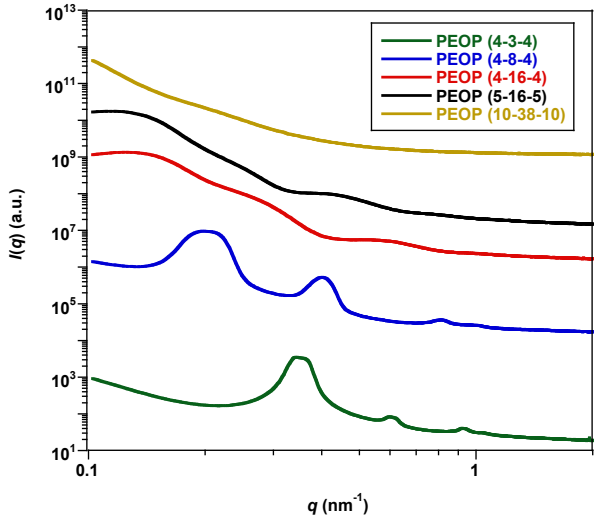

b)

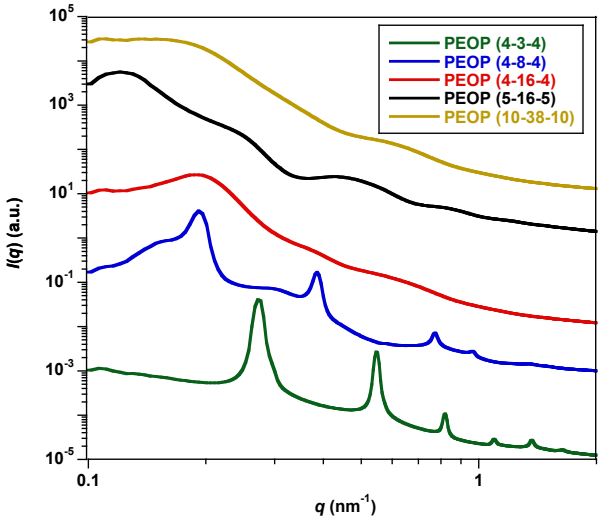

Figure 5.6 SAXS profiles for PEOP samples in the absence (a) and presence (b) of LiTFSI, at 120 °C.

The effect of LiTFSI addition on domain spacing and morphology was established by performing analogous SAXS experiments on salt-doped polymer. The results of these experiments are summarized in Figure 5.6b. In general the presence of LiTFSI had little quantitative effect on the structure of PEOP block copolymers. The intermediate-M_n PEOP samples have no significant change in d upon the addition of salt, and appear to retain the relatively low degree of long range order in the lamellar phase seen in the salt-free cases. Several important differences are important to identify. PEOP (4-3-4) underwent a transition in ordered morphology upon salt addition, from hexagonally-packed cylinders to lamellae. This can be rationalized in terms of the change of ϕ. Under the assumption of complete LiTFSI solubilization by PEO phases, the minor phase increases from $\phi_{PEO} = 0.24$ to conductive phase volume fraction $\phi_c = 0.27$. It is reasonable to expect that the change in ϕ experienced by PEOP (4-3-4) could be sufficient to drive the formation of a lamellar phase in place of the cylindrical phase. A second significant difference between the salt-free profiles is found for PEOP (10-38-10). Interestingly, the addition of salt evidently changes the structure of this polymer such that it is possible to resolve the location of q^* for the mixture.

We used RSoXS to fully resolve the morphology of PEOP (10-38-10). While RSoXS has been demonstrated to be useful for characterizing the structure of a variety of block copolymer-based materials,[59,60] its value for this work lies in the ability to tune the accessible q range, allowing study of large-d materials. In Figure 5.7 we show the RSoXS profile obtained for neat PEOP (10-38-10), as well as the PEOP (4-3-4) in the absence and presence of salt, to demonstrate the close correspondence of results

obtained from SAXS and RSoXS. In the case of neat PEOP (4-3-4), it is clear that the location of q^*_{RSoXS} is in reasonable agreement with q^*_{SAXS} (d_{RSoXS} = 16.4 nm compared with d_{SAXS} = 18.0 nm). The lack of quantitative agreement is probably due to multiple scattering effects in the presence of X-ray absorption. Similar agreement is found for PEOP (4-3-4) doped with LiTFSI. In addition, the RSoXS profile for PEOP (4-3-4) with LiTFSI was obtained for a q range which allowed resolution of a higher order peak at $2q^*$, indicating that the method could resolve the higher order peaks indicative of long range order in some cases. For PEOP (10-38-10), the X-ray λ was tuned to extend the low-q range in order to clearly identify the location of q^*. It is evident from Figure 5.7 that this was successful, as the profile thus obtained has a clear, albeit broad

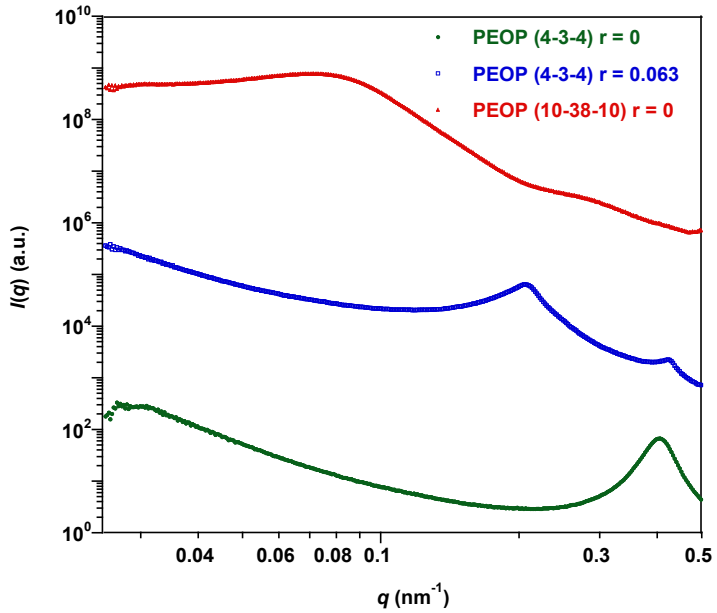

Figure 5.7 RSoXS profiles for PEOP (4-3-4) in the absence and presence of LiTFSI and neat PEOP (10-38-10), at 120 °C. Scattering profiles for PEOP (4-3-4) are in good agreement with those obtained *via* SAXS. The use of RSoXS allows access to sufficiently low values of q to resolve the primary scattering peak for PEOP (10-38-10), which is not possible using the SAXS configuration.

peak located at q = 0.0726 nm^{-1}, corresponding to d = 86.5 nm. This value of d is reasonable in comparison to the values of d obtained for the smaller-M_n polymers. The RSoXS profile of PEOP (10-38-10) lacks distinctive signatures of long range order, presumably due to the slow diffusion of long chains. Nevertheless, the use of RSoXS allows successful characterization of block copolymers with large domain spacing.

The ionic conductivity σ of the PEOP electrolytes doped with LiTFSI as a function of 1000 / T is summarized in Figure 5.8. For comparison σ has also been determined for the PEOP (4-16-4) polymer in the absence of LiTFSI (*i.e.*, r = 0). Only the data corresponding to the cooling scan and subsequent (second) heating scan are presented. In the temperature range explored, the data obtained for neat PEOP (4-16-4) shows evidence of two different regimes, with a transition at about 50 °C corresponding to $T_{m,PEO}$.[61] In contrast, the LiTFSI-doped PEOP electrolytes do not exhibit such a transition even at the depressed values of $T_{m,PEO}$ observed in DSC results for the salt-doped polymers in Figure 5.4a. The presence of LiTFSI strongly decreases the crystallinity of the PEO domain, and its solubility in PEO provides a route to the elevated values of σ. Furthermore, there is no impact on σ when passing through $T_{m,PP}$. It is important to note that neat PEOP (4-16-4) was found to have σ in the range of 3×10^{-6} to 1×10^{-5} S/cm at T > 50 °C. Remaining impurities from the synthetic procedure are likely the source of this observation. Purification processes are under way to remove any trace impurities from the PEOP samples. The effect of this "background" ionic motion represents less than 5% of the total ionic conductivity when LiTFSI is added to the PEOP (4-16-4) polymer and falls well within the experimental error bars reported in Figure 5.8.

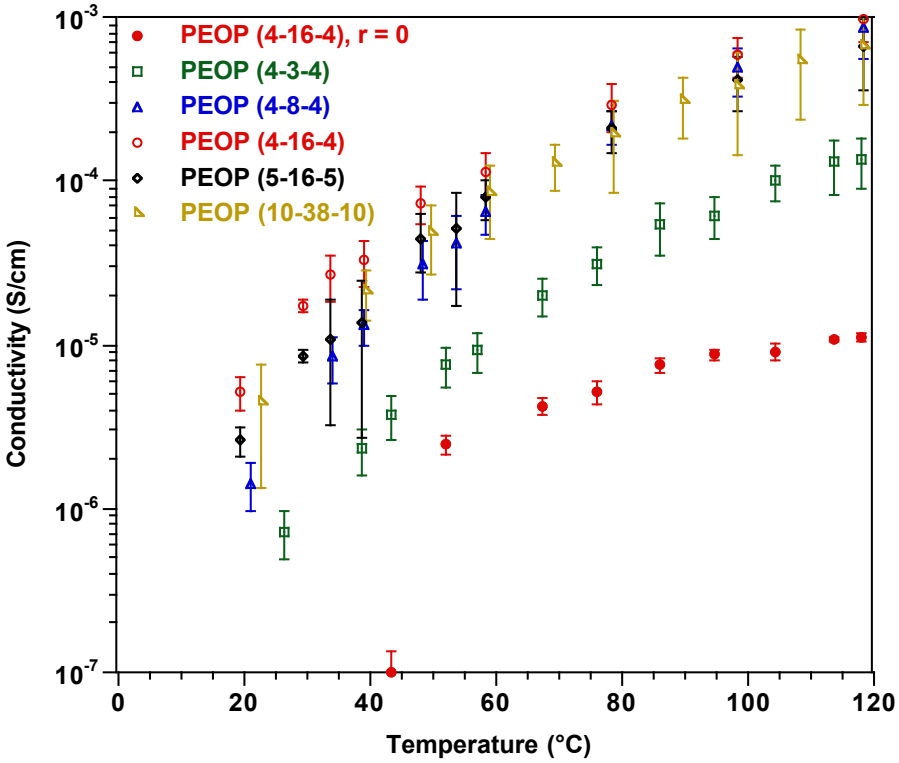

Figure 5.8 Ionic conductivity of LiTFSI-doped PEOP block copolymers as a function of temperature.

Over the entire T range, it was found that σ is higher for the PEOP (4-16-4) compared with PEOP (4-8-4). This observation can be rationalized in context of previous work on PEO-containing block copolymer electrolytes, where an increase in σ has been shown with increasing $M_{n,PEO}$.[30] Furthermore, for higher values of ϕ_c, σ is found to increase, as evidenced by comparing the results for PEOP (4-16-4) and PEOP (5-16-5). At 90 °C, σ for the PEOP electrolytes containing $M_{n,PEO}$ in the range of 8 – 16 kg/mol are on the order of 4×10^{-4} S / cm. This value of σ is comparable to that for high M_n diblock copolymer electrolytes with a polystyrene mechanical block.[30]

The presence of a peak σ as a function of M_n distinguishes PEOP electrolytes

from previously studied polymer electrolytes. In the case of homopolymer electrolytes such as LiTFSI-doped PEO, σ was found to decrease monotonically with increasing M_n due to the decrease in full chain diffusion beyond the entanglement molecular weight for PEO (M_e ~ 1.7 kg/mol).[62] Conversely, diblock copolymer electrolytes studied by Balsara and workers (and others) have generally found σ to increase monotonically with M_n, particularly in the high-M_n limit.[30] A caveat to that is the recent demonstration that in the low-M_n limit, SEO electrolytes have σ inversely proportional to M_n.[58] In contrast to the previous literature, PEOP electrolytes studied in this work have a peak in σ as a function of M_n, as seen in Figure 5.9. This result can be attributed to several possible factors. The lack of long-range order, as indicated by relative breadth of scattering peaks and absence of higher-order peaks, suggests that the coherent grains of the block copolymer are likely quite small. This is due, in part,

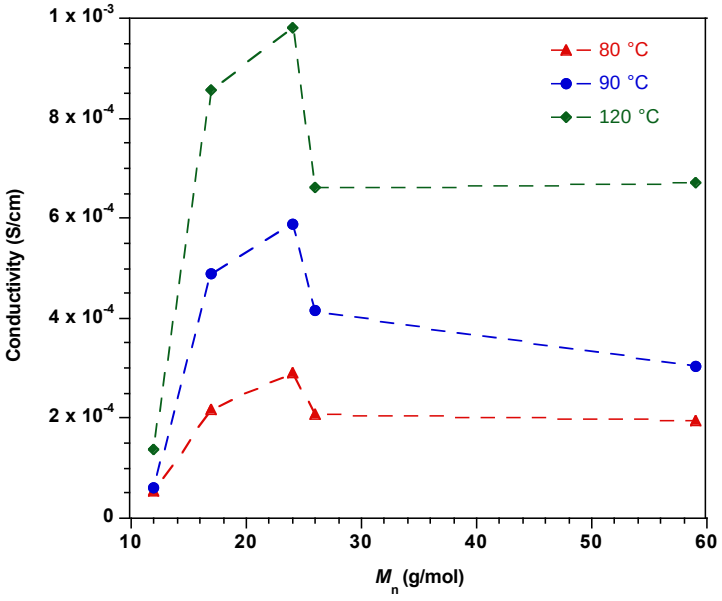

Figure 5.9 Dependence of σ on M_n for PEOP electrolytes at three temperatures (T = 80, 90, and 120 °C).

to the nature of triblock copolymers, where a significant energetic penalty is required to achieve significant rearrangement of individual molecules. The polymers studied here evidently are far from a disordering transition, even in the case of the lowest M_n sample. The interaction parameter χ between sPP and PEO must be large in order to maintain strongly-segregated domains at elevated temperatures. Thus there is a strong resistance for PEOP chains to diffuse across phase boundaries, which would be required to obtain highly ordered samples. It has been shown that the presence of grain boundaries can promote high σ in SEO block copolymers.[63] However high-*T* annealing of these electrolytes results in the minimization of grain boundaries and a concomitant decrease in ion transport. By effectively eliminating the ability of the polymers to reassemble into well-ordered domains *via* the annealing process, the triblock architecture appear to exhibit sustained high performance, independent of thermal processing history.

5.4 Conclusions

In summary, we have synthesized and characterized the properties and self-assembly of syndiotactic polypropylene-*block*-poly(ethylene oxide)-*block*-syndiotactic polypropylene triblock copolymers, and established their unusual behavior as solid polymer electrolytes. Using DSC and scattering experiments, we determined the thermal and structural properties of the polymers, and the effect of doping with lithium bis(trifluoromethanesulfonyl)imide salt. We studied the ionic conductivity of the salt-doped polymers and found that the triblock architecture played a crucial role in the anomalous behavior and identified it as an important methodology to design future materials with superlative performance.

5.5 Experimental

5.5.1 General

All manipulations of air- and/or water sensitive compounds were carried out under dry nitrogen using a Braun UniLab drybox or standard Schlenk techniques. ^{1}H and ^{13}C NMR spectra were collected in deuterated solvents on a Varian INOVA 400 or Varian 500 (^{13}C, 125 MHz). The spectra were referenced internally to residual protio solvents (^{1}H) or to deuterio-solvent signals (^{13}C) and are reported relative to tetramethylsilane (δ = 0 ppm). Syndiotactic polypropylene (sPP) samples were dissolved in $CDCl_3$ and NMR spectra were collected at 60 °C. Molecular weights of the end-functionalized sPP and PEO samples were determined using end group analysis of quantitative ^{1}H NMR spectra and are given in Table 5.1 as $M_{n,sPP}$ and $M_{n,PEO}$. The length of each block in number of repeat units, relative to a reference unit volume v_0 = 0.1 nm^3, is given as N_{sPP}^{*} and N_{PEO}^{*} (where N_i^{*} is defined by $M_{n,i} \cdot v_i / M_i \cdot v_0$). The propylene repeat unit is defined with respect to a dimer of the propylene monomer (*i.e.*, C_6H_{12}) by convention. M_P and M_{EO} are the repeat unit molar masses of propylene (84.16 g / mol) and ethylene oxide (44.05 g / mol), respectively. v_P and v_{EO} are the repeat unit volumes of propylene (0.176 nm^3) and ethylene oxide (0.069 nm^3), respectively, at a reference temperature of 140 °C.

5.5.2 Methods

Toluene was purified over columns of alumina and copper (Q5). Tetrahydrofuran for block copolymer synthesis was purified over alumina column and degassed by three freeze-pump-thaw cycles before use. Propylene (Airgas, research purity) was purified over columns of BASF catalyst R3-12, BASF catalyst R3-11, and

4 Å molecular sieves. Polymethylaluminoxane (PMAO-IP, 13 wt% Al in toluene, Akzo Nobel) was dried *in vacuo* to remove residual trimethyl aluminum and used as a white solid powder. Sodium azide, PEO polymers (M_n: 3, 8, 16 and 38 kg/mol; M_w/M_n = 1.1), *para*-toluenesulfonyl chloride, sodium hydride (60% dispersion in mineral oil), tripropargyl amine (98%), tetrakis(acetonitrile)copper(I) hexafluorophosphate (97%), 2,6-lutidine (>99%), borane-tetrahydrofuran complex (1.0 M solution in THF, stabilized with 0.005 M N-isopropyl-N-methyl-tert-butylamine), propargyl bromide solution (80 wt.% in toluene), and copper bromide were purchased from Sigma-Aldrich and used as received. Acetonitrile (HPLC grade) was obtained from Mallinckrodt Baker and used as received. Benzyl azide (94%) was purchased from Alfa-Aesar and used as received. $CDCl_3$ was purchased from Cambridge Isotope Laboratories (CIL) and used as received. Dry tetrahydrofuran (THF) for electrolyte preparation was obtained from Sigma Aldrich and used as received in an argon-filled glove box. Dry LiTFSI was obtained from Novolyte under argon, brought into the glove box, and dried under vacuum in the glove box antechamber at 120 °C for three days prior to use.

Allyl-terminated sPP (M_w/M_n = 1.9) was prepared according to a previously reported procedure.[46,64] The extent of syndiotacticity of sPP samples was determined from ^{13}C NMR spectroscopy using the fraction of fully syndiotactic pentads [*rrrr*] and was found to be 0.80. Tris-(benzyltriazolylmethyl)amine (TBTA) ligand for alkyne-azide "click" chemistry was synthesized according to the literature procedure.[49]

5.5.3 Synthesis

5.5.3.1 General procedure for the synthesis of dipropargyl-terminated PEO

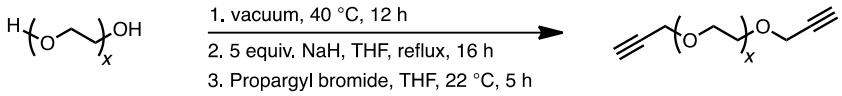

Scheme 5.1 General scheme for the synthesis of dipropargyl-terminated poly(ethylene oxide).

An oven-dried three neck round bottom flask was cooled under vacuum and charged with PEO (7.9 g, 5.3 mmol OH functional groups). The polymer was heated at 40 °C under vacuum for 12 h to ensure that it is completely dry. Sodium hydride (0.640 g, 15.8 mmol) was added to the cooled flask under nitrogen. THF (150 mL) was then cannula transferred to the flask under nitrogen and the reaction mixture was refluxed for 16 h. The flask was cooled to room temperature and propargyl bromide (1.76 mL, 11.8 mmol) was injected into the reaction mixture via gastight syringe. The mixture was stirred at 22 °C for 5 h and then quenched with minimum amount of ethanol. After the effervescence ceased, the mixture was slowly poured into hexanes. The precipitated polymer was collected, dissolved in dichloromethane and filtered through a glass frit layered with Celite. Dichloromethane was removed; the polymer was again precipitated in hexanes and dried *in vacuo* to constant weight (6.9 g, 87% yield). ^{1}H NMR (500 MHz, $CDCl_3$) δ 4.16 (d, J = 2.4 Hz, 4H), 3.60 (s, 340H), 2.41 (t, J = 2.4 Hz, 2H). ^{13}C NMR (126 MHz, $CDCl_3$) δ 79.68, 74.64, 70.51, 69.11, 58.42.

5.5.3.2 General procedure for the synthesis of hydroxyl-terminated sPP[46]

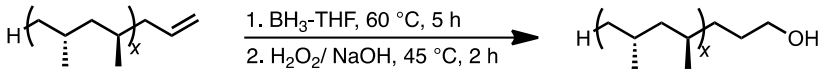

Scheme 5.2 General scheme for the synthesis of hydroxyl-terminated syndiotactic polypropylene.

An oven dried 250 mL Schlenk adapted round bottom flask was cooled under vacuum and charged with allyl-terminated sPP (2.7 g, 0.51 mmol). THF (100 mL) was cannula transferred into the flask under nitrogen and the mixture was heated at 45 °C. BH_3-THF solution (5.1 mL, 5.1 mmol) was added to the reaction flask *via* a gastight syringe and the solution was heated at 60 °C for 5 h. The solution was cooled to 45 °C and sodium hydroxide solution (1.0 M in H_2O, 41 mmol) was added followed immediately by a hydrogen peroxide solution (1.2 M in THF, 41 mmol). The solution was stirred at 45 °C for 2 h and poured slowly into methanol (200 mL). The polymer was collected, dissolved in hot toluene and filtered through a glass frit layered with silica. Toluene was removed and the polymer was precipitated in methanol. Polymer was isolated and dried *in vacuo* to constant weight (2.5 g, 94% yield). ^{1}H NMR (500 MHz, $CDCl_3$, 60 °C) δ 3.63 (q, J = 6.4 Hz, 2H), 1.82 – 0.58 (m, 960H). ^{13}C NMR (126 MHz, $cdcl_3$) δ 46.83, 27.83, 20.04.

5.5.3.3 General procedure for the synthesis of tosyl-terminated sPP

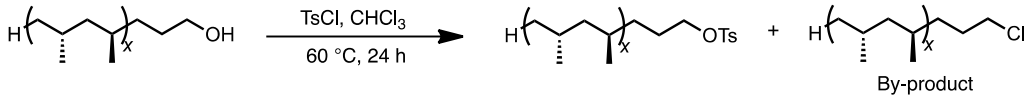

Scheme 5.3 General scheme for the synthesis of tosyl-terminated syndiotactic polypropylene.

A 250 mL round bottom was charged with hydroxyl-terminated sPP (2.7 g, 0.61 mmol), *para*-toluenesulfonyl chloride (3.43 g, 18.0 mmol), and chloroform (60 mL). Pyridine (1.45 ml, 18.0 mmol) was added to the mixture *via* a syringe and the solution was heated at 60 °C. After 24 h, the reaction mixture was cooled to room temperature and poured in methanol (200 mL). The polymer was collected, dissolved in hot toluene, and then filtered through a glass frit layered with silica. Toluene was removed and the polymer was precipitated in methanol. The polymer was collected and dried *in vacuo* to constant weight (2.6 g, 97% yield). ^{1}H NMR (500 MHz, $CDCl_3$, 60 °C) δ 7.82 – 7.77 (m, 2H), 7.34 (d, J = 8.1 Hz, 2H), 4.01 (t, J = 6.6 Hz, 2H), 3.52 (t, J = 6.9 Hz, 2H), 2.45 (s, 3H), 1.85 – 0.59 (m, 1080H). ^{13}C NMR (126 MHz, $CDCl_3$, 60 °C) δ 46.83, 27.83, 20.04.

5.5.3.4 General procedure for the synthesis of azido-terminated sPP

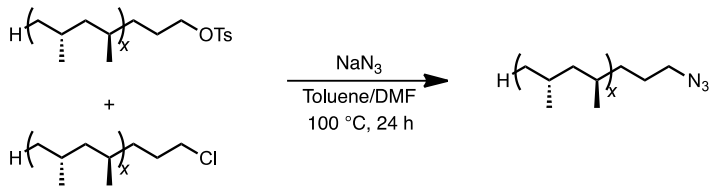

Scheme 5.4 General scheme for the synthesis of azido-terminated syndiotactic polypropylene.

An oven-dried 100 mL Schlenk adapted round bottom was charged with tosyl-terminated sPP (1.3 g, 0.21 mmol) and sodium azide (0.28 g, 4.3 mmol). Toluene (21.0 mL) and dimethyl formamide (10.5 mL) were cannulated into the flask under N_2 and the reaction mixture was heated at 100 °C for 24 h. After cooling to room temperature, the solution was poured into methanol (100 mL) to precipitate the polymer. The polymer was isolated, dissolved in hot toluene, and filtered through a plug of silica. Toluene was removed and the polymer was precipitated in methanol. Polymer was collected and dried *in vacuo* to constant weight (1.1 g, 86% yield). ^{1}H NMR (500 MHz, $CDCl_3$, 60 °C) δ 3.25 (t, J = 7.0 Hz, 2H), 1.82 – 0.61 (m, 825H). ^{13}C NMR (126 MHz, $CDCl_3$, 60 °C) δ 46.83, 27.83, 20.04.

5.5.3.5 General procedure for the synthesis of sPP-*b*-PEO-*b*-sPP triblock copolymer

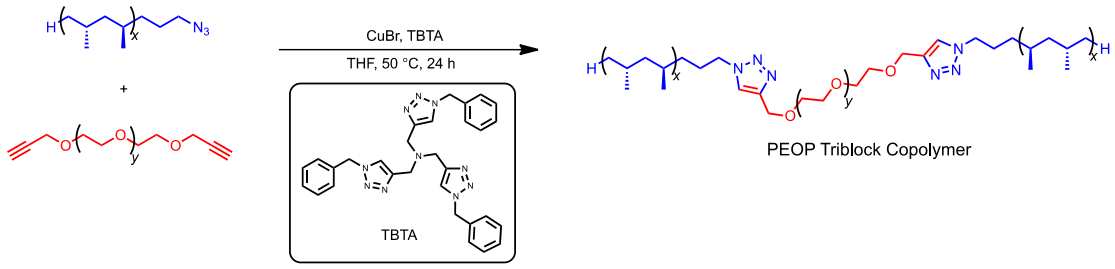

Scheme 5.5 General scheme for the synthesis of PEOP triblock copolymer.

In the glovebox, a 100 mL Schlenk tube was charged with azido-terminated sPP (0.60 g, 0.070 mmol N_3 functional groups), dipropargyl-terminated PEO (0.36 g, 0.085 mmol functional propargyl groups), CuBr (3 mg, 0.02 mmol), and TBTA ligand (11 mg, 0.020 mmol). THF (7.1 mL) was added and the Schlenk tube was heated at 50 °C for 24 h. After the reaction had completed, the mixture was cooled to room temperature, and the polymer was precipitated in methanol. The resultant light green polymer was thoroughly washed with methanol to remove the copper catalyst and excess PEO. Insoluble polymer was isolated by vacuum filtration, washed with methanol, and dried *in vacuo* to constant weight (0.85 g, 94% yield). ^{1}H NMR (400 MHz, $CDCl_3$, 60 °C) δ 7.55 (s, 2H), 4.69 (s, 4H), 4.31 (t, J = 7.4 Hz, 1H), 3.64 (s, 1010H), 1.70 – 0.58 (m, 2664H). ^{13}C NMR (126 MHz, $CDCl_3$, 60 °C) δ 70.85, 46.74, 27.74, 19.97.

5.5.4 NMR Spectra

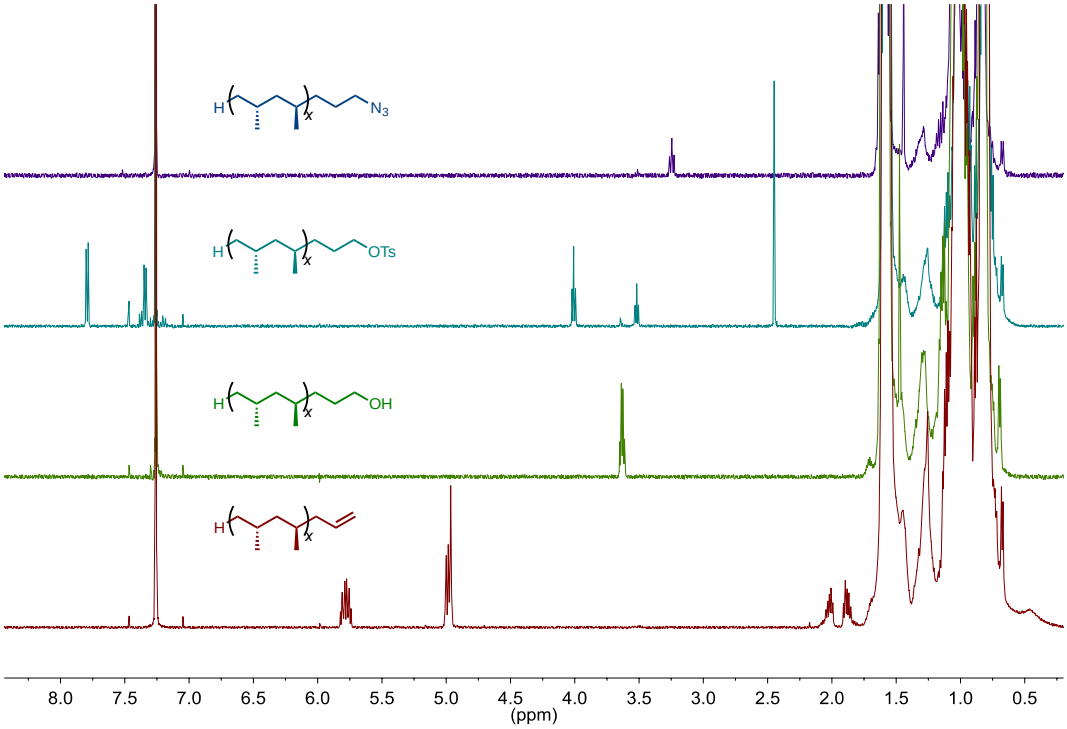

Figure 5.10 ^{1}H NMR spectra ($CDCl_3$, 60 °C) of sPP-$CH_2CH{=}CH_2$ (red), sPP-$(CH_2)_3$-OH (green), sPP-$(CH_2)_3$-OTs (teal), and sPP-$(CH_2)_3$-N_3 (blue).

5.5.5 Electrolyte preparation

PEOP polymers were brought into an argon-filled glove box for electrolyte preparation after drying in the glove box antechamber at 100 °C for one day. In the glove box, a mixture of PEOP polymer and dry LiTFSI was co-dissolved in THF. For all samples the amount of LiTFSI added was predetermined to obtain a molar ratio *r* of lithium ions (Li^+) to ethylene oxide (EO) moieties equal to 0.063 ± 0.06. This concentration of salt was previously shown to give the highest ionic conductivity for SEO-based electrolytes.[28] The solution was stirred for several hours at 90 °C until complete dissolution could be observed visually, and then the THF was allowed to evaporate to obtain a solid polymer-salt mixture. Subsequently, the electrolyte was dried further in the glove box antechamber under vacuum at 90 °C for at least 8 hours prior to characterization.

For each electrolyte the volume fraction of the conducting phase, ϕ_c, is determined taking into account the contributions of both PEO and LiTFSI as defined by:

$$\phi_c(r) = \frac{V_{EO} + r \cdot V_{LiTFSI}}{V_{EO} + r \cdot V_{LiTFSI} + \frac{2 \cdot M_{n,sPP} \cdot M_{EO}}{M_P \cdot M_{n,PEO}} V_P} \qquad (2)$$

where V_{EO}, V_{LiTFSI}, and V_P are the molar volumes of EO monomer units (41.56 cm^3 / mol),[42] LiTFSI (141.9 cm^3 / mol),[58] and propylene repeat units (105.99 cm^3 / mol),[42] respectively, at a reference temperature of 140 °C. Eq. 1 is derived according to the assumption of no volume change of mixing.

5.5.6 Characterization Procedures

5.5.6.1 Differential Scanning Calorimetry (DSC)

The thermal properties of polymers were studied *via* DSC experiments. Pure PEOP polymers and the related electrolytes were sealed in aluminum hermetic pans in an argon-filled glove box. DSC experiments were performed on a TA Instruments DSC Q200 instrument. All samples were studied with an identical scan program: samples were heated from room temperature to 120 °C at 10 °C / min, after which two cooling/heating scan were run at 10 °C / min, between −40 °C and 120 °C. For each sample $T_{m,i}$ of the PEO and sPP phases were determined at the maximum of each endothermic peak on the last cycle.[65] The integration of the area of each endothermic peak gives the enthalpy of melting, $\Delta H_{m,i}$, for each phase *i* (*i* = PEO or sPP). The crystallinity, $X_{c,i}$, for the phase *i* is given by:

$$X_{c,i} = \frac{\Delta H_{m,i}}{w_i \cdot \Delta H^0_{m,i}} \quad (3)$$

where w_i is the weight fraction of phase *i* and $\Delta H^0_{m,i}$ is the enthalpy of melting of pure *i*. $\Delta H^0_{m,PEO}$ and $\Delta H^0_{m,sPP}$ values are 195.8 J / g and 206.7 J / g, respectively.[66,67]

5.5.6.2 Small angle X-ray scattering (SAXS)

SAXS experiments were performed at beamline 7.3.3 at the Advanced Light Source (ALS) at Lawrence Berkeley National Laboratory and at beamline 1-4 at the Stanford Synchrotron Radiation Lightsource to determine the morphology and domain spacing of each block copolymer as well as the related electrolyte. SAXS samples were assembled in an argon-filled glove box by hot-pressing solid polymer into

approximately 150 μm thick spacers (Garolite G-10) at 90 °C. The samples were sealed in air-tight aluminum sample holders with Kapton windows, and annealed at 120 °C for several days prior to experiments. Samples were mounted in a custom-built sample stage with *T* control. At each *T* examined, samples were annealed for a minimum of 20 min prior to data collection. SAXS data analysis was performed using the Nika program written for Igor Pro.[68] Silver behenate was used as a standard to calibrate beam center and sample-to-detector distance. The measured two-dimensional scattering data were azimuthally averaged to obtain intensity, *I*, as a function of the scattering vector magnitude, *q*. The relationship between *q* and the wavelength of the X-rays, λ, and the scattering angle, θ is given by:

$$q = \frac{4\pi}{\lambda} \sin\left(\frac{\theta}{2}\right) \tag{4}$$

The X-ray energy for SAXS experiments was approximately 10 keV in all cases, corresponding to λ = 0.124 nm^{-1}. SAXS data from all the samples were obtained at room temperature and between 60 °C and 120 °C in increments of 20 °C. The location of the primary scattering peak at a scattering vector magnitude *q** enables determination of the domain spacing, *d*:

$$d = \frac{2\pi}{q^*} \tag{5}$$

The ratio between *q** and higher order scattering peaks were used to determine the nanostructured morphology, *e.g*. integer multiples as indication of lamellar morphology (*q* / *q** = 2, 3, 4, *etc*.).

5.5.6.3 Resonant soft X-ray scattering (RSoXS)

RSoXS experiments were performed at beamline 11.0.1.2 at ALS to determine the domain size and morphology of high molecular weight samples for which values q^* could not be resolved by SAXS experiments ($q_{min,SAXS} \approx 0.1$ nm^{-1}). RSoXS experiments could be performed over a range of incident X-ray energy values, which allows λ to be tuned and thus varies q_{min} according to equation 3 ($q_{min,RSoXS} \approx 0.03$ nm^{-1}). Samples for RSoXS experiments were made by drop-casting in an argon-filled glove box to obtain thin samples which minimize X-ray absorption. Pure PEOP and LiTFSI-doped PEOP samples were made by dissolving the appropriate material in THF at a concentration of ~ 1 mg / mL solids at room temperature. Solutions were stirred overnight to ensure complete dissolution. The solutions were dropped onto silicon nitride substrates (Norcada) and dried overnight to obtain thin films on the order 1 – 5 μm thick. The substrates consisted of 200 μm thick silicon frame with dimensions 5 × 5 mm with a 100 nm thick silicon nitride top layer exposed in a 1.5 × 1.5 mm window. Samples were stored under argon until immediately before placement in the ultrahigh vacuum chamber used for RSoXS. Incident X-ray energies were tuned near the carbon K-edge to 280 eV. Samples were attached to a stage with carbon tape that was capable of heating samples to ~ 130 °C. Data were reduced and analyzed using a modified version of the Nika program for Igor Pro, and normalized by subtracting out a dark image to obtain $I(q)$.[69]

5.5.6.4 Symmetrical cell assembly and characterization

Inside an argon-filled glove box, the polymer electrolyte was hand-pressed at 90 °C into a 30 μm thick Kapton spacer with a 0.3 cm diameter hole that defines the

active area *S* of the cell. Two stainless steel blocking electrodes were then placed on each side of the electrolyte-spacer assembly and pressed at 90 °C. At each step of the assembly the overall thickness was measured to monitor the electrolyte thickness, *l*. An aluminum tab was taped on each stainless steel electrode and the assembly was vacuum sealed in pouch material (Showa Denko).

The cells were mounted into a custom heating stage and connected to a Bio-Logic VMP3. Impedance spectroscopy was performed using an excitation signal between 10 and 40 mV in a frequency range between 10^6 and 1 Hz. The *T* program consisted of an initial heating scan from room temperature to 120 °C in 10 °C steps, followed by cooling to room temperature, and then a second heating scan was carried out from 30 °C to 120 °C in 10 °C steps. Data was analyzed from the cooling scan and subsequent heating scan. For each *T*, the resistance of the electrolyte, R_{el}, was monitored as a function of time and the impedance spectra was measured only when R_{el} became stable. The equilibrated value of R_{el} was extracted from the impedance spectra by fitting the profile with an equivalent electrical circuit consisting of a resistor and a constant phase element.[70] After the experiments, the cells were returned to the argon-filled glove box and disassembled to determine the final value of *l*. This *l* value was used to calculate σ according to equation 6:

$$\sigma(T) = \frac{l}{S \cdot R_{el}(T)} \tag{6}$$

at each *T* considered.

5.5.6.5 Wide-angle X-ray Scattering (WAXS)

WAXS experiments were performed at beamline 1-4 at the Stanford Synchrotron Radiation Lightsource (SSRL) at SLAC National Laboratory to determine the effect of salt on the crystallinity of PEO and sPP blocks. WAXS samples were assembled in an argon-filled glove box by hot-pressing solid polymer into approximately 150 μm thick spacers (Garolite G-10) at 90 °C. The samples were sealed in air-tight aluminum sample holders with Kapton windows, and annealed at 120 °C for several days prior to experiments. Samples were mounted in a custom-built sample stage with *T* control. At each *T* examined, samples were annealed for a minimum of 20 min prior to data collection. WAXS data analysis was performed using the Nika program written for Igor Pro.[68] Silver behenate was used as a standard to calibrate beam center and sample-to-detector distance. The measured two-dimensional scattering data were azimuthally averaged to obtain *I* as a function of *q*. WAXS data from all the samples were obtained at 30 °C and 90 °C. Several prominent WAXS features were identified by comparison with literature reports on the characterization of polyethylene-PEO diblock copolymers (*i.e.*, the PEO(120) peak at q = 13.2 nm^{-1}),[71] and sPP-poly(ethylene-*co*-propylene)-sPP triblock copolymers (*i.e.*, the sPP(200) peak at q = 8.7 nm^{-1} and the sPP(020) peak at q = 11.0 nm^{-1}).[72,73]

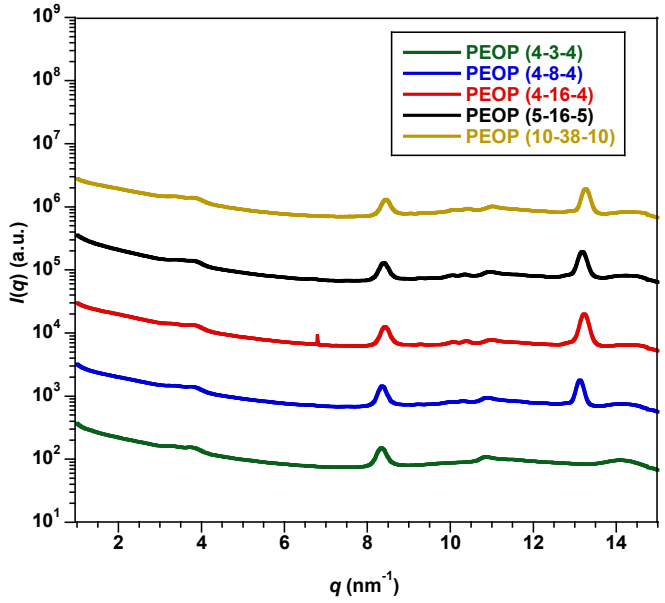

Figure 5.11 Wide angle X-ray scattering profiles of neat PEOP block copolymers at 30 °C. Important features include the PEO(120) peak at q = 13.2 nm^{-1}, the sPP(200) peak at q = 8.7 nm^{-1}, and the sPP(020) peak at q = 11.0 nm^{-1}.

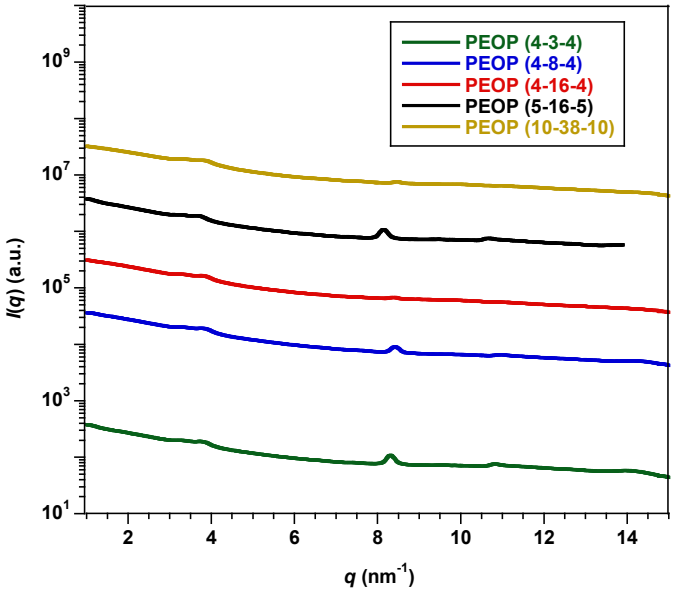

Figure 5.12 Wide angle X-ray scattering profiles of LiTFSI-doped PEOP block copolymers (r = 0.063) at 30 °C. The profiles are characterized by the absence of PEO(120) peak at q = 13.2 nm^{-1}.

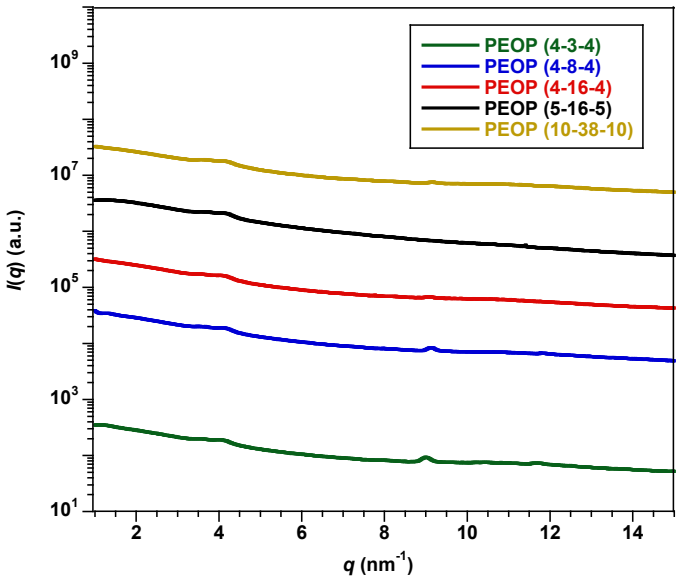

Figure 5.13 Wide angle X-ray scattering profiles of LiTFSI-doped PEOP block copolymers (r = 0.085) at 90 °C. Similar to the profiles of Figure 5.12, these profiles are characterized by the absence of PEO(120) peak at q = 13.2 nm^{-1}. Furthremore, there is a reduction in the sharpness of the peak attributed to the sPP(200) feature at q = 8.7 nm^{-1}, and the sPP(020) feature at q = 11.0 nm^{-1}, as $T_{m,sPP}$ is approached.

REFERENCES

(1) Tarascon, J. M.; Armand, M. *Nature* **2001**, *414*, 359–367.

(2) Armand, M.; Tarascon, J.-M. *Nature* **2008**, *451*, 652–657.

(3) Fenton, D. E.; Parker, J. M.; Wright, P. V. *Polymer* **1973**, *14*, 589–589.

(4) Armand, M. B. C., J. M.; Duclot, N. J. *Fast Ion Transport in Solids: Electrodes, and Electrolytes*; Lake Geneva, Wisconsin, U.S.A., May 21−25, 1979; Vashishta, P.; Mundy, J. N.; Shenoy, G. K., Eds; North Holland: New York, 1979.

(5) Armand, M. *Solid State Ionics* **1983**, *9-10*, 745–754.

(6) Armand, M. *Solid State Ionics* **1994**, *69*, 309–319.

(7) Baril, D.; Michot, C.; Armand, M. *Solid State Ionics* **1997**, *94*, 35–47.

(8) Shi, J.; Vincent, C. A. *Solid State Ionics* **1993**, *60*, 11–17.

(9) Diddens, D.; Heuer, A.; Borodin, O. *Macromolecules* **2010**, *43*, 2028–2036.

(10) Vallée, A.; Besner, S.; Prudhomme, J. *Electrochim. Acta* **1992**, *37*, 1579–1583.

(11) Lascaud, S.; Perrier, M.; Vallée, A.; Besner, S.; Prudhomme, J.; Armand, M. *Macromolecules* **1994**, *27*, 7469–7477.

(12) Dollé, M.; Sannier, L.; Beaudoin, B.; Trentin, M.; Tarascon., J.-M. *Electrochem. Solid-State Lett.* **2002**, *5*, A286–A289.

(13) Rosso, M.; Brissot, C.; Teyssot, A.; Dollé, M.; Sannier, L.; Tarascon, J. M.; Bouchet, R.; Lascaud, S. *Electrochim. Acta* **2006**, *51*, 5334–5340.

(14) Hou, W. H.; Chen, C. Y.; Wang, C. C.; Huang, Y. H. *Electrochim. Acta* **2003**, *48*, 679–690.

(15) Liang, Y. H.; Wang, C. C.; Chen, C. Y. *Eur. Pol. J.* **2008**, *44*, 2376–2384.

(16) Snyder, J. F.; Carter, R. H.; Wetzel, E. D. *Chem. Mater.* **2007**, *19*, 3793–3801.

(17) Hayamizu, K.; Aihara, Y.; Price, W. S. *J. Chem. Phys.* **2000**, *113*, 4785–4793.

(18) Sadoway, D. R. *J. Power Sources* **2004**, *129*, 1–3.

(19) Trapa, P. E.; Acar, M. H.; Sadoway, D. R.; Mayes, A. M. *J. Electrochem. Soc.* **2005**, *152*, A2281–A2284.

(20) Trapa, P. E.; Won, Y. Y.; Mui, S. C.; Olivetti, E. A.; Huang, B. Y.; Sadoway, D. R.; Mayes, A. M.; Dallek, S. *J. Electrochem. Soc.* **2005**, *152*, A1–A5.

(21) Hu, Q.; Osswald, S.; Daniel, R.; Zhu, Y.; Wesel, S.; Ortiz, L.; Sadoway, D. R. *J. Power Sources* **2011**, *196*, 5604–5610.

(22) Niitani, T.; Shimada, M.; Kawamura, K.; Kanamura, K. *J. Power Sources* **2005**, *146*, 386–390.

(23) Leibler, L. *Macromolecules* **1980**, *13*, 1602–1617.

(24) Matsen, M. W.; Thompson, R. B. *J. Chem. Phys.* **1999**, *111*, 7139–7146.

(25) Matsen, M. W. *J. Chem. Phys.* **2000**, *113*, 5539–5544.

(26) Abetz, V.; Goldacker, T. *Macromol. Rapid Commun.* **2000**, *21*, 16–34.

(27) Niitani, T.; Amaike, M.; Nakano, H.; Dokko, K.; Kanamura, K. *J. Electrochem. Soc.* **2009**, *156*, A577–A583.

(28) Singh, M.; Odusanya, O.; Wilmes, G. M.; Eitouni, H. B.; Gomez, E. D.; Patel, A. J.; Chen, V. L.; Park, M. J.; Fragouli, P.; Iatrou, H.; Hadjichristidis, N.; Cookson, D.; Balsara, N. P. *Macromolecules* **2007**, *40*, 4578–4585.

(29) Mullin, S. A.; Stone, G. M.; Panday, A.; Balsara, N. P. *J. Electrochem. Soc.* **2011**, *158*, A619–A627.

(30) Panday, A.; Mullin, S.; Gomez, E. D.; Wanakule, N.; Chen, V. L.; Hexemer,

A.; Pople, J.; Balsara, N. P. *Macromolecules* **2009**, *42*, 4632–4637.

(31) Gomez, E. D.; Panday, A.; Feng, E. H.; Chen, V.; Stone, G. M.; Minor, A. M.; Kisielowski, C.; Downing, K. H.; Borodin, O.; Smith, G. D.; Balsara, N. P. *Nano Lett.* **2009**, *9*, 1212–1216.

(32) Lobitz, P.; Fullbier, H.; Reiche, A.; Illner, J. C.; Reuter, H.; Horing, S. *Solid State Ionics* **1992**, *58*, 41–48.

(33) Alloin, F.; Sanchez, J.-Y.; Armand, M. *Electrochim. Acta* **1992**, *37*, 1729–1731.

(34) Saunier, J.; Alloin, F.; Sanchez, J.-Y. *Electrochim. Acta* **2000**, *45*, 1255–1263.

(35) Jankova, K.; Jannasch, P.; Hvilsted, S. *J. Mater. Chem.* **2004**, *14*, 2902–2908.

(36) Ionescu-Vasii, L. L.; Abu-Lebdeh, Y.; Armand, M. *Solid State Ionics* **2005**, *176*, 2769–2775.

(37) Huang, J.; Tong, Z.-Z.; Zhou, B.; Xu, J.-T.; Fan, Z.-Q. *Polymer* **2013**, *54*, 3098–3106.

(38) Soo, P. P.; Huang, B. Y.; Jang, Y. I.; Chiang, Y. M.; Sadoway, D. R.; Mayes, A. M. *J. Electrochem. Soc.* **1999**, *146*, 32–37.

(39) Ruzette, A.-V. G.; Soo, P. P.; Sadoway, D. R.; Mayes, A. M. *J. Electrochem. Soc.* **2001**, *148*, A537–A543.

(40) Trapa, P. E.; Huang, B. Y.; Won, Y. Y.; Sadoway, D. R.; Mayes, A. M. *Electrochem. Solid-State Lett.* **2002**, *5*, A85–A88.

(41) Huang, B.; Cook, C. C.; Mui, S.; Soo, P. P.; Staelin, D. H.; Mayes, A. M.; Sadoway, D. R. *J. Power Sources* **2001**, *97/98*, 674–676.

(42) Balsara, N. P.; Eitouni, H. B. In *Physical Properties of Polymers Handbook,*

Second Edition; Mark, J. E., Ed.; Springer: New York, 2007, p 339–356.

(43) Jannasch, P. *Chem. Mater.* **2002**, *14*, 2718–2724.

(44) See Experimental Section for details.

(45) Anderson, A. M., Cornell University, 2010.

(46) Anderson-Wile, A. M.; Coates, G. W.; Auriemma, F.; De Rosa, C.; Silvestre, A. *Macromolecules* **2012**, *45*, 7863–7877.

(47) Hillmyer, M. A.; Bates, F. S. *Macromolecules* **1996**, *29*, 6994–7002.

(48) Liu, R.; Li, Z. Y.; Mai, B. Y.; Wu, Q.; Liang, G. D.; Gao, H. Y.; Zhu, F. M. *J. Polym. Res.* **2013**, *20*, 64–74.

(49) Chan, T. R.; Hilgraf, R.; Sharpless, K. B.; Fokin, V. V. *Org. Lett.* **2004**, *6*, 2853–2855.

(50) Rodriguez-Arnold, J.; Zhang, A.; Cheng, S. Z. D.; Lovinger, A. J.; Hsieh, E. T.; Chu, P.; Johnson, T. W.; Honnell, K. G.; Geerts, R. G.; Palackal, S. J.; Hawley, G. R.; Welch, M. B. *Polymer* **1994**, *35*, 1884–1895.

(51) Deplace, F.; Wang, Z.; Lynd, N. A.; Hotta, A.; Rose, J. M.; Hustad, P. D.; Tian, J.; Ohtaki, H.; Coates, G. W.; Shimizu, F.; Hirokane, K.; Yamada, F.; Shin, Y.-W.; Rong, L.; Zhu, J.; Toki, S.; Hsiao, B. S.; Fredrickson, G. H.; Kramer, E. J. *J. Pol. Sci., Part B: Pol. Phys.* **2010**, *48*, 1428–1437.

(52) Ho, R. M.; Chung, T. M.; Tsai, J. C.; Kuo, J. C.; Hsiao, B. S.; Sics, I. *Macromol. Rapid Commun.* **2005**, *26*, 107–111.

(53) Radulescu, A.; Mathers, R. T.; Coates, G. W.; Richter, D.; Fetters, L. J. *Macromolecules* **2004**, *37*, 6962–6971.

(54) Ballesteros, O. R. d.; Auriemma, F.; Rosa, C. D. *Macromolecules* **2007**, *40*,

611–622.

(55) Rosa, C. D.; Ballesteros, O. R. d.; Auriemma, F. *Macromolecules* **2004**, *37*, 7724–7735.

(56) Sánchez-Soto, P. J.; Ginés, J. M.; Arias, M. J.; Novák, C.; Ruiz-Conde, A. *J. Therm. Anal. Calorim.* **2002**, *67*, 189-197.

(57) Allen, F. I.; Watanabe, M.; Lee, Z.; Balsara, N. P.; Minor, A. M. *Ultramicroscopy* **2011**, *111*, 239–244.

(58) Yuan, R.; Teran, A. A.; Gurevitch, I.; Mullin, S. A.; Wanakule, N. S.; Balsara, N. P. *Macromolecules* **2013**, *46*, 914–921.

(59) Virgili, J. M.; Tao, Y.; Kortright, J. B.; Balsara, N. P.; Segalman, R. A. *Macromolecules* **2007**, *40*, 2092–2099.

(60) Wong, D. T.; Wang, C.; Beers, K. M.; Kortright, J. B.; Balsara, N. P. *Macromolecules* **2012**, *45*, 9188–9195.

(61) Bouchet, R.; Lascaud, S.; Rosso, M. *J. Electrochem. Soc.* **2003**, *150*, A1385–A1389.

(62) Fetters, L. J.; Lohse, D. J.; Richter, D.; Witten, T. A.; Zirkel, A. *Macromolecules* **1994**, *27*, 4639–4747.

(63) Mullin, S. A.; Teran, A. A.; Yuan, R.; Balsara, N. P. *J. Pol. Sci., Part B: Pol. Phys.* **2013**, *51*, 927–934.

(64) Cherian, A. E.; Lobkovsky, E. B.; Coates, G. W. *Macromolecules* **2005**, *38*, 6259–6268.

(65) Marzantowicz, M.; Krok, F.; Dygas, J. R.; Florjanczyk, Z.; Zygadlo-Monikowska, E. *Solid State Ionics* **2008**, *179*, 1670–1678.

(66) Buckley, C. P.; Kovacs, A. J. *Colloid Polym. Sci.* **1976**, *254*, 695–715.

(67) Supaphol, P. *J. Appl. Polym. Sci.* **2001**, *79*, 1603–1609.

(68) Ilavsky, J. *J. Appl. Crystallogr.* **2012**, *45*, 324–328.

(69) Gann, E.; Young, A. T.; Collins, B. A.; Yan, H.; Nasiatka, J.; Padmore, H. A.; Ade, H.; Hexemer, A.; Wang, C. *Review of Scientific Instruments* **2012**, *83*, 045110.

(70) Devaux, D.; Bouchet, R.; Glé, D.; Denoyel, R. *Solid State Ionics* **2012**, *227*, 119–127.

(71) Cao, W. Y.; Tashiro, K.; Hanesaka, M.; Takeda, S.; Masunaga, H.; Sasaki, S.; Takata, M. *J. Phys. Chem. B* **2009**, *113*, 2338–2346.

(72) De Rosa, C.; Circelli, T.; Auriemma, F.; Mathers, R. T.; Coates, G. W. *Macromolecules* **2004**, *37*, 9034–9047.

(73) Deplace F.; Wang, Z. G.; Lynd, N. A.; Hotta, A.; Rose, J. M.; Hustad, P. D.; Tian, J.; Ohtaki, H.; Coates, G. W.; Shimizu, F.; Hirokane, K.; Yamada, F.; Shin, Y. W.; Rong, L. X.; Zhu, J.; Toki, S.; Hsiao, B. S.; Fredrickson, G. H.; Kramer, E. J. *J. Pol. Sci., Part B: Pol. Phys.* **2010**, *48*, 1428–1437.

APPENDIX A

Exploring Different Poly(ethylene oxide)-Based Cross-Linked Polymer Electrolytes:

A) Comb Polymers

B) Polymers Bearing Cyclic Carbonate Side Chains

APPENDIX A

Exploring Different Poly(ethylene oxide)-Based Cross-Linked Polymer Electrolytes:

A) Comb Polymers

B) Polymers Bearing Cyclic Carbonate Side Chains

A.1 Cross-Linked Comb Copolymers

In Chapter 2, we reported plasticized polyethylene/poly(ethylene oxide) (PE/PEO) polymer electrolytes with high ionic conductivity values at ambient temperatures. In particular, the electrolyte composition containing 40 wt% poly(ethylene glycol) (PEG; M_n = 275 Da) plasticizer exhibited ionic conductivity of 2.0×10^{-4} S/cm at 25 °C. We were interested in the effect of a covalently bound plasticizer in the network polymer on the ionic conductivities of these polymer electrolytes. Herein, we report comb cross-linked polymer electrolytes wherein the short PEG grafts were employed as immobile internal plasticizers.

Ring opening metathesis polymerization (ROMP) is a powerful synthetic tool to obtain macromolecular architectures with tunable molecular weight, size, shape, and function.[1,2] We used ROMP to copolymerize a PEO functionalized cross-linker (PEOX) with PEG-*grafted*-cyclooctene (PEG-*g*-COE) in the presence of LiTFSI salt to obtain cross-linked comb polymer electrolytes (Figure A.1). Short PEG grafts (average repeat units of ethylene oxide, b = 6) were immobilized on the polymer backbone and we expected that the molecular motion of these ethylene oxide (EO) units would be faster compared to the PEO chains constrained between the cross-links. Furthermore, we anticipated that the faster molecular motion of these PEG grafts

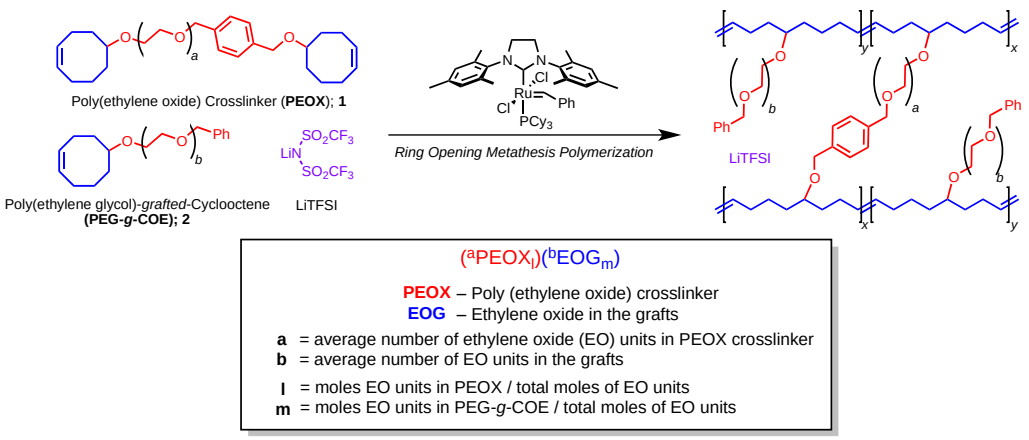

Figure A.1 Synthesis and nomenclature of PEO cross-linked comb polymers.

might facilitate the Li-ion conduction in the polymer matrix and increase the ionic conductivity. In the present work, thin polymer films were obtained by copolymerizing PEOX with PEG-*g*-COE using Grubbs second-generation catalyst in a Teflon-lined dish at 50 °C with a gradual evaporation of solvent from the dish.[3]

To test the effect of immobilization of the internal plasticizer on the polymer backbone, five different polymer electrolyte compositions were prepared at different [**PEOX**]:[**PEG-*g*-COE**] ratios. The nomenclature used for these comb polymers is described in the Figure A.1; each component is given a name, the average number of repeat units for each of the components are shown in the superscript, and the mole fraction of EO contained in each of these components is mentioned in the sub-scripts. The compositions and the thermal properties of these cross-linked comb polymers are listed in Table A.1. The data for the polymer electrolyte without any internal plasticizer (i.e. homopolymer of PEOX cross-linker) is not listed in the table because these polymer membranes were extremely brittle, which made the ionic conductivity measurements challenging. One would predict that an increase in the mole fraction of

Table A.1 Compositions and thermal properties of PEO cross-linked comb polymers[a]

entry	Sample Name	mmoles of EO	[PEOX]:[PEG-*g*-COE][b]	T_g[c] (°C)	DC Ionic Conductivity at 25 °C[d] (S/cm)
1	$(^{36}PEOX_{0.92})(^{6}EOG_{0.08})$	5.4	2:1	−44	2.1×10^{-5}
2	$(^{36}PEOX_{0.86})(^{6}EOG_{0.14})$	5.2	1:1	−45	2.9×10^{-5}
3	$(^{36}PEOX_{0.75})(^{6}EOG_{0.25})$	5.0	1:2	−45	2.3×10^{-5}
4	$(^{36}PEOX_{0.67})(^{6}EOG_{0.33})$	4.8	1:3	−45	1.3×10^{-5}
5	$(^{36}PEOX_{0.61})(^{6}EOG_{0.39})$	4.7	1:4	−43	9.7×10^{-6}

[a]All films had [EO]:[Li] composition of 15:1; where EO means ethylene oxide units contained both in the **PEOX** cross-linker and **PEG-*g*-COE**. [b][**PEOX**]:[**PEG-*g*-COE**] is defined as the molar ratio of **PEOX** cross-linker to **PEG-*g*-COE** in the cross-linked comb polymer. [c]Glass transition temperature (T_g) was determined by differential scanning calorimetry of the second heat cycle. [d]Determined by dielectric spectroscopy measurements. See General Method Section for more details.

PEG-*g*-COE would cause a decrease in the cross-linking density of these network comb polymers, and might lead to lower glass transition temperatures (T_gs) due to plasticizing effect of the PEG grafts. However, no significant changes in the T_gs of PEO segments in the network were observed, when the mole fraction of EO in the PEG-*g*-COE was changed from 0.08 to 0.39 (Table 1, entries 1–5). In contrast, Watanabe and coworkers reported a slight decrease in T_g from −56 °C to −60 °C when the internal plasticization was increased from 0 to 65% in the network polyether polymers.[4] Presumably, the graft length (i.e. 6 repeat units) in the comb polymers reported herein is still too large and hence these internal plasticizers have little effect on the segmental motion of the PEO chains in the network polymer, leading to no observed changes in the glass transition temperatures of these polymers.

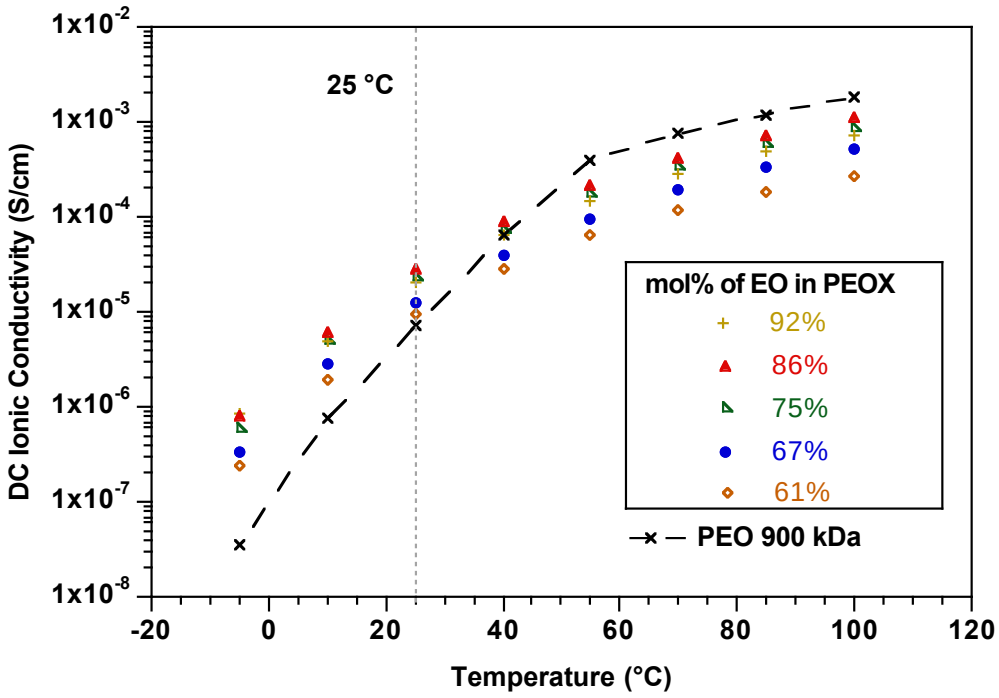

Figure A.2 Variable temperature conductivity of PEO cross-linked comb polymers.

The variable temperature conductivities of the cross-linked comb polymers containing different mole fractions of EO in the PEOX cross-linker are shown in Figure A.2. A LiTFSI-doped PEO (M_n 900 kDa) sample is also shown for comparison purposes. Of the tested comb polymer electrolyte compositions, the samples with higher cross-linking density and a lower mole fraction of the covalently bound plasticizing agent (i.e. entries 1 and 2) show relatively higher ionic conductivity (~ 2.5 × 10^{-5} S/cm at 25 °C) compared to the compositions containing higher mole fraction of EO grafts (~ 1.0 × 10^{-5} S/cm at 25 °C). It is currently unclear why the comb electrolyte compositions with higher mole fraction of internal plasticizer exhibits lower conductivity. Nonetheless, all the comb polymers exhibit higher ionic

conductivity values compared to the standard PEO sample at lower temperatures (below 40 °C). However, above the melting temperature of PEO (i.e. at temperatures >60 °C), PEO standard exhibits relatively higher ionic conductivity. Presumably, this is due to the fact that significant volume fraction of the network polymer electrolyte also contain unsaturated PE components, resulting in lower ethylene oxide content relative to the PEO homopolymer.

A.2 Cross-Linked Polymers with Cyclic Carbonate Side Chains

Ethylene carbonate and dimethyl carbonate are excellent solvents for dissolving the lithium salts, and they are currently used as lithium battery electrolyte components in commercially available lithium-ion batteries.[5] We wanted to incorporate similar cyclic carbonate moieties in our polymer electrolyte structure and examine their effect on the ionic conductivity of these electrolytes. We sought to develop PE/PEO cross-linked electrolytes with varying mole fraction of cyclic carbonate (CC) moieties using orthogonal-tandem catalysis (Figure A.3).[6] A cyclooctene monomer with cyclic carbonate containing side chain (**COE-CC**) was synthesized and used as a comonomer for ROMP chemistry. This synthetic route provides several advantages: a) facile incorporation of highly polar and lithium solubilizing components such cyclic carbonate in the polymer structure, b) fine-tuning of the mole fractions of PEO, PE, and cyclic carbonates in the polymer electrolytes, and c) tunability of the thermal properties of these network polymer electrolytes.

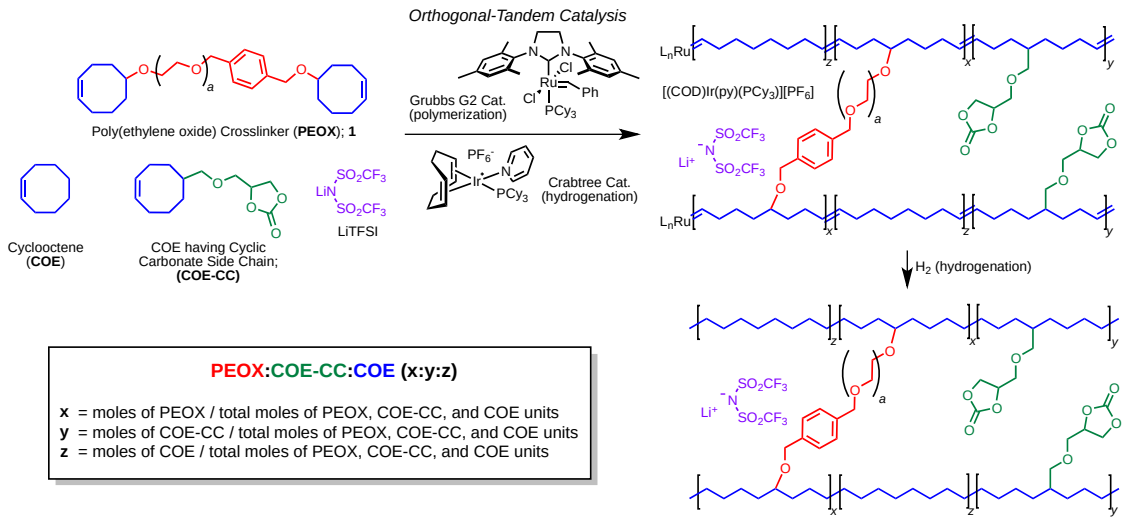

Figure A.3 Synthesis and nomenclature of the cross-linked polymers bearing cyclic carbonate side chains.

The nomenclature for these cyclic carbonate bearing polymer electrolytes is shown in Figure A.3. It was expected that the cyclic carbonate moieties in the polymer network would affect the ionic conductivity by virtue of the high dielectric constants of these materials. To examine the effects of the cyclic carbonate side chains on the ionic conductivity, three different polymer electrolytes were developed containing varying mole fraction of the cyclic carbonate monomer. The compositions and thermal properties of these polymer electrolytes are listed in Table A.2. Among all the tested compositions, the T_gs of the PEO components in the polymer electrolytes are comparable. An increase in the cyclic carbonate mole fraction (Table 1, entries 1–3) does not lead to an increase in the ionic conductivity. Ion transport is a complex phenomena and it is possible that the ionic conductivity is determined not only by the solvation of Li^+ ion by cyclic carbonate, but also by the concentration of the free Li^+ ions in the polymer matrix.

Table A.2 Compositions and thermal properties of PEO cross-linked polymers with cyclic carbonate side chains[a]

entry	x:y:z[b]	mmoles of EO	T_g[c] (°C)	DC Ionic Conductivity at 25 °C[d] (S/cm)
1	0.09:0:0.91	3.3	−43	6.5×10^{-6}
2	0.06:0.26:0.68	2.5	−40	4.2×10^{-6}
3	0.06:0.34:0.60	2.2	−41	5.0×10^{-6}

[a]All films had PEOX cross-linker with 36 EO units in the cross-links. [EO]:[Li] composition of 15:1; where EO means ethylene oxide units contained in the PEOX cross-linker. [b]x is the mole fraction of [**PEOX**] cross-linker, y is the mole fraction of the **COE-CC**, and z is the mole fraction of **COE** in the cross-linked polymer electrolyte. [c]Glass transition temperature (T_g) was determined by differential scanning calorimetry of the second heat cycle. [d]Determined by dielectric spectroscopy measurements. See General Method Section for more details.

Surprisingly, the ionic conductivity of CC bearing polymer electrolytes is similar to that of the LiTFSI-doped PEO standard sample at room temperature. However, notable differences were observed at higher temperatures (>60 °C). The PEO standard exhibited almost an order of magnitude higher conductivity than the CC bearing cross-linked polymer electrolytes (Figure A.4). The strong dipole-dipole interactions between the polar CC units of the polymer chains lead to a significant decrease in the segmental motion of PEO chain in the cross-linked polymer electrolyte. Furthermore, it is possible that any gain in the ion-pair dissociation of LiTFSI salt caused by the higher dielectric constant of these CC units is offset by the decrease in the segmental motion of the PEO chains.

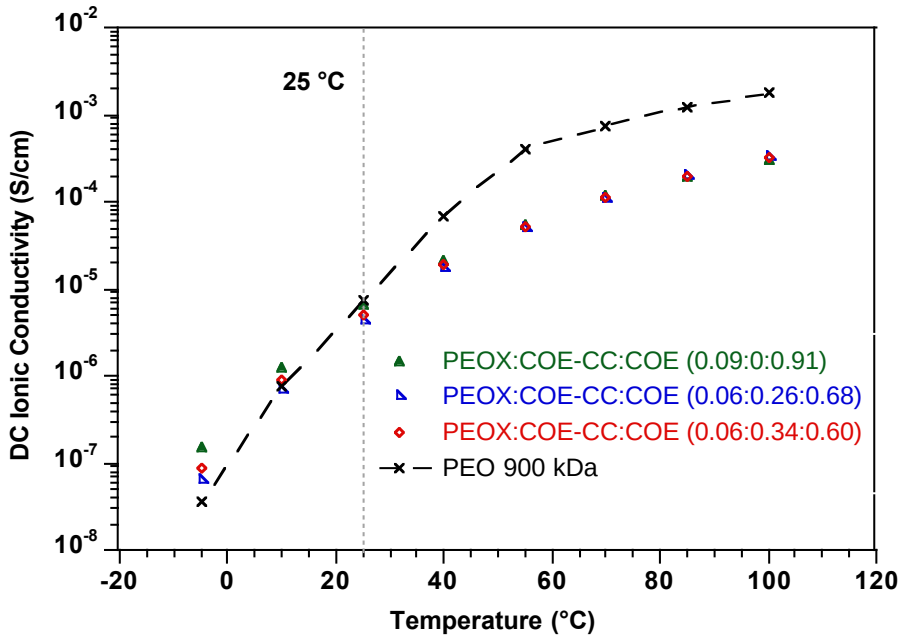

Figure A.4 Variable temperature conductivity of cross-linked polymers with cyclic carbonate side-chains.

A.3 Experimental

A.3.1 General Methods

All reactions and manipulations of air and moisture sensitive compounds were carried out under dry nitrogen using a Braun UniLab drybox or standard Schlenk line techniques unless otherwise specified. ^{1}H NMR spectra were collected in deuterated solvents on a Varian INOVA 400 or Varian INOVA 500 spectrometer and referenced with residual non-deuterated solvent shifts ($CHCl_3$ = 7.24 ppm) and are reported relative to tetramethylsilane (δ = 0 ppm). ^{13}C NMR spectra were recorded on a Varian INOVA (^{13}C, 100 MHz) or Varian INOVA (^{13}C, 125 MHz) spectrometer and referenced to chloroform (δ 77.23 ppm).

Gel permeation chromatography (GPC) analyses were carried out using an

Agilent PL-GPC 50 integrated system, equipped with UV and refractive index detectors, and 2 PL gel Mini-MIX C columns (5 micron, 4.6 mm ID). The GPC columns were eluted with tetrahydrofuran at 30 °C at 0.3 mL/min and were calibrated with monodisperse polystyrene standards. Differential scanning calorimetry (DSC) analyses of polymer samples were performed on either a TA Instruments Q1000 instrument equipped with liquid nitrogen cooling system or a Mettler Polymer DSC instrument equipped with a chiller. Polymer samples on TA Instruments Q1000 instrument were made in aluminum pans and heated under nitrogen from −100 °C to 180 °C at a rate of 10 °C per minute and then cooled to −100 °C at a rate of 10 °C per minute, followed heating to 180 °C at a rate of 10 °C per minute. The glass transition temperature (T_g) and the melting temperature (T_m) were recorded from the second heating run.

The conductivity data of the polymer electrolytes were obtained over a range of frequency (0.1 to 3×10^6 Hz) and temperature (−5 °C to 100 °C) using a Novocontrol Dielectric Broadband Spectrometer fitted with a Quatro temperature control system. Conductivity measurements were performed using blocking/solid polymer electrolyte/blocking cell orientation, using gold plated stainless steel electrodes.

A.3.2 Materials

Sodium hydride (95%), 1,5-cyclooctadiene, *cis*-cyclooctene (95%), *meta*-chloroperoxybenzoic acid (≤77%), epichlorohydrin (99%), Grubbs 2nd Generation catalyst (Cl_2(iMes)(PCy_3)Ru=CHPh), and Crabtree's catalyst [(COD)Ir(py)(PCy_3)]PF_6 were purchased from Sigma-Aldrich and used as received.

Bis(trifluoromethane)sulfonimide lithium salt, LiTFSI (99.95% trace metals basis) was purchased from Sigma-Aldrich and dried *in vacou* at 90 °C for 24 h and transferred directly into the glove box. Ethylene oxide was purchased from Sigma-Aldrich and dried over *n*-BuLi before use. Dibromo-*p*-xylene (97%) was purchased from Alfa Aesar and used as received. Sodium hydroxide and sodium chloride were purchased from Mallinckrodt and used as received. HPLC grade tetrahydrofuran was purchased from Fisher Scientific and dried over an alumina column and degassed by three freeze pump thaw cycles before use. Chloroform was dried over P_2O_5 and distilled prior to use. Hydrogen (99.99%) and CO_2 were purchased from Airgas. $CDCl_3$ was purchased from Cambridge Isotope Laboratories (CIL) and used as received. High-resolution mass spectrometry (HRMS) analyses were performed at the Mass Spectrometry Laboratory at the University of Illinois at Urbana-Champaign.

Following a literature procedure,[7] 5-hydroxy-1-cyclooctene was prepared, dried over activated 3 Å sieves, and degassed by three freeze pump thaw cycles before use. Potassium naphthalenide in THF was prepared from naphthalene and potassium at a concentration of 0.35 M (titrated with a standard benzoic acid solution until a persistent green color was observed as an end-point of the titration) and degassed by three freeze pump thaw cycles before use.

A.3.3 Synthesis

A.3.3.1 Synthesis of the PEO Functionalized Cross-linker (PEOX; 1)

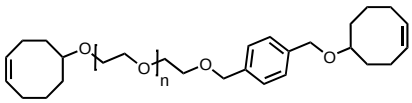

For the synthesis of PEO functionalized cross-linker (**1**), see Section 2.5.3.1

A.3.3.2 Synthesis of poly(ethylene glycol)-*grafted*-cyclooctene (PEG-*g*-COE)

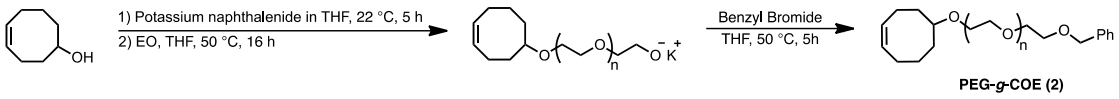

Scheme A.1 Synthesis of PEG-*g*-COE (**2**).

Preparation of PEG-*g*-COE (2): In a N_2 filled glovebox, a Fischer-Porter bottle was charged with 5-hydroxycyclooct-1-ene (2.43 g, 19.3 mmol) solution in THF (2.0 mL). A solution of potassium naphthalenide in THF (32.5 mL of 0.59 M, 19.2 mmol) was added to the alcohol solution dropwise resulting in a dark green solution. The vessel was sealed with the reactor head and the apparatus was removed from the box and stirred at 22 °C for 1 h. The solution was cooled to −78 °C and ethylene oxide (5.46 g, 124 mmol) was then condensed into it. The solution was allowed to warm to room temperature over 16 h. After 16 h, the living alkoxide was capped with benzyl bromide (2.8 mL, 24 mmol), which resulted in immediate precipitation of white KBr salt. The reaction mixture was stirred at 50 °C for 5 h and then allowed to warm to

room temperature. The salts formed were filtered over a Celite plug and the filtrate was partially concentrated on rotary evaporator. PEG-*g*-COE was then washed with hexanes (2 × 200 mL). The resulting viscous oil (7.7 g, 85%) was dried in vacuum at 30 °C for several hours until its mass was constant. ^{1}H NMR (500 MHz, $CDCl_3$) δ 7.26 (m, 4H), 5.77 – 5.48 (m, 2H), 4.55 (s, 2H), 3.83 – 3.44 (m, 24H), 3.40 – 3.29 (m, 1H), 2.45 – 1.28 (m, 10H). ^{13}C NMR (126 MHz, $CDCl_3$) δ 138.34, 130.10, 129.53, 128.41, 127.79, 127.63, 81.01, 73.29, 70.93, 70.61, 69.49, 67.71, 34.21, 33.48, 25.87, 25.71, 22.72. M_n(NMR) = 470 g/mol; M_n(THF GPC) = 390 g/mol, PDI = 1.1.

A.3.3.3 Synthesis of (*Z*)-4-((cyclooct-4-en-1-ylmethoxy)methyl)-1,3-dioxolan-2-one

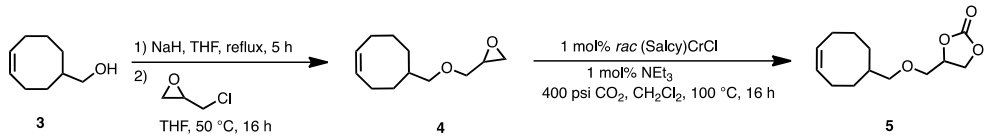

Scheme A.2 Synthesis of (*Z*)-4-((cyclooct-4-en-1-ylmethoxy)methyl)-1,3-dioxolan-2-one (**5**).

Preparation of (*Z*)-cyclooct-4-en-1-ylmethanol (3): For the synthesis of **3**, see section B.2.3.1.

Preparation of (*Z*)-2-((cyclooct-4-en-1-ylmethoxy)methyl)oxirane (4): A suspension of NaH (0.290 g, 11.5 mmol) in anhydrous THF (15 mL) was treated dropwise with 5-methylhydroxycyclooct-1-ene (1.0 g, 7.1 mmol) at room temperature. Upon complete addition of the alcohol, the resulting solution was heated to 70 °C under N_2 for 5 h. Epichlorohydrin (1.2 mL, 15 mmol) was added to this mixture, and the resultant solution was heated at 50 °C for 16 h. The dark brown reaction mixture

was passed through a Celite plug and rinsed with diethyl ether. The product was extracted with diethyl ether (3 x 50 mL), washed with saturated brine, and dried over anhydrous sodium sulfate. After the solvent was removed under reduced pressure, the residue was purified by column chromatography on silica using 1:9 ethyl acetate/hexanes. The desired product was isolated as colorless oil (0.9 g, 64%). ^{1}H NMR (400 MHz, $CDCl_3$) δ 5.84 – 5.52 (m, 2H), 3.68 (ddt, *J* = 11.6, 3.1, 1.5 Hz, 1H), 3.35 (ddd, *J* = 11.6, 5.8, 1.2 Hz, 1H), 3.31 – 3.17 (m, 2H), 3.12 (ddt, *J* = 5.5, 3.9, 2.7 Hz, 1H), 2.78 (td, *J* = 4.7, 4.1, 1.3 Hz, 1H), 2.65 – 2.53 (m, 1H), 2.39 – 1.00 (m, 10H). ^{13}C NMR (126 MHz, $CDCl_3$) δ 130.11, 77.91, 51.03, 44.36, 37.92, 32.18, 29.91, 28.13, 25.97, 24.74.

Preparation of (*Z*)-4-((cyclooct-4-en-1-ylmethoxy)methyl)-1,3-dioxolan-2-one (5): A glass sleeve with a magnetic stir bar was charged with *rac* (salcy)CrCl catalyst (41 mg, 0.065 mmol), compound **4** (1.27 g, 6.47 mmol), triethylamine (10 μL, 0.072 mmol), and dichloromethane (2 mL) and placed in a Parr reactor. It was pressurized to 400 psig with CO_2 and then vented down to 100 psig. This process was repeated twice more to purge the reactor of air, then pressurized to 400 psig and heated to 100 °C. After 16 h, the Parr reactor was cooled to room temperature and vented. The crude reaction mixture was passed through a pad of silica, rinsed with ethyl acetate, and the filtrate was concentrated under reduced pressure to yield the product as a light brown oil (1.3 g, 81%). ^{1}H NMR (300 MHz, Chloroform-*d*) δ 5.72 – 5.55 (m, 2H), 4.79 (ddt, *J* = 7.7, 5.9, 3.8 Hz, 1H), 4.57 – 4.33 (m, 2H), 3.61 (qd, *J* = 11.0, 3.5 Hz, 2H), 3.27 (dd, *J* = 6.8, 1.5 Hz, 2H), 2.41 – 1.03 (m, 10H). ^{13}C NMR (126 MHz, $CDCl_3$) δ

155.10, 130.17, 78.26, 75.23, 69.75, 66.38, 37.73, 31.91, 29.82, 28.01, 25.92, 24.66. HR-MS (ESI) m/z calculated for $C_{13}H_{21}O_4$ ($M + H^+$) 241.1440, found 241.1443.

A.3.3.4 Synthesis of Cross-Linked Comb Polymers

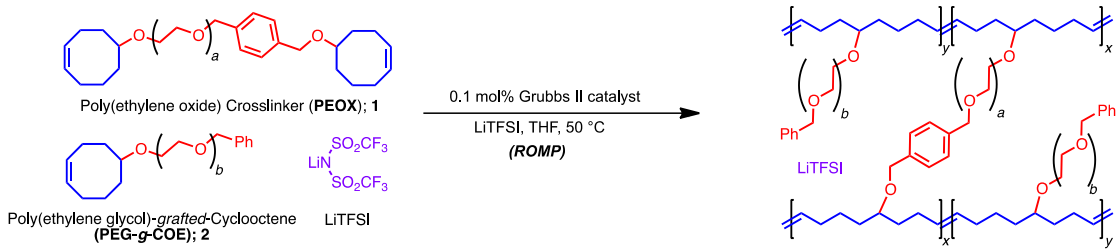

Scheme A.3 Synthesis of cross-linked comb polymer electrolytes.

Nomenclature Cross-Linked Comb SPE

(^{a}PEOX$_l$)(^{b}EOG$_m$)

where **PEOX**: PEO in the cross-linker; **EOG:** Ethylene oxide in the grafts; **a**: average number of ethylene oxide (EO) units in PEOX cross-linker; **b**: average number of EO units in PEG-*g*-COE**; l**: moles of EO units in the PEOX/ total moles of EO units; **m**: moles EO units in the PEG-*g*-COE/ total moles of EO units; **l + m** = 1

Calculations for l and m

l′ = (mmoles of PEOX) × a

m′ = (mmoles of PEG-*g*-COE) × b

$$\mathbf{l} = \frac{\mathbf{l'}}{\mathbf{l'} + \mathbf{m'}}$$

$$\mathbf{m} = \frac{\mathbf{m'}}{\mathbf{l'} + \mathbf{m'}}$$

Representative procedure for the Synthesis of Cross-Linked Comb SPE, (^{36}PEOX$_{0.92}$)(^{6}EOG$_{0.08}$): Cross-linker **1** (270 mg, 0.140 mmol) with 36 EO units in the cross-linker and PEG-*g*-COE (34 mg, 0.072 mmol) with 6 EO units in the graft were combined and dissolved in 1.5 mL of THF. Grubbs' 2nd generation catalyst (0.3 mg, 0.4 μmol) dissolved in 0.5 mL of THF was added to the monomer mixture, followed by the addition of LiTFSI (98 mg, 0.34 mmol) solution in THF (0.5 mL). The reaction mixture was then transferred to a metal dish (fluoropolymer-lined, diameter of 5.25 cm and depth of 3.0 cm) placed in a volume glass chamber bearing two Kontes glass valves on top. The chamber was placed on top of the hot plate equipped with a metal plate to ensure uniform heating and film was casted under N_2 flow at 50 °C for 3 h. After the solvent evaporated off, the Kontes valves were closed and the glass chamber was taken in the glove box. Hexane was added to the metal dish in order to release the film from the dish. The film was dried *in* vacuum at 22 °C for 24 h.

A.3.3.5 Synthesis of Cyclic Carbonate Containing Cross-linked Polymers

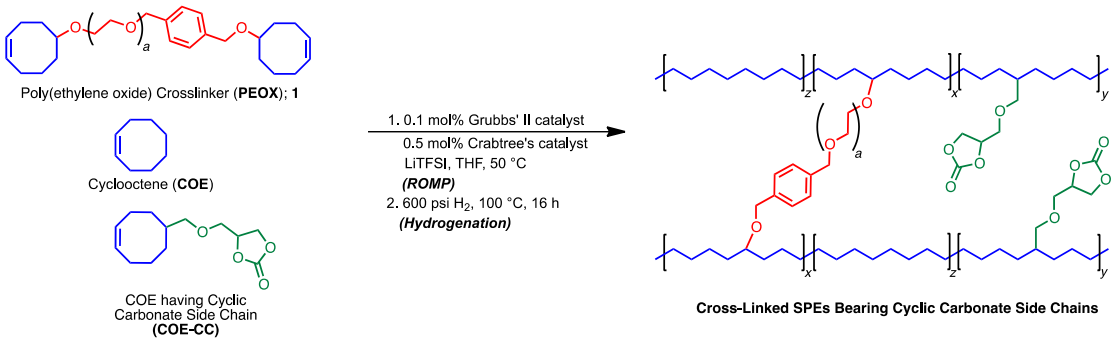

Scheme A.4 Synthesis of cross-linked polymer electrolytes bearing cyclic carbonate side chains.

Nomenclature of Cross-Linked SPE with Cyclic Carbonate Side Chains

PEOX:COE-CC:COE (x:y:z)

where **PEOX**: PEO in the cross-linker; **COE-CC:** Cyclic carbonate functionalized cyclooctene; **COE:** cyclooctene; **x**: moles of PEOX / total moles of PEOX, CC-COE, and COE; **y**: moles of CC-COE / total moles of PEOX, CC-COE, and COE; **z:** moles of CC-COE / total moles of PEOX, CC-COE, and COE.

Representative procedure for the Synthesis of Cross-Linked SPE bearing Cyclic Carbonate Side Chain, PEOX:COE-CC:COE (0.06:0.26:0.68: Cross-linker **1** (137 mg, 0.0785 mmol) with 32 EO units in the cross-linker, comonomer **5** (76 mg, 0.32 mmol) and COE (108 µL, 0.79 mmol) were combined and dissolved in 1.5 mL of THF. Grubbs' 2nd generation catalyst (1.1 mg, 0.0013mmol) dissolved in 0.5 mL of THF was added to the monomer mixture, followed by addition of LiTFSI (49 mg, 0.19 mmol). Crabtree's catalyst (5.1 mg, 0.0063 mmol) dissolved in 0.5 mL $CHCl_3$ was

added to the resultant solution and shaken vigorously for one minute. It was then transferred to a metal dish (fluoropolymer-lined, diameter of 5.25 cm and depth of 3.0 cm) placed in a volume glass chamber bearing two Kontes glass valves on top. The chamber was placed on top of the hot plate equipped with a metal plate to ensure uniform heating and film was casted under N_2 flow at 50 °C for 3 h. After the solvent evaporated off, the Kontes valves were closed and the glass chamber was taken in the glove box. Hexane was added to the metal dish in order to release the film from the dish. The film was dried in vacuum at 22 °C for 24 h and then placed in a Parr reactor equipped with an overhead stirrer and sealed. It was pressurized to 600 psig with hydrogen and then vented down to 50 psig. This process was repeated twice more to purge the reactor of air, then pressurized to 600 psig and heated to 100 °C. After 16 h, Parr reactor was cooled, vented and the plasticized SPE was dried under vacuum at 22 °C for 24 h.

A.3.4 DC Ionic Conductivity

A.3.4.1 DC Ionic Conductivity of PEO Cross-Linked Comb Polymers

Table A.3 DC ionic conductivities of PEO cross-linked comb polymer electrolytes[a]

entry	Sample Name	DC Ionic Conductivity (S/cm)[b]							
		−5 °C	**10 °C**	**25 °C**	**40 °C**	**55 °C**	**70 °C**	**85 °C**	**100 °C**
1	$(^{36}PEOX_{0.92})(^{6}EOG_{0.08})$	8.5×10^{-7}	4.9×10^{-6}	2.1×10^{-5}	6.3×10^{-5}	1.5×10^{-4}	2.9×10^{-4}	4.9×10^{-4}	7.4×10^{-4}
2	$(^{36}PEOX_{0.86})(^{6}EOG_{0.14})$	8.2×10^{-7}	6.3×10^{-6}	2.9×10^{-5}	9.1×10^{-5}	2.2×10^{-4}	4.2×10^{-4}	7.2×10^{-4}	1.1×10^{-3}
3	$(^{36}PEOX_{0.75})(^{6}EOG_{0.25})$	5.8×10^{-7}	4.9×10^{-6}	2.3×10^{-5}	7.3×10^{-5}	1.7×10^{-4}	3.3×10^{-4}	5.7×10^{-4}	8.6×10^{-4}
4	$(^{36}PEOX_{0.67})(^{6}EOG_{0.33})$	3.3×10^{-7}	2.8×10^{-6}	1.3×10^{-5}	4.0×10^{-5}	9.6×10^{-5}	1.9×10^{-4}	3.4×10^{-4}	5.2×10^{-4}
5	$(^{36}PEOX_{0.61})(^{6}EOG_{0.39})$	2.4×10^{-7}	2.0×10^{-6}	9.7×10^{-6}	2.8×10^{-5}	6.3×10^{-5}	1.2×10^{-4}	1.8×10^{-4}	2.8×10^{-4}
6	PEO 900 kDa	3.6×10^{-8}	7.5×10^{-7}	7.2×10^{-6}	6.6×10^{-5}	3.9×10^{-4}	7.6×10^{-4}	1.2×10^{-3}	1.8×10^{-3}

[a]All films had [EO]:[Li] composition of 15:1; where EO means ethylene oxide units contained both in the **PEOX** cross-linker and **PEG-*g*-COE**. [b]Determined by dielectric spectroscopy measurements.

A.3.4.1 DC Ionic Conductivity of PE/PEO Cross-Linked Polymer Electrolytes Bearing Cyclic Carbonate Side Chains

Table A.4 DC ionic conductivities of cross-linked polymer electrolytes bearing cyclic carbonate side chains[a]

entry	x:y:z[b]	DC Ionic Conductivity (S/cm)[c]							
		−5 °C	**10 °C**	**25 °C**	**40 °C**	**55 °C**	**70 °C**	**85 °C**	**100 °C**
1	0.09:0:0.91	1.5×10^{-7}	1.3×10^{-6}	6.5×10^{-6}	2.2×10^{-5}	5.6×10^{-5}	1.2×10^{-4}	2.0×10^{-4}	3.0×10^{-4}
2	0.06:0.26:0.68	6.3×10^{-8}	6.8×10^{-7}	4.2×10^{-6}	1.7×10^{-5}	4.8×10^{-5}	1.1×10^{-4}	2.0×10^{-4}	3.3×10^{-4}
3	0.06:0.34:0.60	8.8×10^{-8}	8.8×10^{-7}	5.0×10^{-6}	1.9×10^{-5}	5.1×10^{-5}	1.1×10^{-4}	2.0×10^{-4}	3.2×10^{-4}
4	PEO 900 kDa	3.6×10^{-8}	7.5×10^{-7}	7.2×10^{-6}	6.6×10^{-5}	3.9×10^{-4}	7.6×10^{-4}	1.2×10^{-3}	1.8×10^{-3}

[a]All films had [EO]:[Li] composition of 15:1; where EO means ethylene oxide units in the **PEOX** cross-linker. [b]x is the mole fraction of [**PEOX**] cross-linker, y is the mole fraction of the **COE-CC**, and z is the mole fraction of **COE** in the cross-linked polymer electrolyte. [c]Determined by dielectric spectroscopy measurements.

A.3.5 NMR Spectra

(*Z*)-2-((cyclooct-4-en-1-ylmethoxy)methyl)oxirane (4)

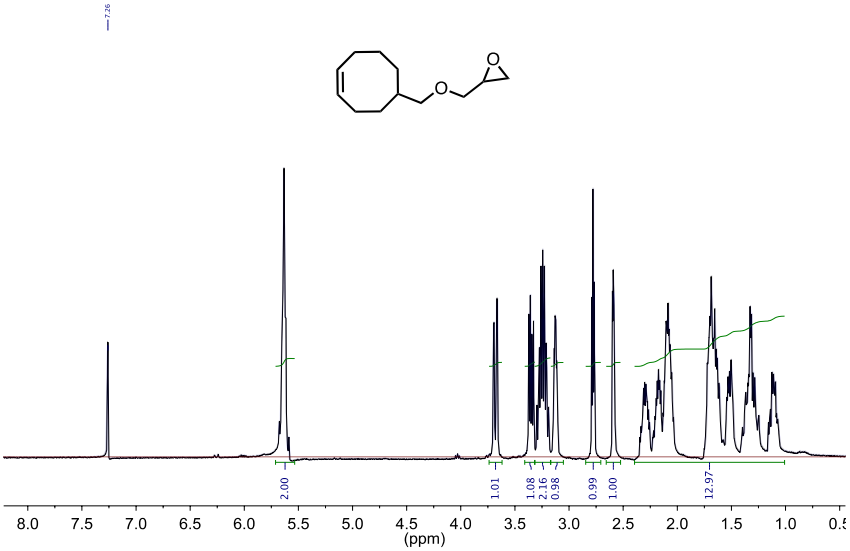

Figure A.5 ^{1}H NMR spectrum of (*Z*)-2-((cyclooct-4-en-1-ylmethoxy)methyl)oxirane (**4**). Signal at 7.26 ppm is residual $CHCl_3$.

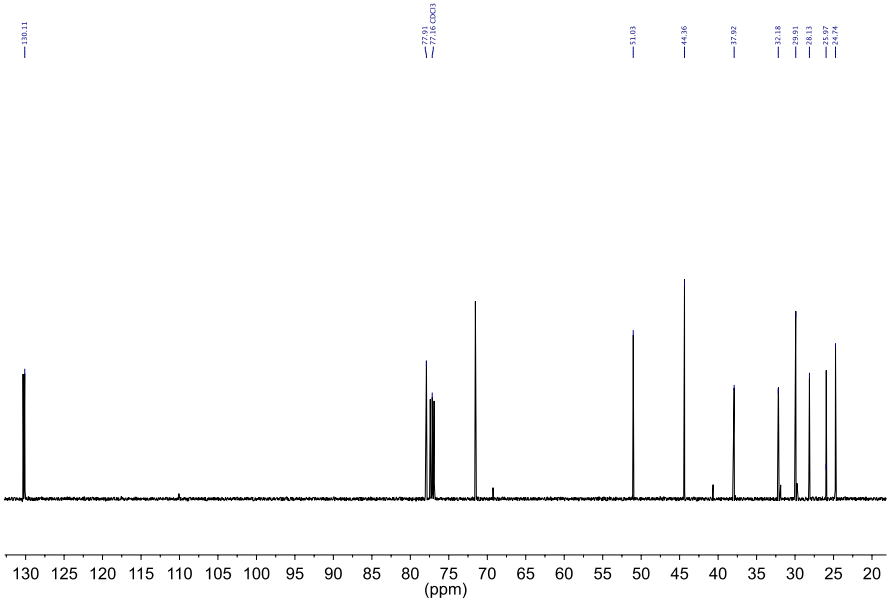

Figure A.6 ^{13}C NMR spectrum of (*Z*)-2-((cyclooct-4-en-1-ylmethoxy)methyl)oxirane (**4**). Signal at 77.16 ppm is residual $CDCl_3$.

(*Z*)-4-((cyclooct-4-en-1-ylmethoxy)methyl)-1,3-dioxolan-2-one (5)

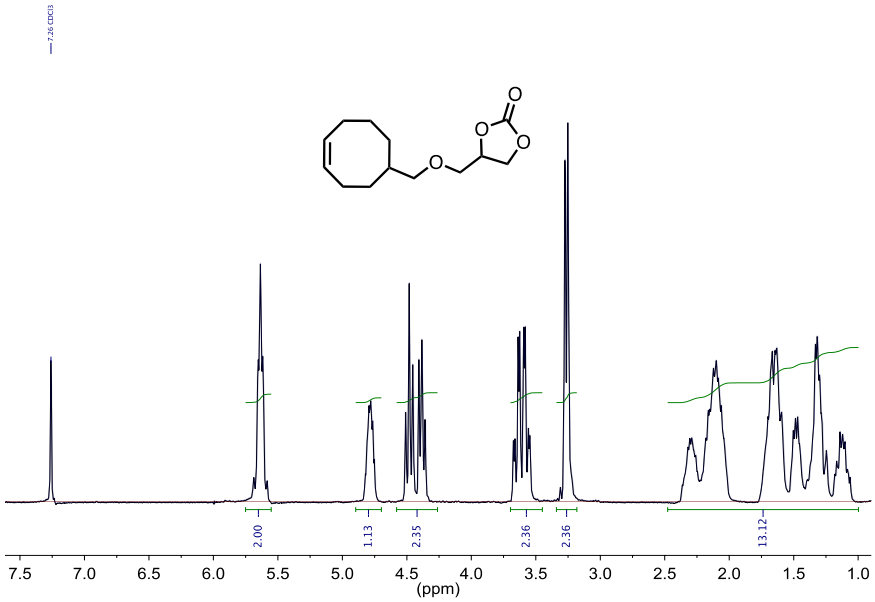

Figure A.7 ^{1}H NMR spectrum of (*Z*)-4-((cyclooct-4-en-1-ylmethoxy)methyl)-1,3-dioxolan-2-one (**5**). Signal at 7.26 ppm is residual $CHCl_3$.

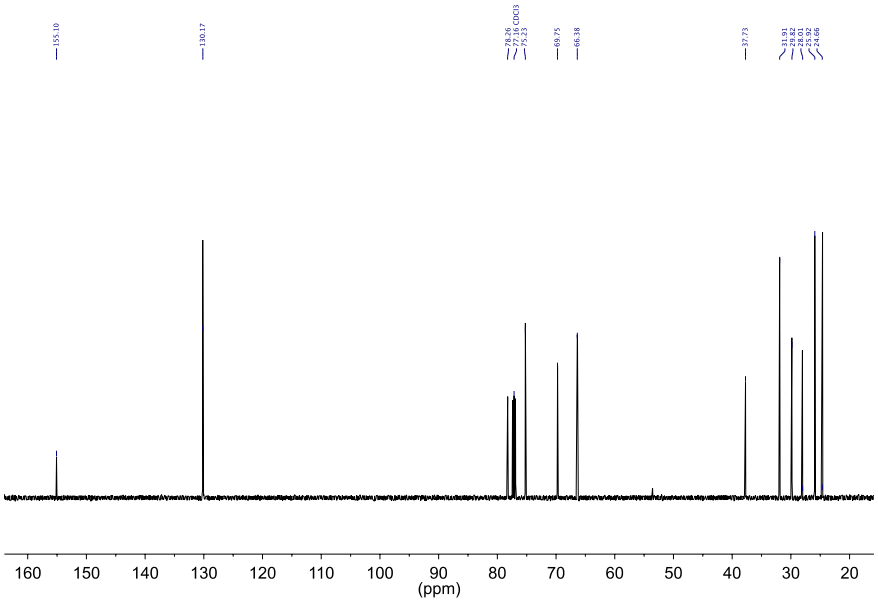

Figure A.8 ^{13}C NMR spectrum of (*Z*)-4-((cyclooct-4-en-1-ylmethoxy)methyl)-1,3-dioxolan-2-one (**5**). Signal at 77.16 ppm is residual $CDCl_3$.

Poly(ethylene glycol)-*grafted*-cyclooctene (PEG-*g*-COE; 2)

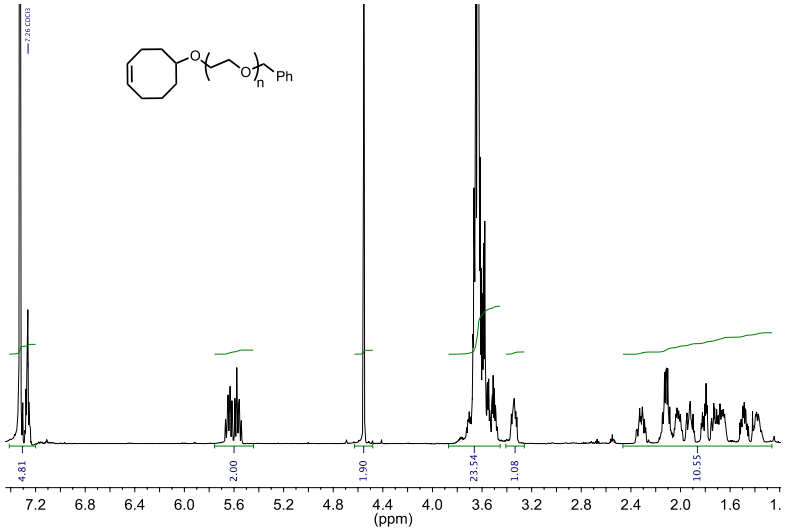

Figure A.9 ^{1}H NMR spectrum of PEG-*g*-COE (**2**) of molecular weight 0.5 kDa. Signal at 7.26 ppm is residual $CHCl_3$.

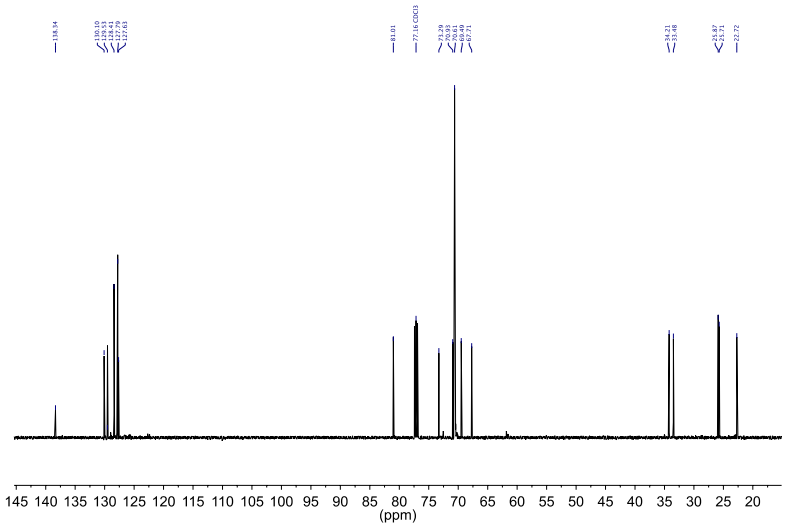

Figure A.10 ^{13}C NMR spectrum of PEG-*g*-COE (**2**) of molecular weight 0.5 kDa. Signal at 77.16 ppm is residual $CDCl_3$.

PEO functionalized cross-linker (1)

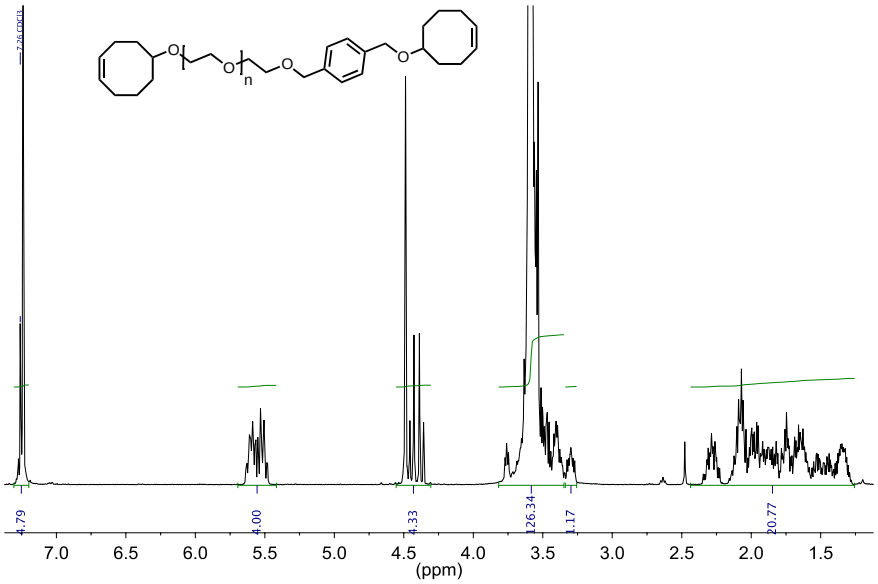

Figure A.11 ^{1}H NMR spectrum of PEO functionalized cross-linker (**1**) of molecular weight 1.8 kg/mol. Signal at 7.26 ppm is residual $CHCl_3$.

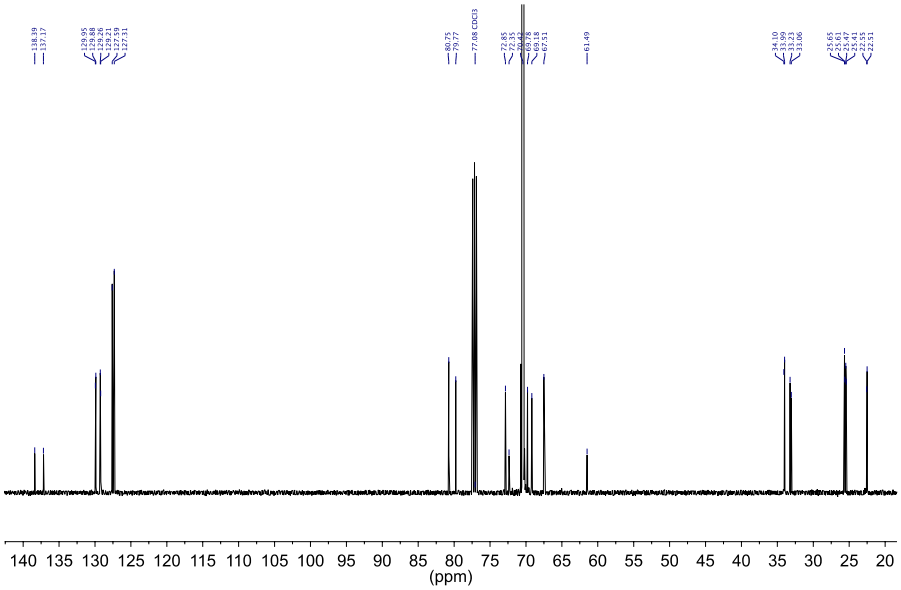

Figure A.12 ^{13}C NMR spectrum of PEO functionalized cross-linker (**1**) of molecular weight 1.8 kg/mol. Signal at 77.16 ppm is residual $CDCl_3$.

REFERENCES

(1) Bielawski, C. W.; Grubbs, R. H. *Prog. Polym. Sci.* **2007**, *32*, 1–29.

(2) Sutthasupa, S.; Shiotsuki, M.; Sanda, F. *Polym. J.* **2010**, *42*, 905–915.

(3) See Experimental Section for details.

(4) Kono, M.; Hayashi, E.; Watanabe, M. *J. Electrochem. Soc.* **1998**, *145*, 1521–1527.

(5) Xu, K. *Chem. Rev.* **2004**, *104*, 4303–4417.

(6) Shindoh, N.; Takemoto, Y.; Takasu, K. *Chem.—Eur. J.* **2009**, *15*, 12168–12179.

(7) Hillmyer, M. A.; Laredo, W. R.; Grubbs, R. H. *Macromolecules* **1995**, *28*, 6311–6316.

APPENDIX B

Synthesis and Characterization of Tetrakis(perfluorophenyl)borate Containing Monomers for Ring Opening Metathesis Polymerization

APPENDIX B

Synthesis and Characterization of Tetrakis(perfluorophenyl)borate Containing Monomers for Ring Opening Metathesis Polymerization

B.1 Introduction

Weakly coordinating organoborate anions are widely used as counterions to stabilize the highly reactive cationic transition metal catalysts in olefin polymerization.[1,2] Other promising areas for the applications of weakly coordinating anions (WCAs) include ionic liquids,[3] Li-ion battery electrolytes,[4] and supporting electrolytes in electrochemistry.[5,6] Few examples of borate containing WCAs that have been extensively used due to their reduced coordinating ability and/or poor lewis basicity include $[BPh_4]^-$, $[B(PhF_5)_4]^-$, and $B[3,5\text{-}(CF_3)_2C_6H_3]_4]^-$. While the efficacy of these WCAs have been corroborated by their wide range of applications,[7] only few reports exist where these non-coordinating anions were immobilized on a polymer backbone.[8,9] Uozumi and co-workers developed polymer supported organoborate for use as cocatalysts in metallocene catalyzed ethylene and propylene polymerization.[8] Jäkle and co-workers reported amphiphilic organoborate polymers, where one of the blocks was functionalized with weakly coordinating borate anions.[9] Recently, these WCAs were also used as building blocks for the synthesis of dendrimers[10] and anionic network polymers.[11,12]

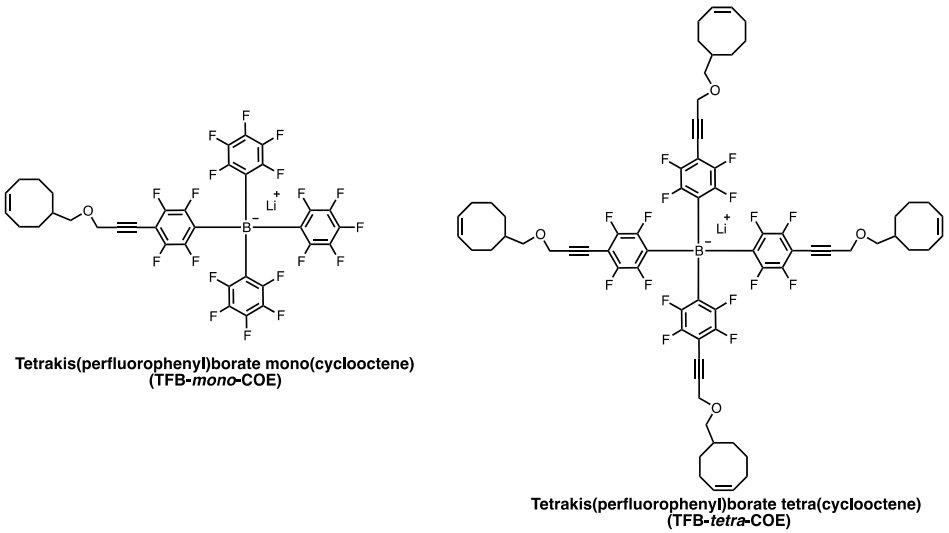

Figure B.1 Monomers containing weakly coordinating anions. Left: tetrakis(perfluorophenyl)borate mono(cyclooctene) (TFB-*mono*-COE) and right: tetrakis(perfluorophenyl)borate tetra(cyclooctene) (TFB-*tetra*-COE).

We were intetested in developing ionomer membranes containing weakly coordinating perfluorinated organoborate anions for Li-ion battery applications. Functionalized cyclooctene monomers (Figure B.1), which could be polymerized using Grubbs' second generation catalyst (G2 catalyst) by ring opening metathesis polymerization (ROMP) were selected. We sought to develop WCA tethered polymers using ROMP due to the functional group tolerance of G2 catalyst. Moreover, this synthetic strategy would allow one to modulate the architecture, ionic content, and molecular weight of the proposed ionomers. While tetrakis(perfluorophenyl)borate mono(cyclooctene) (TFB-*mono*-COE) would provide accessibility to solvent processable ionomers, the tetrakis(perfluorophenyl)borate tetra(cyclooctene) (TFB-*tetra*-COE) monomer would allow the formation of Li-ion conducting network organoborate polymers.

B.2 Experimental

B.2.1 General

All reactions and manipulations of air and moisture sensitive compounds were carried out under dry nitrogen using a Braun UniLab drybox or standard Schlenk line techniques unless otherwise specified. ^{1}H NMR spectra were collected in deuterated solvents on a Varian INOVA 400 or Varian INOVA 500 spectrometer and referenced to residual non-deuterated solvent shifts ($CHCl_3$ = 7.24 ppm) and are reported relative to tetramethylsilane (δ = 0 ppm). ^{13}C NMR spectra were recorded on a Varian INOVA (^{13}C, 100 MHz) or Varian INOVA (^{13}C, 125 MHz) spectrometer and referenced to chloroform (δ 77.23 ppm). ^{19}F NMR were recorded on a Varian INOVA (^{19}F, 376 MHz) and referenced to an external standard (hexafluorobenzene). ^{11}B NMR were recorded on a Varian INOVA (160 MHz) and referenced to an external standard ($BF_3.O(C_2H_5)_2$).

Thermogravimetric analysis (TGA) from 20-1000 °C was carried out on a TA Instruments Q500 Thermogravimetric Analyzer in nitrogen atmosphere using a 10 °C/min ramp without equilibration delay.

High-accuracy mass data was obtained using MALDI, ESI and DART sources. MALDI mass spectra were obtained on a Waters Micro MX MALDI-TOF mass spectrometer using negative ion mode and a reflectron detector. Samples were prepared by depositing the analyte dissolved in a saturated dithranol solution onto a stainless steel sample plate. The plate was dried in air before loading it into the instrument. ESI and DART mass spectra were obtained on a Thermo Scientific Exactive spectrometer in negative ion mode, using a Thermo Scientific heated ESI

source and an IonSense DART-SVP source, respectively. ESI samples were dissolved in acetone and infused directly via a syringe pump. DART samples were analyzed in the solid state using a melting point capillary to position the analytes in the DART gas.

B.2.2 Materials

Sodium hydride (95%), 1,5-cyclooctadiene, propargyl bromide (80 wt.% in toluene), tetrakis(triphenylphosphine)palladium(0) (99%), copper(I) iodide (99.99% trace metals basis), diisopropyl amine (purified by redistillation, 99.95%), 1,4-dibromotetrafluorobenzene (>99%), and boron trichloride solution (1.0 M solution in heptane) were purchased from Sigma-Aldrich and used as received. Lithium aluminum hydride, powder, 97% (Alfa Aesar), tris(pentafluorophenyl)borane, 95% (Strem Chemicals), and *n*-butyllithium solution (1.7 M in hexanes, Acros) were used as received. Sodium hydroxide, anhydrous sodium sulfate, and sodium chloride were purchased from Mallinckrodt and used as received. HPLC grade tetrahydrofuran and diethyl ether were purchased from Fisher Scientific and dried over an alumina column and degassed by three freeze pump thaw cycles before use. NMR solvents ($CDCl_3$ and acetone-d_6) were purchased from Cambridge Isotope Laboratories (CIL) and used as received.

Following a literature procedure,[13] (*Z*)-*tert*-butyl cyclooct-4-enecarboxylate (**A**) was prepared and dried over activated 3 Å sieves before use.

B.2.3 Synthesis

B.2.3.1 Synthesis of tetrakis(perfluorophenyl)borate mono(cyclooctene) monomer

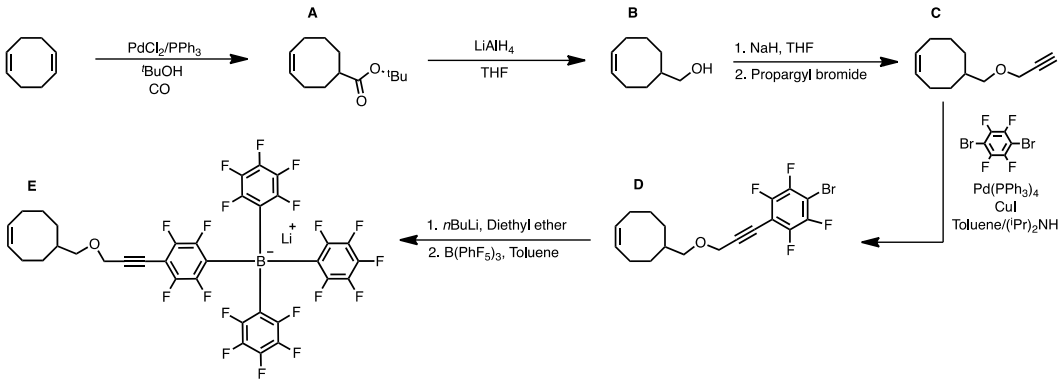

Scheme B.1 Synthesis of tetrakis(perfluorophenyl)borate mono(cyclooctene) monomer (**E**).

Preparation of (*Z*)-cyclooct-4-en-1-ylmethanol (B): Lithium aluminum hydride (4.70 g, 124 mmoles) was added to a 500 mL Schlenk adapted round bottom flask under a flow of nitrogen. Dry THF (~150 mL) was then cannula transferred to the flask under standard Schlenk conditions to obtain a suspension. The resultant suspension was cooled to 0 °C and a solution of compound **A** (15.4 g, 73.2 mmoles) in 100 mL of dry THF was slowly cannula transferred to it. The solution was stirred at 0 °C for 2 hours and was then slowly warmed to room temperature. After stirring for 16 h at room temperature, the solution was cooled back to 0 °C and slowly quenched with 1M HCl. The salts were filtered and washed with diethyl ether. The resultant solution was extracted with diethyl ether (3 × 200 mL). The ether extracts were combined, washed with saturated brine (200 mL), dried over anhydrous sodium sulfate, and

concentrated under reduced pressure to yield a colorless oil (10 g, 97%). ^{1}H NMR (500 MHz, $CDCl_3$) δ 5.77 – 5.57 (m, 2H), 3.52 – 3.26 (m, 2H), 2.45 – 1.02 (m, 11H). ^{13}C NMR (126 MHz, $CDCl_3$) δ 130.28, 130.12, 69.08, 40.54, 31.85, 29.69, 28.07, 25.94, 24.70. HRMS (DART) *m/z* calculated for ($M + H^+$) 141.1279, found 141.1270.

Preparation of (*Z*)-5-((prop-2-yn-1-yloxy)methyl)cyclooct-1-ene (C): A suspension of NaH (1.27 g, 50.3 mmol) in anhydrous THF (100 mL) was made in a three-neck Schlenk adapted round bottom flask equipped with a reflux condenser. This suspension was treated dropwise with a solution of **B** (4.72 g, 33.7 mmol) in 30 mL dry THF and heated to 70 °C under N_2 for 16 h. After cooling to room temperature, a solution of propargyl bromide (8.8 mL, 59.2 mmol) was *slowly* added to the alkoxide solution under standard Schlenk conditions at 22 °C (exotherm was observed during the addition). The resulting mixture was refluxed for 2 h, which yielded a brown solution. The reaction mixture was cooled to room temperature and filtered through a pad of celite. The filtrate was concentrated on a rotary evaporator to yield a red-brown oil, which was further purified by column chromatography on silica using 1:9 ethyl acetate/hexanes. The desired product was isolated as a mixture of C and C′ (5.4 g, 91%). The R_f of the compounds C and C′ (Figure B.2) were very similar and could not be purified on the silica column chromatography, and therefore the mixture was used without further purification for the next step (i.e. for the synthesis of Compound D). ^{1}H NMR (500 MHz, $CDCl_3$) δ 5.79 – 5.54 (m, 2H), 4.24 – 4.05 (m, 2H), 3.42 – 3.16 (m, 2H), 2.40 (m, 1H), 2.36 – 1.06 (m, 11H). ^{13}C NMR (126 MHz, $CDCl_3$) δ 131.22, 130.33, 130.19, 128.34, 80.25, 77.16, 76.67, 76.60, 74.59, 74.15, 74.13, 58.76, 58.28,

58.20, 39.95, 37.80, 32.23, 30.05, 29.46, 28.74, 28.16, 27.81, 26.01, 25.93, 24.75, 24.26. HR-MS (DART) *m/z* calculated for ($M + H^+$) 178.1352, found 179.1422.

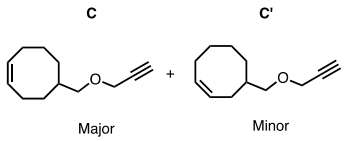

Figure B.2 Chemical structures of compounds C and C′.

For the HSQC and HMBC analysis of the mixture of compounds C and C′, see Section B.2.6.

Preparation of (*Z*)-5-(((3-(4-bromo-2,3,5,6-tetrafluorophenyl)prop-2-yn-1-yl)oxy) methyl)cyclooct-1-ene (D): A 250 mL round bottom Schlenk flask was charged with 1,4-dibromotetrafluorobenzene (6.58 g, 21.4 mmol), $Pd(PPh_3)_4$ (0.518 mg, 0.450 mmol), CuI (0.174 g, 0.910 mmol) and anhydrous toluene (120 mL) under nitrogen. The resultant solution was subjected to three freeze-pump-thaw cycles, and backfilled with nitrogen. A mixture of compounds C and C′ (2.73 g, 15.3 mmol) was dissolved in degassed diisopropylamine (35 mL) under standard Schlenk conditions and was <u>*slowly*</u> cannula transferred to the solution of 1,4-dibromotetrafluorobenzene under standard Schlenk conditions. The resultant solution was stirred 2 h at 70 °C, cooled to room temperature, filtered through celite, and washed with CH_2Cl_2 (150 mL). The solvent was evaporated and the crude product was purified by column chromatography on silica using 1:3 CH_2Cl_2/hexanes to yield a mixture of D and D′ (Figure B.3) as a pale yellow oil (1.98 g, 32%). ^{1}H NMR (500 MHz, $CDCl_3$) δ 5.80 – 5.55 (m, 2H), 4.41 (d, *J* = 8.1 Hz, 2H), 3.46 – 3.29 (m, 2H), 2.47 – 1.09 (m, 11H). ^{19}F NMR (376 MHz,

$CDCl_3$) δ −131.57 (m, 2 F), −133.69 (m, 2F). $^{13}C\{^1H\}$ NMR (126 MHz, $CDCl_3$) δ 147.26 (ddt, *J* = 255, 15, 4 Hz), 144.93 (dddd, *J* = 248, 15, 5, 3 Hz), 131.35, 130.30, 130.24, 128.23, 103.76 (tm, *J* = 18 Hz), 100.98 (tm, *J* = 23 Hz), 99.65 (t, *J* = 4.0 Hz), 74.96 , 71.01 (t, *J* = 4 Hz), 58.93 , 58.86 , 39.99 , 37.87 , 32.21 , 30.08 , 29.48 , 28.75 , 28.17 , 27.80 , 26.03 , 25.97 , 24.75 , 24.26 . $^{13}C\{^{19}F\}$ NMR (126 MHz, $CDCl_3$) δ 147.26, 144.93, 103.75, 100.99, 99.64 (t, *J* = 7 Hz), 71.00 (t, *J* = 5 Hz). HR-MS (DART) *m/z* calculated for ($M + H^+$) 405.047165, found 405.04656.

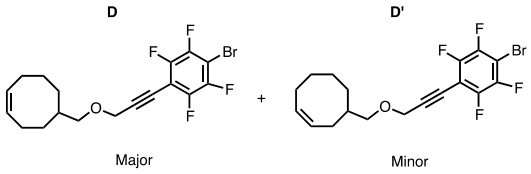

Figure B.3 Chemical structures of compounds D and D′.

Preparation of Lithium (*Z*)-(4-(3-(cyclooct-4-en-1-ylmethoxy)prop-1-yn-1-yl)-2,3,5,6-tetrafluorophenyl)tris(perfluorophenyl)borate (E): A solution of mixture of compounds **D and D′** (0.40 g, 0.99 mmol) in 5 mL anhydrous diethyl ether was cooled to −78 °C under nitrogen. Butyllithium (0.69 mL, 1.6 M solution in hexanes, 1.10 mmol) was slowly added to the reaction mixture and it was stirred for 4 h at −78 °C. A solution of tris(pentafluorophenylborane) (0.48 g, 0.94 mmol) in toluene (4 mL) was then added to the lithiated compound *via* a gas tight syringe under standard Schlenk conditions at −78 °C and the reaction mixture was slowly warmed to room temperature. The resulting solution was refluxed for 2 h, cooled to room temperature, and concentrated under reduced pressure to yield a white crystalline powder (0.78 g, 98%). The final product was a mixture of two regioisomers E and E′ (Figure B.4) ^1H

NMR (500 MHz, Acetone-d_6) δ 5.69 – 5.58 (m, 2H), 4.40 (s, 2H), 3.54 (s, 2H), 3.37 – 3.28 (m, 2H), 2.41 – 1.12 (m, 11H). $^{13}C\{^{1}H\}$ NMR (126 MHz, Acetone-d_6) δ 149.05 (dm, J = 240 Hz), 146.64 (dd, J = 249, 24 Hz), 139.07 (dt, J = 240, 13 Hz), 137.07 (ddd, J = 250, 19, 13 Hz), 131.55, 130.99, 130.67, 129.17, 99.85 (t, J = 18 Hz), 97.51, 76.94, 74.94, 72.61, 66.11, 59.09, 59.01, 40.73, 38.62, 32.79, 30.65, 29.32, 28.76, 28.32, 26.45, 26.34, 25.24, 24.78, 15.60. $^{13}C\{^{19}F\}$ NMR (126 MHz, Acetone-*d*6) δ 149.05, 148.96, 146.66, 139.06, 137.07, 124.98 (q, $J_{C,11B}$ = 51 Hz), 124.77 (q, $J_{C,11B}$ = 52 Hz), 99.86, 97.49 (t, J = 8 Hz), 72.59, 59.02.^{19}F NMR (376 MHz, Acetone-d_6) δ –130.51 (m, 9F), –140.45 (m, 2F), –161.75 (t, J = 20 Hz, 1F), –161.90 (t, J = 20 Hz, 2F), –165.80 (m, 6F). ^{11}B NMR (160 MHz, Acetone-d_6) δ −15.07. HR-MS (ESI) *m/z* calculated for (M^-) 837.1063, found 837.1065.

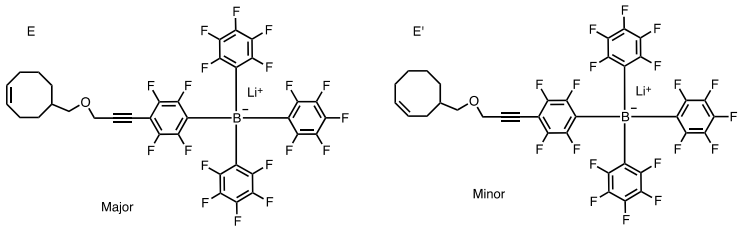

Figure B.4 Chemical structures of compounds E and E′.

B.2.3.2 Synthesis of tetrakis(perfluorophenyl)borate tetracyclooctene monomer

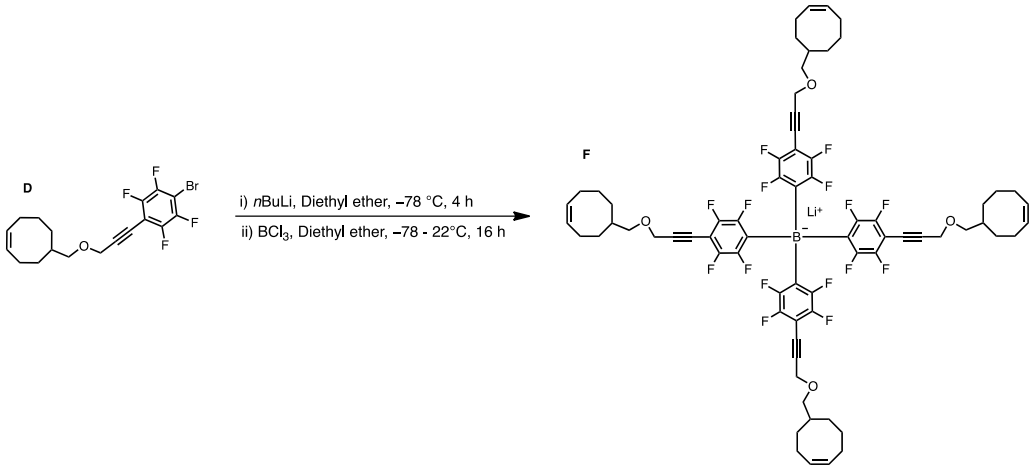

Scheme B.2 Synthesis of tetrakis(perfluorophenyl)borate tetracyclooctene monomer (**F**).

Preparation of (*Z*)-5-(((3-(4-bromo-2,3,5,6-tetrafluorophenyl)prop-2-yn-1-yl)oxy) methyl)cyclooct-1-ene (D): See Section B.2.3.1 for the synthesis details.

Preparation of lithium tetrakis(4-(3-((*Z*)-cyclooct-4-en-1-ylmethoxy)prop-1-yn-1-yl)-2,3,5,6-tetrafluorophenyl)borate (F): A solution of mixture of compounds D and D′ (1.0 g, 2.5 mmol) in 12 mL anhydrous diethyl ether was cooled to −78 °C under nitrogen. Butyllithium (1.7 mL, 1.6 M solution in hexanes, 2.7 mmol) was slowly added to the reaction mixture and it was stirred for 4 h at −78 °C. A solution of boron trichloride (0.61 mL, 1.0 M in heptane, 0.61 mmol) was then added to the lithiated compound *via* a gas-tight syringe under standard Schlenk conditions at −78 °C. The cooling bath was removed and the mixture was stirred at room temperature for 16 h. Distilled water (20 ml) was added and the mixture was stirred for 1 h. The aqueous

phase was separated from the organic phase and was extracted two times with diethyl ether (3×25 mL). The organic layers were combined, dried with 3Å molecular sieves, and concentrated under reduced pressure to yield a pale yellow powder. The powder obtained was thoroughly washed with hexanes and dried under high vacuum at 22 °C until constant weight (0.36 g, 44%). The final product was a mixture of regioisomers of F and F′. ^{1}H NMR (400 MHz, Acetone-d_6) δ 5.77 – 5.52 (m, 8H), 4.41 (s, J = 6.8 Hz, 8H), 3.56 – 3.17 (m, 8H), 2.40 – 1.03 (m, 44H). ^{13}C{^{1}H} NMR (126 MHz, Acetone-d_6) δ 131.15, 130.81, 77.06, 59.16, 38.77, 32.95, 30.79, 28.89, 26.61, 25.40. ^{13}C{^{19}F} NMR (126 MHz, Acetone-d_6) δ 149.00, 146.65, 99.92, 97.52 (t, J = 7.4 Hz), 72.66 (t, J = 4.4 Hz), 60.18, 59.01. ^{19}F NMR (376 MHz, Acetone-d6) δ −130.2 (s, 8F), −140.5 (s, 8F). ^{11}B NMR (160 MHz, Acetone-d_6) δ −14.56. HR-MS (ESI) *m/z* calculated for (M^-) 1311.4950, found 1311.4944.

B.2.4 Thermal Gravimetric Analysis (TGA)

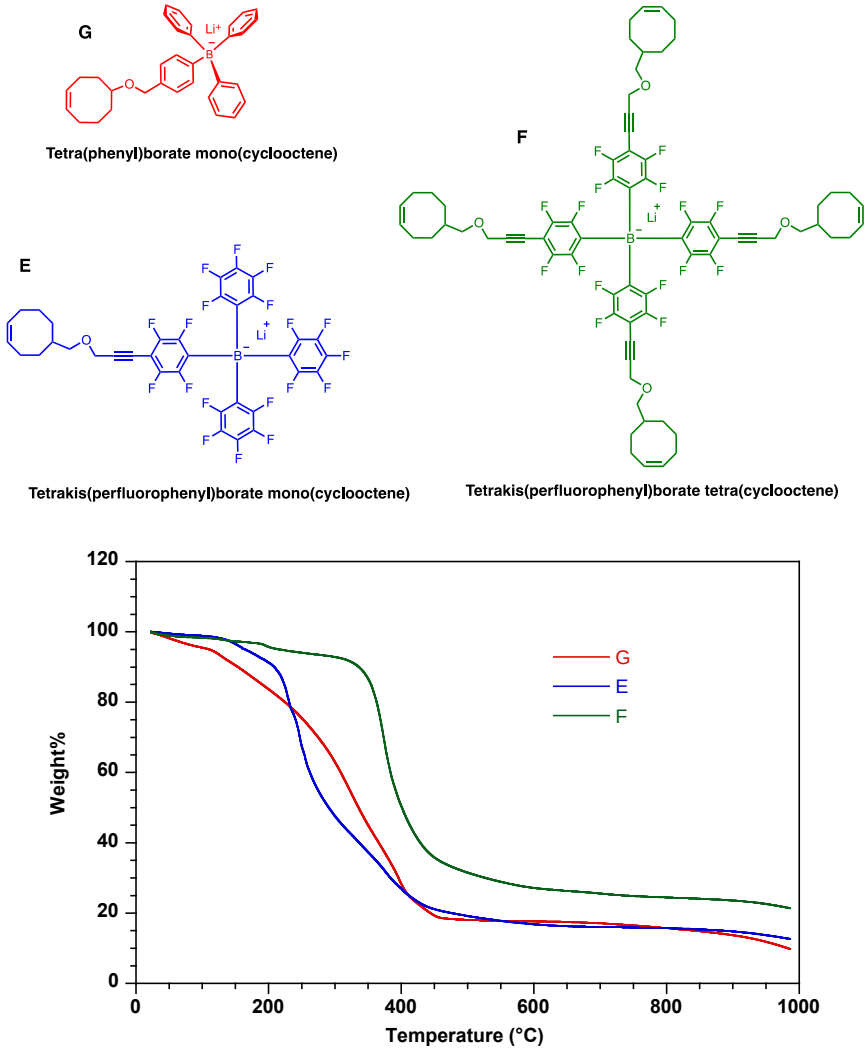

Figure B.5 TGA traces of **G** (red), **E** (blue), and **F** (green).

To determine the thermal stability of the borate monomers, TGA analysis was done. The onset decomposition tempertaures for the organoborate monomers are shown in Figure B.5. Among the non-coordinating borate monomers, the bulky perfluorinated monomer with four cycloctenes (**F**) showed the highest decomposition temperature of 355 °C, which is approximately 100 °C higher than **G** and **E** organoborate monomers.

B.2.5 MALDI-TOF Data

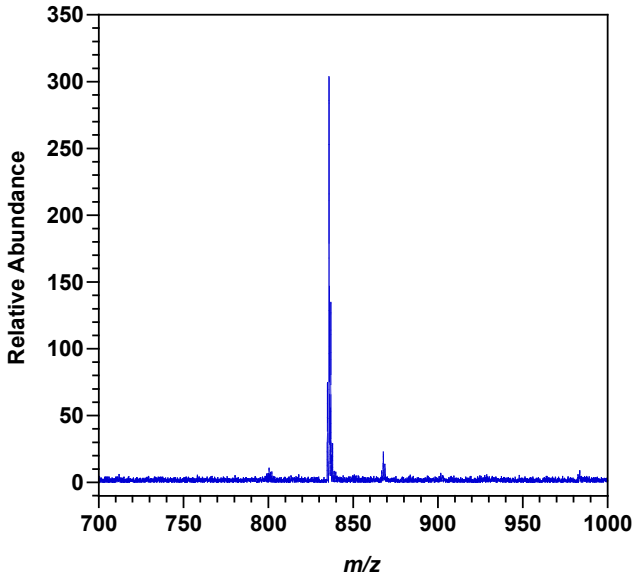

Figure B.6 MALDI-TOF spectrum of lithium (*Z*)-(4-(3-(cyclooct-4-en-1-ylmethoxy)prop-1-yn-1-yl)-2,3,5,6-tetrafluorophenyl)tris(perfluorophenyl)borate (**E**) (F). *m/z* calculated for (M^-) 837.11, found 837.87.

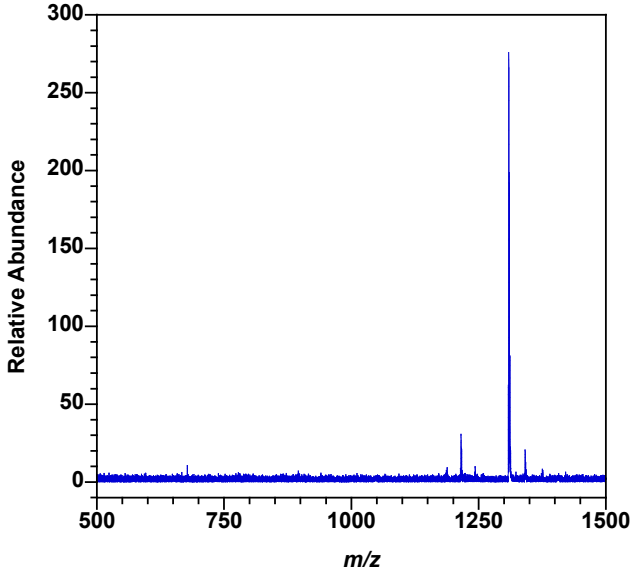

Figure B.7 MALDI-TOF spectrum of lithium tetrakis(4-(3-((*Z*)-cyclooct-4-en-1-ylmethoxy)prop-1-yn-1-yl)-2,3,5,6-tetrafluorophenyl)borate (**F**). *m/z* calculated for (M^-) 1311.50, found 1311.54.

B.2.6 NMR Spectra

Compound B

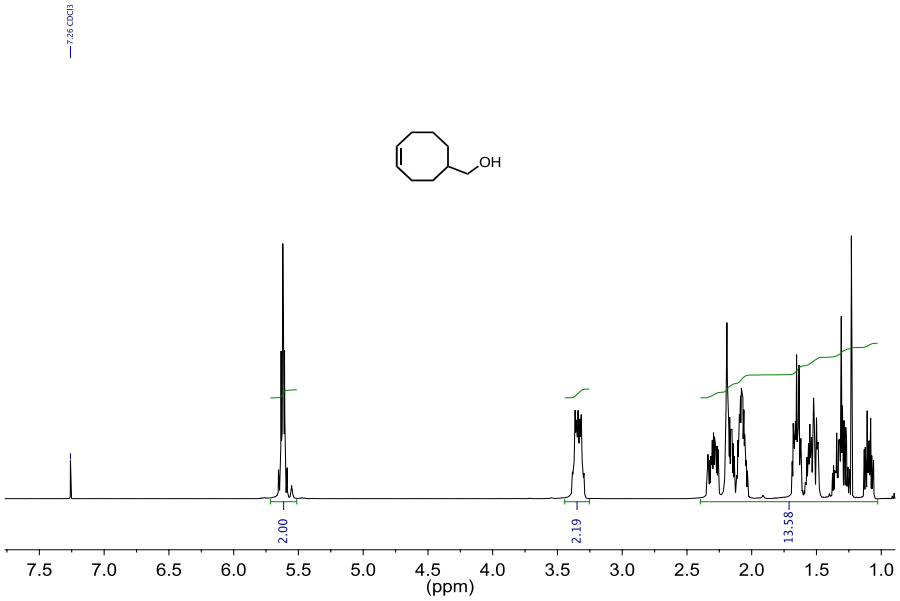

Figure B.8 ^{1}H NMR spectrum of compound **B**. Signal at 7.24 ppm is residual $CHCl_3$.

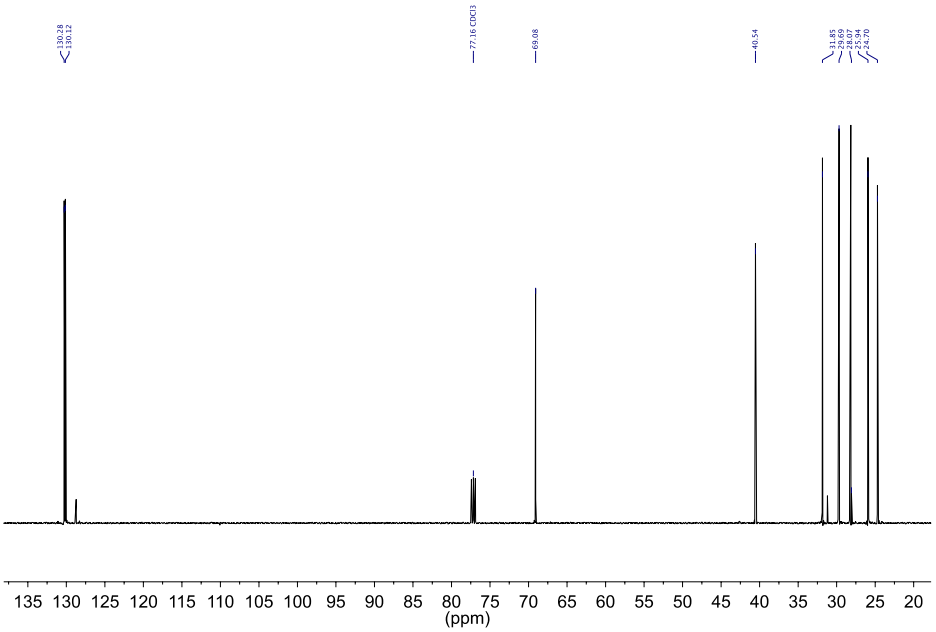

Figure B.9 ^{13}C NMR spectrum of compound **B**. Signal at 77.16 ppm is residual $CDCl_3$.

Compound C and C′

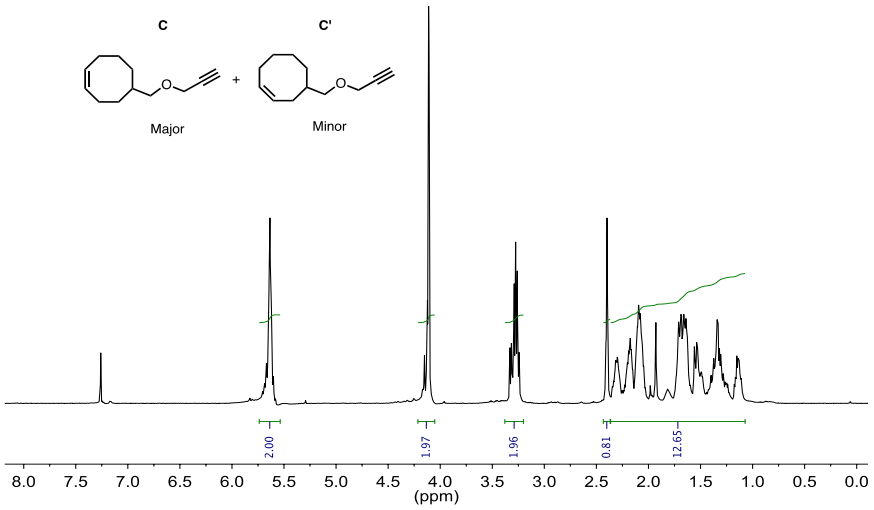

Figure B.10 ^{1}H NMR spectrum of mixture of compounds **C** and **C′**. Signal at 7.24 ppm is residual $CHCl_3$.

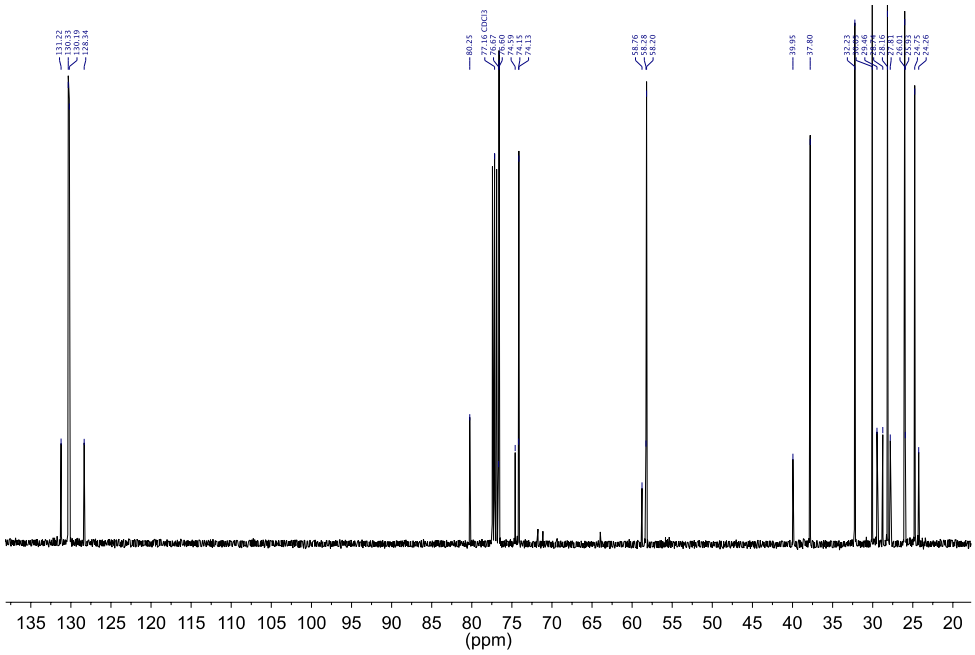

Figure B.11 ^{13}C NMR spectrum of mixture of compounds **C** and **C′**. Signal at 77.16 ppm is residual $CDCl_3$.

Table B.1 ^{1}H and ^{13}C NMR assignments for mixture of compounds **C** and **C′** based on HMBC and HSQC analysis.

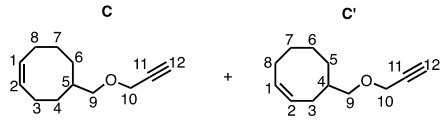

Assignments for Compound C

Atom	^{13}C shift (ppm)	^{1}H shift (ppm)
1	130.06	5.68
2	130.18	5.65
3	24.61	2.09, 2.32
4	32.11	1.16. 1.70
5	37.67	1.72
6	29.92	1.56, 1.32
7	28.04	1.36, 1.66
8	25.90	2.12, 2.19
9	76.46	3.29
10	58.07	4.13
11	80.13	n.a.[a]
12	73.99	2.42

Assignments for Compound C′

Atom	^{13}C shift (ppm)	^{1}H shift (ppm)
1	128.21	5.62
2	131.08	5.69
3	27.67	2.09, 2.24
4	39.82	1.83
5	28.61	1.26, 1.66
6	24.14	1.43, 1.66
7	29.32	1.50, n.d.[b]
8	25.80	2.06, 2.20
9	74.46	3.34
10	58.15	4.14
11	80.10	n.a.[a]
12	74.02	2.43

[a]n.a. not applicable
[b]n.d. not determined

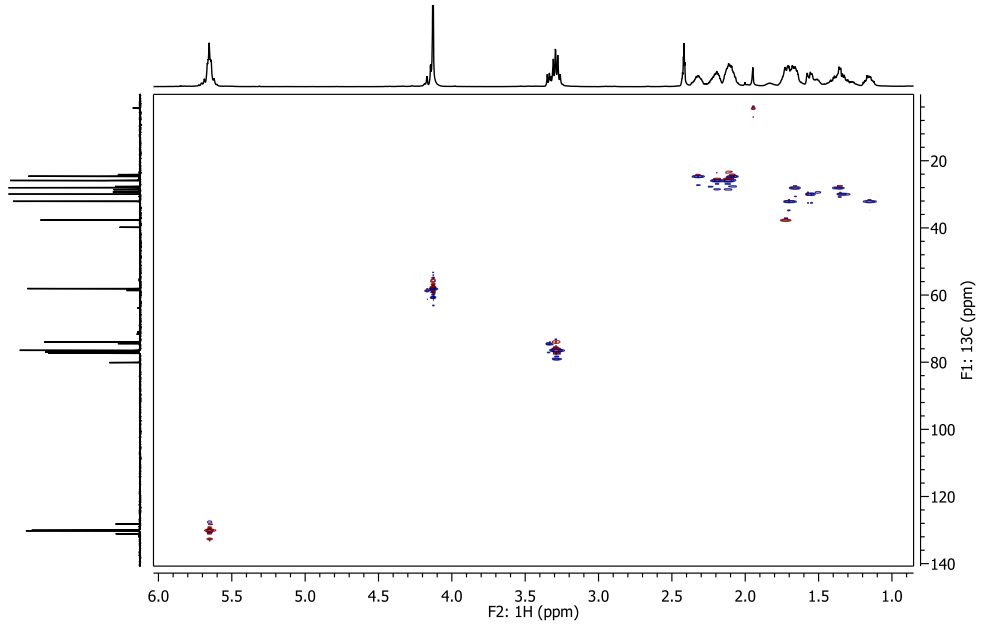

Figure B.12 $^{1}H/^{13}C$ multiplicity-edited HSQCAD NMR spectrum of mixture of compounds **C** and **C′**. Positive (red) contours correspond to CH and CH_3, negative contours (blue) correspond to CH_2.

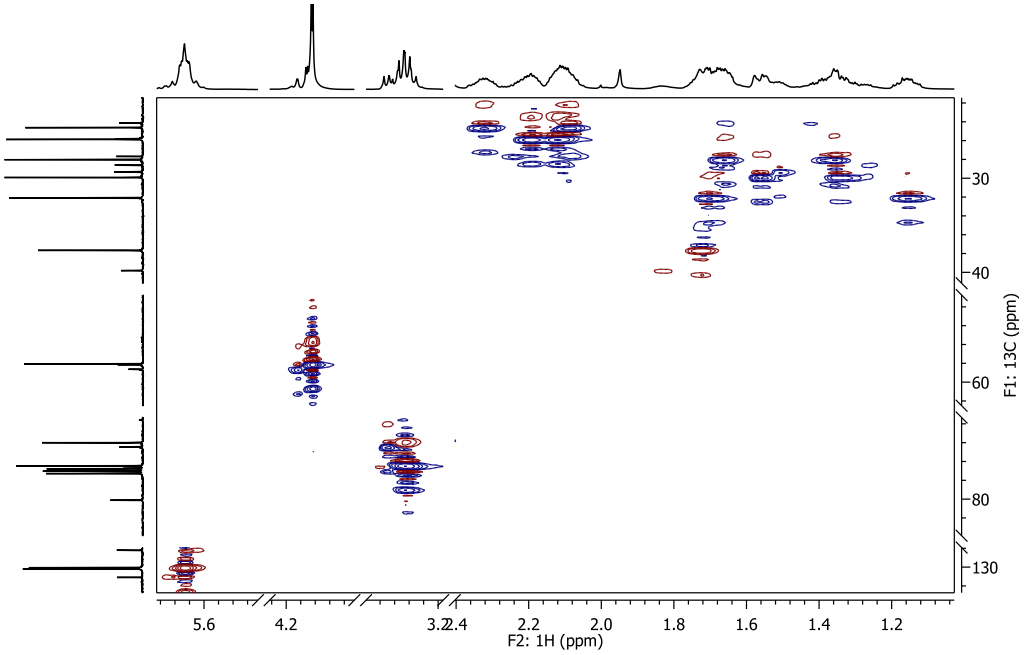

Figure B.13 $^{1}H/^{13}C$ multiplicity-edited HSQCAD NMR spectrum of mixture of compounds **C** and **C′**. Positive (red) contours correspond to CH and CH_3, negative contours (blue) correspond to CH_2. Displaying only regions of interest.

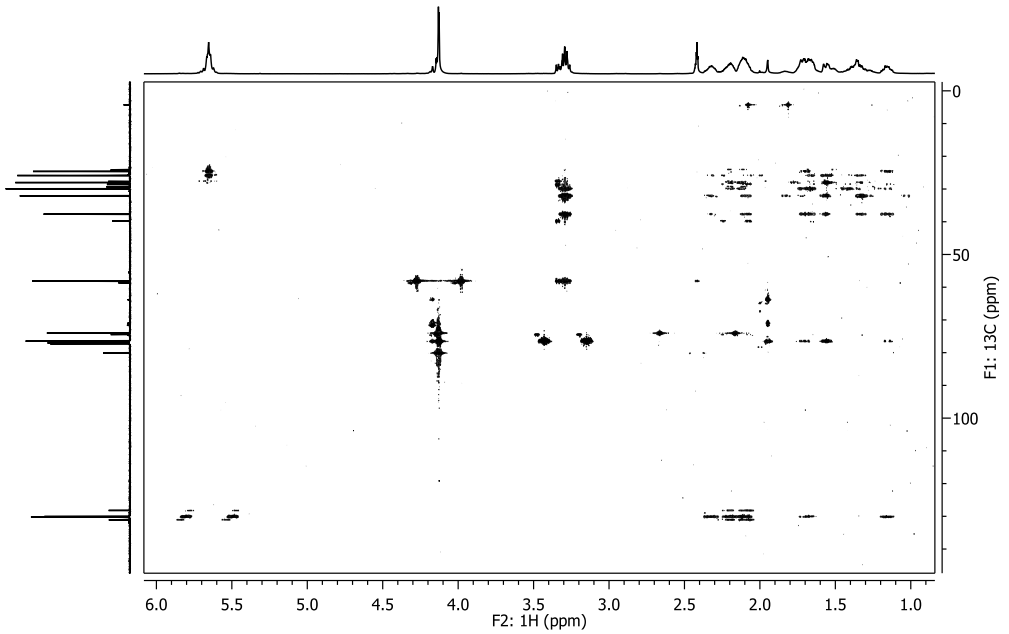

Figure B.14 $^{1}H/^{13}C$ HMBCAD NMR spectrum of mixture of compounds **C** and **C′**.

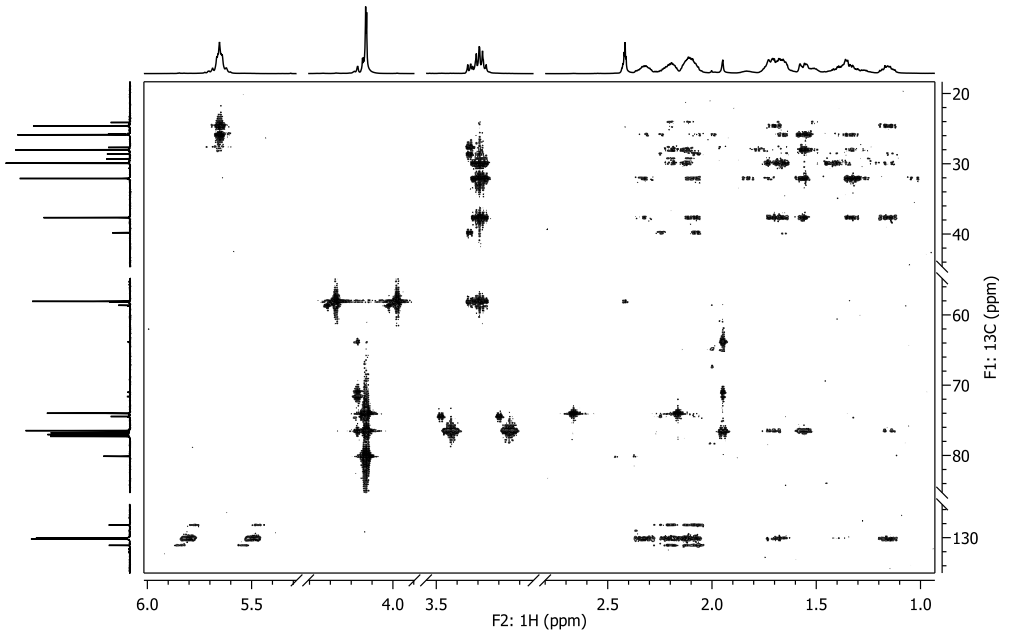

Figure B.15 $^{1}H/^{13}C$ HMBCAD NMR spectrum of mixture of compounds **C** and **C′**. Expanded display showing only regions of interest.

Compounds D and D′

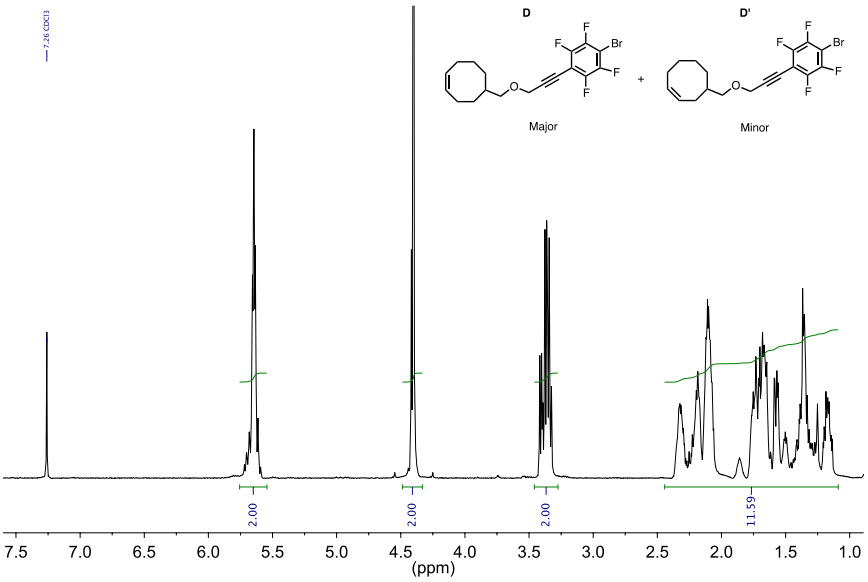

Figure B.16 ^{1}H NMR spectrum of mixture of compounds **D** and **D′**. Signal at 7.24 ppm is residual $CHCl_3$.

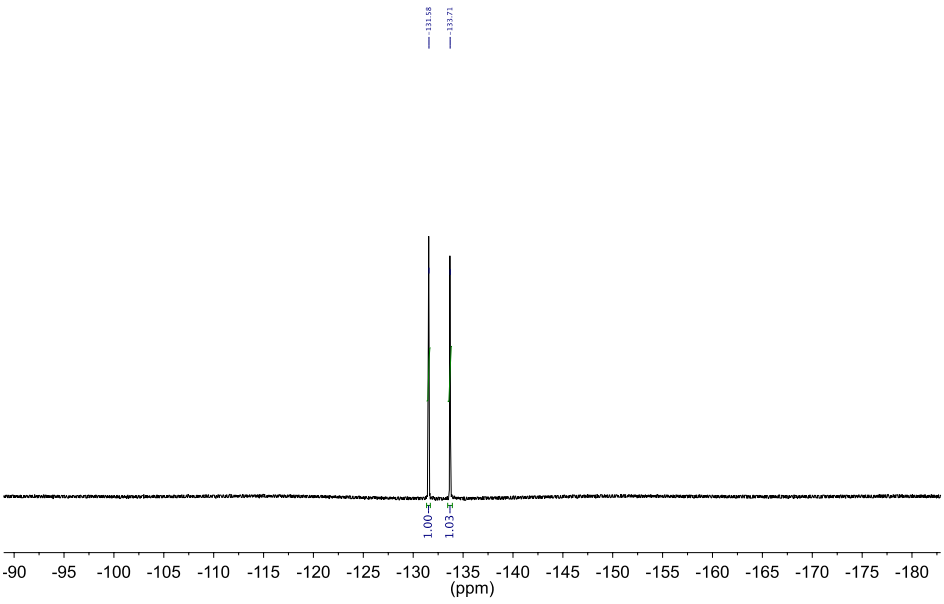

Figure B.17 ^{19}F NMR spectrum of mixture of compounds **D** and **D′**. Spectrum was referenced externally to C_6F_6 ($\delta = -165$ ppm).

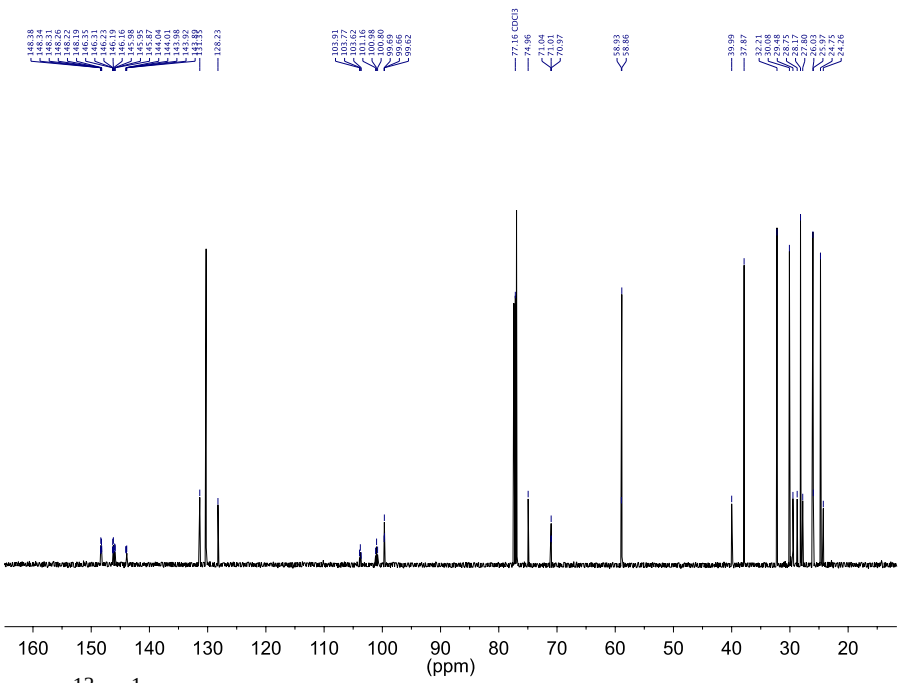

Figure B.18 $^{13}C\{^{1}H\}$ NMR spectrum of mixture of compounds **D** and **D′**. Signal at 77.16 ppm is residual $CDCl_3$.

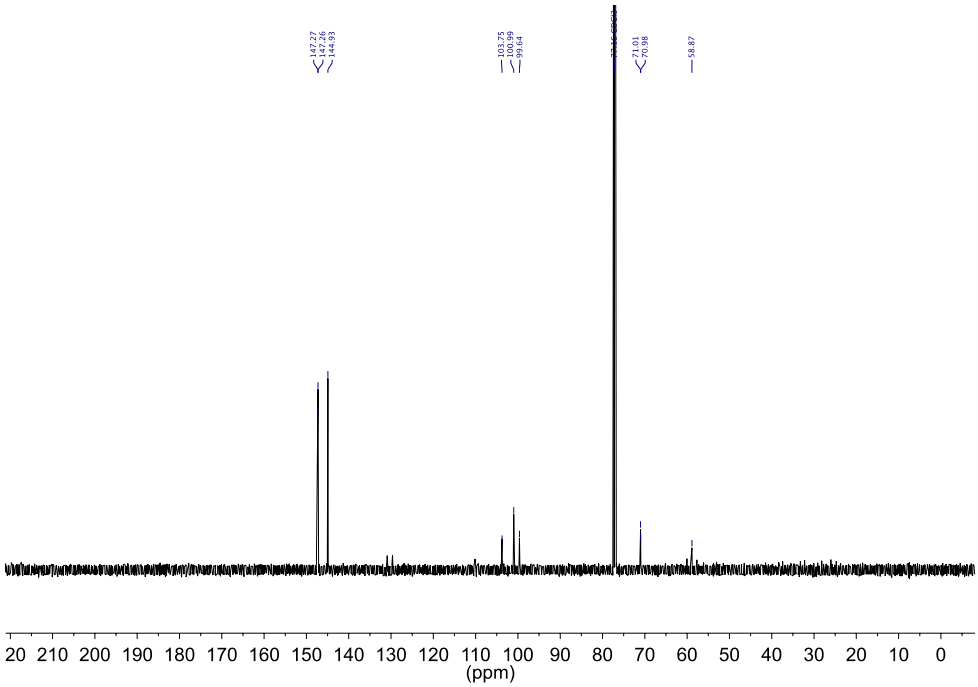

Figure B.19 $^{13}C\{^{19}F\}$ NMR spectrum of mixture of compounds **D** and **D′**. Signal at 77.16 ppm is residual $CDCl_3$.

Lithium (*Z*)-(4-(3-(cyclooct-4-en-1-ylmethoxy)prop-1-yn-1-yl)-2,3,5,6-tetrafluoro phenyl) tris(perfluorophenyl)borate (E)

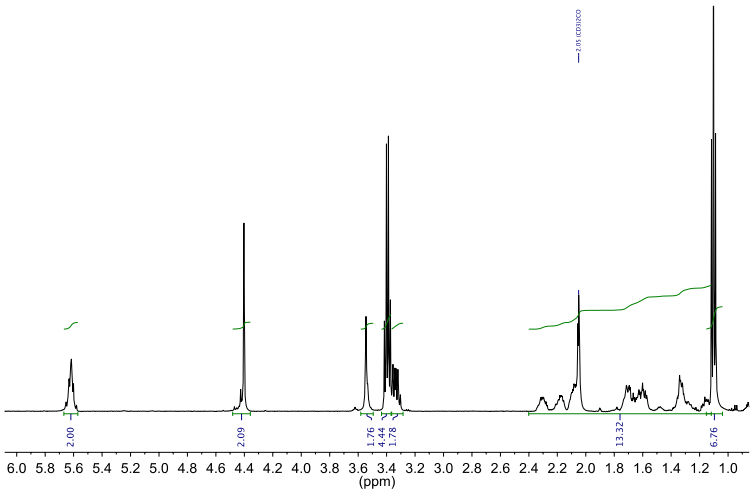

Figure B.20 ^{1}H NMR spectrum of lithium (*Z*)-(4-(3-(cyclooct-4-en-1-ylmethoxy)prop-1-yn-1-yl)-2,3,5,6-tetrafluorophenyl)tris(perfluorophenyl)borate (**E**). The compound has one molecule of diethyl ether bound to it (signals at 1.10 and 3.40 pm). Signal at 2.06 ppm is residual acetone.

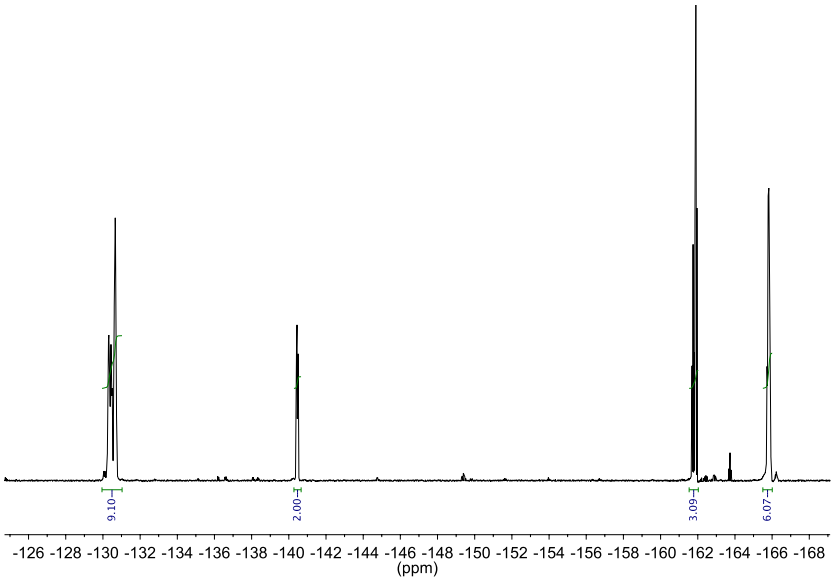

Figure B.21 ^{19}F NMR spectrum of lithium (*Z*)-(4-(3-(cyclooct-4-en-1-ylmethoxy)prop-1-yn-1-yl)-2,3,5,6-tetrafluorophenyl)tris(perfluorophenyl)borate (**E**). Spectrum was referenced externally to C_6F_6 ($\delta = -165$ ppm).

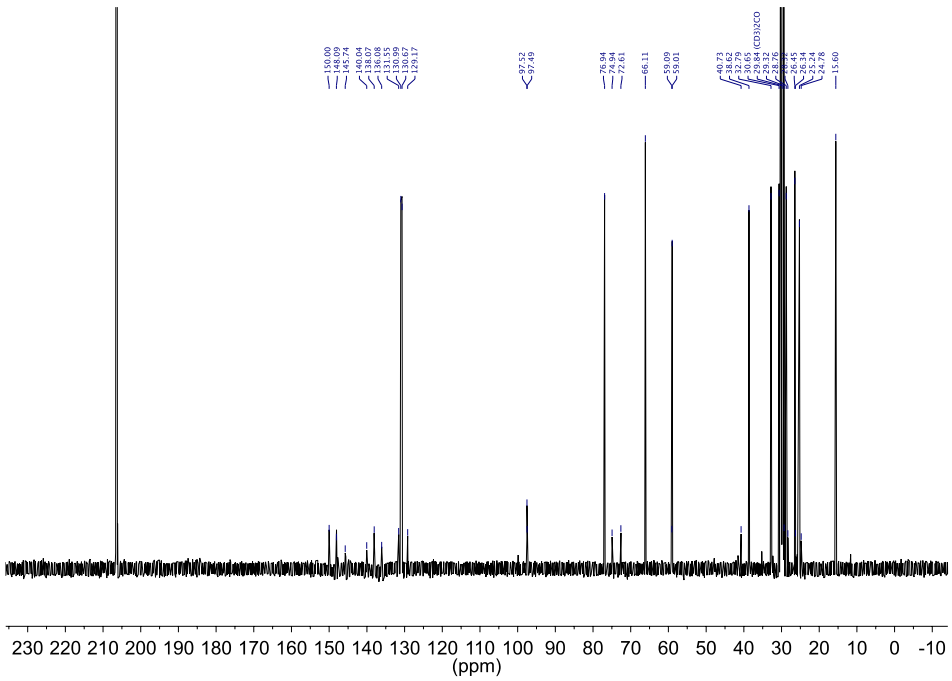

Figure B.22 $^{13}C\{^{1}H\}$ NMR spectrum of lithium (*Z*)-(4-(3-(cyclooct-4-en-1-ylmethoxy)prop-1-yn-1-yl)-2,3,5,6-tetrafluorophenyl)tris(perfluorophenyl)borate (**E**).

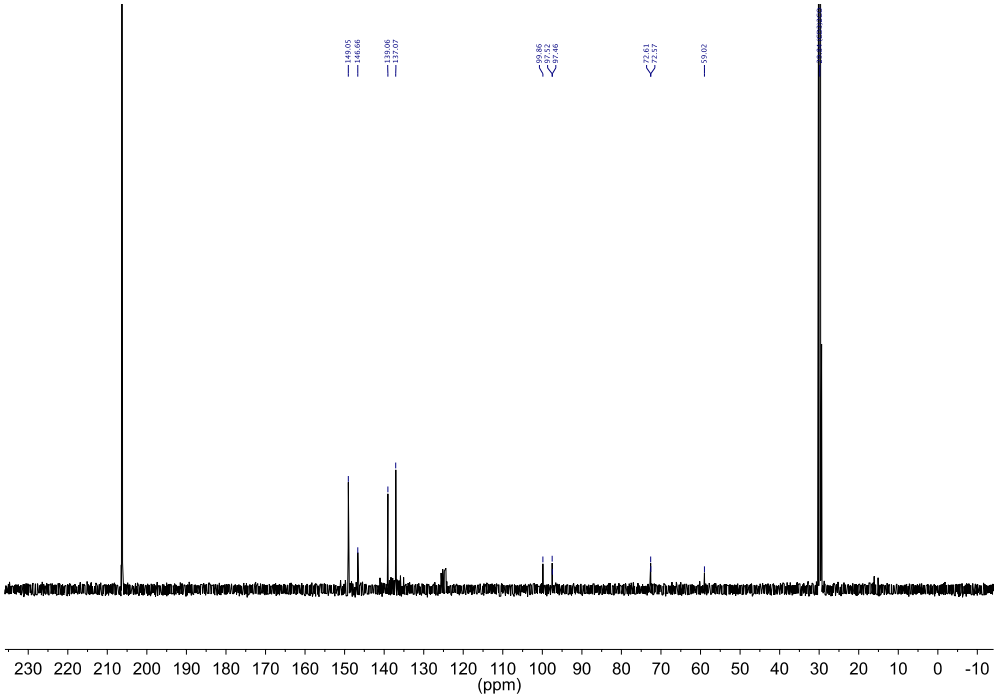

Figure B.23 $^{13}C\{^{19}F\}$ NMR spectrum of lithium (*Z*)-(4-(3-(cyclooct-4-en-1-ylmethoxy)prop-1-yn-1-yl)-2,3,5,6-tetrafluorophenyl)tris(perfluorophenyl)borate (**E**).

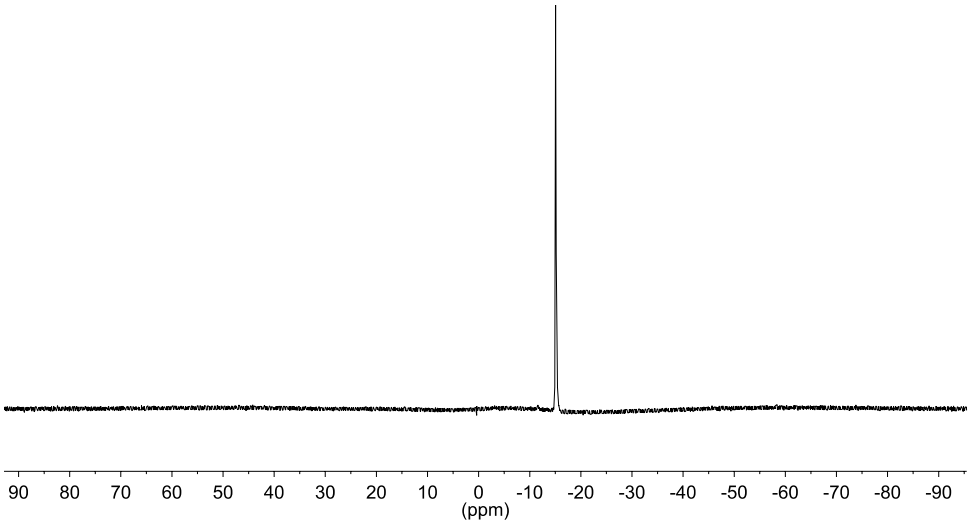

Figure B.24 ^{11}B NMR spectrum of lithium (*Z*)-(4-(3-(cyclooct-4-en-1-ylmethoxy)prop-1-yn-1-yl)-2,3,5,6-tetrafluorophenyl)tris(perfluorophenyl)borate (**E**). Spectrum was referenced externally to $BF_3.Et_2O$ ($\delta = 0$ ppm).

Lithium tetrakis(4-(3-((*Z*)-cyclooct-4-en-1-ylmethoxy)prop-1-yn-1-yl)-2,3,5,6-tetrafluorophenyl)borate (F)

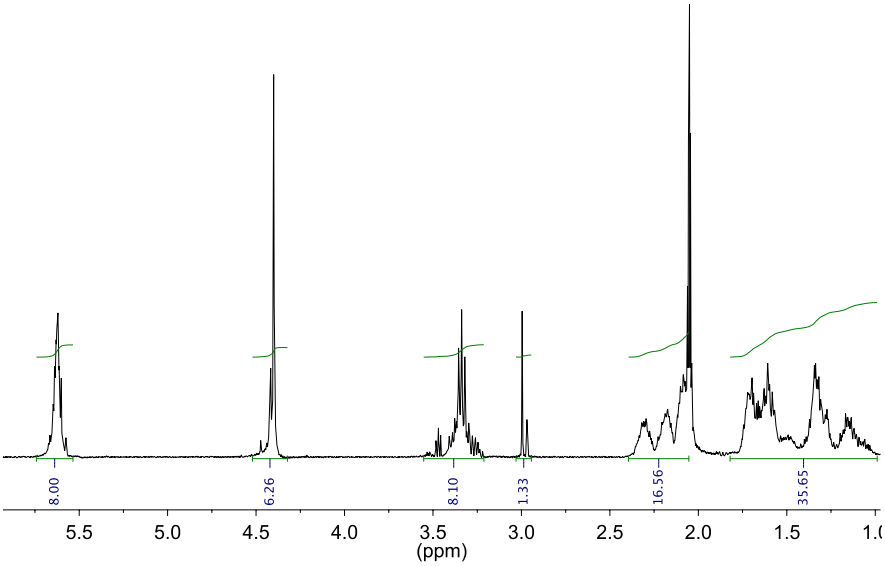

Figure B.25 ^{1}H NMR spectrum of lithium tetrakis(4-(3-((*Z*)-cyclooct-4-en-1-ylmethoxy)prop-1-yn-1-yl)-2,3,5,6-tetrafluorophenyl)borate (**F**).

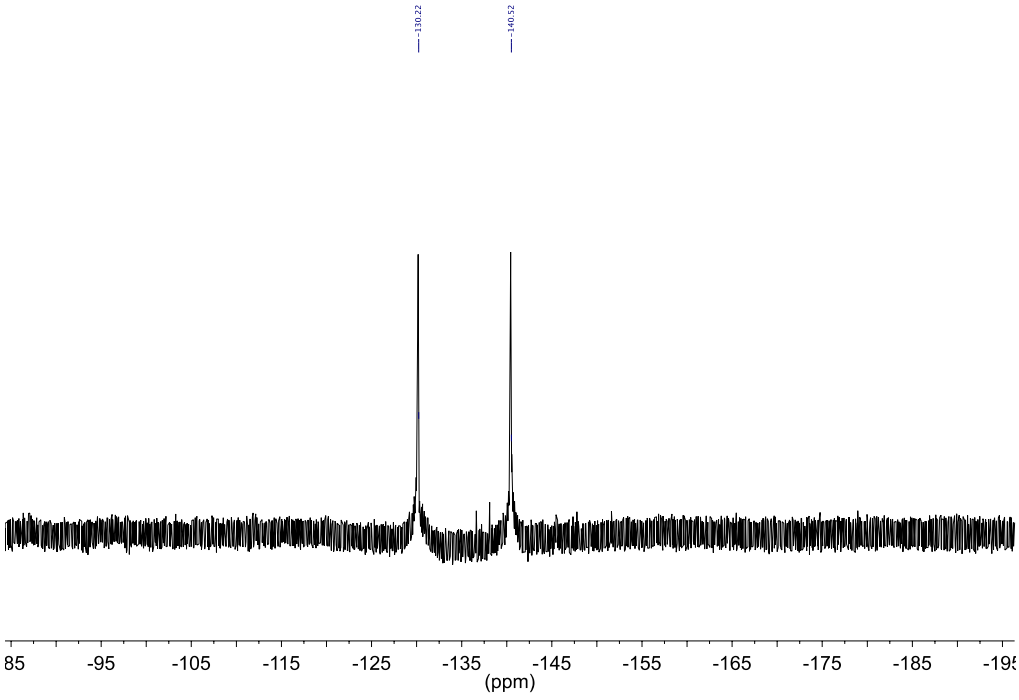

Figure B.26 ^{19}F NMR spectrum of lithium tetrakis(4-(3-((*Z*)-cyclooct-4-en-1-ylmethoxy)prop-1-yn-1-yl)-2,3,5,6-tetrafluorophenyl)borate (**F**). Spectrum was referenced externally to C_6F_6 ($\delta = -165$ ppm).

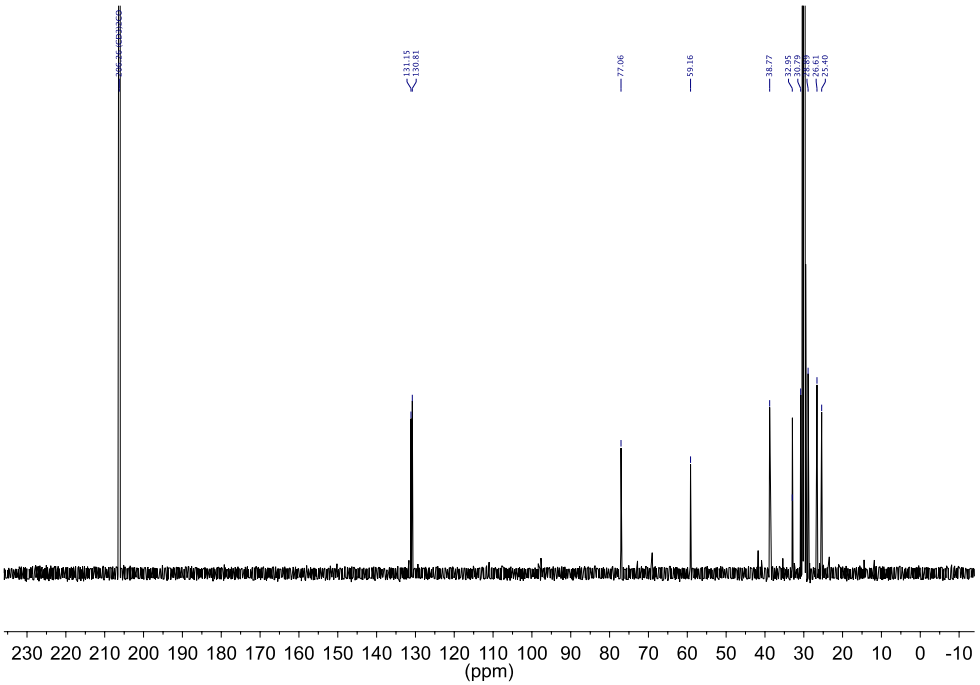

Figure B.27 $^{13}C\{^{1}H\}$ NMR Spectrum of compound **F**. Signals at 29.84 and 206.12 ppm are from the residual acetone.

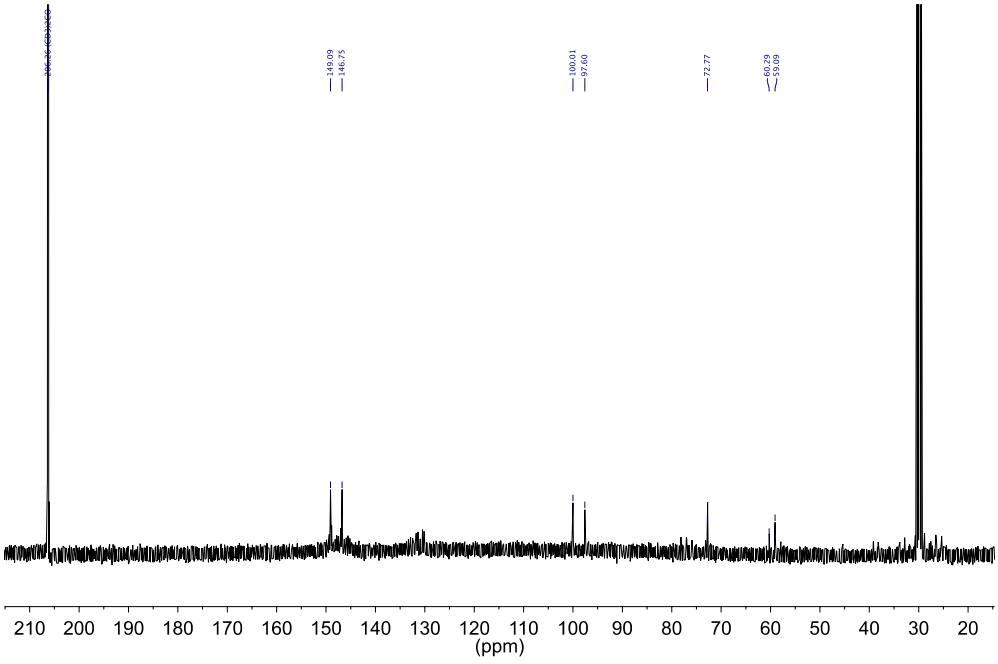

Figure B.28 $^{13}C\{^{19}F\}$ NMR spectrum of compound **F**. Signals at 29.84 and 206.12 ppm are from the residual acetone.

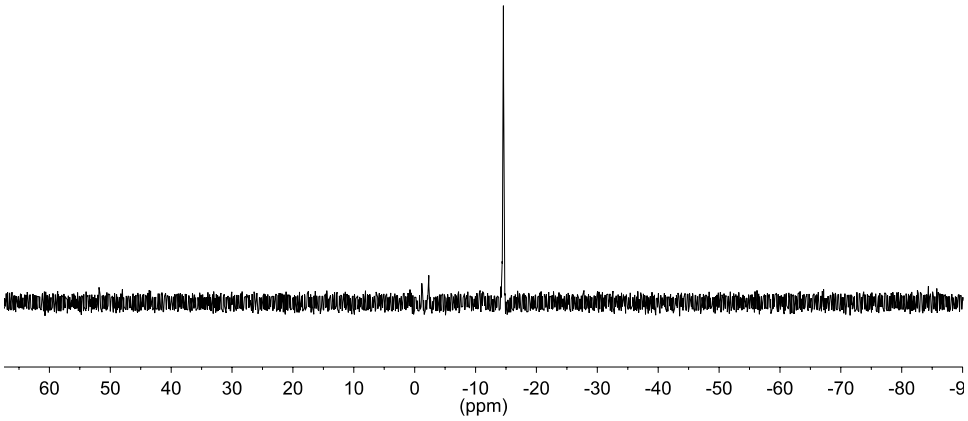

Figure B.29 ^{11}B NMR spectrum of lithium tetrakis(4-(3-((*Z*)-cyclooct-4-en-1-ylmethoxy)prop-1-yn-1-yl)-2,3,5,6-tetrafluorophenyl)borate (**F**). Spectrum was referenced externally to $BF_3.Et_2O$ ($\delta = 0$ ppm).

REFERENCES

(1) Strauss, S. H. *Chem. Rev.* **1993**, *93*, 927–942.

(2) Chen, E. Y. X.; Marks, T. J. *Chem. Rev.* **2000**, *100*, 1391–1434.

(3) Bosmann, A.; Francio, G.; Janssen, E.; Solinas, M.; Leitner, W.; Wasserscheid, P. *Angew. Chem. Int. Ed.* **2001**, *40*, 2697–2699.

(4) Ivanova, S. M.; Nolan, B. G.; Kobayashi, Y.; Miller, S. M.; Anderson, O. P.; Strauss, S. H. *Chem.—Eur. J.* **2001**, *7*, 503–510.

(5) Barriere, F.; Camire, N.; Geiger, W. E.; Mueller-Westerhoff, U. T.; Sanders, R. *J. Am. Chem. Soc.* **2002**, *124*, 7262–7263.

(6) LeSuer, R. J.; Geiger, W. E. *Angew. Chem. Int. Ed.* **2000**, *39*, 248–250.

(7) Krossing, I.; Raabe, I. *Angew. Chem. Int. Ed.* **2004**, *43*, 2066–2090.

(8) Kishi, N.; Ahn, C. H.; Jin, J.; Uozumi, T.; Sano, T.; Soga, K. *Polymer* **2000**, *41*, 4005–4012.

(9) Cui, C. Z.; Bonder, E. M.; Jakle, F. *J. Am. Chem. Soc.* **2010**, *132*, 1810–1812.

(10) Turp, D.; Wagner, M.; Enkelmann, V.; Mullen, K. *Angew. Chem. Int. Ed.* **2011**, *50*, 4962–4965.

(11) Fischer, S.; Schmidt, J.; Strauch, P.; Thomas, A. *Angew. Chem. Int. Ed.* **2013**, *52*, 12174–12178.

(12) Furukawa, Y.; Kokado, K.; Sada, K. *Chem. Lett.* **2012**, *41*, 667–668.

(13) Robertson, N. J.; Kostalik, H. A.; Clark, T. J.; Mutolo, P. F.; Abruña, H. D.; Coates, G. W. *J. Am. Chem. Soc.* **2010**, *132*, 3400–3404.